Flight Simulations of High Speed Runway Exits

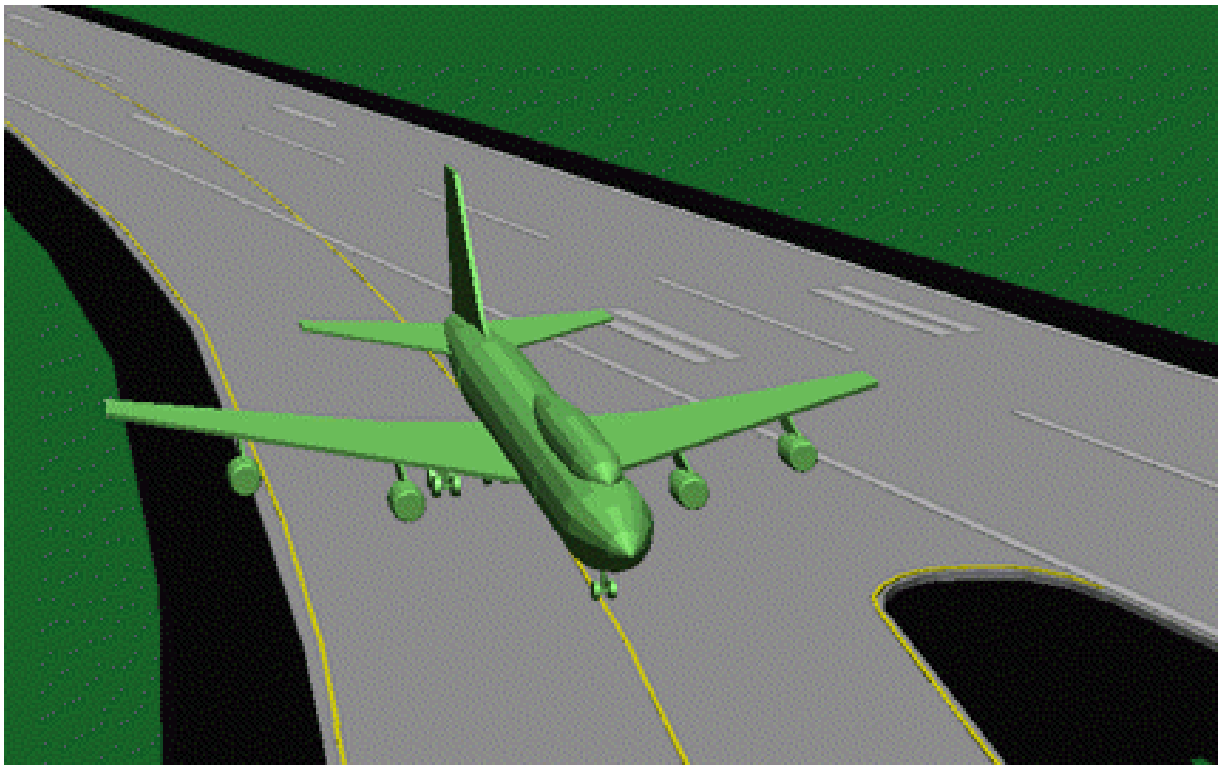

A.A. Trani, J. Cao, B.J. Kim, X. Gu,
C.Y. Zhong and M.T. Tarrago-Trani

Virginia Tech University
Department of Civil Engineering
Transportation Systems Laboratory
Blacksburg, VA 24061

:

Foreword

This report describes the work accomplished in the development of a computer simulation/optimization model to: 1) estimate optimal runway locations and 2) assess the feasibility and acceptance of high speed runway turnoffs. This work has been carried out for the Federal Aviation Administration (FAA) as part of a research grant with Virginia Tech.

The model described here and named REDIM 2.1 is a simulation and optimization model to evaluate existing runways and to estimate optimal runway exit locations for new runway facilities. The model described in this report has been coded in Microsoft Basic 7.0 compiler and can be executed as a stand-alone model in any personal computer using the DOS operating system.

The work presented here would not have been possible without the contribution of many individuals. Special thanks to Tom Tomita, Jim White, Archie Dillard and Satish Agarwal from the Federal Aviation Administration. Jim White acted project monitor for this research project. Archie Dillard provided invaluable insights to the development of the flight simulation experiments and also coordinated the flight simulation experiments at the FAA Mike Monroney Aeronautical Center. We would like to acknowledge the professionalism of all FAA pilots involved in these experiments. Their comments and insight provided the research team with a valuable feedback to improve and rationalize the proposed high speed exits.

We would also like to thank the TRACON and Control Tower personnel at Atlanta, Washington National, Dulles, Charlotte and Raleigh-Durham for the hospitality and help offered during our visits to each airport. The data gathered at these facilities made possible the calibration and improvement of the models described in this report.

A.A. Trani, X. Gu, C. Zhong, J. Cao, B.J. Kim, and M.T. Tarrago-Trani

Blacksburg, Virginia

Executive Summary

This report presents the results of a study performed by the Transportation Systems Laboratory at Virginia Polytechnic Institute and State University concerning the development of a computer program to estimate the optimal locations and geometric design requirements of high-speed runway turnoffs and flight simulation experiments to validate the same computer program. This study was conducted for the Federal Aviation Administration System Technology Division to assess the impact of optimal turnoff locations in runway occupancy time and ultimately in the assessment of possible runway capacity gains. The report covers the third and last phase of this research effort and emphasizes in the development of a micro-computer program to ascertain the impact of turnoff placement in the expected weighted average runway occupancy time for a given runway/aircraft mix configuration.

The resulting simulation/optimization model called REDIM 2.1 (runway exit design interactive model) is a stand alone application requiring minimal computer hardware (i.e., an IBM or compatible personal computer and EGA capabilities) that can be used in the planning and design of new runway turnoff upgrades or in the location of turnoffs for future runway facilities. REDIM 2.1 is capable of handling all existing turnoff geometries (including "wide throat" geometries) for added flexibility as well as newly proposed high-speed geometries with user-defined turnoff angles.

The main conclusions found during the development of the REDIM 2.1 computer model can be summarized as follows:

- The computer program developed uses a combination of a Monte Carlo simulation and a Polynomial Dynamic Programming algorithm to estimate turnoff candidates and optimize locations that minimize the aircraft weighted average runway occupancy time (WAROT).

- The model results computed for various runway/turnoff configurations seem to be in good agreement with empirical observations made by previous researchers [Koenig, 1978; Weiss and Barrer, 1984, Weiss, 1985 and Ruhl, 1990]. It must be pointed out that most of the previous data grouped aircraft according to approach speed [except for Ruhl, 1990] while the model described in this report considers the differences in landing aircraft dynamics between individual vehicles even if they belong to the same approach speed group classification.
- Significant reductions in runway occupancy time are possible with the optimal location and geometric tailoring of turnoff geometries for a known aircraft population. Single runway reductions in WAROT of up to 15% are possible with the use of proposed super-acute angle exits (i.e., 20 degree turnoff angle) compared to standard 30 degree angle geometries. Further reductions are possible by converting right angle turnoffs to super-acute angle exits. This reduction in WAROT could translate into moderate gains in runway capacity under mixed operations due to the stretching effect on the departure slots.
- Reductions in WAROT down to 36-40 seconds seem feasible with the use of optimally located super-acute turnoffs. This WAROT could support a 2.0 nautical mile interarrival separation (assuming some advances in terminal ATC automation take place and solutions to the wake vortex problem are found).
- Six degree of freedom aircraft simulations seem to indicate that super-acute turnoff geometries could allow consistent exit speeds of up to 35 m./s. (78 m.p.h.) for transport type aircraft operations. While the land use requirements of these turnoffs are high, it might well payoff in runways operated almost exclusively by transport-type aircraft over a 20 year life cycle.
- Proposed lateral separation distance nomographs between a runway and parallel taxiways were derived for all types of high-speed geometries using fairly conservative aircraft deceleration assumptions on the tangent portion of a turnoff. These nomographs could be used in preliminary airport planning to estimate land use requirements.
- The airfield observations confirm that REDIM 2.1 can indeed predict the weighted ROT parameter for many aircraft individually. In several occasions the WAROT values predicted by the model are within 2-3 seconds of those observed. Chapter 4 of this report addresses this issue in more detail.
- The landing roll airfield observations reported in this study fill an important gap in aviation operations today. The data was derived from video sources thus making it more reliable than standard counts taken at airports in previous studies.
- The flight simulation experiments conducted at the FAA Mike Monroney Aeronautical Center confirm that high speed exits are being misused in practice by conservative practices. These results also show that widening the throat of high speed exits has a substantial effect in the perception of high speed geometries by pilots.

- The flight simulation results indicate that pilots could take four new high speed exit geometries at higher speeds than the FAA acute angle standard. The data showed however, that in doing so pilots did not feel any safety compromises in the process. The exits tested have spiral transitions based upon the aircraft inertia and not based on geometric principles.

Several recommendations derived from this report are:

- Investigate in detail the aircraft landing gear dynamics associated with the proposed high-speed turnoffs as this might eventually be a deterrent for their operational implementations from the airline point of view. This will require actual aircraft runs and not just flight simulations in order to assess landing gear loads realistically.
- An extension to the existing model is possible where further consideration is given to the complex interactions between existing taxiway/runway subsystems and the placement of new runway turnoff locations. Also some consideration could be given in this analysis to airline/ATC motivational practices in locating runway turnoffs.
- Implement the algorithms of REDIM in a real-time ground control advisory system to help ATC personnel to make decisions regarding exit assignment in real time. This automated advisory system could in principle reduce ground delays prevalent at major airports by assigning aircraft to unused taxiways and runway exits. This project could easily tie the algorithmic development done here with ASTA-2 automation initiatives.
- Implement new lateral distance guidelines between runway and taxiway centerlines in FAA AC/150-5300-13 to provide minimum requirements for the implementation of high-speed runway turnoffs. Most pilots considered that 225 m (750 ft) was a minimum to execute high speed roll-outs from real runways. New high speed runway exit standards are proposed in this report.

CHAPTER 1 Introduction

1.1 Background of the Problem

Air transportation delays have a clear economic impact on the users and the suppliers of the aviation system. Recent statistics indicate that nearly $1 billion dollars are paid by airlines due to airport delays in the U.S. according to the Federal Aviation Administration [FAA, 1993]. According to FAA the number of congested airports will increase to thirty five by the end of the century [FAA,1993] with one-seventh of them possibly experiencing more than 50,000 hours of system imposed delays. The construction of new airports to alleviate this problem is a slow and iterative process due to the scarcity of land, limited financial resources and, local opposition due to possible environmental pollution. The FAA is currently engaged in the development of system wide strategies to increase the National Airspace System (NAS) capacity in several fronts ranging from upgrades to the existing Air Traffic Control System to methods to reduce the runway service time.

To increase the capacity of the existing air transportation system several topics of interest have been identified by FAA one of them being the possible reduction of runway occupancy time and its variance.

Runway occupancy time (ROT) of aircraft is one of the important factors affecting the capacity of a runway which in turn translates in an airport capacity. ROT is the time that an aircraft occupies the runway until a new operation (arrival or departure) can be processed.

Some of the most important factors that influence runway capacity are:

- Intrail separations
- Aircraft population mix
- Exit locations and their type

Several studies have suggested that by improving some of these factors there would be an increase in capacity of a single runway by 20% [Barrer and Diehl, 1988]. This report addresses some of the issues associated with the use of high speed exits and explores a methodology to optimally place runway turnoffs to minimize runway occupancy time. The report also details some of the steps taken to calibrate several computer models developed in the course of the past three years at Virginia Tech University to justify high speed turnoffs. Finally, this project also conducted flight simulation experiments to ascertain subjective pilot responses on the possible benefits and improvement to high speed exits.

1.2 Previous Research

Research on the subject started with the pioneering work of Robert Horonjeff in the late fifties [Horonjeff, et al., 1959, 1960 and 1961]. Horonjeff proposed standards for 45 and 30 degree angle geometries that later were adopted by the FAA and ICAO with subtle differences [FAA, 1989; ICAO, 1986]. This work was the first one to recognize the critical relationship between turnoff location and turnoff geometry and the research culminated with the developed a mathematical model to locate exit taxiways for a limited number of scenarios (i.e., two exit taxiway speeds and a reduced aircraft population). The results of this model concluded that the optimum location of runway turnoffs is quite sensitive to aircraft population, number of exits, and exit speeds. The same model used external atmospheric corrections to modify the baseline results due to meteorological and geographical conditions. However, only two exit speeds (i.e., 40 and 60 m.p.h.) and a limited number of aircraft populations were investigated thus making the model of limited use. Furthermore, since the aircraft populations used comprised “old” aircraft by current standards the results need revision. The pioneering effort of the Horonjeff team, however, generated a good amount of information regarding the cornering capabilities of aircraft and also obtained data on several lighting schemes to help pilots negotiate these turnoffs under adverse weather conditions. The Horonjeff team performed extensive experiments to find the acceptable turning radius at a given exit speed. The results suggested two centered curves for the turnoff geometry approximating the tracks derived from empirical observations for a Boeing KC-135 aircraft.

In 1970, FAA proposed standards for high speed exits using Horonjeff's results for 30 and 45 degree geometries. A 1800 ft. radius of curvature was adopted for the centerline track of the turnoff for the 30 degree exit geometry with a baseline design speed of 26.7 m./sec. (60 m.p.h.). According to Horonjeff’s findings the 45 degree turnoff was rated at 17 m./sec. (40 m.p.h.). The high speed turnoff incorporated a straight 61 m. entrance track emulating a large radius of curvature suggested by Horonjeff. ICAO adopted the Horonjeff standard using two radii of curvature (ICAO, 1977).

Schoen et. al. [Schoen et. al., 1985] investigated the turnoff trajectory of high speed taxiing aircraft in an isolated basis. The resulting shape of the aircraft turnoff was a variable curvature geometry with a continuously decreasing radius of curvature. The end result of this research was a computer program to calculate the (x, y) coordinates of the geometry, considering exit speed and aircraft turning ability. The findings of this research suggested that aircraft moment of inertia played an important factor in dictating the initial trajectory of the

turnoff maneuver. This research also showed that ROT values of 30 seconds are possible at the expense of large turning radius and extremely high exit speeds (e.g., 110 MPH for a Boeing 747). Very high-speed turnoff results should, however, be treated cautiously since at such high speeds the controllability of aircraft on the ground could become a serious operational deterrent.

Another important study on turnoff geometries was conducted by Aviation Department staff of Dade County, Florida (Carr et. al., 1980; Witteveen, 1987; and Haury, 1987).After testing various types of geometries, lighting, and marking scenarios in an L1011 flight simulator a “wide throat” geometry was derived having an entrance spiral length of 244 m. (800 ft.) and tapering off with a 122 m. (400 ft.). radius of curvature.Figure A.3 in Appendix A depicts graphically the peculiarities of this turnoff geometry. This type of turnoff geometry has been implemented at Miami International, Baltimore-Washington International, Indianapolis and Orlando International Airports. The wide entrance throat of this geometry is appealing in situations where lateral spacing restrictions between the runway and the nearest parallel taxiway are severe (i.e., less than 183 m.). However, the ending radius of curvature of only 244 m. might be a limiting factor in the operational capabilities of this exit to handle large aircraft above 17 m./s. (37 knots) in a routine basis. Subsequently, Marinelli evaluated the acceptance of this wide throat geometry against that of acute angle geometries with clear results favoring the standard 30-degree angle turnoffs.

The publication of Advisory Circular 150/5300-12 [FAA, 1983] incorporated several significant changes to the well established thirty degree angle exit geometry adopted in the early seventies.The most notable change has been the incorporation of a 427 m. (1400 ft.) spiral transition curve to smooth the initial aircraft path while transitioning from a straight line path (i.e., an infinite radius centerline track) to a finite centerline turnoff trajectory.

Regarding the optimal location of runway turnoffs the problem has been researched in at least four well documented instances. Horonjeff et al. [Horonjeff et al., 1961] proposed an optimization model based upon the maximization of the aircraft arrival acceptance rate under saturated operational conditions. The main problem with this model however, was the uncertainty of input parameters in terms of bivariate random variables represented by the mean distance and time for an aircraft to decelerate to a predetermined exit speed. This model could not address airfield specific environmental factors nor aircraft operational variables (e.g., aircraft landing weight variations) dictating the landing distance and time distributions.

In 1974, Daellenbach [1974] developed a dynamic programming model which in many respects is equivalent to the Horonjeff's approach with added extensions. Daellenbach removed the assumption of a specific arrival pattern thus adding more realism to the model. Daellenbach's model, however, also requires the knowledge of joint landing distributions which are in fact difficult to assess unless extensive data is available under many scenarios.

In a parallel effort Joline [Joline, 1974] developed another dynamic programming model to find the optimal number of exits and their locations with respect to the combined objective function of ROT and exit construction cost. While Horonjeff's model and Daellenbach's model required the joint distributions of landing distance and time for each aircraft type, Joline's model used a univariate distribution of 'ideal exit location' for a mixed aircraft pop-

ulation. Joline classified aircraft into three categories based on the aircraft size, and found the distributions of ideal exit locations for these three aircraft classes based on the observations of aircraft landing operations in Chicago O'Hare Airport. The ideal exit location distribution for entire aircraft population was found by combining the three distributions according to the proportions of the three aircraft classes. As mentioned earlier, there are several factors influencing the aircraft landing distance such as the design exit speed, landing weight, etc. Joline's model, like the previous models, did not address these variables.

The last effort in the optimal location of runway exits was performed at the Center for Transportation Research at Virginia Tech. The effort in the previous research phase was to develop algorithms suitable to be used in a realistic airport environment with the inclusion of several aircraft specific variables in the model developed. This work suggested the use of a combination of a dynamic programming algorithm with continuous simulation producing a first generation REDIM model [Sherali et al., 1991; Trani et al., 1990]. This new phase tries to expand on the notions previously reported and incorporates more flexibility and realism to the existing REDIM model.

1.3 Research Objectives

The purpose of this research is to investigate the viability of optimizing the location and geometric design of rapid runway turnoffs and develop a computer simulation model to execute these tasks in a routine and interactive basis. The model has been calibrated using real airport data collected at five major airports in the U.S. Also, flight simulation experiments were conducted to look at pilot’s concerns and views when high speed exits are used. This report represents the results of a third phase in a task to fully develop and implement rapid runway turnoffs under realistic airport scenarios as part of the research program sponsored by the Federal Aviation Administration. The ultimate goal of providing high speed exits is to reduce the service time of current and future runway facilities and thus reduce the possibility that runways in fact become bottlenecks of the air transportation system. This report builds upon algorithms to developed in Phases I and II using an integrated dynamic simulation and dynamic programming approach to estimate optimal runway turnoff locations minimizing the weighted average runway occupancy time, WAROT. This phase enhances the features of the Runway Exit Design Interactive Model (REDIM) whose preliminary development was reported in FAA/DOT research reports RD-90/32,I and RD-92/16,II [Trani and Hobeika et al., 1990].The model was revised to provide variable angle turnoffs consistent with FAA safety standards and ultimately to design guidelines and operational issues associated with newly developed turnoff geometries.

The Runway Exit Design Interactive Model version 2.1 (REDIM 2.1) developed in this research effort, incorporates several upgrades from its predecessor in order to provide added flexibility in the estimation of optimal turnoff locations and geometries. The model, like its predecessor, addresses specific airfield variables that affect the landing performance of the aircraft as well as important operational constraints (e.g., aircraft mix) that have a direct impact on the selection of the turnoff location and their geometry. The model is composed of three modules: 1) an interactive input module, 2) a dynamic simulation and optimization module to estimate the ROT times for individual aircraft and their optimal exit locations

and 3) an output module to show graphically and in tabular form the suggested runway turnoff configuration and display some measures of effectiveness of aircraft landing operations. The program contains a library of geometric and operational aircraft characteristics to allow the analyst to choose from a wide selection of aircraft operating under realistic airport conditions. Enhancements to the input module allow quick prototyping of various runway scenarios through very simple data input screens.Also enhancements to the output capabilities of the program have been made to facilitate the output of hard copies in a variety of printers.

The program considers four broad types of analyses: 1) evaluation of an existing runway, 2) improvement of an existing runway 3) design of a new runway facility and 4) individual aircraft landing roll behavior. In the evaluation mode, REDIM estimates several measures of effectiveness indicative of the operational capabilities of an existing runway facility. In this mode the user inputs the number, type and location of existing turnoffs as well as the relevant aircraft population data and the model predicts the average runway occupancy time (WAROT), the particular exit(s) that an aircraft can take, and the probability of each aircraft taking the assigned exit(s). Another potential use of this mode is to serve as a benchmark to perform valid comparisons between different runway alternatives.

The second mode of operation deals with the redesign of a runway facility. In this scenario it is expected that the user might want to explore the possibility of adding new high-speed turnoffs to an existing facility and examine their impact in the operational efficiency of the facility. Inputs in this mode are the number and type of existing turnoffs, their locations, the number of new turnoffs to be constructed and a reliability parameter. The outputs are the location and geometry of each new turnoff, the weighted average runway occupancy time, and an aircraft assignment table containing individual runway occupancy times and the individual aircraft probabilities of taking every existing and new exits.

In the third mode of operation REDIM estimates the optimal location of runway turnoffs and their corresponding geometries. An assignment table is given to the user indicating the turnoff(s) associated with each aircraft and their individual runway occupancy times. The weighted average runway occupancy time is also estimated as a global runway operational parameter and sensitivity studies can easily be conducted by changing the number of turnoffs allocated to a specific runway. Inputs by the user in this mode are the number of exits to be constructed and the desired exit reliability parameter.

The fourth mode addresses an individual aircraft landing roll scenario where the user wants to know specific results about the expected runway occupancy time and landing roll dynamics of a particular aircraft. This mode is primarily envisioned to serve as an individual calibration tool for critical aircraft analyses.

More detailed descriptions of these four modes of operation will be given in the remaining chapters of this report. REDIM blends the principles of continuous simulation with those of mathematical optimization to find the best turnoff locations and corresponding turnoff geometries for a myriad of possibilities. The program was designed to be interactive and a great effort was made to reduce the number of inputs expected from the user. A large aircraft data base is included to simplify the analyst input task but flexibility is also built-in to allow future aircraft additions. The overall effort was to make the program interactive and

easy to use. Many suggestions from previous users have been incorporated in this new version and extra features have been added to extend the flexibility of the program.

1.4 Methodology

1.4.1 Monte Carlo Simulation Technique

In the development of REDIM 2.1 a great deal of effort has been made to realistically simulate aircraft operations as they would occur in actual practice. Due to the stochastic nature of aircraft landing roll deviations observed in practice [HNTB, 1975; Koenig, 1978; Ruhl, 1989] it was decided to use a Monte Carlo simulation procedure in the dynamic simulation algorithms embedded into REDIM 2.1. The Monte Carlo simulation technique used primarily to estimate landing roll distance dispersions using aircraft normal distributions for some of the aircraft parameters dictating landing roll performance.

1.4.2 Interactive Software Package

The software package developed as part of this research consists of three important modules: 1) Input, 2) Dynamic Simulation/Optimization and 3) Output routines. The model called REDIM 2.1 incorporates significant improvements over its predecessor, REDIM 1.5, described in detail by Trani et al. [Trani et al., 1990]. Chapter 5 in this report fully documents the software package developed as part of this research. A users manual of the software is also available.

1.5 Differences with Previous REDIM Model

REDIM 2.1 incorporates several enhancements from its predecessor that add flexibility to every analysis. Differences in the new program encompass all three modules but specifically the dynamic and optimization routines have been improved to allow Monte Carlo simulations of landing aircraft operations. Additions to the new program have been primarily to account more realistically for variations in the aircraft landing dynamics. The aircraft dynamic characteristics have been improved using actual landing roll profiles observed at five busy airports in the East Coast. Also, results of flight simulation experiments have been added whenever applicable to make the algorithms more robust. Weight factors have been added to the program to represent more accurately aircraft landing conditions at the airport facility of interest.

1.5.1 Aircraft Landing Weight Factors

The aircraft weight factor is a nondimensional parameter varying from 0 to 1 representing the proportion of the useful load carrying capacity of an aircraft at any point in time. The landing load factor is a major determinant of the aircraft nominal approach speed of a vehicle. The load carrying capacities of certain aircraft make their approach speed range large enough to justify the inclusion of this parameter in REDIM 2.1. A Boeing 727-200

for example has a 30 knot differential between the approach speeds at the operating empty and maximum landing weights and ISA, wet airfield conditions [Boeing, 1986].The reference landing runs at these two extreme landing weights are 1190 and 1615 m., respectively, thus providing an idea of the large variations in landing roll performance for transport-type aircraft.

1.5.2 Aircraft Landing Data Generation Methods

In the optimization procedure used in REDIM it is necessary to emulate a large number of aircraft operations through a Monte Carlo simulation procedure in order to assess accurately the landing distance dispersions of a large aircraft population.This procedure although more accurate necessitates considerably longer running times. Chapter 3 in this report describes in detail the basic assumptions regarding the aircraft kinematic behavior and the probability density functions used in estimating landing roll parameters.

1.5.3 Range Solution f or Exit Locations

Due to the stochastic nature of the problem the solutions provided by REDIM 2.1 represent ranges of solutions to locate turnoff exit locations rather than a deterministic location as in REDIM 1.0. The motivation behind this approach is to provide optimal location ranges where the construction of a new turnoff yields near similar WAROT values for a given aircraft population and airport environmental conditions.This approach should point out the analyst sensitivity of the model to input parameters.The range of solutions for turnoff locations are derived from five internal iterations performed for all the aircraft data selected by the user. All five runs use different pseudorandom numbers and therefore have the same weight in the solutions presented. More details of this method are presented in Chapter 3 of this report.

CHAPTER 2

Computer Model Description REDIM 2.1

This chapter describes the functional organization of REDIM 2.1 and provides details of the mathematical optimization and simulation procedures used internally. The chapter ends with a series of examples that will help the reader to understand the use and applications possible with REDIM 2.1. A separate version of this chapter is available in form of a user manual for those individuals not concerned with the mathematical details of the model and who would only like to run and interpret the program results.

2.1 REDIM 2.1 Computer Model Organization

The structure of REDIM 2.1 is shown graphically in Figure 2.1. The model is comprised of four modules: 1) Input, 2) Simulation, 3) Optimization and 4) Output. The modules interact with three data files containing aircraft related information (master and working files) and an output file generated after the end of each run. The following paragraphs describe in some detail the peculiarities of each module and the input/output structure of the program.

2.1.1 Main Menu

The "Main Menu" placed at the top level of the flow chart has five modes: 1) "Edit", 2) "Analysis", 3) "Output", 4) "Print", and 5) “Quit". The Main Menu always appears at the top of the computer screen. The ‘edit’ mode invokes the procedures of Input Module, where the user may edit the Data File or Master File. The ‘analysis’ mode invokes the analysis procedures. REDIM 2.1 provides four types of analyses: ‘design,’ ‘improvement,’ ‘evaluation’ and ‘individual” run modes. The ‘output’ modes connects the user with the output module where the user may view the various output screen.

2.2 Input Module

The Input Module comprises a series of interactive screens that allow the user to input and edit data necessary for the analysis portion of the program (i.e. Simulation and Optimization Modules). This module is controlled by menus or key-stroke commands such as "Esc" key.

Input data is classified into six broad categories: 1) analysis type and related data, 2) aircraft mix, 3) airport operational data, 4) airport environmental data, 5) runway gradients and 6) surface conditions. All of these are necessary for the analysis, and should be saved in a 'Working Data File' specified by the user with an arbitrary name. For the convenience of the user, all predefined aircraft characteristics are kept in a Master Data File named "MASTREV.DAT" and are transferred to the Working Data File automatically if necessary.

FIGURE 2.1 REDIM 2.1 Model Structure.

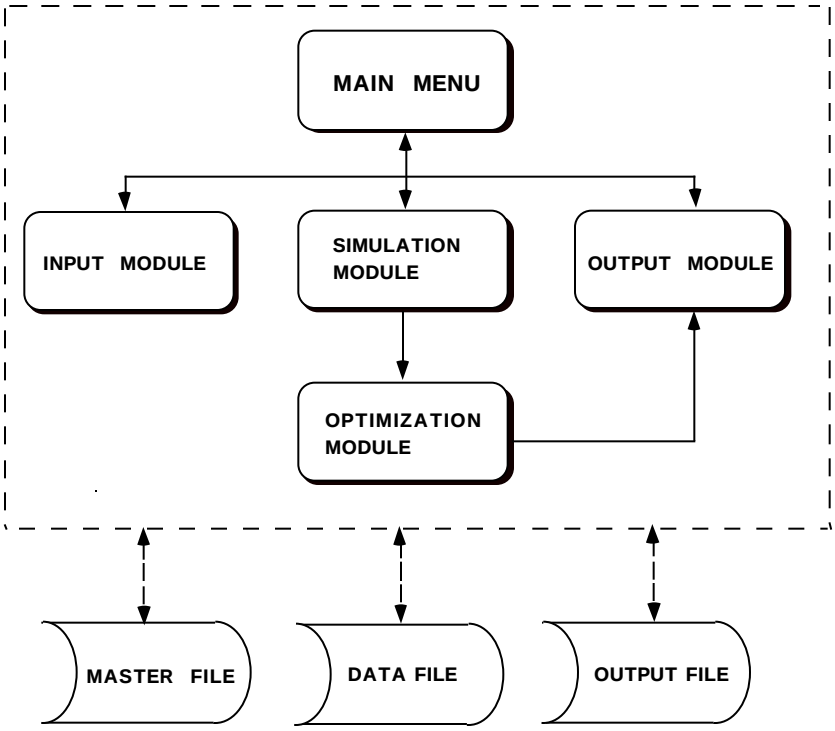

2.2.1 Data Classification

In REDIM 2.1 there are three kinds of data needed for analysis: 1) input data, 2) constant data, and 3) calculated data. Among these kinds of data, constant data and calculated data are determined in the Simulation and Optimization Module. Input data is

provided by the user via the Input Module and its user-friendly screens. The input data is classified into six categories as mentioned previously. The following paragraphs define the categories in more detail.

Analysis Type and Related Data

The program provides the user with four choices for the type of analysis to be performed. For each type of analysis, there are some pieces of data needed to execute the model properly. “Design” analysis asks the user to input the number of new exits, the lateral distance between the runway and the parallel taxiway, the exit angle, the speed at the junction of exit and taxiway and the exit speed of each aircraft category. “Evaluation” analysis requires the information on the existing exit configuration including the number of existing exits, the locations and the types, the entry speed for each existing exit and availability. For the “improvement” analysis, the user has to input all the data above. The “individual” mode requires only the aircraft type and surface condition.

Aircraft Mix

In this category, the percentages of the aircraft comprising the airport population mix are included. The maximum number of aircraft for a mix is restricted as twenty because this number seems to be a practical limit and because the memory requirements of the software should not exceed 640k dictated by the DOS operating system.

Airport Operational Data

In this category, the free roll time between the touchdown and the beginning of braking, the free roll time between the end of braking and the beginning of turn off are included. A safety factor for the impending skidding condition is also part of this category.

Airport Environmental Data

The following parameters are included in this category: wind speed, wind direction, airport elevation, airport temperature, runway orientation and runway width. This will affect the optimal placement of turnoffs, since they have effect on airport landing roll performance.

Runway Gradient

In this category, runway length, and the effective gradient for every one tenth of runway are included. The runway gradient affects the effective aircraft deceleration used in the kinematic equations of motion.

Weather

The relative frequency of dry and wet runway surface conditions are included in this category. The percentages should reflect the expected conditions predominant at the airport facility.

2.2.2 Data Input Method

In the Input Module, there are three different input methods used: 1) menu input, 2) line input, and 3) table input. Menu input arises when the user selects his choice among the list displayed on the screen using the arrow and enter keys. The flow in the program is controlled by the menu input method. The main menu, edit menu for working data file, edit menu for master data file, selection of a analysis type, etc. are the examples of the menu input method. Line input occurs when the user puts a numerical value like runway length or a string datum like a data file name at the position specified on a screen. The user inputs file names (data and/or output file), the number of exits, etc. using this method. Table input is similar to line input. However, table input is used in order to get several numerical data on the same screen, while line input is used in order to get one numerical or string datum on a line. By the table input method the user inputs aircraft mix data, exit speeds etc.

2.2.3 Procedures Used in the Input Module

If the user selects ‘Edit’ from the Main Menu, the program shows the user ‘Edit Menu’ which offers the user with two choices: ‘Edit Data File’ and ‘Edit Master File.’

Editing the Data File

This portion of the program allows the user to modify existing data file. If the user selects this mode from the Edit Menu, the list of the data categories, which are explained in Section 2.3.1, are shown on the screen. The user may select one from the list, and then modify the values of data items in that category.

Editing the Master File

While the function of "Edit Data" mode is editing the working data file, the function of "Edit Master File" is editing the master data file which keeps the aircraft names and their geometric characteristics. If "Edit Master File" mode is selected, the Edit Menu for master data file appears. In this menu, there are two choices: 1) "Add a New Aircraft" and 2) "Change some Specific Data." If the user chooses the first, he/she has to select one out of five aircraft categories (TERPS A-E) and input the new aircraft name. Then a screen for editing aircraft characteristics appears. If the user opts for the second choice, he/she has to select one aircraft category and one aircraft name included in the category selected. Then a screen for editing aircraft characteristics appears.

2.2.4 Analysis Types and Their Input/Output Relationships

As stated earlier, the user can select one of four types of analysis: 1) design of a new runway system, 2) improvement of an existing runway system, 3) evaluation of an existing runway system and 4) analysis of individual aircraft landing performance.

The'design' option assumes a hypothetical situation with no exits on the runway. The number of new exits and the design exit speed for each aircraft category are inputs for this type of analysis. The results are 1) optimal exit locations, 2) aircraft assignment to the new exits, 3) the weighted average ROT which is minimized by the optimal exit locations, and 4) turnoff geometries of the exits.

The'improvement' option assumes that a few exits would be added to an existing runway. This analysis requires the number of new exits which will be constructed and all information on the existing exits, which includes 1) the number of existing exits, 2) the locations and types of existing exits and 3) availability of existing exits. The design exit speed for each aircraft category is also required. The results are similar in nature to those of the 'design' option. The only difference is that this option takes into account the existing exits as well as the new exits for aircraft assignment

The purpose of ‘evaluation’ option is to estimate the average ROT of a given aircraft mix assuming only existing exits are utilized. All information on the existing exits are required for this analysis. The aircraft assignment to the existing exit and the resultant average ROT are the major outputs of this analysis, while the user may view the geometry of the existing exits.

The ‘individual’ option is added in Phase II research for analyzing the landing behavior of an aircraft in more detail. The aircraft type and surface condition are the inputs for this analysis. The five percentile values (95%, 90%, 80%, 70% and 50%) of landing distance and ROT are then found for six predefined exit speeds.

2.3 Computational Modules

The Simulation Module and the Optimization Module are the collections of subroutines made for computations. These computational modules are responsible for the aircraft landing roll dynamic simulation so as to generate turnoff locations for each aircraft and the dynamic programming optimization so as to decide the exit locations. For example, the Simulation Module involves the subroutines for aircraft dynamics and the subroutines for random number generation from the truncated normal distribution. The Optimization Module includes the subroutines for exit candidate generation and for the dynamic programming algorithm. The details of these computations are described below.

2.4 Aircraft Stochastic Simulation Model

The aircraft landing maneuver simulated in REDIM 2.1 starts at the runway threshold crossing point and ends at a point where the aircraft wingtip clears the imaginary, vertical plane defined by the runway edge. The aircraft landing phases modeled in REDIM 2.1 are: 1) an air phase, 2) a free roll segment between touchdown and the initiation of braking, 3) a braking phase, 4) a second free roll phase between the end of the braking phase and the start of the turnoff maneuver and 5) the turnoff maneuver phase. These landing phases are depicted graphically in Fig. 2.2. It can be seen from this figure that the major contributors

to runway occupancy time are the braking and turnoff phases as these usually take about 60% and 25%, respectively of the total ROT

FIGURE 2.2 Aircraft Landing Roll Phases Modeled.

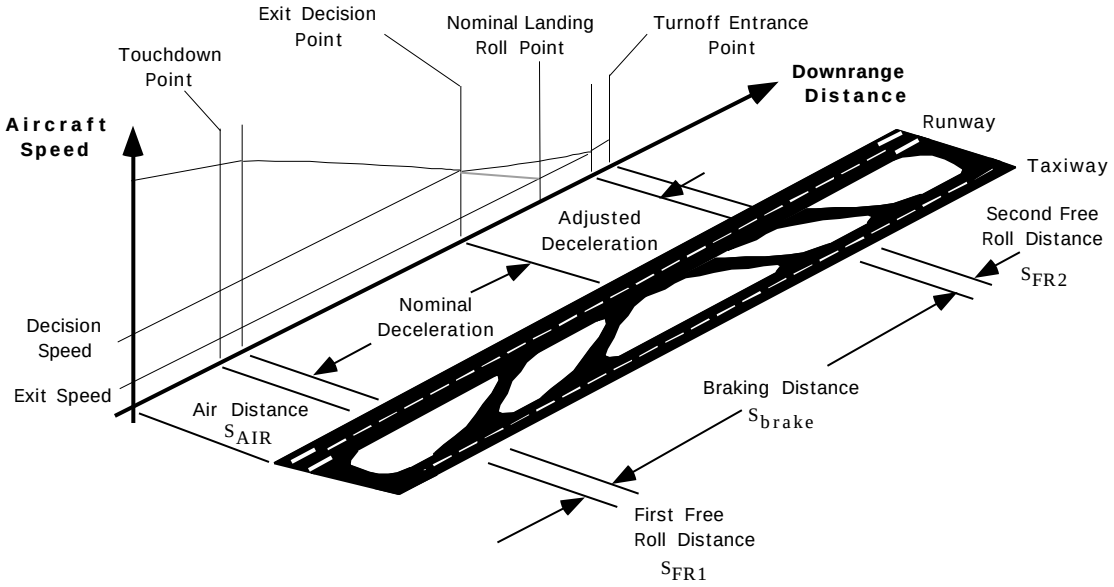

2.4.1 Air Phase

The air distance can be estimated assuming the longitudinal flight path of landing aircraft is a combination of a linear descent path and a circular arc flare maneuver. Lan and Roskam [Lan and Roskam, 1981] suggested an analytical expression for estimating air distance with these two terms. However, our analysis indicates that pilots have a tendency to float more on long runways than in short ones to reduce the sink rate at touchdown thus a third term is added to the previously known expressions shown in Equation 2.1.

$$S_{air} = \frac{h_{th}}{\gamma} + \frac{V_{fl}^2}{2g(n_{fl}-1)} + \Delta S(RL) \qquad \textbf{(2.1)}$$

Where: h_{th} is the threshold crossing height, γ is the flight path angle, V_{fl} is the flare speed, n_{fl} is flare load factor, V_{ap} is the approach speed, V_{td} is the touchdown speed, and $\Delta S(RL)$ is a correction factor to account for aircraft floating over the runway. The first and the second terms of Eqn. 2.1 represent three distinct segments used to model the air distance as shown graphically in Fig. 2.3.

The aircraft approach speed is determined from the basic steady state lift equation (Trani et al. 1992a):

$$V_{fl} = K \times \sqrt{\frac{2Mg}{\rho c_{atm} C_{lmax} A_w}} \quad \textbf{(2.2)}$$

Where: K is an empirical flare speed correction factor, M is the aircraft mass, g is the gravity acceleration, ρ is the standard atmosphere air density, c_{atm} is a correction factor for ρ, C_{lmax} is maximum landing lift coefficient, and A_w is the aircraft wing area. From our field observations the aircraft approach speed has been determined to be about 1.05 times of the flare speed (Trani et al. 1992a). K factors have been derived from airfield observations for medium and short range transport aircraft and used in the simulation model instead.

FIGURE 2.3 Initial Landing Path Diagram.

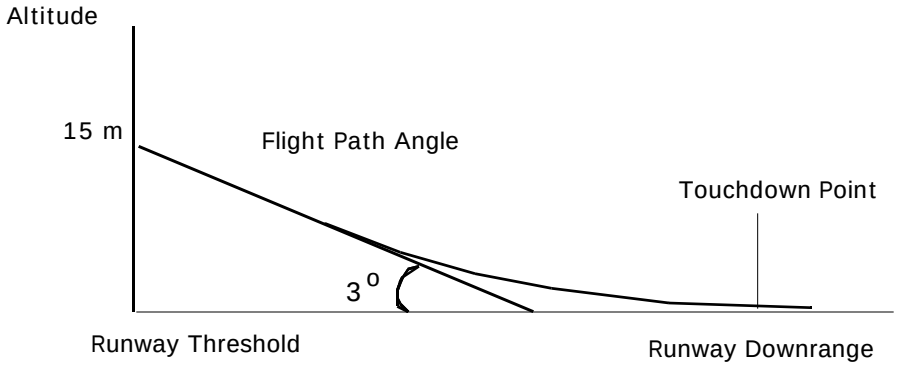

2.4.2 Free Roll Phases

First Free Roll Phase: The first free roll phase accounts for a time lag perceived in the activation of aircraft thrust reversers and brakes. The first free roll phase starts at the point where the main gear touches down and ends when thrust reverse and brakes are applied. The aircraft is assumed to travel at a near constant speed for about 1 to 3 seconds.

$$S_{fr1} = V_{td} t_1 \quad \textbf{(2.3)}$$

Where: S_{fr1} is the first free roll distance and t_1 is the travel time.

Braking Phase: The braking phase starts from the ending point of the first free roll phase until the aircraft decelerates to an acceptable exit design speed, V_{ex}. In this phase the aircraft uses a nominal deceleration rate to decelerate to a speed called decision speed (V_{dec}). The model checks for the existence of a coasting distance segment, S_{coast}, under the assumption that the aircraft uses the nominal deceleration rate to reach the selected exit after coasting. If this distance is within certain range, l_{dec}, the aircraft uses the adjusted deceleration rate to reach the exit's design speed without coasting. If the distance exceeds l_{dec}, the aircraft coasts for some time using a lower deceleration rate dec_{ct} with the decision speed as a initial speed and then uses the nominal deceleration rate to reach the exit. The nominal deceleration rate (dec) is generally derived from the aircraft manufacturer published data

under sea level International Standard Atmospheric conditions (ISA) and adjusted by runway local gradient, surface conditions (wet or dry) and the aircraft assigned gate location. The decision speed used in the model has been obtained by using detailed kinematic analysis of aircraft landings collected at various airports (Trani et al. 1993). Equations 2.4 and 2.5 are used to estimate the braking phase distance, S_{br}, and time, t_{br}, respectively.

$$S_{br} = l_{ex} - (S_{air} + S_{fr1} + S_{fr2}) \tag{2.4}$$

$$t_{br} = \begin{cases} \dfrac{2\left(S_{br} - \dfrac{V_{td}^2 - V_{dec}^2}{2dec}\right)}{V_{dec} + V_{ex}} + \dfrac{V_{td} - V_{dec}}{dec} & if \;\; S_{coast} < l_{dec} \\ \dfrac{V_{td} - V_{dec}}{dec} + \dfrac{V_{dec} - V_x}{dec_{ct}} + \dfrac{V_x - V_{ex}}{dec} & if \;\; S_{coast} \geq l_{dec} \end{cases} \tag{2.5}$$

Where: l_{ex} is the distance from a selected exit to the runway threshold, S_{coast} is the possible coasting distance which can be calculated by using equation 3.7and V_x is the ending speed in the coasting period given by using equation 2.7.

$$S_{coast} = \frac{l_{ex} - \left(S_{air} + S_{fr1} + S_{fr2} + \dfrac{V_{td}^2 - V_{ex}^2}{2dec}\right)}{\left(1 - \dfrac{dec_{ct}}{dec}\right)} \tag{2.6}$$

$$V_x = \sqrt{\frac{dec_{ct}(V_{td}^2 - V_{ex}^2) + (dec - dec_{ct})V_{dec}^2 - 2dec_{ct}decS_{br}}{dec - dec_{ct}}} \tag{2.7}$$

An exit choice model is used in the braking phase to determine the most likely exit to be used. This model is described later in this report.

Second Free Roll Phase: The second free roll phase is scheduled after the braking phase just before the aircraft starts turning off from the runway. This phase is associated with the pilot identification and decision procedure to take a feasible exit. The aircraft will travel at a constant speed (i.e., the exit speed) for about 1 to 3 seconds in this phase.

$$S_{fr2} = V_{ex} t_2 \tag{2.8}$$

Where: S_{fr2} is the second free roll distance, t_2 is the travel time and V_{ex} is the exit speed.

Turnoff Phase: The turnoff phase is used to describe the aircraft exit turnoff behavior and estimate the turnoff time. This phase starts as the aircraft begins the turnoff maneuver and ends at the point where the aircraft clears the runway. The turnoff time, t_{tof}, is estimated through numerical integration using a 4th order Rung-Kutta algorithm as indicated in equation 2.9.

$$t_{tof} = f(V_{ex}, b_{tail}, b_{wing}, Rw, ET) \tag{2.9}$$

Where: b_{tail} is the aircraft tail plane span, b_{wing} is the aircraft wing span, R_w is the runway

width and ET is the selected exit type. As described above, the aircraft runway occupancy time ROT can be estimated by adding all individual times in all phases.

$$ROT = t_{air} + t_1 + t_{br} + t_2 + t_{tof} \quad \textbf{(2.10)}$$

2.4.3 Turnoff Phase

The purpose of the turnoff phase is to trace the aircraft path throughout the exit maneuver and to estimate the time consumed in the turnoff up to the clearance point. A model is adopted with some modifications to perform this purpose. The exiting maneuver begins when the aircraft decelerates to the user-defined exiting speed and ends with a complete clearance of the runway as depicted in Fig. 2.3. It is assumed that the wingtip dictates the clearance of runway, which is generally true for all aircraft exiting at high speeds. The only exceptions occur at low exit speeds or when an aircraft has an abnormally large tail-plane span (STOL aircraft). Since the objective of this research is to investigate the effectiveness of high speed exits, these exceptions would seldomly be studied.

The turning motion of an aircraft at a speed, at which aerodynamic forces are insignificant, can be simply characterized by forces acting on the nose gear. An algorithm developed by Schoen et al. and used in a previous NASA research effort on this topic, considers three side force contributions acting on the aircraft nose gear: 1) the centripetal force, 2) the aircraft inertia, and 3) the tire scrubbing resistance to the turn [Schoen et al., 1985]. That is, the total side force acting on the aircraft nose gear is composed of the centripetal force, the aircraft inertia and the tire scrubbing force. The side friction coefficient (f_{skid}) is the sum of the coefficients of above three contributions. Mathematically,

$$f_{skid} = f_c + f_{sc} + f_{Izz} \quad \textbf{(2.11)}$$

where: f_{skid} is the nose gear tire skid friction coefficient, f_{sc} is the tire scrubbing coefficient, f_{Izz} is the aircraft inertia contribution to the nose gear skidding friction coefficient, and f_c is the centripetal acceleration contribution to skidding.

Originally, Schoen et al. (Schoen et al., 1983) fixed the skid friction coefficient as a conservative value (0.2). However, it is well documented in the literature that the skid friction coefficient is a function of aircraft tire pressure and speed, among other variables [Harrin, 1958: Wong, 1978]. A summary of this functional relationship is depicted graphically in Fig. 2.3, where four aircraft type categories are represented (i.e., four tire pressures characteristic of each aircraft approach speed category). The upper curve corresponds to a tire pressure of 50 PSI which is a representative value of Class A category aircraft. Similarly, the fourth lowest curve corresponds to a tire pressure of 200 PSI, a typical tire pressure of current transport aircraft. Instead of using a single value as the skid friction coefficient, the coefficient is selected from Fig. 2.4 considering the exit speed and aircraft type.

As shown in Eq. 2.11, the skid friction coefficient is modeled as the sum of three terms. These terms are calculated as follows:

FIGURE 2.4 Side Skid Friction Coefficient Variations with Speed.

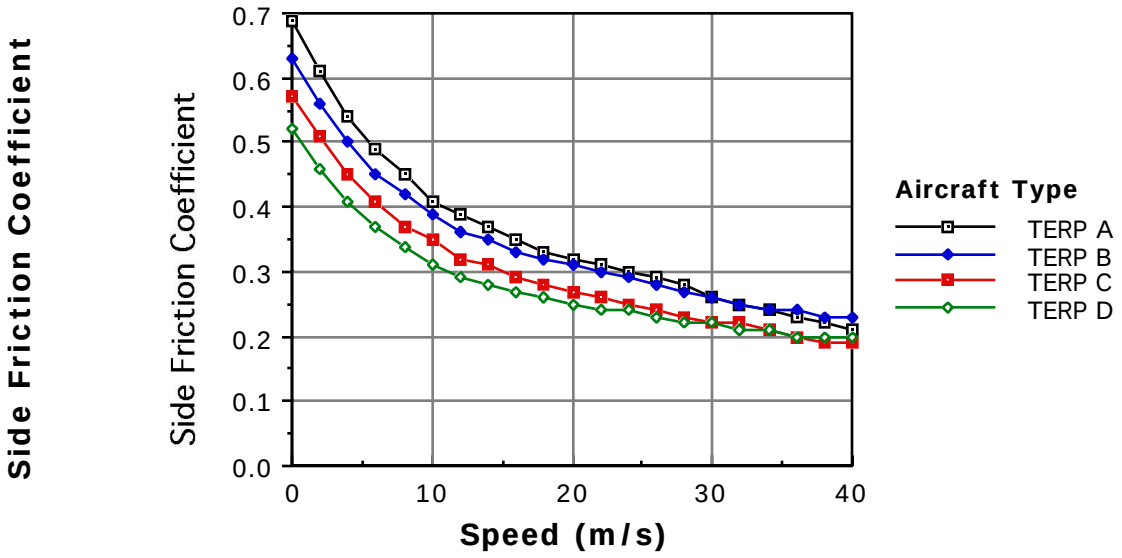

The contribution of the centripetal acceleration is:

$$f_c = \frac{V^2}{gR} \tag{2.12}$$

where: V is the aircraft instantaneous speed, R is the instantaneous radius of the curvature followed by the aircraft, and g is the acceleration of gravity. The tire scrubbing resistance contribution (f_{sc}) is determined by aircraft mass and the instantaneous radius. The relationship of these variables is depicted in Fig. 2.5.

At last, the contribution of aircraft inertia to side load on nose gear is:

$$f_{Izz} = \frac{I_{zz}\left(\frac{V\dot{R}}{R^2}\right)}{mg\left(1 - \frac{l_m}{100}\right)w_b\left(\frac{l_m}{100}\right)} \tag{2.13}$$

where: I_{zz} is the moment of inertia around the z axis, V is the aircraft speed, l_m is the percent load on the main gear, w_b is the wheelbase, m is the aircraft mass, and $\dot{R}$ is the instantaneous rate of change of the radius of curvature.

FIGURE 2.5 **Variations of Tire Scrubbing Coefficient with Radius of Curvature (Adapted from Schoen et al. 1989).**

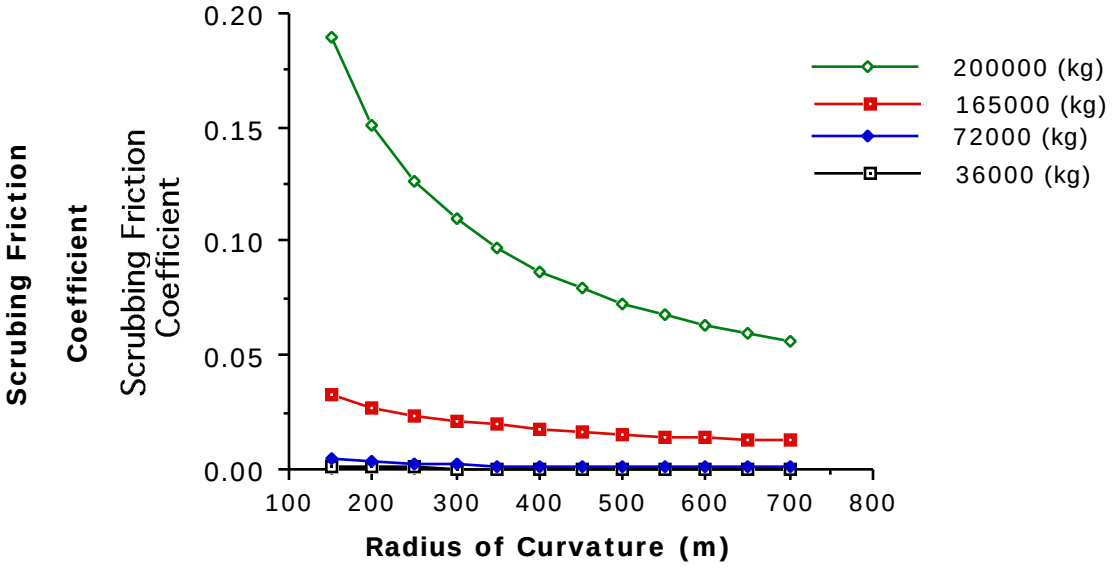

Solving Eq.2.14 for $\dot{R}$ gives:

$$\dot{R} = \frac{f_{Izz} R^2}{I_{zz} V}(mgw_b)\left(\frac{l_m}{100}\right)\left(1 - \frac{l_m}{100}\right) \quad \textbf{(2.14)}$$

With a given aircraft type, for every instantaneous speed and instantaneous radius of curvature, the values of f_{skid}, f_{sc} and f_c can be found via Figs.2.4 and.2.5 and Eq.2.12. By substituting these values into the Eq.2.10, the value of f_{Izz} is found. By substituting the value of f_{Izz} into Eq.2.14, can be computed for every instance.With the instantaneous values of $\dot{R}$ and V, the transient radius of curvature, R_t can be calculated by integrating forward in time. That is,

$$R_t = R_{t-1} + \int_{(t-1)}^{t} \dot{R}_t dt \quad \textbf{(2.15)}$$

The coordinates of an aircraft's turning path can be calculated by integrating the instantaneous speed multiplied by the sine and cosine values of the heading angle, φ. That is,

$$X_t = X_{t-1} + \int_{(t-1)}^{t} V\cos(\varphi)dt \quad \textbf{(2.16)}$$

$$Y_t = Y_{t-1} + \int_{(t-1)}^{t} V \sin(\varphi)\, dt \qquad \textbf{(2.17)}$$

where: X_t and Y_t are the longitudinal and lateral cartesian coordinates of the aircraft at any time t, V_t is the aircraft instantaneous speed, and φ is the heading angle with respect to the runway heading.

It should be noted that this simplification may apply only to a speed up to two thirds of the touchdown speed, because this speed is known to be the threshold for significant aerodynamic control for conventional aircraft [Miller and Thomas, 1963]. Even with this restriction, the evaluation of turnoff maneuvers can be accomplished for a large variety of aircraft whose turnoff speed ranges from 10 to 45 m/s (22.3 - 100.4 m.p.h). Turnoff design speeds above 45 m/s are unlikely to ever be used due to possible aircraft ground control problems. The lifting forces acting on the aircraft at high speed can be included in the above equations by modifying the aircraft mass term accordingly.

Another modification on this algorithm is the incorporation of the free roll deceleration during the turnoff phase. Since turnoff phase requires a fairly large amount of time unlike the free roll phase, the free roll deceleration should not be neglected in the turnoff phase. The free roll deceleration is assumed to be -0.375 m/s^2. Hence, the instantaneous speed in the above equations is reduced by this deceleration rate.

The integration of Eqs.2.14 to 2.16 is computed numerically for every 0.01 of a second. Along with the x-y coordinates of the turning path, the position of the wingtip is also computed at every step in the numerical integration until the wingtip leaves the runway boundary. Turnoff time is defined as the duration from the beginning of the turning maneuver to the instance when the wingtip leaves the runway boundary.

2.4.4 Deceleration Distance and ROT

Runway occupancy time as defined in this report represents the time interval between the aircraft threshold crossing point and when the aircraft wingtip has cleared the runway edge imaginary line. The estimations of runway occupancy time encompasses the five landing phases explained previously. The corresponding time parameters are: 1) time to touchdown, 2) one free roll time between touchdown and the initiation of braking, 3) braking time, 4) a second free roll time between the end of the braking phase and the start of the turnoff maneuver and 5) the turnoff time. Although at first glance it might seem that the contribution of the turnoff component is not significant even for moderate speeds (using a typical high-speed turnoff), it could amount to 12-13 seconds or about one fourth of the total runway occupancy time.

By definition, the total distance for an aircraft to decelerate to a given exiting speed is calculated as the sum of distances in the air, free roll, and braking phases, and that ROT is

found as the sum of durations of the air, free roll, braking, and turnoff phases. Mathematically,

$$S_{tot} = S_{air} + S_{fr1} + S_{fr2} + S_{br} \quad \textbf{(2.18)}$$

$$t_{tot} = t_{air} + t_{fr1} + t_{fr2} + t_{br} + t_{off} \quad \textbf{(2.19)}$$

2.4.5 Data Generation via Monte Carlo Simulation

The landing roll performance of an aircraft is stochastic in nature. For example, the touchdown location and deceleration rate varies for each landing resulting in the different total landing roll distances. In order to incorporate this stochastic nature of landing process into the model, four variables are selected as random variables: the threshold crossing altitude, final flight path angle, landing weight and deceleration. By FAA regulations [FAR 25], the pilots are requested to maintain the threshold crossing altitude and flight path angle as 15m and 3 degree, respectively. To represent the variations in the altitude and the angle, the standard deviation of the altitude and the flight path angle are set to 1.5m and 0.15 degrees, respectively. The mean and standard deviation of landing weight factors for each category is given by the analyst. The mean deceleration rate is estimated by the method explained in section 2.1 and the standard deviation of deceleration rate is set to 7% of the mean value. To improve the model's capability to predict the actual aircraft landing performance, these parameters were calibrated with field observations and with high fidelity flight simulators such as those conducted at the FAA B727-200 simulator in Oklahoma City. During the third phase of this research, the calibration of these parameters was performed according to the procedures described in Chapter 7.

For an optimization analysis, 200 landing distance data points are generated for each aircraft type via a Monte Carlo simulation. The Monte Carlo simulation is a tool for analyzing a stochastic system by generating random numbers for each random variable involved in the system. For analyzing the landing roll performance, each landing distance value is generated via following steps:

1. Generate four random numbers from the uniform distribution on the interval [0, 1]
2. Generate the values of the threshold crossing altitude, flight path angle, landing weight factor and deceleration rate from truncated normal distribution using the random numbers generated in step 1
3. Calculate the landing distance and deceleration time by substituting the values of four random variables into the dynamic formulation described in section 2.1
4. Repeat the step 1 to 3 two hundred times.

Step 1 is performed by utilizing the RND0 function of Microsoft BASIC version 7.0. Step 2 is performed by inverse transform method using truncated normal distributions with parameters described previously. Since normal distribution does not have a simple closed form of the inverse cumulative density function, a polynomial approximation of inverse cumulative density function is used to generate the random numbers from normal distribu-

tions [Beasley and Springer, 1977]. The method for generating random variables from a truncated distributions is described in Law and Kelton [Law and Kelton, 1982]. Step 3 is a simple calculation, because all the equations and the values of all the variables are known.

2.4.6 Second Order Landing Aircraft System

The new braking algorithm incorporates a new exit "seeking" deceleration procedure that changes the deceleration of the vehicle as a function of the distance to go to the next available exit. The inclusion of feedback from the current aircraft position on the runway allows shorter runway occupancy times and also seems to represent the pilot's behavior under real airport conditions. To illustrate this new method adopted in REDIM 2.1 refer to Fig. 2.2. Two distinct aircraft deceleration phases are identified: 1) a nominal deceleration phase where the pilot applies an average braking effort and 2) an adjusting braking phase where the pilot modifies continuously the aircraft deceleration schedule to achieve a predefined turnoff speed at the next available runway exit location. A decision point is defined in order to establish the transition between the nominal and the adjusted deceleration phases.

The decision point will generally be a function of variables such as the pilot's eye position with respect to the ground, the airport visibility, the aircraft state variables (i.e., speed, deceleration, etc.), the pilot's situational awareness (i.e., information of various exit locations and their design speeds), and the instantaneous crew workload. Since many of these variables are difficult to validate a simple heuristic rule is used in this approach to determine the decision point in terms of aircraft approach speed solely. This simplification seems valid if one considers that in general the approach speed will dictate to some extent the average workload expected during a typical landing. The faster the aircraft flies in the approach phase, the sooner decisions will have to be made in order to maintain a reasonable safety margin in the landing roll operations. Also, the approach speed is somewhat correlated with the pilot's eye position in the cockpit for commercial aircraft. This implies that heavy jets will have a definite advantage over general aviation aircraft in reaching their decision point at an earlier stage as pilots have a much better perspective of the location of downrange turnoffs.

In practice, pilots flying into an airport facility will probably have knowledge of the approximate exit locations and types of turnoff available for the active runway. therefore it is likely that they will adjust the aircraft behavior to reach a comfortable exit location at or near a desired exit speed. Figure 2.6 illustrates this heuristic principle using data typical of a Boeing 727-200.

The computer simulation results show the adjusted deceleration algorithm and the corresponding individual runway occupancy time for five different turnoff locations and a desired exit speed of 15 m/s. From Figure 2.6 one can see that the braking adjustments start at the decision point for all runs since the same aircraft speed parameters were used in the simulation. The differences in runway occupancy time are solely due to the different adjusting braking rates present once the decision point has been reached. Using the same aircraft and varying the decision point parameter from 100 to 400 m. yields results shown

in Figure 2.7. Notice that increments in situational awareness (i.e., increasing the decision point distance) will allow pilots to adjust earlier for a given exit location thus resulting in smaller runway occupancy times. Note that in both cases the adjustments made to the deceleration rate can be easily linearized with little loss in accuracy. This linear approximation of deceleration rate has been embedded into REDIM to simplify the number of internal computations of the model thus reducing CPU time.

FIGURE 2.6 Aircraft Nonlinear Deceleration Model (Runway Exit Location Sensitivity).

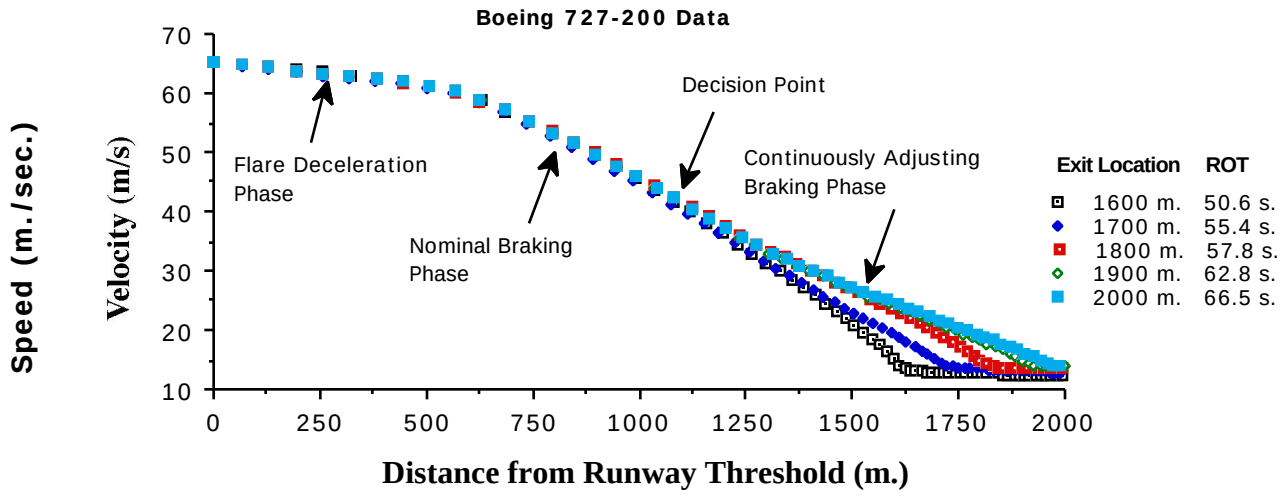

FIGURE 2.7 Aircraft Nonlinear Deceleration Model (Decision Point Location Sensitivity).

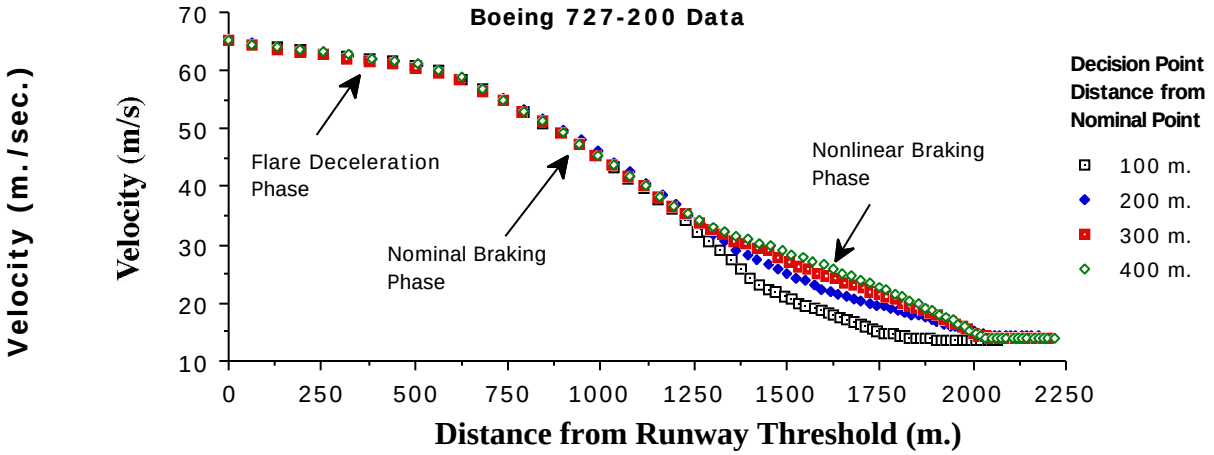

2.4.7 Aircraft Landing Weight Factors

The aircraft weight factor is a nondimensional parameter varying from 0 to 1 representing the proportion of the useful load carrying capacity of an aircraft at any point in time. The landing load factor is a major determinant of the aircraft nominal approach speed of a vehicle. The load carrying capacities of certain aircraft make their approach speed range large enough to justify the inclusion of this parameter in REDIM 2.1. A Boeing 727-200 for example has a 30 knot differential between the approach speeds at the operating empty and maximum landing weights, respectively [Boeing, 1986].The reference landing runs at these two extreme landing weights are 1190 and 1615 m., respectively for a wet runway scenario and sea level standard conditions [Boeing, 1985].

Mathematically the weight factor is defined as follows:

$$w_f = \frac{W_{land} - W_{OEW}}{W_{MLW} - W_{OEW}} \tag{2.20}$$

where, w_f is the weight factor for a specific aircraft landing event, W_{land} is the aircraft landing weigh, W_{OEW} is the aircraft operating empty weight, and W_{MLW} is the aircraft maximum allowable landing weight. From this definition it is clear that the landing weight of an aircraft can be easily defined in terms of the weight factor as shown below.

$$W_{land} = W_{OEW} + w_f(W_{MLW} - W_{OEW}) \tag{2.21}$$

In practical situations the weight factor is a parameter readily available to the airport engineer and planner since airlines are usually charged landing fees dependent upon the values of landing weights (from which the weight factor can be readily obtained) at all airport facilities. In this fashion it is possible to predict with more accuracy the locations of turnoff geometries for specific airport/airline operational conditions. If data on weight factors is not available the engineer and planner should use high values of w_f in order to provide some degree of conservatism in the computations. REDIM 2.1 provides default values of w_f in order to ease the task of the analyst as shown in Table 2.1.

TABLE 2.1 Baseline Landing Weight Factors Parameter Values Used in REDIM 2.1.

Parameter	TERP A	TERP B	TERP C	TERP D
w_f	0.8	0.8	0.6	0.6
σ_{wf}	0.1	0.1	0.1	0.1

Variations of w_f depend heavily upon various airline policies such as fuel reserve factors and stage length segments flown. Data on weight factors can be obtained from airline statistics and should be used in the estimation of runway turnoff locations as this will have a

significant payoff in aircraft operations. Airline data suggests that weight factors can in fact be approximated using normal distributions [Credeur and Caprone, 1989]. With this in mind one can approximate the weight factor as a normal distribution with mean w_f and standard deviation σ_{wf} representing operational dispersions of aircraft landing weights. Figure 2.8 depicts a typical weight factor distribution for United Airlines Boeing 737-200A aircraft landing at a major airport facility [Credeur and Capron, 1989].

It is interesting to note that many short haul operations will have weight factors means very close to 0.5 and their standard deviations seem to be below 0.2. In general it is expected that values of landing w_f will increase as the size of the aircraft decreases since the fuel fractions of general aviation aircraft are usually smaller than those of long range transport aircraft [Torenbeek, 1987] thus resulting in proportionately lower landing weights. The airport planner and designer is encouraged to investigate specific values of w_f applicable to airlines operating in the facility to be upgraded. If a new facility is to be constructed the planner should also contact airlines in order to have a better assessment of aircraft weight factors

FIGURE 2.8 PDF Plot of Boeing 737-200 Weight Factor Variations (Adapted from Credeur and Capron, 1989).

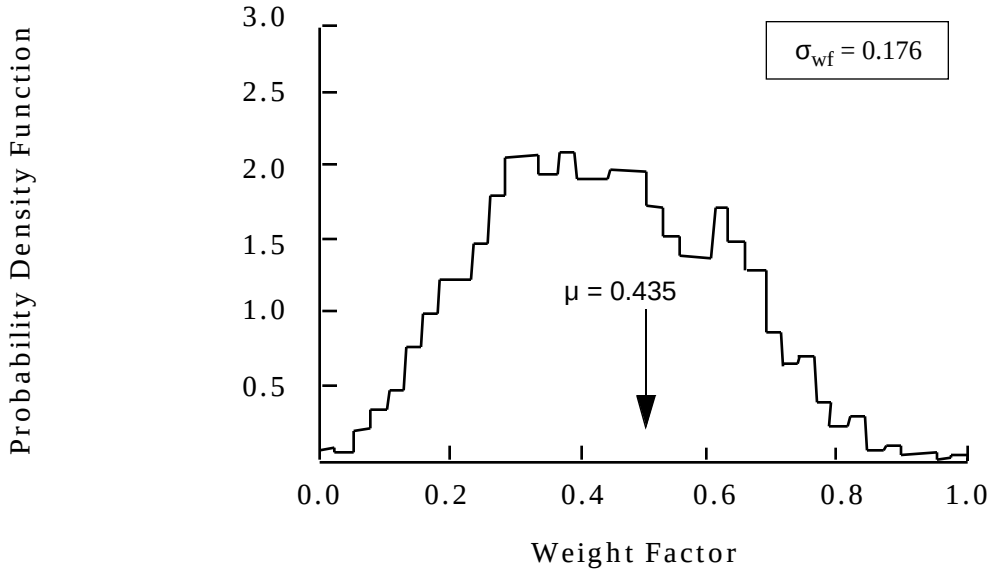

Figure 2.9 illustrates the expected landing roll distance variations (down to 15 m/s) for a twin engine, heavy aircraft using a high mean weight factor (0.8) and a standard deviation of 0.1. These results were derived from REDIM 2.1 and represent typical values expected in airline practice. In order to have an appreciation of landing roll distance deviations for the same vehicle under different weight factors refer to the same figure where low w_f are also included.

FIGURE 2.9 **Landing Roll Distance Histogram for Airbus A300-600 (High and Low w_f).**

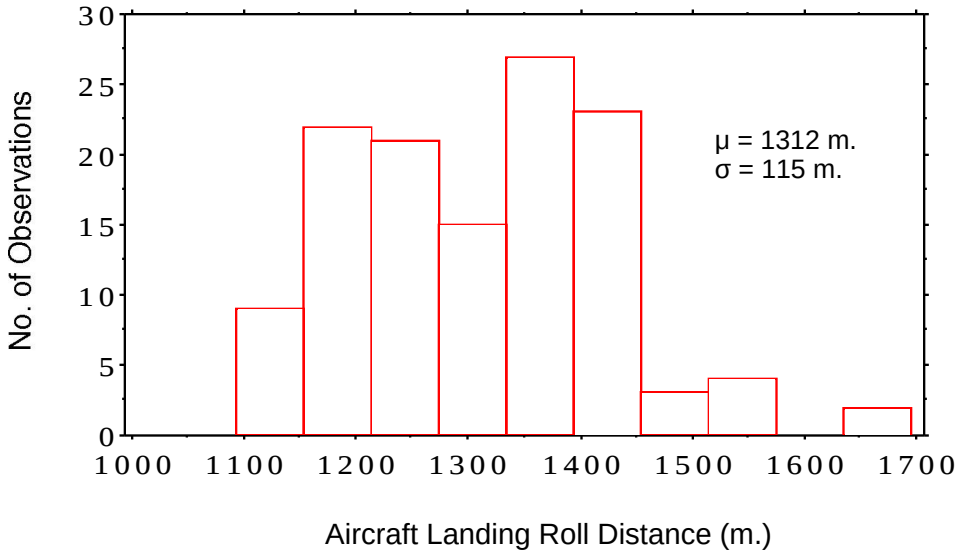

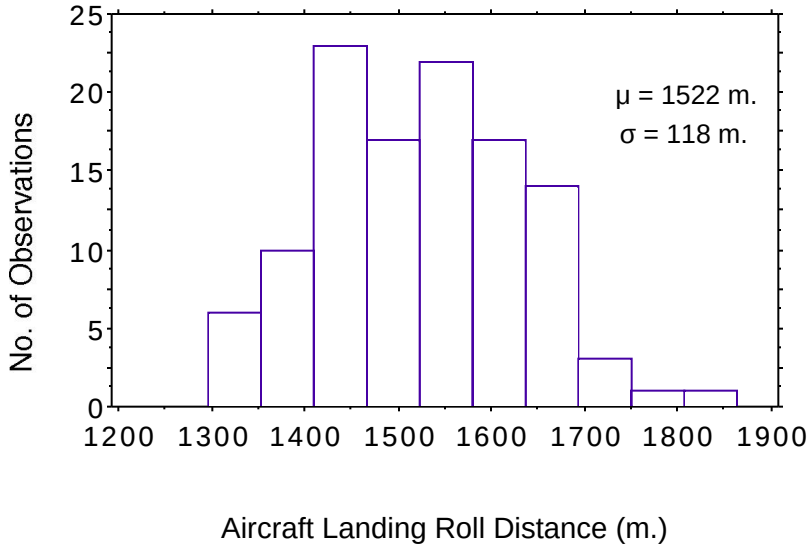

2.4.8 Turnoff Time Estimation

The computation of turnoff times is explicitly modeled for every aircraft/exit candidate as turnoff times generally account for 15-25% of the total runway occupancy time depending upon the exit type being analyzed. This estimation is executed in REDIM 2.1 using a continuous simulation algorithm predicting the turnoff trajectory of every aircraft from point

of curvature to the point where the aircraft wingtip clears the runway edge imaginary plane.The equations of motion for this simulation are shown in detail in Chapter 3.

2.4.9 Touchdown Variations with Runway Length

It has been observed in practice that pilots have a clear tendency to vary their touchdown point depending upon specific runway characteristics such as location of terminal buildings, runway length, obstacles in the final approach path, etc. Ruhl, for example, observed significant variations in the touchdown point for the same type of transport aircraft for various airport conditions [Ruhl. 1989].

Koenig also observed important motivational behaviors in pilots from various airlines as they landed at two major airport facilities [Koenig, 1974]. With these factors in mind it is possible to establish a correspondence between the touchdown point and the runway length. An even more important consideration from the pilot standpoint is the remaining runway distance available as this is an important parameter the pilot can assess easily from his own experience or looking at runway distance remaining signs. Current FAA regulations for precision runways operated by turbofan/turbojet aircraft mandate the use of runway distance remaining signs providing pilots with direct visual cues on runway length remaining during a landing or takeoff maneuver [FAA, 1991].

2.5 Optimization Model

A runway exit location optimization model is described in this chapter. The object of this model is to estimate the best runway exit locations which minimize the average aircraft runway occupancy time thus maximizing the runway capacity. A dynamic programming algorithm based on previous research at Virginia Tech (Sherali et al. 1992) is used as the basis to solve this problem. Several improvements are made and implemented to make the model more realistic.

2.5.1 Problem Description

The object of this model is to minimize the weighted average runway occupancy time of a given landing aircraft mix. The following is the mathematical description of this model:

$$\text{Minimize} \quad \sum_{r=1}^{R} \sum_{k=1}^{K} w_r p_k E[IROT(x_1, \quad , x_N)]_{rk} \tag{2.22}$$

Subject to $x_{i+1} - x_i \geq D_{min} \quad for \quad i = 1, \quad , N-1$

$x_1 \geq 0 \quad and \quad x_N \leq RL$

Where: w_r is the proportion of aircraft type *r*, p_k is the chance of *kth* environmental scenario occurring, *IROT* is the individual aircraft runway occupancy time taking the *ith* exit, x_i is the *ith* exit location, *N* is the total number of exits to be located, D_{min} is a minimum distance between two adjacent exits, and *RL* is the length of the runway.

For a given *rk* combination, the expected individual runway occupancy time, *E[IROT]*, is calculated by averaging the aircraft ROT of *M* landing trials. That is,

$$E[IROT(x_1, \quad , x_N)]_{rk} = \frac{1}{M}\sum IROT^m(x_1, \quad , x_N) \qquad \textbf{(2.23)}$$

where: $IROT^m(x_1, \quad , x_N)$ is the individual ROT given exit types and locations $(x_1, \quad , x_N)$ on landing trial *m*.

2.5.2 The Dynamic Programming Formulation

Referring to Sherali (Sherali, 1991) and Trani et al. (Trani et al., 1992), the dynamic programming problem is presented as follows:

Stage *n* for $n \quad \{1, \quad , N\}$, corresponds to a situation in which up to n exits can be located to the right of the last exit already located (i.e., *N-n* exits are assumed to have been constructed close to runway threshold). Stage 0 is a dummy initial stage.

State s_n at stage *n* represents the possible location of the exit currently located. For stage $n \quad \{1, \quad , N-1\}$, the set of possible value for s_n, is $\{x;(N-n-1)\times D_{min} \le x \le RL\}$. For stage *N*, $s_N \equiv -D_{min}$ (which means an imaginary exit location of $-D_{min}$ ahead of runway threshold).

Decision d_n at stage *n* and state *n* corresponds to the location of next exit to be constructed to the right of s_n. The set of possible value of d_n is $\{ d;d = 0 \; or \; (N-n)\times D_{min} \le d \le RL \}$, where $d_n = 0$ means that no more exits will be constructed to the right of current located exit.

The immediate return function, $c_n(s_n, d_n)$, is the cost incurred at stage *n* by making decision d_n in state s_n. This cost corresponds to the additional aircraft assignments which can be made to the given new exit located at d_n.

$$c_n(s_n, d_n) = \begin{cases} \infty & if \quad d_n - s_n < D_{min} \quad and \quad d_n \neq 0 \\ \sum_{r=1}^{R}\sum_{k=1}^{K}\sum_{m=1}^{M} w_r \, p_k \, IROT_{rk}^m(s_n, d_n) & if \quad d_n - s_n \ge D_{min} \quad and \quad d_n \neq 0 \\ 0 & if \quad d_n = 0 \end{cases} \qquad \textbf{(2.24)}$$

Given a stage *n* and having made a decision d_n, the next stage in the process is given by the following stage transition function:

$$T_n(d_n) = \begin{cases} (n-1) & if \quad d_n \neq 0 \\ 0 & if \quad d_n = 0 \end{cases} \tag{2.25}$$

Given a stage *n* and a state s_n, and having made a decision d_n, the next state in stage $T_n(d_n)$ is given by the following state transition function:

$$s_{T_n(d_n)}(s_n) = \tau_n(s_n, d_n) = \begin{cases} d_n & if \ d_n \neq 0 \\ s_n & if \quad d_n = 0 \end{cases} \tag{2.26}$$

Let $f_n(s_n)$ be the optimal accumulated return function for a given input state s_n at stage *n*, then a backward recursive formula can be given by the following function:

$$f_n(s_n) = \underset{d \quad \{d;(s_n + D_{min} \le d \le RL)\}}{Minimum} \quad [c_n(s_n, d_n) + f_{T_n(d_n)}\{\tau_n(s_n, d_n)\}] \quad \{0\} \tag{2.27}$$

Where the initial condition is given by

$$f_0(s_0) = \sum_{r=1}^{R} \sum_{k=1}^{K} \sum_{m=1}^{M} w_r p_k IROT_{rk}^{m}(s_0, RL) I(s_0, RL) d_{rk}^{m} \tag{2.28}$$

The subscript "0" means the dummy initial stage, and s_0 means the location of the last exit. The initial condition, $f_0(s_0)$ is the sum of ROT of all aircraft landings which miss the last exit and execute a turnoff using a ninety degree angled exit located at the end of the runway.

To validate the DP approach for this problem, let the objective function in equation 2.22 be the global return function. That is,

$$R_N\{r_N(s_N, d_N), \quad , r_1(s_1, d_1)\} = \sum_{r=1}^{R} \sum_{k=1}^{K} w_r p_k E[IROT(x_1, \quad , x_N)]_{rk} \tag{2.29}$$

Notice that s_n and d_n are the locations of the (*n-1*)th and nth exits, respectively. The immediate return function at each stage *n*, for $n = 1, \quad , N$, can be stated as:

$$r_N(s_N, d_N) = c_n(s_N, d_N) + I_N(n) f_0(s_0) \tag{2.30}$$

Where: $I_N(n) = 1$ if $n = N$ or 0 otherwise, $c_n(s_N, d_N)$ and $f_0(s_0)$ are the same as defined in the previous formulation. Then

$$R_N\{r_N(s_N, d_N), \quad , r_1(s_1, d_1)\} = \sum_{n=1}^{N} r_n(s_n, d_n) \tag{2.31}$$

As the global return function is a separable and monotonic non-decreasing function. The principle of optimality holds, thus validating the DP approach for this problem.

2.5.3 Solution Algorithm

Algorithms to solve this dynamic programming runway exit location optimization problem are presented to illustrate differences between the previous methods and the approach proposed here.

Beginning with stage 1, the DP algorithm proceeds recursively through stage *N* using the recursive formula (equation 2.27). At any stage *n* in this process, the state s_n corresponds to the location of the rightmost exit among the already constructed *(N-n)* exits and the decision d_n corresponds to the location of the next exit (if decision is zero, no more exits will be constructed). Since the state space and decision space are continuous over the real line from 0 to *RL*, the optimal decision, d_n , and the corresponding optimal intermediate return function $f_n(s_n)$ should be expressed as functions of s_n at every stage *n*. The exact solution may be found on a specific problem with given values of *N, R, K* and the deceleration distance (d^m) and deceleration time (t^m) for all $r = 1, \quad ,R$, $k = 1, \quad ,K$, $m = 1, \quad ,M$.

To reduce the search space in this problem an approximate algorithm is used to solve this problem. Assume that exits are located among the points generated by discretizing the runway with a certain search interval, Δd (25 m), instead of any point on the runway. For each s_n, we could find $f_n(s_n)$ using equation 4.5 over all possible values of d_n in a backward search manner. The corresponding optimal decision d_n is stored along with the value of $f_n(s_n)$. The value of $f_N(s_N)$ ($f_N(0)$) at final stage *N* gives the optimal objective function value of the problem. The optimal exit locations $x_1, \quad ,x_N$ can be found by tracing the optimal decisions from d_1 to d_N using stage and state transition functions.

Let *I* be the total number of search intervals over the entire runway. At each stage, we have *I* states and *I* decisions as a worst case scenario. For every single stage-state-decision combination, $O(RI^2)$ computations are involved. Thus, the algorithm is of polynomial complexity $O(NRI^2)$.

2.6 Output Module

The function of the Output Module is to present the analysis results in graphical form or tabular forms. Three types of analysis, 'design', 'improvement' and 'evaluation' share the same formats of the output, which are 'Aircraft Assignment and ROT Table,' 'ROT Statistics,' 'Exit Locations,' 'Exit Centerline Comparison,' and 'Exit Geometry.' The 'Aircraft Assignment and ROT Table' shows exit utilizations of each aircraft type and the corresponding ROT's. The 'ROT Statistics' shows the average ROT for each aircraft type and the grand average ROT of the aircraft mix in a bar chart format. The 'Exit Locations' presents the runway and the taxiway and the exits graphically on a scale. The 'Exit Centerline Comparison' plots the x-y coordinates of turnoff centerlines of the exits selected by the user on a scaled plane. The 'Exit Geometry' shows the complete geometry and the specifications of the exits selected by the user.

The fourth type of analysis ('individual') has only a form of output where the deceleration distances and ROT's of an aircraft type are presented for six different exit speeds and for

five percentile values. Here, the percentile value means the proportions of aircraft landings to execute a turnoff at a given exit location.

2.6.1 REDIM 2.1 Output Summary Report

REDIM 2.1 provides the user with a summary report containing relevant input and output data at the touch of a single keystroke. This printout can be obtained from the Main Menu or the Output Module.The organization of the summary report is shown in Table 2.2.

2.6.2 Print-Screen Output Capabilities

In order to convey more information to the user REDIM 2.1 incorporates two fast assembly language routines to capture any output screen that needs to be printed. The model provides only two types of printer drivers at this time one for HP-compatible laser printers and another one for Epson compatible dot matrix printers. Output screens can be readily obtained while the user is reviewing the output module screens.

TABLE 2.2 REDIM 2.1 Summary Report Contents.

Report Section	Sub-Section	Remarks
I) Input Data Summary	I.1) Analysis Type and Existing Exits	Contains locations, type and entry speed parameters of every turnoff modeled in the current scenario
	I.2) Aircraft Mix and Aircraft Characteristics	Summarizes aircraft population mix entered for current scenario and the aircraft characteristics extracted from the working data file
	I.3) Airfield Operational Data	Lists current values for skid safety factor and the desired minimum separation between adjacent turnoff locations
	I.4) Environmental Data	Contains values of wind speed, runway orientation, temperature and runway width used in current run
	I.5) Runway Gradients	Lists for every tenth of runway length the local horizontal gradient
II) Analysis Results	II.1) Average ROT	Lists the weighted average runway occupancy time obtained for the current run

TABLE 2.2 REDIM 2.1 Summary Report Contents.

Report Section	Sub-Section	Remarks
	II.2) Aircraft Assignment/ROT Table	Assigns aircraft percentages to every exit location for every runway surface condition
	II.3) Turnoff Centerline Geometries	Lists X-Y coordinates of every new or existing turnoff geometry

2.7 REDIM 2.1 Data Files

REDIM 2.1 relies upon user selected information detailing the airport environmental and operational features as well as on aircraft data contained in a Master Data File (Appendix A contains the most current version of the Aircraft master File used in the model). Since it is likely that many users would like to incorporate their own data under several runway scenario conditions the provision of a Working Data File is necessary to avoid critical changes to the Master Data File supplied with the program. Once the user inputs the aircraft mix data, pertinent aircraft data is duplicated from the Master Data File to a user Working Data File.

Every run is then executed using the Working Data File from which modifications can be carried out. The Master Data File contains aircraft characteristics necessary to execute the simplified aircraft landing simulation procedures used in REDIM 2.1. The data file lists aircraft parameters used in the internal computations. Among these are: wing span, empty operational weight, load on main gear, maximum landing weight, wheelbase, etc.

2.8 Model Computational Aspects

In order to provide good measures of dispersion in REDIM 2.1, the model is executed over five trial sets using randomized seeds and twenty replications per trail per aircraft/runway surface condition. This implies that every aircraft/runway surface condition combination is actually executed one hundred times in order to get good estimates of the probability density function describing the aircraft landing roll kinematic behavior. The most intensive computational algorithm in REDIM 2.1, however, is the optimization of exit locations consuming approximately 80% of the CPU time needed to execute a typical analysis. The reader should be aware that the computational effort varies dramatically with the various factors such as the runmode selected (e.g., design, improvement or analysis of runways), the number of exits selected, the runway length, and the mix index. The most prominent factor being the run mode selected. The design mode is the most computationally intensive of all running modes available in REDIM 2.1, as this mode deals with

the optimal placement of turnoffs on a new runway where usually no longitudinal constraints have been specified.

CHAPTER 3

REDIM 2.1 Computer Model Calibration

This chapter explains the procedures used to calibrate REDIM 2.1 using airfield landing observations at five major airports in the United States East Coast. The main objectives of these field observations was to obtain the following data:

- Runway occupancy time data for many types of aircraft
- Runway exit utilization patterns at various airports
- Landing roll velocity profiles for various aircraft

Ultimately, the data was used to calibrate REDIM 2.1 using heuristic rules and statistical techniques.

3.1 Airfield Observations

More than two thousand landing events were recorded at five major airports within the United States in order to establish heuristic trends in the deceleration pattern of aircraft. The observations took place in the period January through July of 1992 and were made at the following airports:

- Charlotte Douglas International Airport
- Atlanta Hartsfield International Airport
- Raleigh-Durham International Airport
- Washington National Airport
- Washington Dulles International Airport

Most of the observations were made under Visual Meteorological Conditions (VMC) ex-

cept for a small sample at Washington National Airport were snow showers prevailed during a two hour period. Some wet runway pavement conditions were also recorded at Washington Dulles International Airport (i.e., during a four hour period) and strong surface wind conditions were encountered at Raleigh-Durham International Airport in an extended one day recording period. Table 3.1 summarizes some of the data sets obtained at these airport locations for five transport aircraft.

TABLE 3.1 Summary of Aircraft Landing Roll Observations at Five U.S. Airports.

Airport	Date of Observations	Total Number of Observations
Atlanta Hartsfield (ATL)	January 22-23, 1992	1,230
National Airport (DCA)	March 20-22, 1992	560
Charlotte Douglas (CLT)	April 20-22, 1992	653
Raleigh-Durham (RDU)	May 20-22, 1992	560
Washington Dulles (IAD)	July 4-6, 1992	460

3.2 Data Collection Method

The method used in the data collection at all airports was a high fidelity (SVHS) video equipment. The video output provided a reliable source to check runway occupancy times (ROT) and points of runway clearance. All observations were made from the Air Traffic Control towers at every site to gain the best vantage point and cover multiple runways whenever possible.

Data gathered from the video equipment included:

- Runway occupancy time from threshold crossing heigth down to the clearance point on the runway
- Aircraft velocity profile trajectories
- Runway exit utilization
- Turnoff times per aircraft type and for every runway exit
- Runway exit speed profiles

The following paragraphs describe in detail the procedures used in the data collection and calibration methods.

A number of aircraft landing operations from the threshold crossing to clearance of the runway were recorded using video equipment from the control tower of selected airports in-

cluding Washington National Airport (DCA), Charlotte Douglas International Airport (CLT) and Atlanta Hartsfield International Airport (ATL). Runway 36 of DCA airport, runway 23 of CLT airport and runway 8L of ATL airport, whose length are 2094 m (6869 ft), 2286 m (7500 ft) and 2742 m (9000 ft), respectively, were exclusively used for arrivals at the times of recording. Frame counter codes were later embedded on these video tapes to allow a streamline data acquisition method. Since the video tape runs at 30 frames per second, it is possible to distinguish the aircraft landing roll trajectory in every 1/30 second. From theses tapes, velocity profiles over roll distance have been extracted for each landing through the following steps:

1) Identify suitable reference points whose positions are known on the active runway. Two adjacent reference points make an interval.
2) Record the frame counter code when an aircraft nose passes a reference point, when the aircraft is at touchdown, and at the clearance of runway. These data were used to find touchdown location and ROT.
3) Find average interval speed by dividing the interval length by the interval passing time. The interval passing time is the difference of frame counter codes of two neighboring reference points. The interval passing time can be measured with an accuracy of 1/30 second.
4) Connect the average interval speed to produce an approximated velocity profile for a landing operation. By overlapping the individual velocity profiles for a particular aircraft type, a velocity profile band for the aircraft type on a specific runway can be generated.

In order to assess the landing velocity profiles of aircraft a set of video cameras was used to compare the position of aircraft on the runway at various reference points. Reference points used in this analysis varied from runway markings to various ancillary equipment located near the runway in question (i.e., runway visual range transmissometers, glideslope antennas, etc.). In general, the accuracy of the method employed to assess aircraft velocity profiles depends upon the method employed to derive each aircraft velocity profile. In this research two methods were used to ascertain speed profiles on the runway: 1) the distance difference method and 2) the aircraft characteristic length method. In the first one measurements on aircraft speed from video tape are made at known geographic locations using runway identifiable points (i.e., RVR transmissiometer, runway markingds, etc.). This method provides accuracies within 2-2.25 m/s for transport aircraft since each video frame offers a resolution of 1/30 of a second. Figure 3.1 illustrates the method to establish specific control point locations. The second method relies on knowledge of the aircraft characteristic length at all points in times to derive a suitable distance-time profile over the runway. This method is suitable for low speeds where appreciable changes in speed are not present.

3.2.1 Data Reduction Pr ocedures

The data was reduced by inscribing the time code on the videotapes and with the use of a personal computer and a video controller discrete aircraft positions on the runway were recorded. From this recording procedure velocity-time and velocity-position profiles were derived using curve fitting techniques. During the aircraft position extraction procedure several milestones were also recorded in parallel indicating important actions by the man-machine system such as deployment of thrust reversers, touchdown position, turnoff starting and turning ending points. These milestones were later used in determining heuristic rules used by pilots in the landing roll sequence to further correct the algorithms used in REDIM 2.1.

Figure 3.2 illustrates a sample on how the reference points were selected. First, the video tapes were reviewed to find distinct objects around the active runway. Second, these objects were placed on a large scale, typically 1:7000, airport layout drawings. By projecting a line from the recording position through the objects to the centerline of the active runway, a reference point was found. As the number of reference points increase, the approximated velocity profile becomes closer to the actual. If the distance between two adjacent reference points, however, is too small, the error in speed measurement induced by one frame mistake becomes unacceptably great. Considering these two contradicting factors, the reference points were selected so as to make the interval size about 152 m (500 ft). In the case of CLT airport, for example, where runway 23 was used for arrivals, some runway marks of both runway 18L and 23 appear clearly on the video image. Therefore both sets of runway marks were used to determine reference points on runway 23. Overall the goal was to use anywhere between 10 and 15 data points to discretize the aircraft velocity profile providing some data countinuity. Similar procedures were repeated at other airports.

For the accuracy and convenience of data reduction, a computer data collection interface software was developed which made it possible to transfer the video signal frame counter code to a an Apple Macintosh computer. The frame counter codes were saved in a data file which in turn was later manipulated to generate velocity profiles, touchdown location, exit utilization and runway occupancy time (ROT). This system is depicted schematically in Figure 3.2.

Figure 3.3 shows examples of the aircraft velocity profiles obtained at Charlotte-Douglas airport (CLT) for short and medium range transport aircraft (Boeing 737-300 and Boeing 727-200, respectively). It is evident from the velocity profile data that different aircraft although belonging to the same class exhibit completely different landing roll behavior as expected from the flight manual.

Figure 3.4 shows a typical velocity profile of Boeing B-737 landing on runway 23 at Charlotte Douglas International airport. Note that we have indicated several milestone segments and points in the plot to illustrate the velocity profile data reduction process. Refering to Figure 3.4 it can be seen that the flare speed was estimated as the average speed during the segment comprised between the threshold crossing point and the touchdown point.

FIGURE 3.1 Two Examples of Reference Points for Aircraft Velocity Profile Extraction.

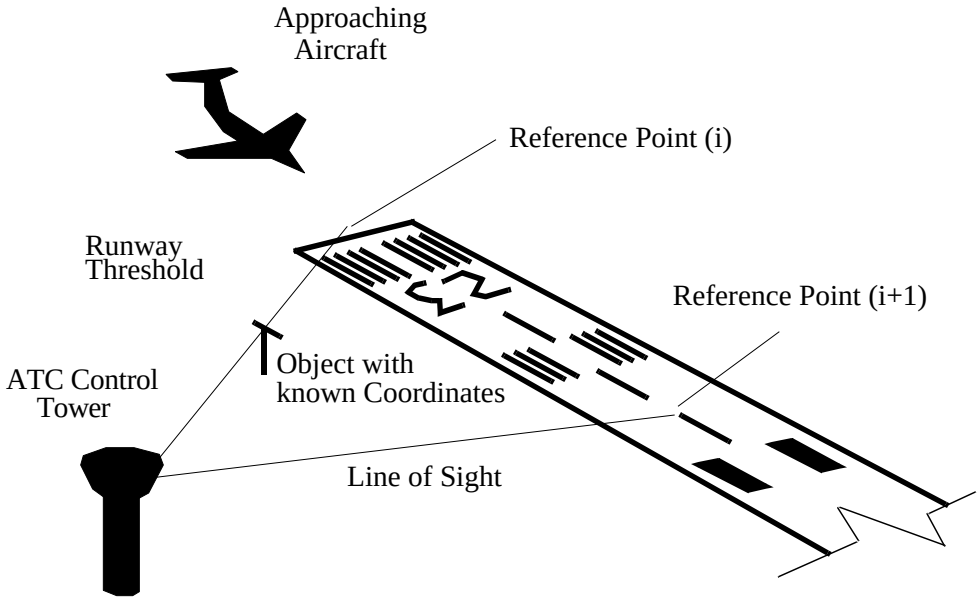

FIGURE 3.2 Data Collection and Reduction Procedure Flowchart.

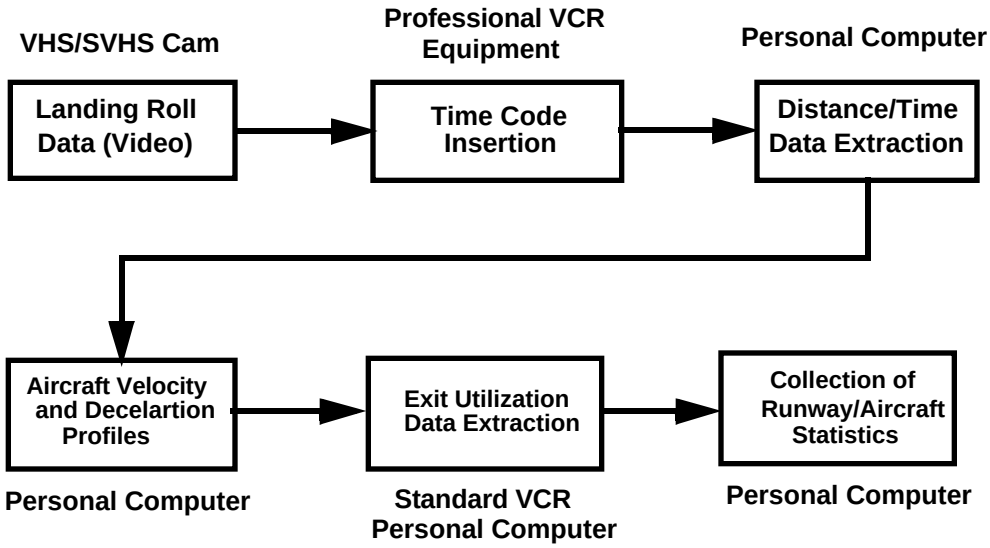

In order to understand and calibrate the landing roll algorithms in REDIM data from three airports (Washington National, Atlanta and Charlotte), five different transport aircraft (Boeing 727-200, 737-300, 400 and 200 series, 757-200, Douglas DC9-30 and McDonnell Douglas MD-80) were used to ascertain pilot bahaviors during the landing roll (see Table 3.2). It must be mentioned that only those aircraft were present at all three airports in significant numbers to unbias the results. Nevertheless, those transport aircraft constitute 89.6% of the total narrow-body jet aircraft population currently in use by airlines in United States [McGraw Hill, 1993]. Table 3.2 presents a summary of landing roll parameters observed at these airports.

TABLE 3.2 Summary of Reduced Aircraft Landing Roll Data.

Airport	A/C Type	No. of Obs.	Flare Speed (m./s)		Touchdown Location (m.)		Average Deceleration (m/s^2)		Landing Distance[a] to reach 30 m/s (m)	
			Mean	S.D.	Mean	S.D.	Mean	S.D.	Mean	S.D.
DCA	B-727	72	66.62	3.03	455	132.1	2.26	0.382	1223	167.9
	B-737	36	65.77	3.99	399.2	80	2.3	0.422	1118	96.5
	B-757	26	65.3	5.78	424.9	97.7	2.14	0.675	1131	125.8
	DC-9	36	65.02	3.54	434.9	105.8	2.08	0.397	1183	158.5
	MD-80	51	68.29	4.51	424.3	94.1	2.14	0.428	1255	169.1
CLT	B-727	13	68.18	3.16	546.9	169.8	1.83	0.511	1733	193.7
	B-737	34	66.08	3.57	400	77.4	2.21	0.573	1336	257.5
	B-757	4	61.55	2.11	489.6	139.7	1.62	0.231	1490	291.6
	DC-9	8	67.34	3.46	425.2	79.6	2.08	0.56	1483	285.6
	MD-80	7	66.6	2.55	550.6	188.3	1.81	0.381	1698	239.5
ATL	B-727	13	70.87	3.87	621.7	164.2	2.11	0.423	1674	166.4
	B-737	12	68.74	4.34	603.3	75.9	2.08	0.497	1563	237.1
	B-757	10	65.28	5.29	699.9	115.4	1.79	0.337	1670	190.5
	DC-9	13	68.85	3.9	594	137.9	1.83	0.341	1690	197.1
	MD-80	28	68.57	4.97	569.7	124.6	1.9	0.302	1625	250.6

a. Landing distance required to decelerate to 30 m/s.

One of the characteristics of REDIM is that it treats aircraft as independent entities rather than grouping aircraft in classes. Therefore, for landing roll performance analysis it was

crucial to validate aircraft behaviors independently. The following hypotheses were tested using standard statistical methods to compare means and standard deviations:

a) The runway length has influence in the touchdown point and possibly in the aircraft deceleration characteristics.

b) Aircraft behaviors during the landing roll are significantly different for various transport aircraft belonging to the same aircraft class or group.

These analyses provided information necessary to ascertain whether the individual behavior approach adopted in REDM 2.1 is indeed justifiable. Moreover, it allowed us to establish the causal relationship between aircraft landing roll behaviors and airport environmental variables such as runway length, gradient and available runway exits.

The total landing distance for an specific speed - the variable our simulation model is designed to predict - can be found from the velocity profile. Finally, an average braking deceleration rate was calculated using the starting and ending locations. The final speed for landing distance computation was set to 30 m/s for the large aircraft. This is consistent with the ultimate purpose of this study to locate high speed exits at airports. The landing distance, for example, for an exit designed for 27 m/s (60 mph) may be found by adding the distance for extra deceleration. Secondly, pilot adjusts the deceleration rate to attain a proper exit speed at the exit he decides to use in real landing operation. The obtained velocity profiles show that this adjustment becomes distinct as the aircraft nears the exit. The simulation model is intended to predict the landing distance for the design of a new runway where no exit is placed. Therefore, it is beneficial not to incorporate the deceleration adjustments reflected in the obtained velocity profiles into the simulation model. The final speed was set to a higher speed than the usual turnoff speed to reduce the deceleration adjustments.

Four landing roll variables considered important in our model were determined from the velocity profile data. These are the landing distance to reach a prespecified speed, the flare speed, the touchdown location and the braking deceleration rate. Sample means of the key variables are plotted in Figure 3.5. Among these variables, the flare speed show an increase, for the same aircraft, from National airport (DCA) to Atlanta Hartsfield (ATL). A plausible explanation for the increasing tendency is that the target reference speed (i.e., “bug” speed in pilot’s jargon) increases as the density altitude increases assuming that landing weight and temperature are the same. Table 3.3 shows the primary runway characteristics at these three airports during the period of observation. All aircraft operations at these three airports occurred under VMC conditions.

The touchdown location plot in Figure 3.5 (part b) shows a clear tendency to increase as the runway length available increases. Note that it is evident that pilots are motivated to touchdown early at National airport (DCA) where the runway is fairly short (1,860 m.) irrespective of the runway turnoff position.

FIGURE 3.3 **Sample Velocity Profiles Observed at Charlotte Douglas Airport for Two Transport Type Aircraft (Boeing727-200 and 737-200/300 series).**

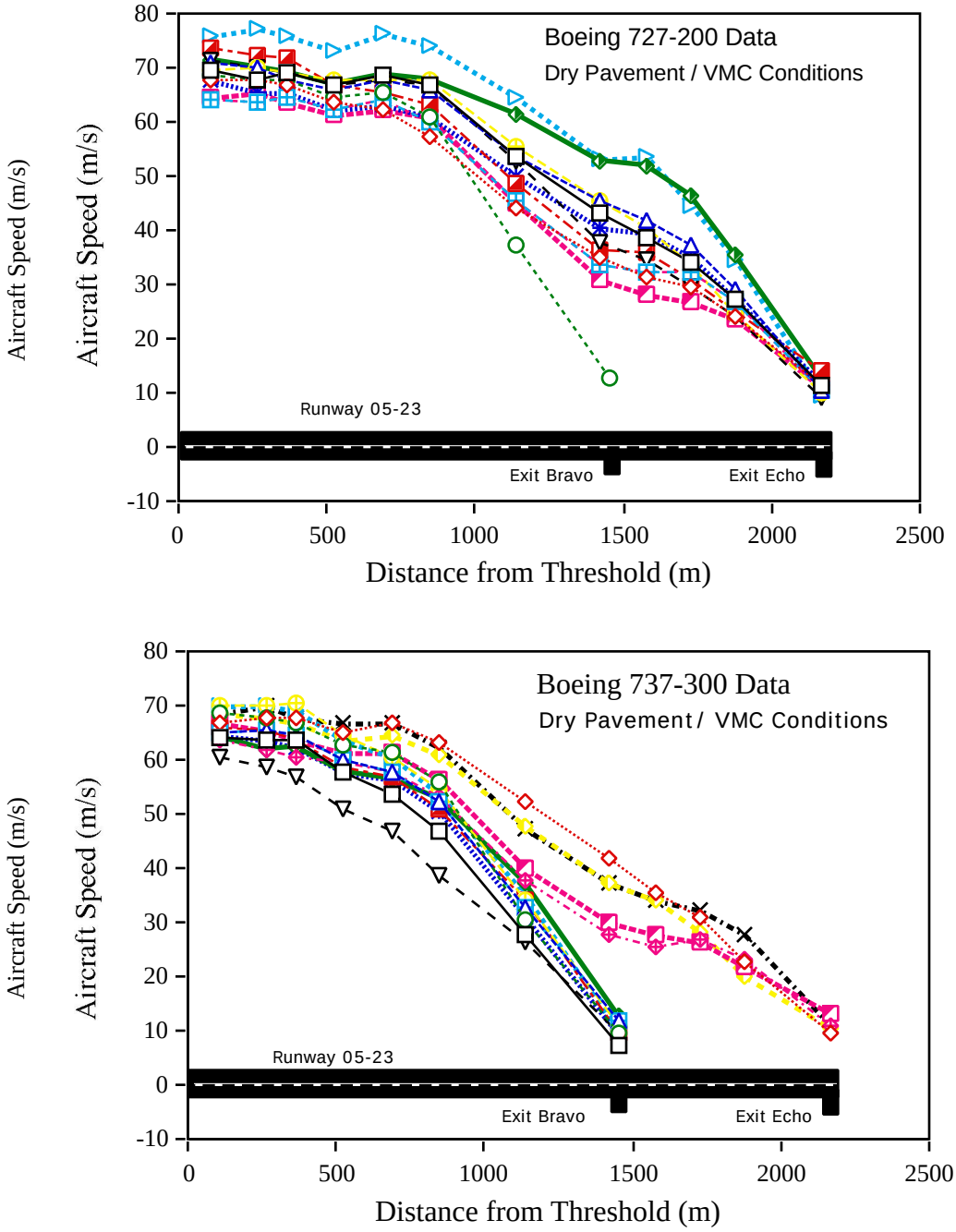

FIGURE 3.4 Typical Aircraft Velocity Profile Data Extraction Procedure (Boeing 737-300 Operating at Charlotte Runway 23).

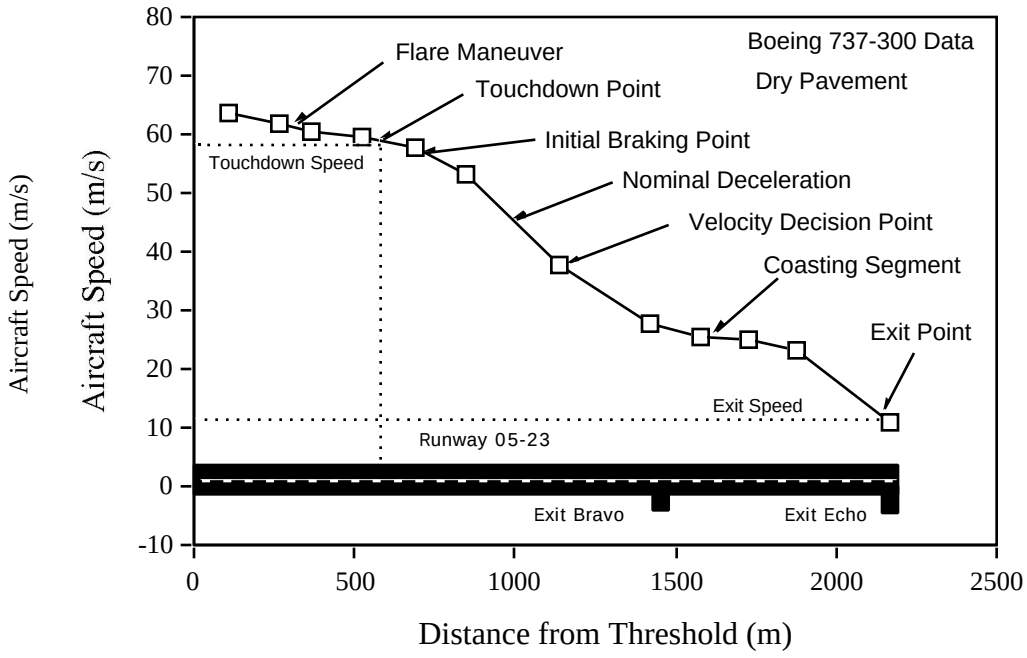

The mean touchdown location was found to be significantly different between the three airports and it was without any doubt primarily influenced by the runway length available for landing as it will be explained later. Table 3.3 shows large differences in runway length for the three airports studied.

TABLE 3.3 Runway Airport Characteristics for Velocity Profile Analysis.

Airport	Runway for Observations	Runway Length (m./ft.)	Elevation MSL (m.)	Average Temperature
National (DCA)	36	2,060 / 6,750		9^{o}C
Charlotte (CLT)	23	2,300 / 7,540		12^{o}C
Atlanta (ATL)	08L	2,750 / 9,100		15^{o}C

In general, it was observed that pilots understandably flare more aggressively in the presence of short runways as they try to aim for the runway touchdown marks. On long runways

pilots flared more relaxed achieving softer landings at the expense of touchdown and ultimately landing distance. This phenomena was fairly evident from all the tapes reviewed. Differences in mean touchdown location varied significantly from 34% for the MD-80 to as high as 65% for the Boeing 757 when comparing data from National and Atlanta airports.

Figure 3.5 also points out that average deceleration rates were high in the presence of short runways as demonstrated by comparing data from National and Atlanta airports for all aircraft. It is interesting to note that the average deceleration data for Boeing 727-200, MD-80 and Boeing 757 aircraft show a non-monotonic behavior as the runway length increases (as it is the case for the Boeing 737 and DC-9 aircraft). This interesting bahavior was caused by the presence of two, highly spaced, exits available at Charlotte's runway 23 (see Figure 3.3). Current exits on runway 23 at Charlotte are located at 1,440 and 2,200 m. from the threshold , respectively, thus resulting in long landing rolls for Boeing 727, Boeing 757 and MD-80 aircraft as they seldom could take Bravo (see Figure 3.3 for Boeing 727-200 velocity profiles on runway 23 at Charlotte). Examination of Figure 3.3 one can see that pilots clearly compensated for turnoff locations that were not optimal for the aircraft being operated.

Figure 3.5 (part c) contains data for Boeing 737-200/300 and Douglas DC9-30 aircraft suggests the use of aggressive braking behavior on runway 23 to use taxiway Bravo (i.e., located at 1,440 m from the threshold). It can be seen that the majority of the population of aircraft in these two categories made it to taxiway Bravo with braking efforts comparable to those recorded at Washington National Airport runway 36.

Graphical depictions such as those shown in Figure 3.6 help to illustrate the qualitative behavior of REDIM 2.1. Figure 3.6 contains sample velocity profiles observed on runway 08-L at Atlanta International Airport for Boeing 737-200/300 and McDonnell Douglas MD-80 aircraft. These plots contain scatter bivariate information of the aircraft landing roll behavior (i.e., distance vs. aircraft speed) and compare it with the landing roll behaviors predicted by REDIM 2.1. Included in Figure 3.6 are the lower, mean and upper bound landing roll trajectories predicted by REDIM 2.1 after 100 landing simulations of Boeing 737-200/300 and Douglas DC9-30 aircraft, respectively. Note that in most cases the observed data falls well within the lower and upper boundaries predicted by REDIM 2.1 thus providing a qualitative assessmentof the predictive capabilities of the model. Appendix J contains fifteen velocity profiles for three airports and five transport aircraft used in the complete calibration of the model.

One observation that should be made about these velocity profiles is that the large bandwidth in the velocity-distance diagram usually results in a very predictable runway exit assignment provided that at least three exits are feasible for one unique type of aircraft (i.e. Boeing 737-200/300). This is evident in Atlanta's runway 08-L where three exit locations seemed preferred by all transport aircraft pilots.

FIGURE 3.5 Comparison of Landing Parameters for Various Aircraft and Airports.

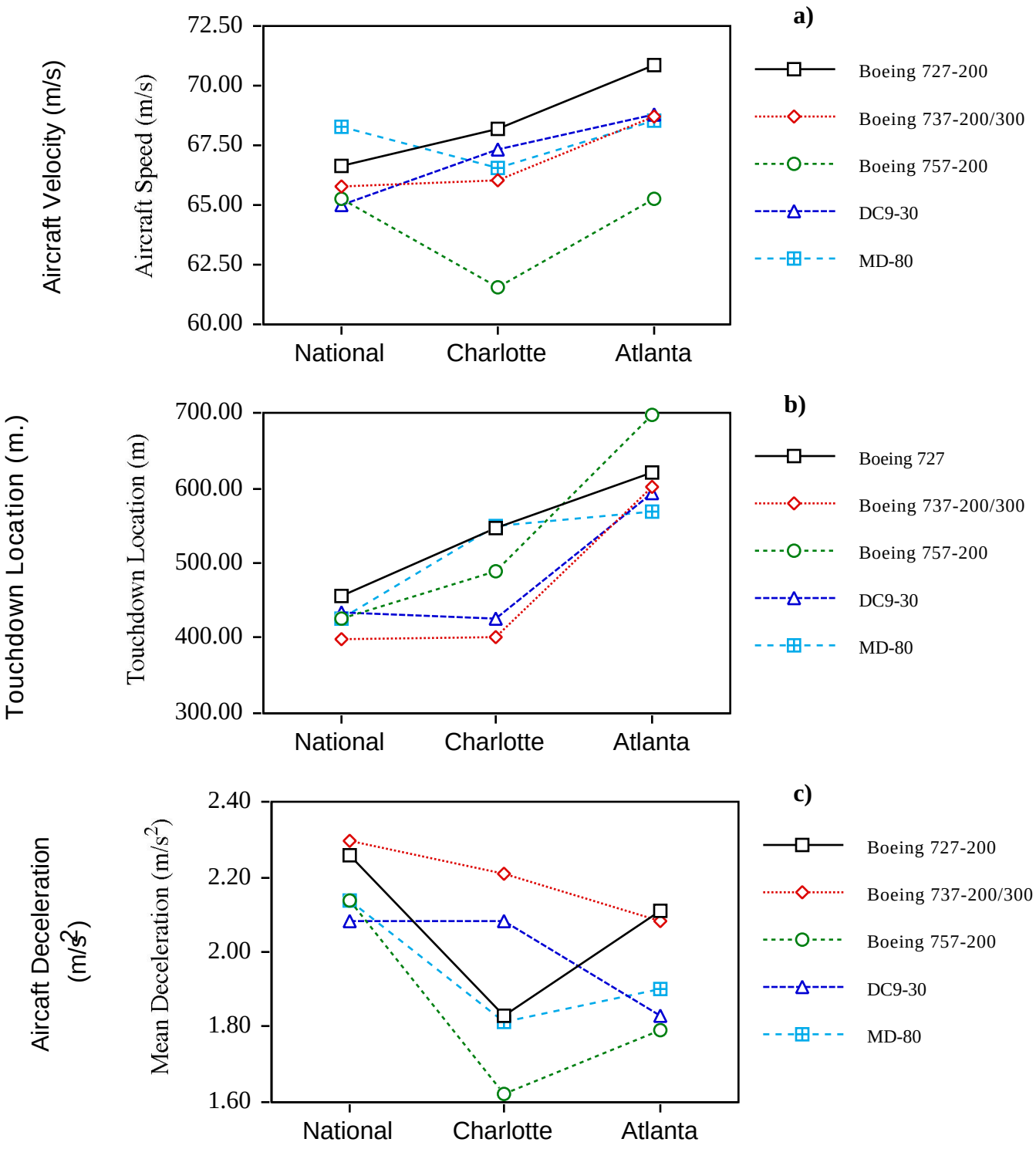

In order to test statistically inter-aircraft and inter-airport type differences we used three key variables in the landing roll model: 1) flare speed, 2) touchdown deceleration, and 3) braking deceleration. A two way analysis of variance (ANOVA) with unequal sample sizes was performed, setting the aircraft type and the airport as main factors. The test results are presented in Table 3.3. The F-statistics were computed based on type III sum of squares as recommended for unequal sample size cases by Neter et al. [1985] and the SAS Institute [1990].

The conclusions of the test are that the interaction effects are weak or negligible and the main effects are significant. This implies that the landing performance prediction should be performed for each aircraft type considering the variations due to the airport. Since many uncontrollable factors such as landing weight factor, flap angle, etc. are involved in the aircraft landing operation, precise explanations for the test results are somewhat difficult. Among the factors which can make the airport effects significant, however, the airfield elevation, the runway length and the runway grade are distinguishable. For the parameter estimation in the following section, the airport effects will be quantified based on the distinguishable factors cited above assuming the other uncontrollable factors are identical throughout the airports.

3.3 Calibration Techniques

The model described in Section 2.3 (see previous chapter) was calibrated in two imporatant areas: 1) comparison of variances and means used in the theoretical model against data observed in the field, and 2) identification of landing techniques and runway exit decision making techniques.

3.3.1 Aircraft Landing Kinematic Profile Characterization

In order to further assess the possible differences between the velocity profiles of various aircraft frequency domain and standard analytical methods were used to further assess the suitability the model for high as well as low speed exits. Typical results comfirm that there is a noticeable difference in the frequency domain and standard distance-velocity profiles of various aircraft as can be observed from Figure 3.7. This figure presents a typical aircraft velocity profile where distinct milestone point have been identified. For example it was identified that most pilots make decisions about potential exit locations while traveling at 40-45 m/s on the runway.

3.4 Runway Turnoff Exit Speed Analysis

Once the major parameters of the aircraft velocity profile have been obtained it is imperative to assess the major contributions of the exit speed to the runway ocuppancy time (ROT) for various types of aircraft and exits.

FIGURE 3.6 **Sample Observed and Predicted Aircraft Landing Roll Velocity Profiles at Atlanta Hartsfield International Airport Runway 08L.**

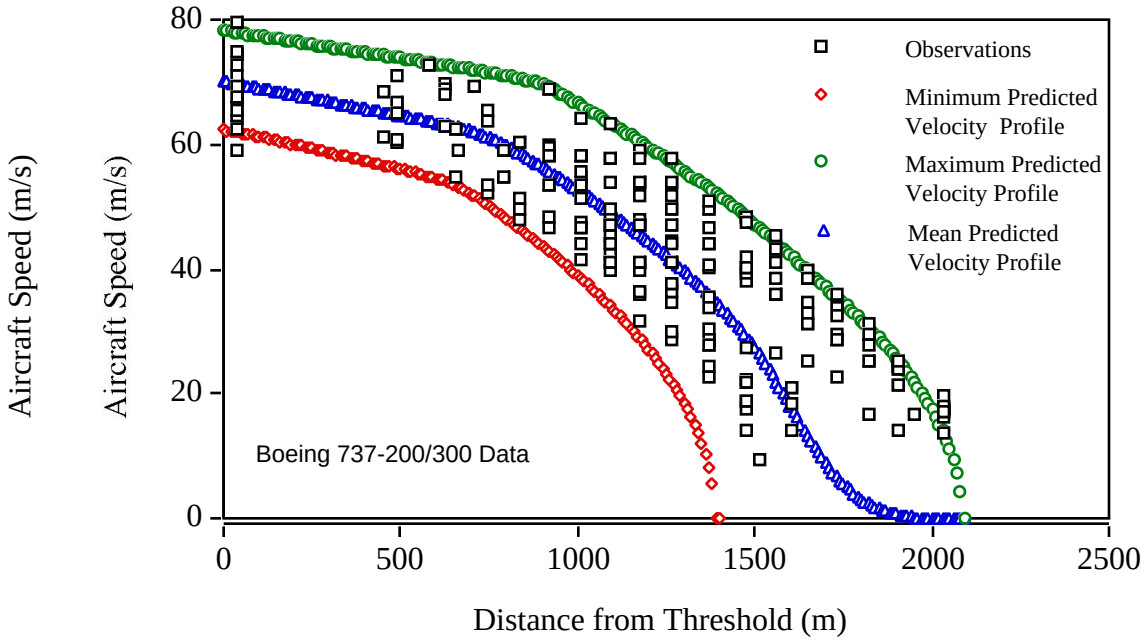

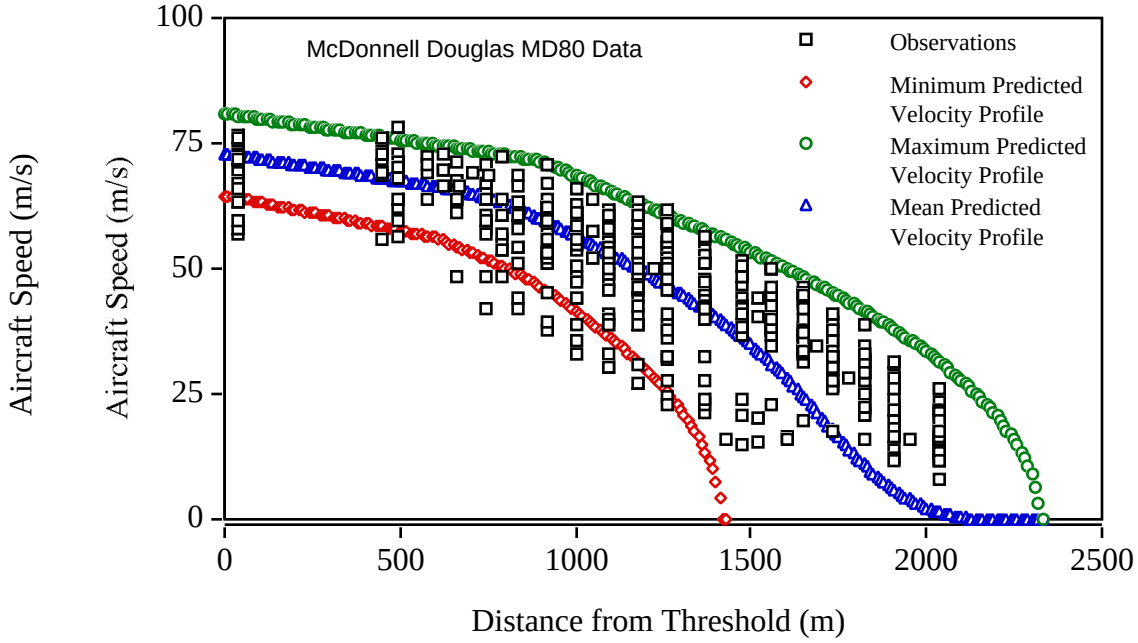

Here we use standard statistical techniques to ascertain exit speeds for each type of geometry observed in the field and whether or not there are differences in turnoff behavior between a sample aircraft population of n vehicles. Our main focus is to find differences in the exit speeds for each turnoff geometry, if any. For example, Figure 3.8 illustrates the observed exit speed histograms obtained for runway 36 at Washington National Airport.

It can be seen that exits labeled “Runway 15-33” and “Hotel” have indeed diferent exit speed characteristics even though the aircraft population taking both exits exhibited similar composition (i.e., the percentages of transport aircraft taking them was the same). One should realize that runway exit “Hotel” is a ninety degree angle exit geometry with a wide entrance radius whereas the intersection of runways 15-33 and 36-18 forms a “pseudo-acute” angle exit capable of sustaining faster exit speeds. The diagrams show clearly differences in their means and standard deviations. These observations were later on proved using standard hypothesis testing criteria.

An interesting point about the observations at National Airport is the normal tendency of the exit speeds recorded for all aircraft landings irrespective of the aircraft and exits taken. This phenomena arises at DCA simply because runway 36-18 has a good balance of exit locations and pilots seem to be highly motivated to clear the runway as quickly as possible due to traffic and short runway conditions.

TABLE 3.4 Statistical Analysis of Aircraft Landing Observations.

Variable	Factor	F-statistics	F-criteria[a]	p-value	Conclusion[b]
	A/C Type	5.44	2.37	0.0003	H1
Flare Speed (m/s)	Airport	8.59	3.00	0.0002	H1
	Interaction	2.00	1.94	0.0461	Marginal
	A/C Type	3.95	2.37	0.0038	H1
T. D. Location (m)	Airport	69.09	3.00	0.0001	H1
	Interaction	2.36	1.94	0.0173	H1
	A/C Type	3.64	2.37	0.0064	H1
Braking Deceleration (m/s^2)	Airport	11.36	3.00	0.0001	H1
	Interaction	1.10	1.94	0.3617	H0

a. F-criteria is set for 5% significant level.
b. H0: The factor does not affect the variable, H1: not H0

FIGURE 3.7 Velocity, Deceleration and Jerk Time Histories used to Derive Man-machine Decision Points.

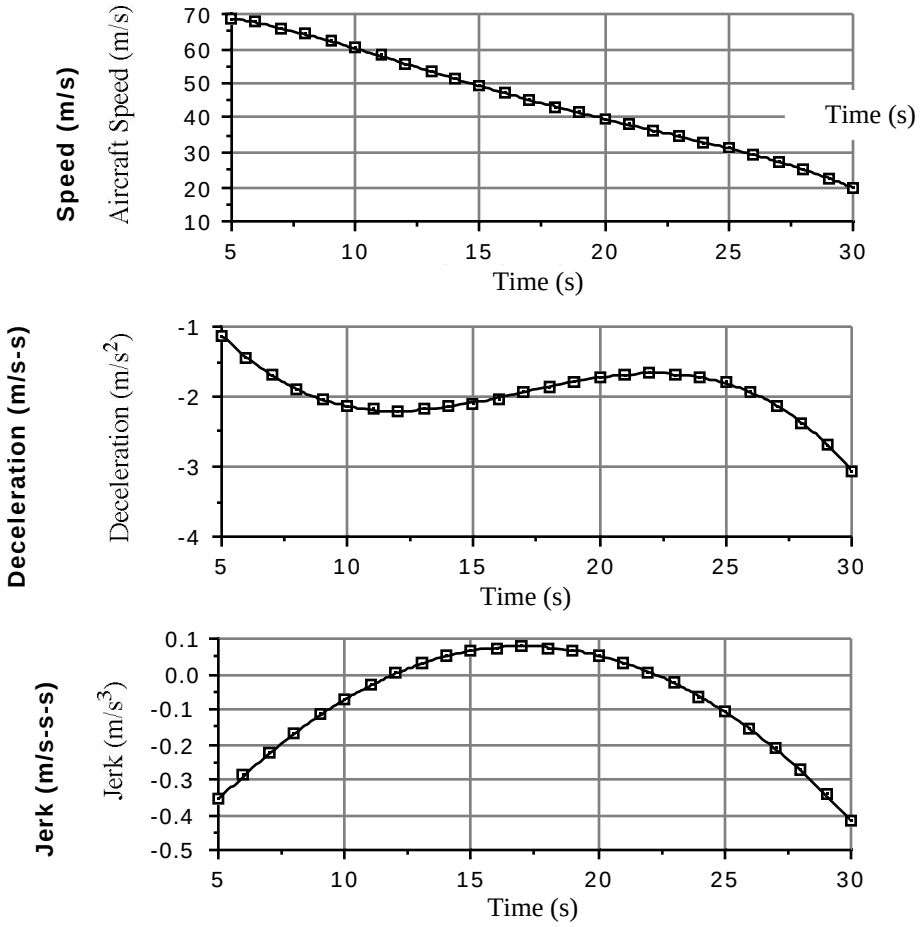

Figure 3.9 shows graphically the cumulative probability density function plots for all observations obtained at National Airport runway 36 and using runway 15-33 as as preferred exit location. The same procedure is repeated for ATL and IAD airports for acute angle exits and transport type aircraft population (see Figures 3.10 and 3.11).

From these observations a mathematical model was developed to estimate the exit speed of transport type aircraft as follows:

$$CPDF = \frac{1}{[1 + \alpha e^{-\beta(V-\gamma)}]} \quad \textbf{(3.1)}$$

where, CPDF is the cumulative value of the exit speed probability density function, α, β and γ are parameters of the model and V is the exit speed in meters per second. Parameters

α and γ were found to be constant at 99 and 6, respectively. Whereas β was found to be sensitive to the distance from the runway to the nearest parallel taxiway centerline. Mathematically, β can be approximated to be:

$$\beta = 3381(d)^{-1.765} \text{ for } 122 < d < 183 \text{ in meters} \quad \textbf{(3.2)}$$

where, d is the distance between the centerline of the runway and the nearest parallel taxiway (in meters). This behavior for β and ultimately for the variations in mean exit speed values can be attributed to pilot behavioral changes when the deceleration distances in the turnoff vary significantly. The data obtained at these airports suggests that pilot confidence increases when the lateral separations between runway and parallel taxiway increase thus making acute angle turnoff more desirable if runway services times are to be reduced. This correlates well with the geometric design standards proposed by Trani et al. (1992b). The usefulness of this simple mathematical model estimating the runway exit speeds like the one presented above is its possible use in more complex runway simulation models (Trani et al. 1995) such as SIMMOD and INM.

A plot of the corresponding probability density functions representing the exit speeds for various high speed exits is presented in Figure 3.14. Note that as the design speedof the turnoff increases the standard deviation of the exits speeds also increases resulting in very large dispersions for high speed turnoffs (i.e., those of Dulles International Airport).

3.5 Runway Exit Usability Results

The calibration of REDIM 2.1 allows one to estimate the runway exit usability for multitude scenarios including runways with low and high speed exits. Using the most current aircraft population data we generate a series of curves containing the probability density functions of exiting a runway as a function of runway downrange distance (see Figures 3.15 through 3.20). These curves represent the expected results of running REDIM 2.1 for the average population operating in the U.S. as of 1994.

Note that three aircraft approach speed groups (B, C, and D) are represented in these results and the curves apply to either dry or wet pavement conditions. Table 3.5 contains the aircraft population mix used in the derivation of these results for further reference. The use of these curves should help airport planners and designers to locate quickly runway turnoffs without running the computer program developed as part of this research. It is anticipated that these results will be made available in the FAA Advisory Circular 150/5300-13 for airport planners and designers.

FIGURE 3.8 Observed Aircraft Exit Speed Histograms at DCA Airport .

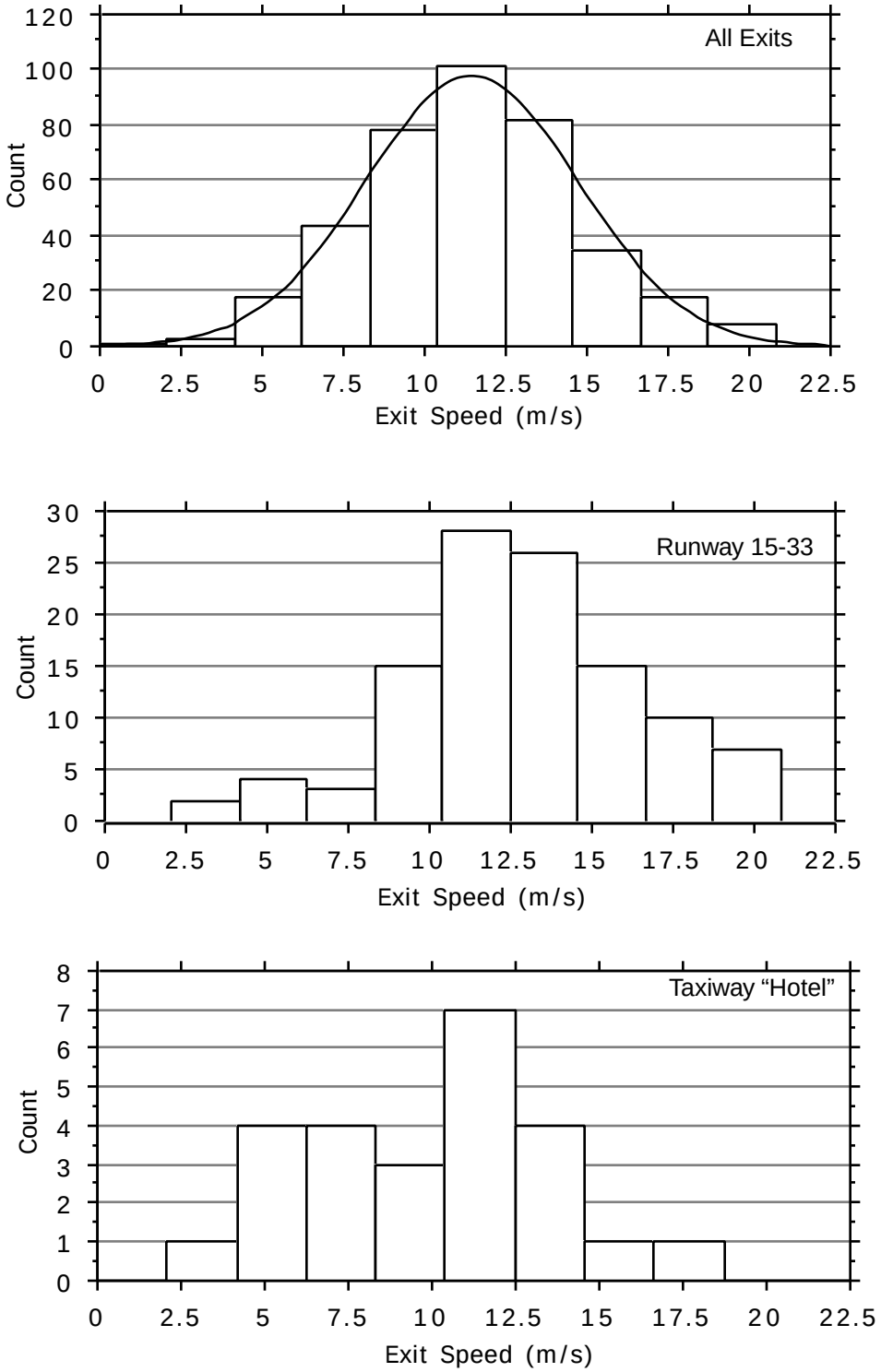

FIGURE 3.9 **Observed and Predicted Cumulative Probability Density Functions for National Airport Data (Runway 15-33 Used as Exit).**

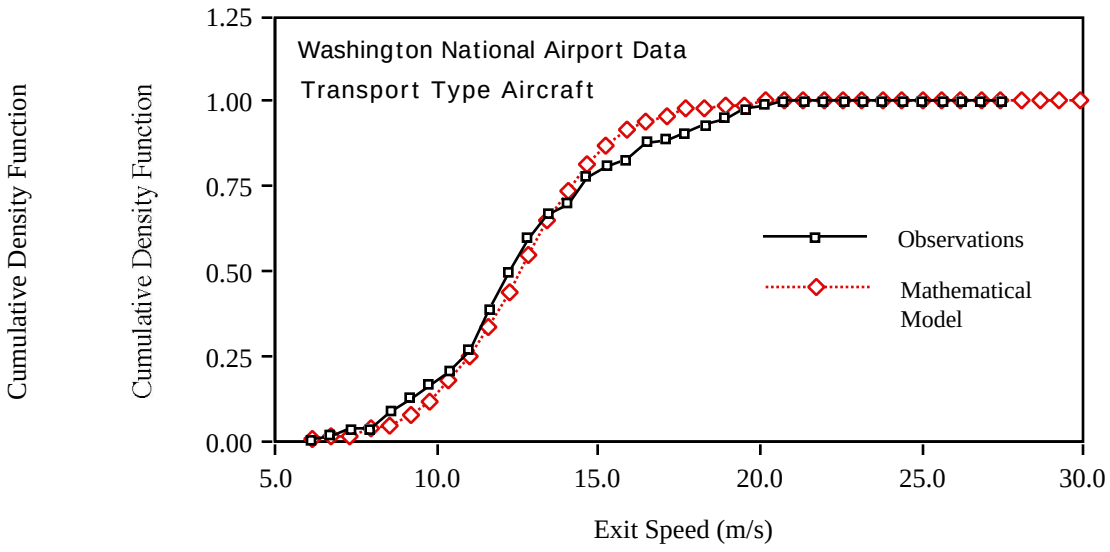

FIGURE 3.10 **Observed and Predicted Cumulative Probability Density Functions for Atlanta Hartsfield International Airport Data Applied to Acute Angle Exits (i.e., 30 degree exit angle).**

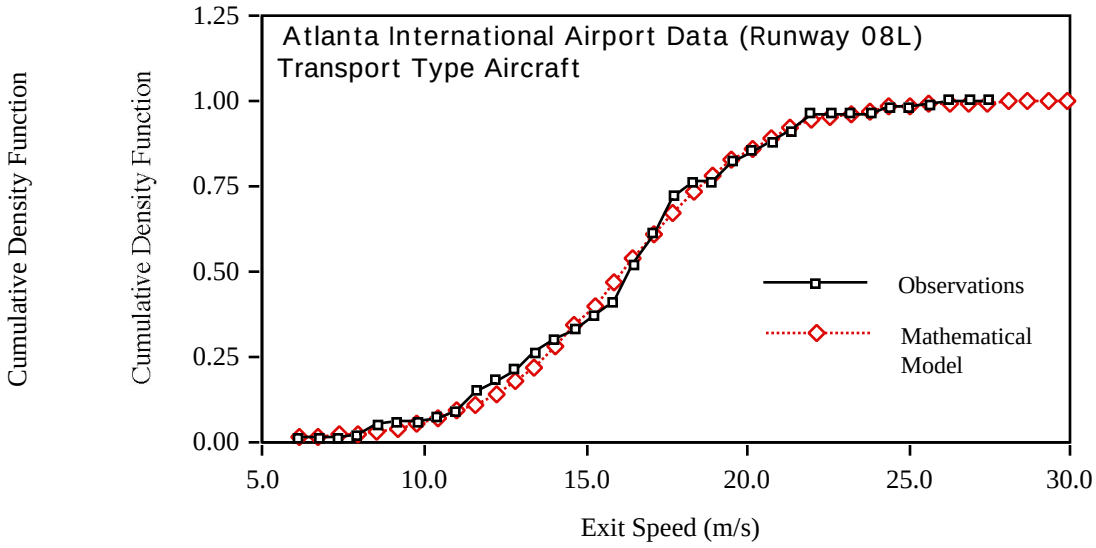

FIGURE 3.11 **Observed and Predicted Cumulative Probability Density Functions for Dulles International Airport Applied to 30 Degree, Acute Angle Exits.**

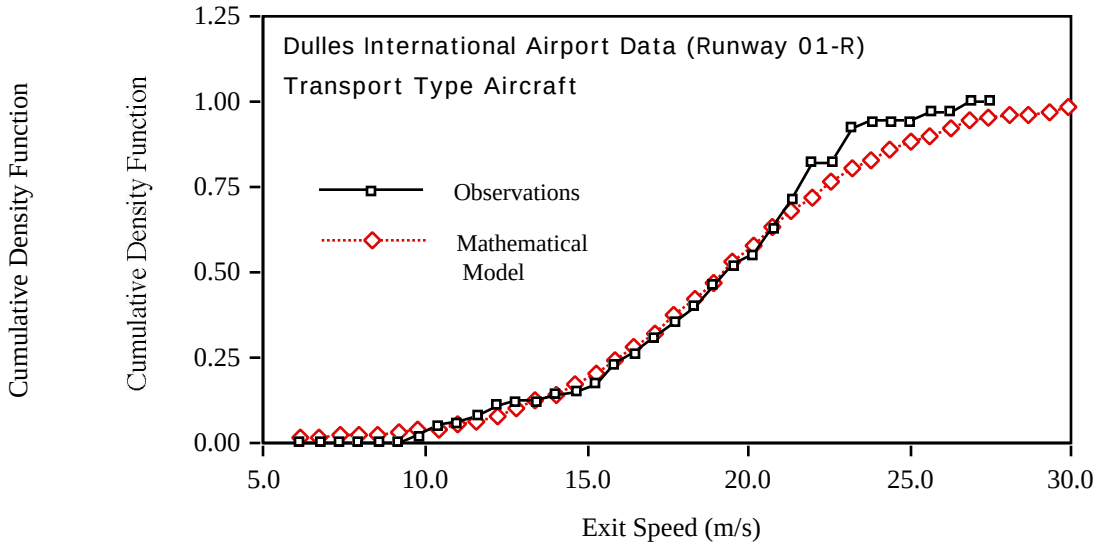

FIGURE 3.12 **Mathematical Models Proposed for Acute Angle Turnoff Exits with Various Lateral Distances Between Runway and Parallel Taxiway.**

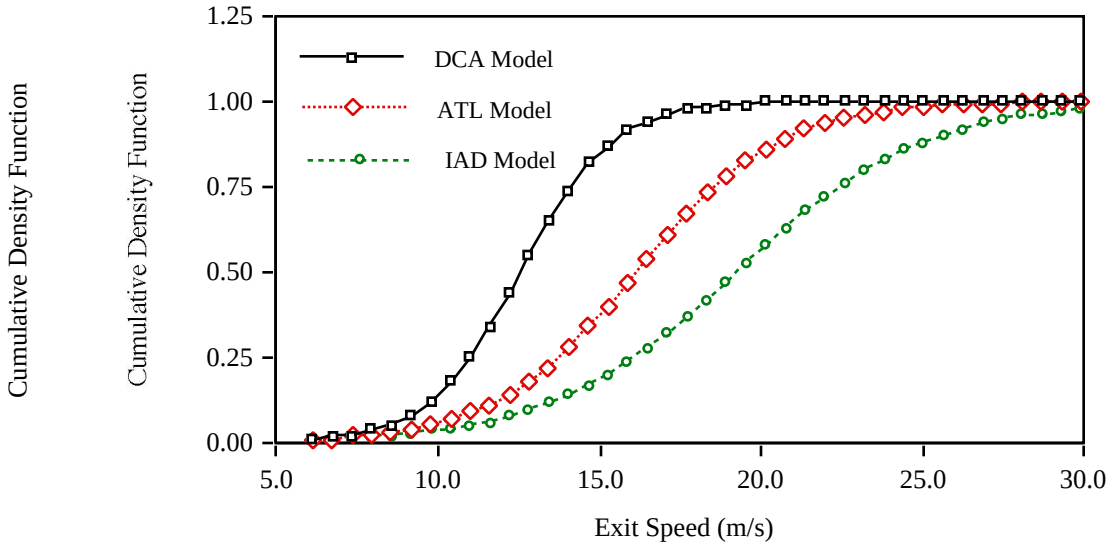

FIGURE 3.13 Parameter β for Various Lateral Distances Between Runway and Parallel Taxiway.

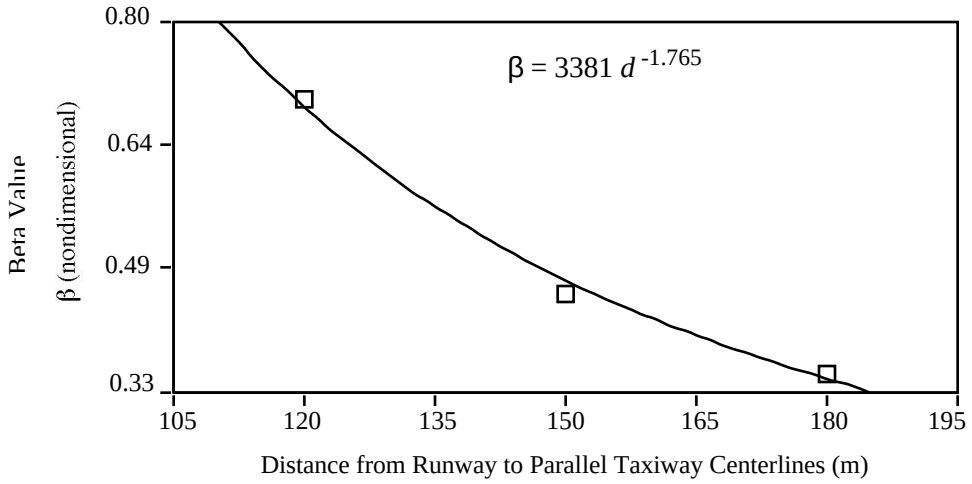

FIGURE 3.14 Probability Density Functions for Proposed Mathematical Models for Acute Angle Turnoff Exits with Various Lateral Distances Between Runway and Parallel Taxiways.

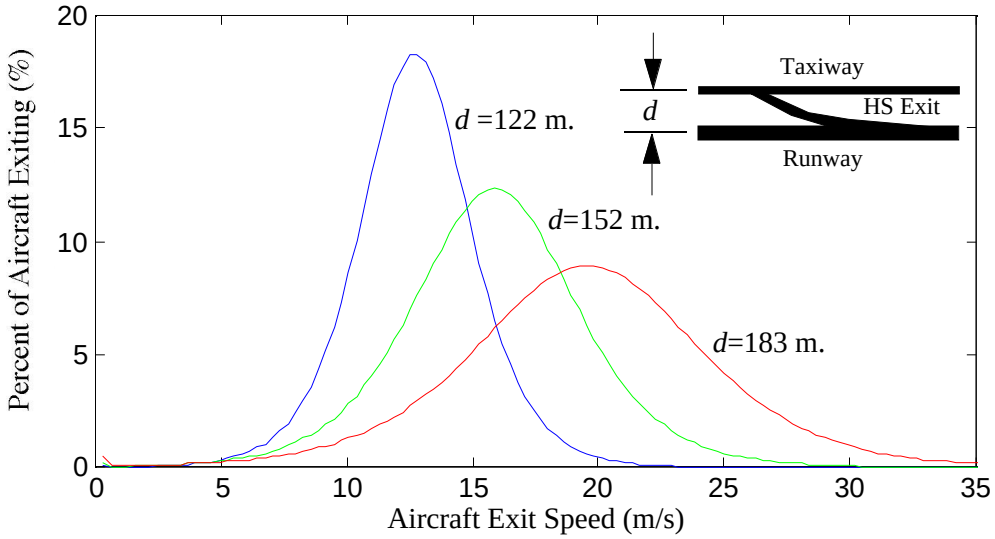

TABLE 3.5 Composition of Transport Aircraft Used for Runway Exit Usability Estimation.

Aircraft Type (Approach Cat. C)	Percentage in US Fleet	Aircraft in US Fleet	Aircraft Type (Approach Cat. D)	Percentage in US Fleet	Aircraft in US Fleet
Boeing 727-200	29.0	1029	Boeing 747-200/300	19.0	178
Boeing 737-200/300	26.0	915	Lockheed L-1011	12.0	113
Boeing 757-200	9.0	328	Douglas DC-10-30	25.0	239
Douglas DC-9-30	12.0	500	Boeing 767-200/300	18.0	170
McDonnell MD-80	17.0	602	Douglas DC-8-70	18.0	168
Avro 146-200	1.0	23	Airbus A300	6.0	58
Airbus A-320	2.0	54	Airbus A310	2.0	21
Fokker 100 / F28	4.0	117			
Total	100.0	3466	Total	100.0	947

FIGURE 3.15 **Runway Exit Assignment Density Functions and Runway Occupancy Times for Aircraft Approach Group B Using Right Angle Exits.**

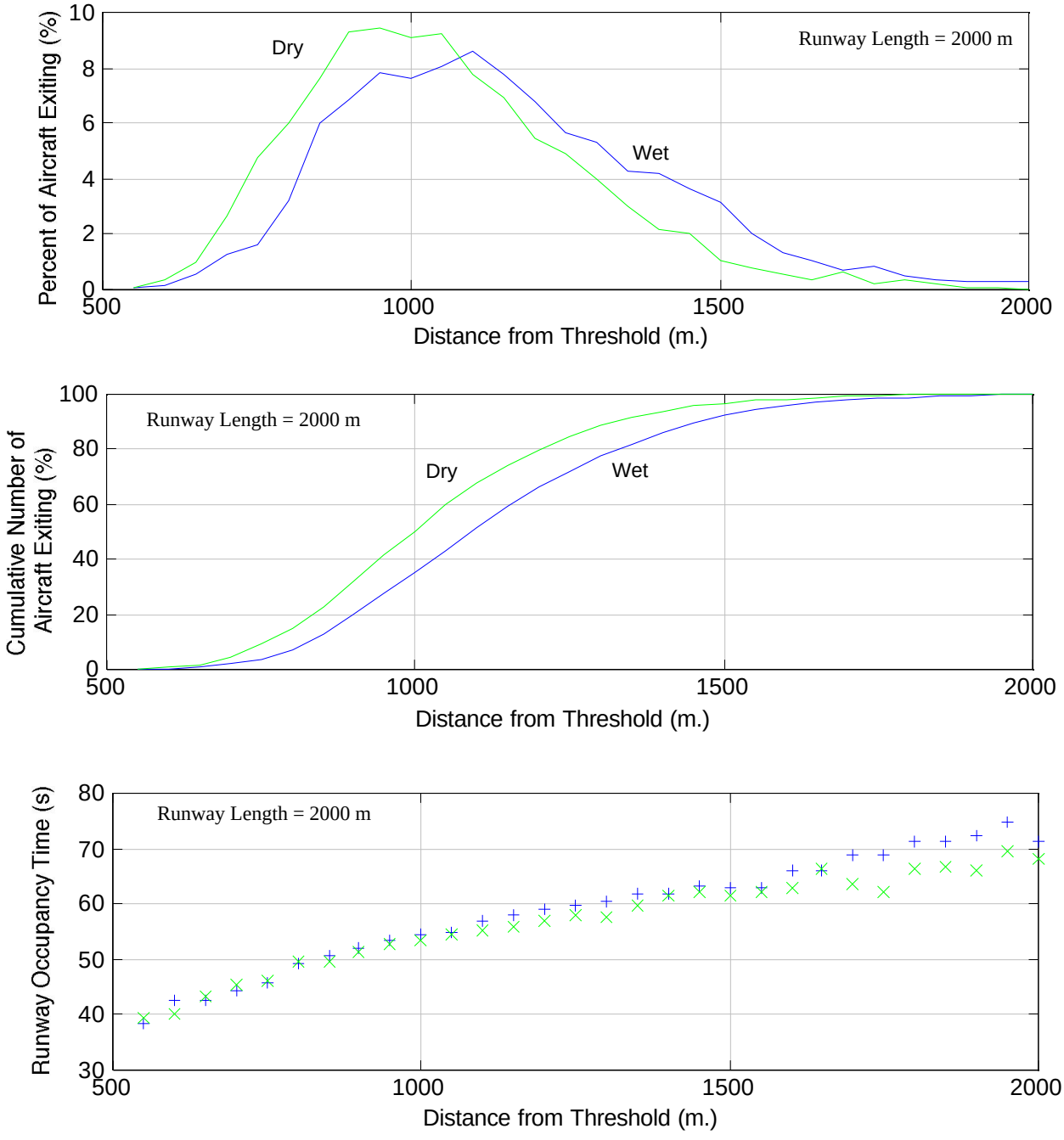

FIGURE 3.16 **Runway Exit Assignment Density Functions and Runway Occupancy Times for Aircraft Approach Group B Using Standard Acute Angle Runway Exits (30 Degree Exit Angle).**

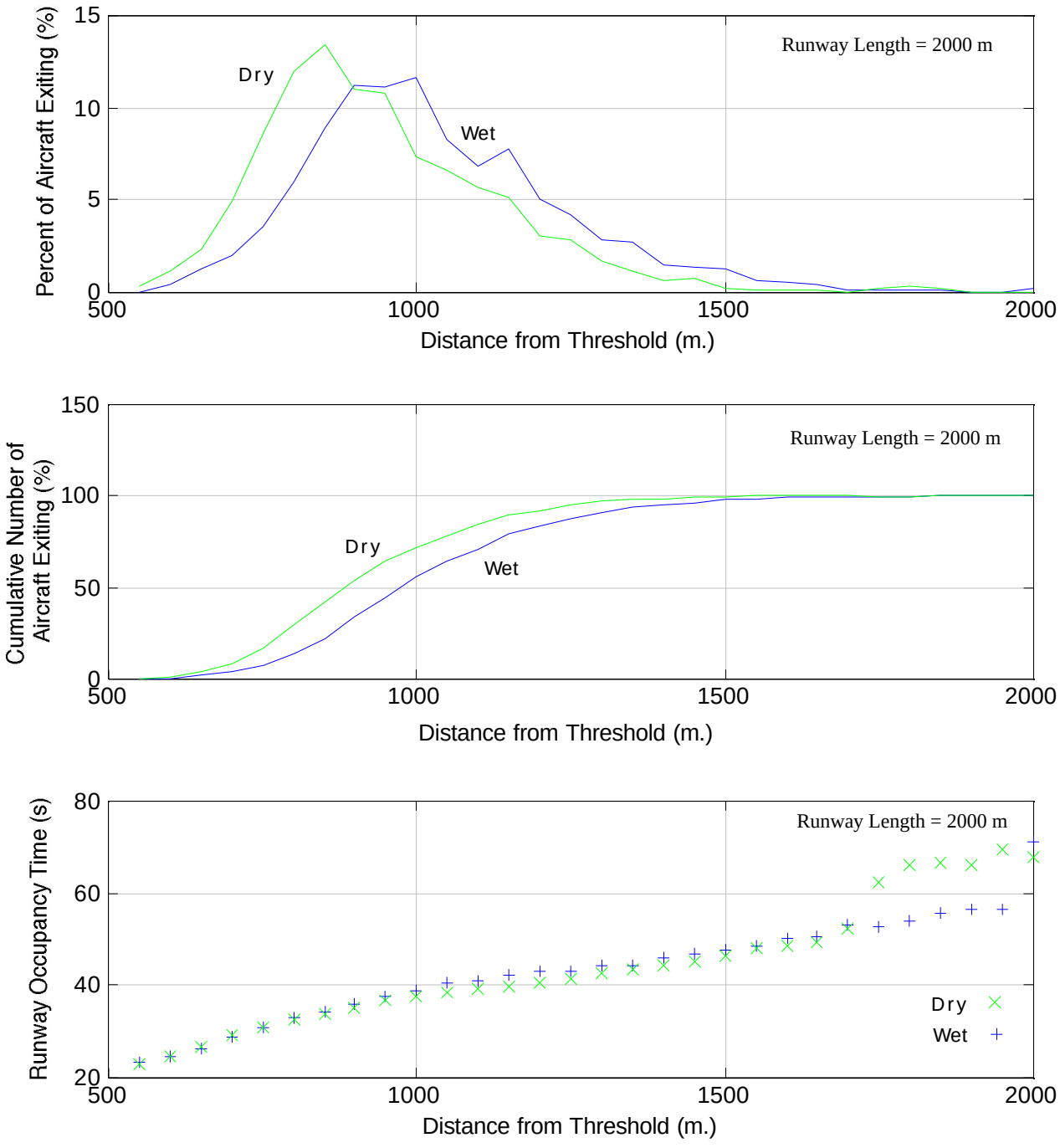

FIGURE 3.17 **Runway Exit Assignment Density Functions and Runway Occupancy Times for Aircraft Approach Group C Using Right Angle Runway Exits.**

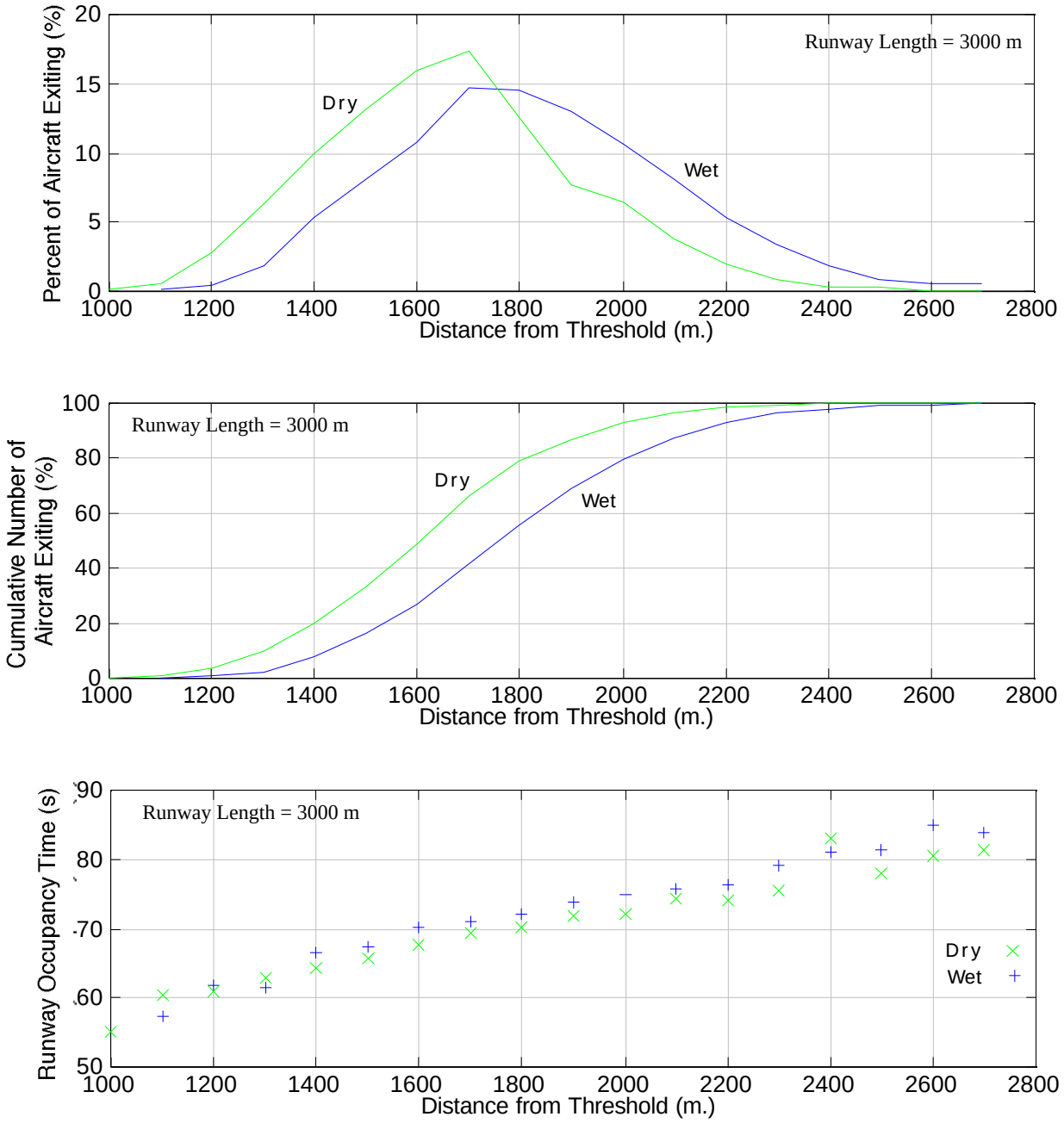

FIGURE 3.18 **Runway Exit Assignment Density Functions and Runway Occupancy Times for Aircraft Approach Group C Using Standard Acute Angle Runway Exits (30 Degree Exit Angle).**

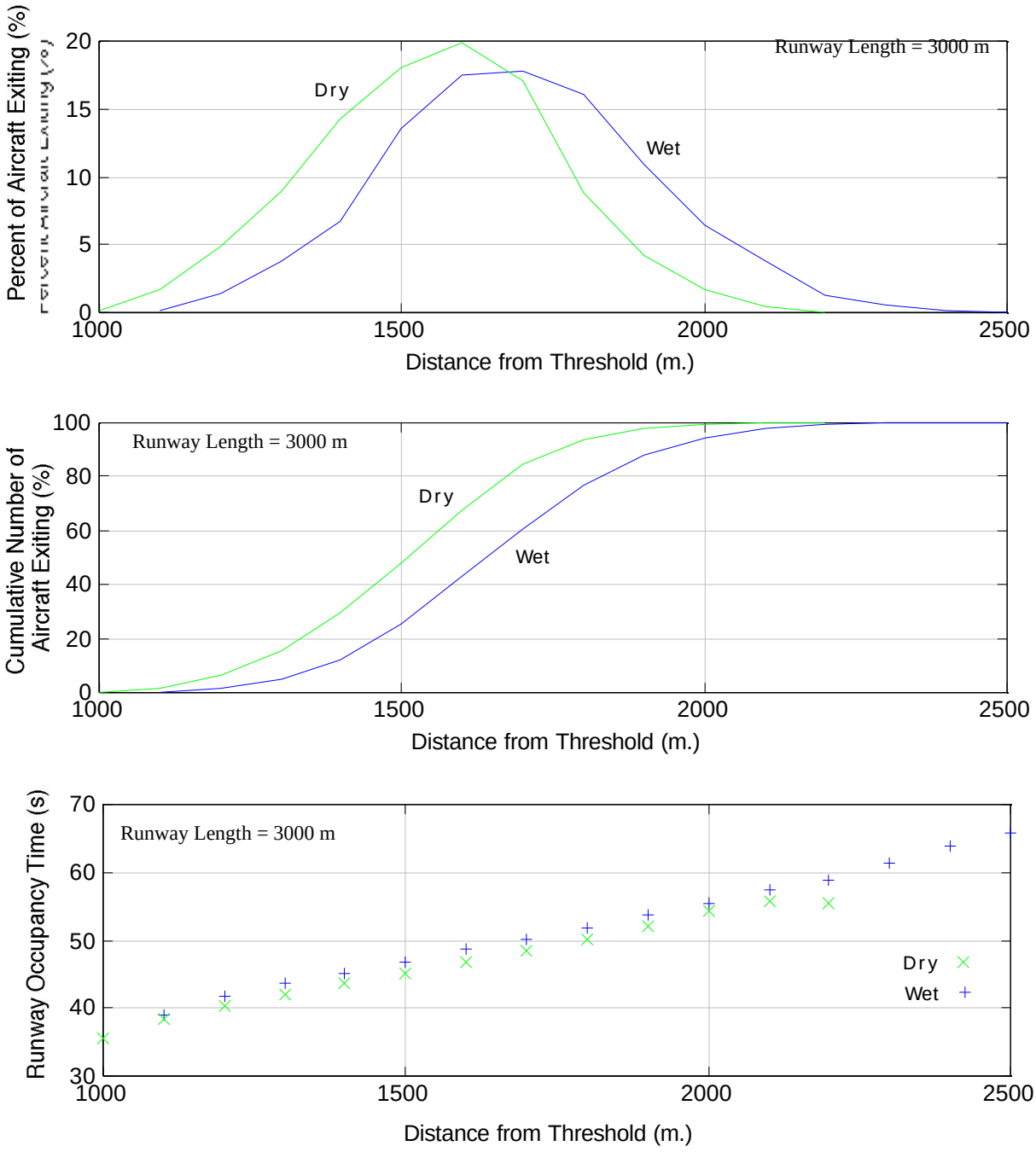

FIGURE 3.19 **Runway Exit Assignment Density Functions and Runway Occupancy Times for Aircraft Approach Group D Using Right Angle Runway Exits.**

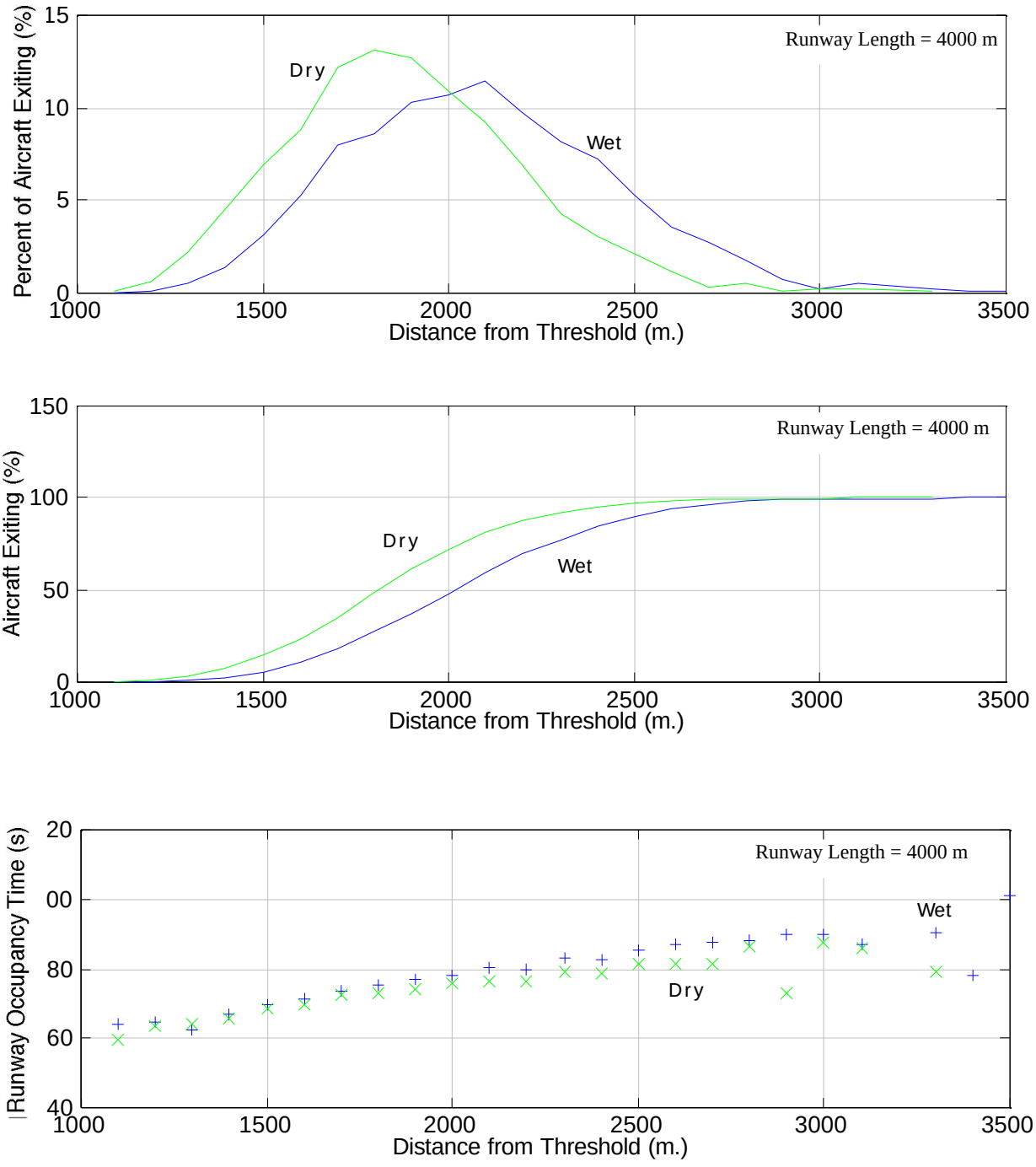

FIGURE 3.20 **Runway Exit Assignment Density Functions and Runway Occupancy Times for Aircraft Approach Group D Using Standard Acute Angle Runway Exits (30 Degree Exit Angle).**

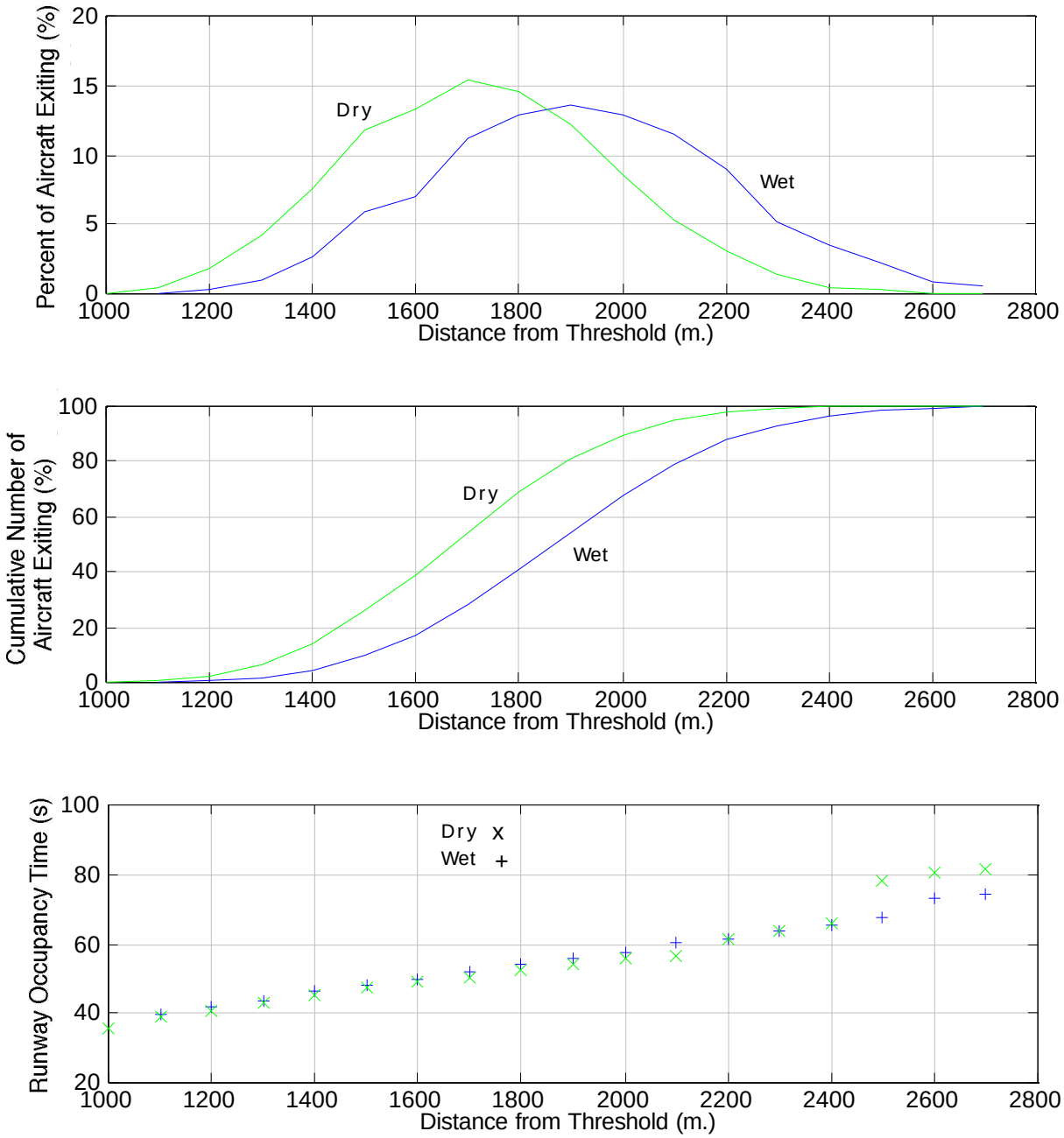

CHAPTER 4

REDIM 2.1 Model Validation

In this chapter we address the model predictive capabilities using various airports as benchmarks for validation. The goal here is to determine how accurate the model calibrated can predict runway ocuppancy time and exit allocations.

4.1 REDIM 2.1 Model Predictive Capabilities

This section compares the results of REDIM 2.1 with the statistics collected by the research team at four major East Coast airport locations. Data from Raleigh-Durham was notused because at the time of our observations, unsually strong wind gust conditions prevailed at this airport making landings a real challenge for pilots. In fact, during the two day visit to RDU three go-arounds motivated by the wind forces. The correlation of the model was made possible by comparing predicted and observed exit utilizations and runway occupancy time data. The results that follow illustrate some of the predictice capabilities of the model at some of these airports.

On runway 36 at DCA airport, four exits are available to the transport type aircraft whose landings were observed. Table 4.1 summarizes the name, location, type and suitable exit speeds of the available exits on runway 36 at National Airport. The suitable exit speeds are set considering the types of exits and the recommended exit speed by the FAA [Airport Design, AC 150/5300-13, 1989]. At DCA airport, some exits have been built with non-standard geometries and thus judgement needs to be used in setting realistic exit speeds. The suitable exit speeds for these non-standard exits are set to those of the closest standard exits without violation of aircraft turnoff capabilities [Trani and Hobeika et al, 1992; Horonjeff, 1961].

TABLE 4.1 Exit Locations and Design Speeds for National Airport Runway 36.

Airport	Exit Number	Location[a] (m)	Name	Type	Speed (m/s)
DCA	1	1008	Hotel	45 degrees	15
DCA	2	1368	India	45 degrees	15
DCA	3	1507	RWY[b]	30 degrees	22
DCA	4	2020	Juliette	90 degrees	10

a. Location is the distance from the threshold to the point of curvature of the runway turnoff.
b. RWY refers to an inactive Crossing Runway.

The simulation model described in Chapter 3 combined with the deceleration adjustment scheme developed in earlier this chapter enables us to evaluate the exit usage and the resultant ROT for every landing aircraft. Figure 4.1 compares the predicted exit utilization and the resultant ROT data with values observed in the field at National Airport. The aircraft mix is determined according to the relative frequencies of aircraft types in the observed data.

The model predicts well the ROT values for each individual exits and the overall average ROT as seen in part a of Figure 4.1. The average error is 1.9 seconds for the individual exits and 0.9 seconds for all airports. However, there is some discrepancy between the prediction and the observation of the exit utilization as appearing in part b. Two reasons seem to contribute to the discrepancy: 1) the limitation of the deceleration distance prediction capability of the simulation model is one, and 2) the pilot's exit choice behavior is the other.

The simulation model predicts the central tendency and magnitude of dispersions of the velocity profile well. However, the model is not able to reproduce the abnormality of the distribution of the landing distance such as skewness and multimodality. The model underestimates the landing distance particularly at CLT airport possibly because of the limited exit availability. This may be the answer to the discrepancy of the exit utilization at CLT airport seen in part b of Figure 4.3. That is, the proportion of the mix using the first exit is predicted 67% by the model while the observed data shows the proportion is 47% partially because of the underestimation of the deceleration distance. However, the discrepancy at DCA airport, where the predicted landing distance data agree on the observed data quite well, is not explained by the reasoning above.

FIGURE 4.1 Comparison of Predictions and Observations at Washington National Airport.

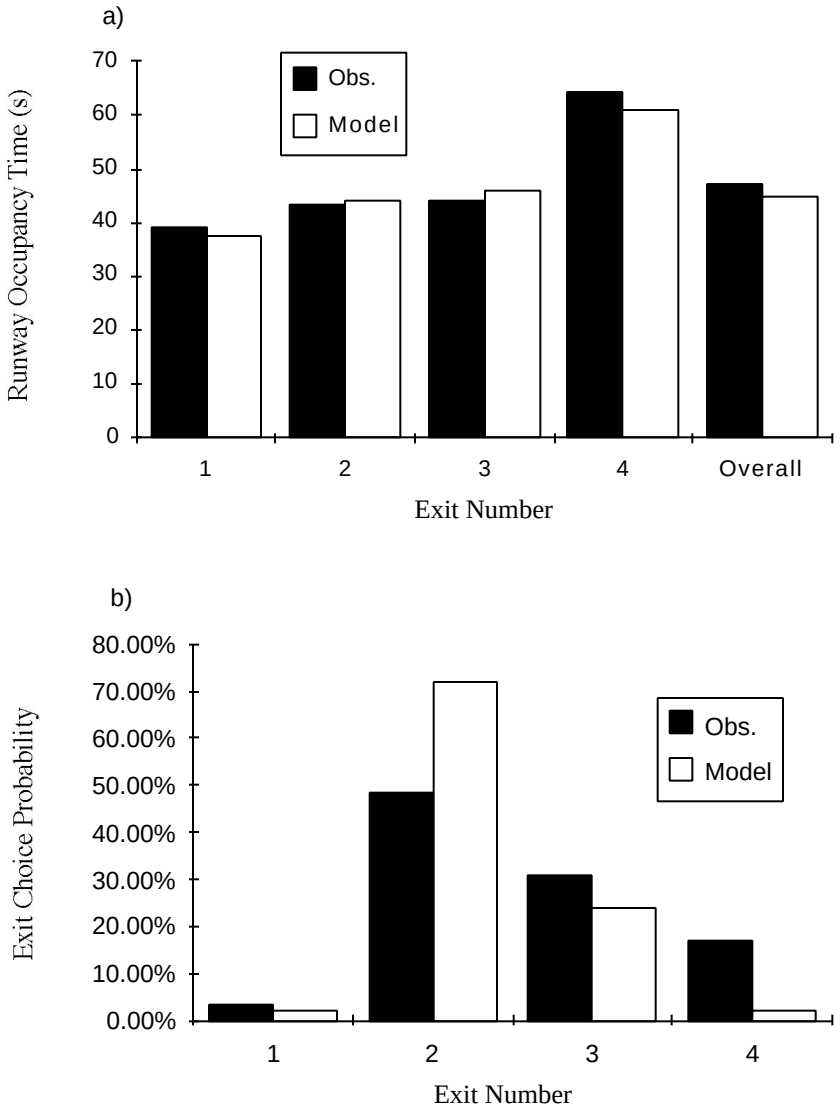

The predictions at Charlotte International runway 23 are more interesting since it is here that pilots display more difficult behaviors in their deceleration profile. Throughout this research, it is assumed that pilots must turn off using the first available exit after they decelerate to the specified exit speed, because this is a desirable behavior for the efficient use of a runway. However, not all the pilots in reality follow this recommendation. The pilots exit choice which does not agree on the assumption seem to play a major role in the exit utilization discrepancy at DCA airport. That is, the simulation model predicts 72 % of the mix turn off using the second exit, while the observed data show that 48.5 % out of 72 % use the second exit and the rest use the third or fourth exits. Twenty three % of the mix (the

difference in the percentage) seem to use the third or fourth exits, though they decelerate to the exit speed (10 m/s) ahead of the second exit.

To verify the effectiveness of the optimization model, 'how much the ROT can be reduced' is investigated by placing three high speed exits suitable for an exit speed of 30 m/s ignoring the existing exits. The only exception is the third exit of the runway 36 at DCA airport, because it is a crossing runway which may not be altered. Figure 4.5 shows the comparison of the observed ROT and the optimized ROT at three airports. The comparison are made for both the overall average and the last exit average, for the last exit ROT, equivalent to the near upper bound value of the ROT at an airport, has a significant effect in determining the runway capacity as well as the overall average.

First, it can be read from part a that the overall average ROT can be reduced by 8 and 7 seconds at DCA and ATL airports and by 15 seconds at CLT airport. Since runway 23 at CLT airport has only two low speed exits angled 90^{o} exits compared to four exits of runway 36 at DCA airport and runway 8L at ATL airport, it seems natural that the ROT reduction for runway 23 at CLT airport is much greater than at the others. Second, while the last exit average ROT can be reduced by 20 seconds and 17 seconds at DCA and CLT airports, the ROT is reduced by only 2.7 seconds at ATL airport. The last exit currently used by the aircraft mix is a high speed exit located at 1830 m as shown in Table 4.3. The last exit ROT comparison clearly illustrates how important the exit speed is in reducing ROT as well as the exit location.

TABLE 4.2 Exit Locations and Design Speeds for Runway Turnoffs for Runway 23 at Charlotte Douglas International Airport.

Airport	Exit Number	Location[a] (m)	Name	Type	Speed (m/s)
CLT	0	900	Romeo	90 degrees	10
	1	1450	Bravo	90 degrees	10
	2	2200	Echo	90 degrees	10

a. Location is the distance from the threshold to the point of curvature of the runway turnoff.

FIGURE 4.2 **Comparison of Predicted and Observated Runway Ocuppancy Times at Charlotte-Douglas International Airport.**

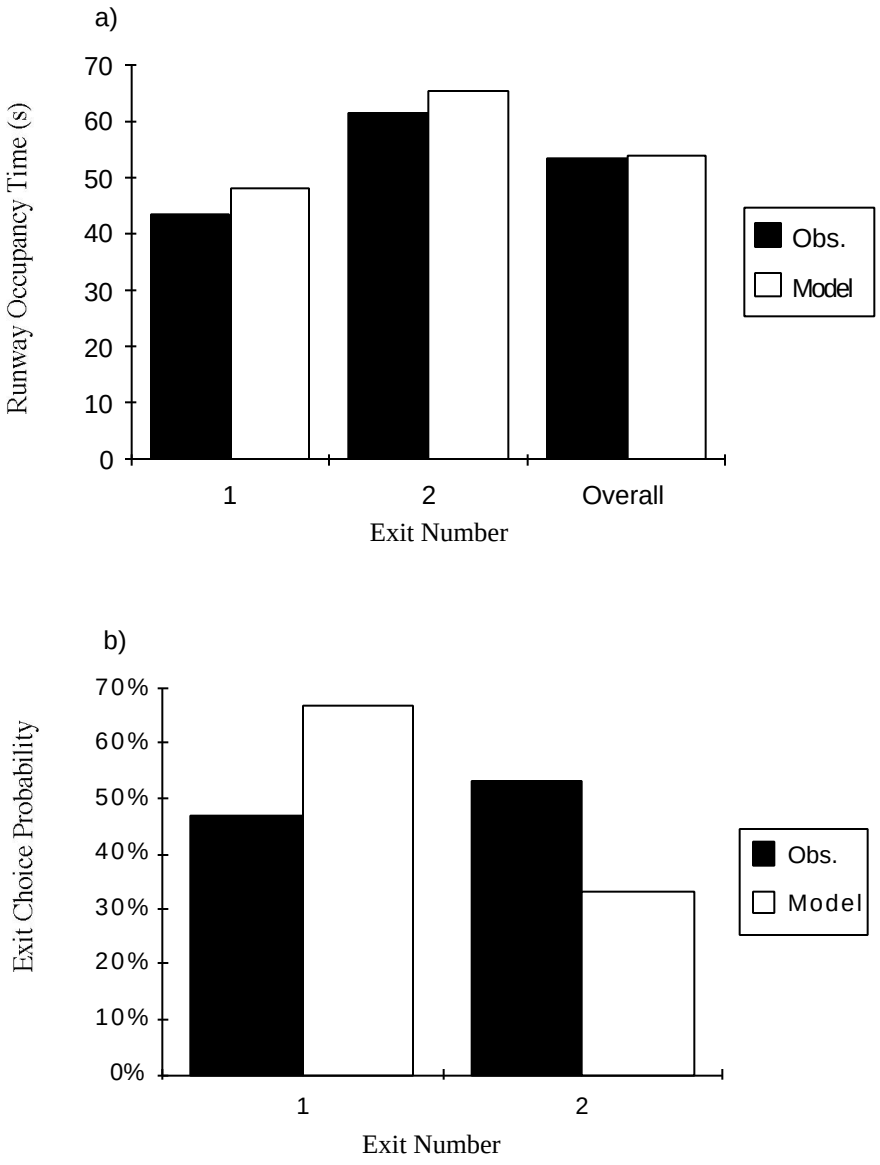

TABLE 4.3 Runway 8L Exit Characteristics at Atlanta Hartsfield International Airport.

Airport	Exit Number	Location[a] (m)	Name	Type	Speed (m/s)
ATL	1	1375	Charlie	90 degrees	10
	2	1470	Delta	90 degrees	10
	3	1500	Bravo-7	30 degree	21
	4	1830	Bravo-11	30 degree	21

a. Location is the distance from the threshold to the point of curvature of the runway turnoff.

FIGURE 3.3 Comparison of Predictions and Observations at Atlanta Hartsfield International Airport.

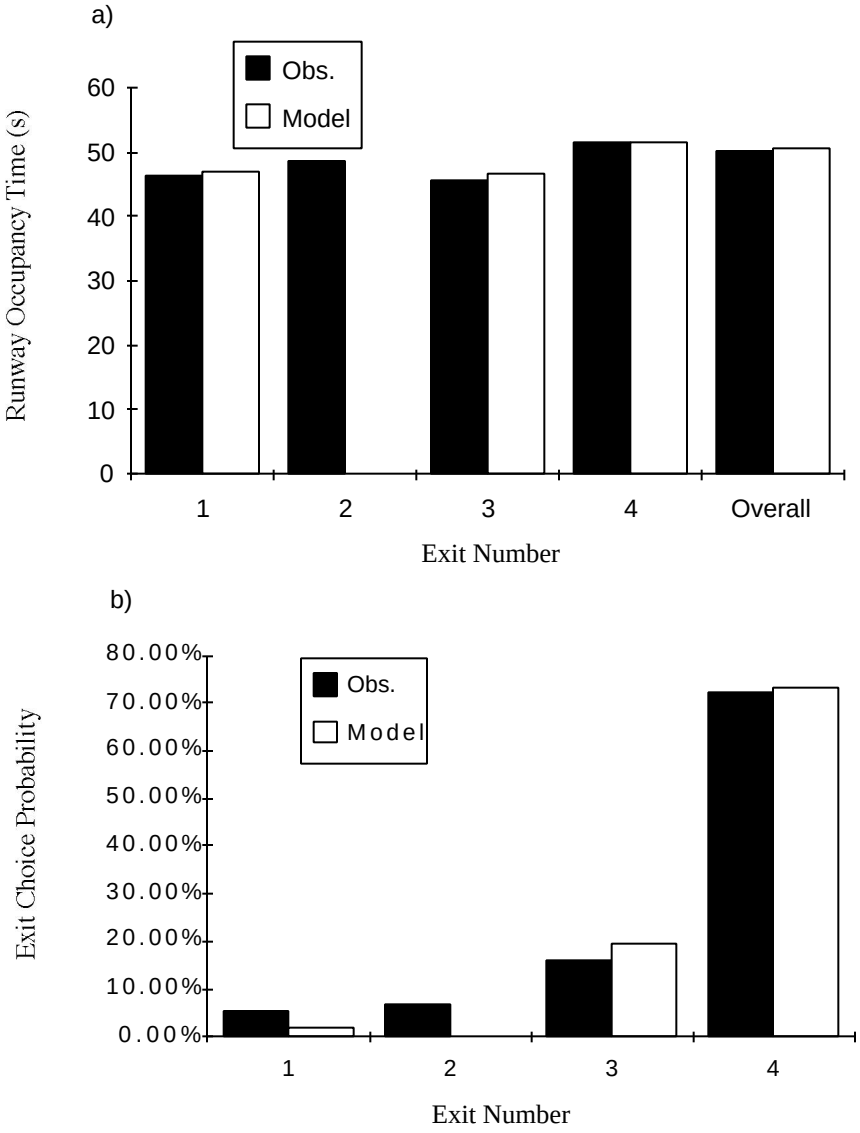

FIGURE 3.4 Comparison of Observed ROT and Optimized ROT for Various Airports.

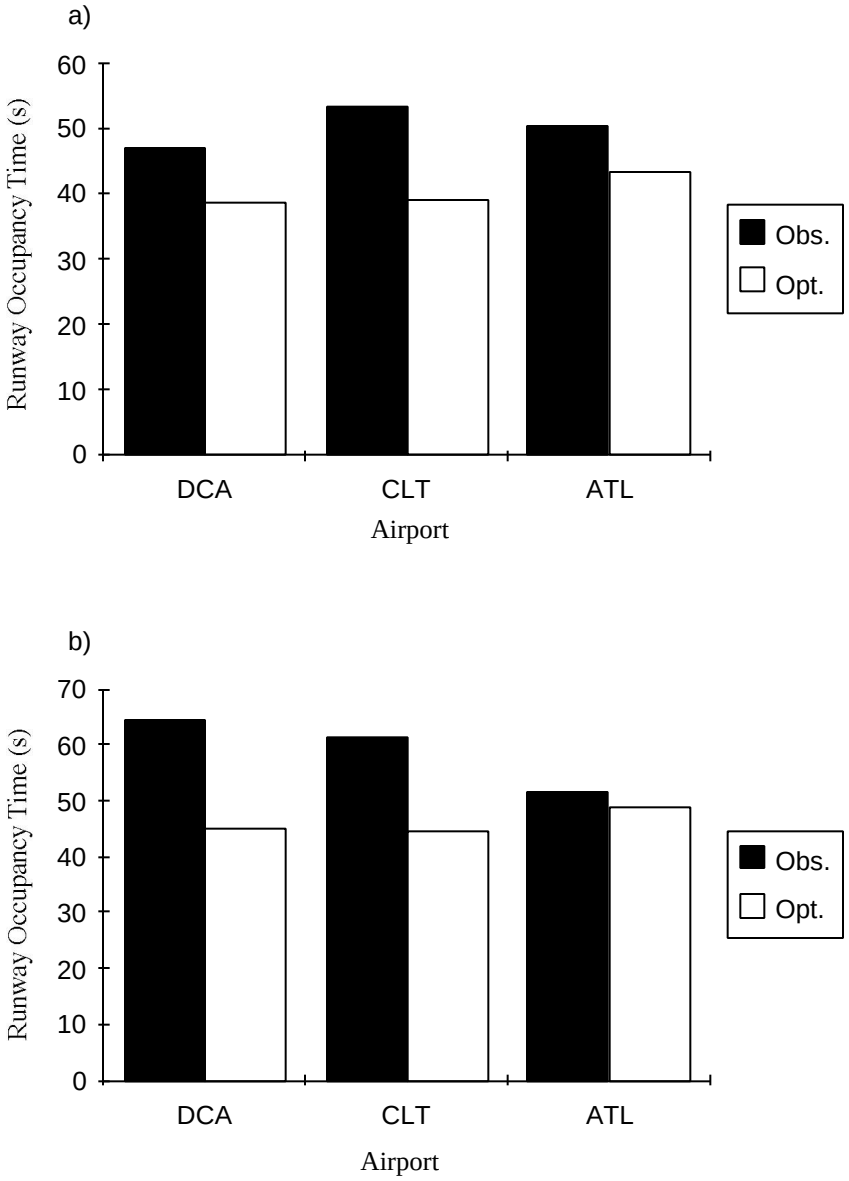

CHAPTER 5

An Economic Methodology to Justify High Speed Runway Exits

This chapter proposes a methodology to quantify the runway capacity gains possible with the actual implementation of high speed turnoff geometries. The method employed here uses the Systems Dynamics methodology to ascertain economic gains associated with the implementation of high speed turnoffs at airports. The method described here relies in the use of several computer simulation/optimization models to estimate capacity and delay changes of a runway configuration once high speed runway turnoff have been implemented.

5.1 A Systems Dynamics Approach

The improvements derived from the use of optimally located geometries require external assessment from macroscopic simulation packages where aircraft terminal airspace and ground operation are simulated and conflicts between arrivals, departures, special operations (i.e., touch-and-go and ground transfers) are resolved. In order to present a unified methodology to study the effects of implementing high speed turnoffs at major airports.

In order to ascertain the capacity gains and corresponding delay reductions in airport operations using high speed turnoff geometries the Systems Dynamics Methodology developed by Jay Forrester at MIT is used. This method incorporates three levels of detail in the modeling process in order to quantify the effects of model variables in dynamic systems. These are: 1) A Verbal model, 2) Causal Diagram and the 3) Mathematical Model. Several tools have been developed to formulate Systems Dynamics models in digital computers and among them STELLA[1] which allows the easy depiction and simulation of causal links between model variables. STELLA is an interactive computer simulation tool used in this context to assess the macroscopic effects of building high speed runway exits at an existing airport. Several computer models have been developed in this research project in order

to estimate capacity gains of high speed exits.

The RUNSIM model (Runway Simulation) is programmed in SIMSCRIPT II.5 and models individual arrival and departure aircraft operations to estimate queues at taxiway holding positions and at terminal airspace nodes [Nunna, 1991]. The model includes the logic necessary to allocate aircraft operations to ten different types of runway exit geometries including REDIM-generated high speed turnoffs. RUNSIM complements the results of REDIM 2.1 and estimates global statistics for arrival and departure operations. The main outputs to this model are the delays incurred by each aircraft arrival and departure operation. In order to demonstrate this a single runway airport scenario was used in order to verify arrival and departure delays under mixed aircraft operations. Using this model it can be shown that airport operations show reductions in the amount of departure delays observed.

5.2 Cost Benefit Analysis

In the assessment of the benefits of high speed turnoffs several cost contributions should be considered: 1) construction, 2) land acquisition, 3) maintenance and operation, 4) administration, 5) user and 6) airline costs. The following paragraphs describe briefly each one of these cost categories and point out some of the most important parameters to ascertain each one in this project.

5.2.1 Construction and Land Acquisition Costs

Since many high-speed turnoffs will be located between an existing runway and a taxiway, there is no extra requirement of land use. Therefore, the land acquisition costs are eliminated in this study. The construction costs and the operation breakdown loss during the construction would be consider in this category.

Mean construction costs per unit area for runways and taxiways can be ascertained from construction manuals. According to the practices of the construction contract administrative authorities, the actual cost could be the reasonable estimated with the historical data and the geographical location. Therefore the cost will be different from area to area and also varied according to construction firms. Technically speaking, an excess cost is reserved based on the cost from the cost-benefit analysis by the planner. To simplify matters, this study will only use a break even cost to evaluate the facility construction cost.

5.2.2 Maintenance, Operation, and Administration Costs of New High-Speed Exits

Operation, maintenance, and administration costs cover the annual costs of operating the facility. It seems that it is difficult to estimate the exact costs of this category for the facility as there are usually many unknowns. These costs will include such items as maintenance, signing, pavement markings, runway/taxiway surface repairs. In the improved airport facility, the number of exits will be changed depending on the aircraft mix and other aircraft

1. STELLA 2.1 is a trademark of High Peformance Systems, Inc., Hanover, New Hampshire.

parameters. Besides the runway delay cost due to this construction, costs are also due to increase corresponding the taxiway/turnoff areas. Compared to the operation and maintenance cost of a complete airport, the marginal cost for this facility is rather small but could be considered as an entity

Administrative costs are somewhat more difficult to estimate, particularly in the case of small projects where increases will not appear as increased staff requirements, but only in marginal increases in workload on the existing staff [Stopher et al, 1976]. The administrative function cost of airport is usually so large compared to the small increase in the numbers of landings and departures that will not increase the cost on the airport administration significantly.

5.2.3 Travel Costs

Users costs are somewhat more complex and include several items. The first one is the direct and indirect airline operating costs, including operating mileage-related maintenance. The second item is time lost costs to passengers.

Airline Operating Cost

Direct operating costs to the airlines due to delay include the cost of fuel, crew time, maintenance, and depreciation. These cost differ by aircraft, type, with larger aircraft costing more to fly. Aircraft operating costs usually were determined by considering direct operating costs but excluding depreciation and insurance costs. These costs were then increase by 25% to account for indirect operating costs. [Milton et, al., 1967]

Historical data on operating cost of aircraft was collected from various sources. Looking at actual operating cost data, it was found that for aircraft classified in category C and D, the operating cost is correlated with the maximum takeoff weight and was applicable to US. airlines [Aviation Week, 1988], including American, Delta, United, USAir, and Northwest Airlines. The data is nonetheless representative of real operations as these megacarriers dominate the air transport market in United States.

An approximate relationship between block hour operating expenses (in 1992 dollars) and maximum and the aircraft maximum allowable takeoff weight has been found to be (Zhong, 1992):

$$C_H = 1254 + 0.0058(W_{MTOG}) \quad \textbf{(5.1)}$$

where, C_H is the hourly aircraft operation cost, and W_{MTOG}. is the aircraft maximum takeoff gross weight expressed in thousand of pounds. This linear regression formulation has a reasonable value of the coefficient of correlation of 0.9821 for twelve types of aircraft ranging from small to heavy transport aircraft.

Passenger Costs

Passenger costs are associated with passengers being delayed. There are at least three approaches to determine the passenger time value: 1) The first method is to value the time ac-

cording to the travelers willingness to pay to avoid delay. 2) The second method is to put the value of passengers travel time as a function of his wage. 3) A more sophisticated approach is the use of derived elasticity of demand function for air travel to compare the value air travelers place on their time.

Each of the three methods above can be used to calculate the passenger time value. However, it should be understood that there is a threshold of the passenger time delay. Passenger delay loss will be of concern only if the delay is above this threshold. According to ATA [Air Transportation Association, 1987] the flight delay statistics show that delays of less than 15 minutes were chronic and widespread, representing 60% of all behind-schedule arrivals. This implies that passenger's delay threshold could be 15 minutes.

Rate of Discount

The appropriated rate of interest or rate of discount is the necessary instrument in present value and capital recovery criteria. A rate of 7% is used as the average annual discount rate.

5.2.4 Peak Hour Operation Cost Analysis

High-speed exits, if used properly, can effectively reduce the average runway occupancy times. The may payoff of high speed exits seems to be concentrated during high demand periods (i.e., near saturation demand conditions) as reductions in ROT result in larger gaps to allow more departures. The cost of airside operations could be reduced by decreasing the airside maneuvering time and benefits could be obtained by letting more aircraft depart during the inter-arrival time gaps resulting from lower runway service times. Thus, the cost analysis should consider the following three categories:

- More departures and arrivals will be allowed per unit of time
- Airside ground maneuvering times could be reduced
- Passenger waiting times could be shorter

Both landing and departure changes are only considered with regard to the benefit of increased departures. In order to compare standard exits with their high speed counterparts it is assumed that in both cases the demands are sufficient to fill all possible landing gaps allowable. Based on this assumption, it is easy to compare the trade-off of cost increases between two equally saturated facilities. It should be emphasized that many congested airports exhibit this behavior during periods of time where heavy airline banking operations are present.

With the same saturated demand, in the do-nothing case, the delay will be increased both for departures and arrivals; in the improved case, the delay of departure and arrivals will decrease and the capacities will increase conditionally. In the improvement case, a certain amount of investments are required for research, development and facility construction purposes. The airside maneuver time and the passenger travel time savings can also be analyzed in an analogous fashion. Two difficulties arise in this analysis: the first one is how to estimate costs and benefits to airlines under the assumption that peak and non-peak hour

pricing is different for some airports. The second one is the consideration of passenger travel time loses in the system. This phenomena is difficult to evaluate under the current schemes used to estimate flight delays.

The airport authority would certainly benefit from more aircraft operations as this implies more revenues through landing fees with the same infrastructure. The major problems in peak hours are capacity related. The utilization of high-speed exits will reduce the runway occupancy time and hence increase the runway capacity under VMC conditions and mixed aircraft operations. By far, this research is concentrated on the reduction of runway occupancy time and delays. The next consideration is how to estimate benefits to a new facility if we can convert the time savings into monetary values. Conceptually, the savings will fall into two categories; the first one is the increased revenue associated with aircraft landing fees.The second one is a possible reduction in taxing times for arriving aircraft if the location of the high speed exits indeed allows for this. In addition, delay reductions at departure queues are possible because under mixed aircraft operations the use of high speed runway exits could open more gaps between arriving aircraft thus allowing, in principle, the release of more departures.

In general, landing fees charged by various airport authorities exhibit important seasonal as well as hourly variations. In most formulations they correlate well with aircraft take off weight [Roskam, 1985]. In this analysis the aircraft landing fees, C_{LF}, are estimated as follows:

$$C_{LF} = f(\overline{W}_{TO}) \tag{5.2}$$

where; f is the landing fee rate in dollars per pound and $\overline{W}_{TO}$ is average aircraft takeoff weight in pounds. The average aircraft takeoff weight is defined as,

$$\overline{W}_{TO} = \sum_{i=1}^{n} n(W_{TO_i}) \tag{5.3}$$

where n is the percent of the *ith* aircraft operating at this airport and W_{TO_i} is the takeoff weight of the *ith* aircraft using this airport facility.

From the assessment of landing fees one can estimate the total departure cost, C_D.

$$C_D = N \sum_{i=1}^{n} A_i P_i T_i \tag{5.4}$$

where: A_i is the cost factor associated with the *i*th aircraft, N is the total number of departing aircraft, P_i is the percentage of aircraft of the *i*th type and T_i is the delay imposed on the aircraft of ith type.

Considering the effect of runway capacity, it is desirable to analyze the sensitivity of depar-

ture cost for various aircraft mixes. Different airports have association with different air transport activities, and these differences can be expressed in terms of varying aircraft mix indices. Thus the aircraft mix index is a major sensitivity parameter in this model. The taxing time cost submodel employed in this analysis is shown in causal diagram form in Figure 5.1. The calculation of runway capacity is executed with the use of an interactive version of the upgraded airport capacity model - ACM - named AIRFRAME [Barrer, 1992].

FIGURE 5.1 Causal Diagram to Estimate Aircraft Delays and Taxing Times Changes.

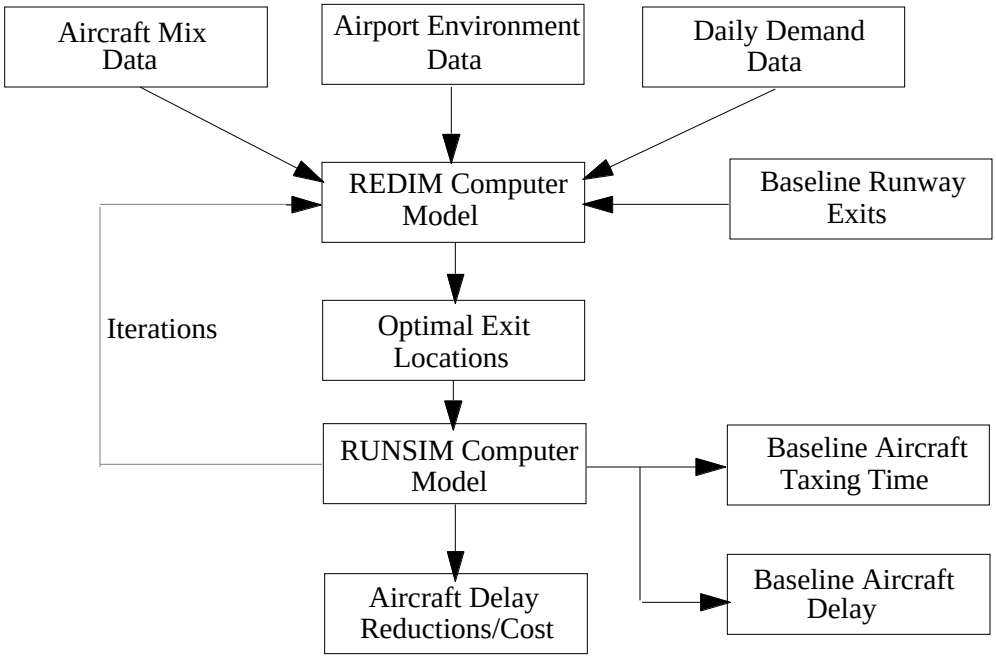

According to the design procedure of high-speed exit design, a typical high-speed cost evaluation analysis consists of the following four steps:

- Estimation of aircraft mix for the peak hour
- Specification of level of service for the facility and estimation of the gap between demand and supply
- Optimization of exit locations and numbers of exits to accommodate the expected aeronautical demand
- Cost/benefit evaluation

According to these four steps, we can see that there is a defined trade off between the level of service, including capacity and delay, and the cost of infrastructure construction. By converting the reductions of weighted average runway occupancy time (WAROT) into runway capacity and delay, we can know how much capacity gain could be obtained. This capacity gain is further converted to a monetary value by estimating the landing fee increases and

airline operation cost reductions caused by the reduced taxiing time. It is obvious that a balance can be reached. The causal diagram of high speed turnoff optimization procedure is shown in Figure 5.1.

The runway occupancy time ROT is an important factor to estimate runway capacity under VMC and IMC conditions. The ROT and the aircraft mix conditionally influence the runway capacity and delay. Landing fees increases and operating cost reductions are derived from the increased capacity and departure delay reductions obtained with the use of high speed runway turnoffs. It should be also noted that the magnitude of these capacity and delay variations is sensitive to the aircraft mix.

Construction cost is also another constrain in the high-speed exit implementation. For a given set of airport and aircraft mix conditions, there is an optimal number of exits. If more exits are build, the benefits of this runway in terms of ROT gains become less and less significant. Therefore the planning of high-speed requires a System Dynamics approach to balance the construction costs with delay reductions and capacity benefits. This is illustrated in Figure 5.1. Figures 5.2 through 5.3 illustrate

FIGURE 5.2 Runway Capacity Estimation Causal Diagram.

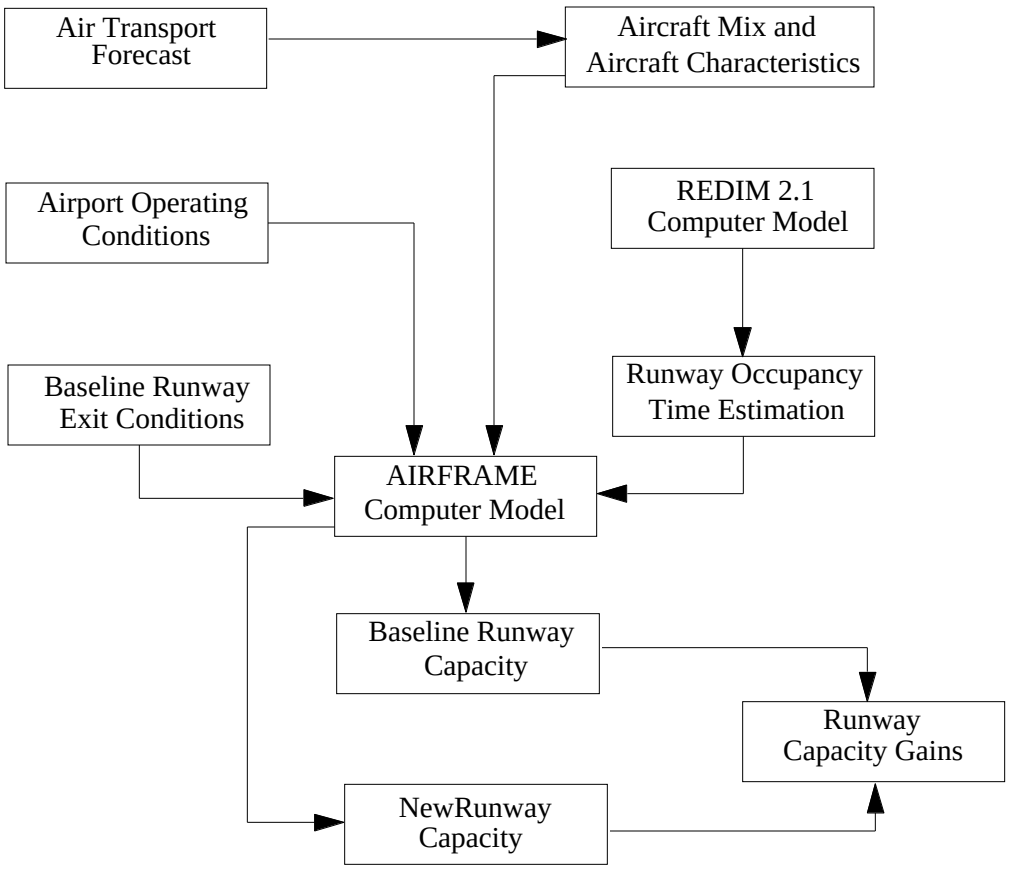

FIGURE 5.3 Taxing Time Reduction Estimation Causal Diagram.

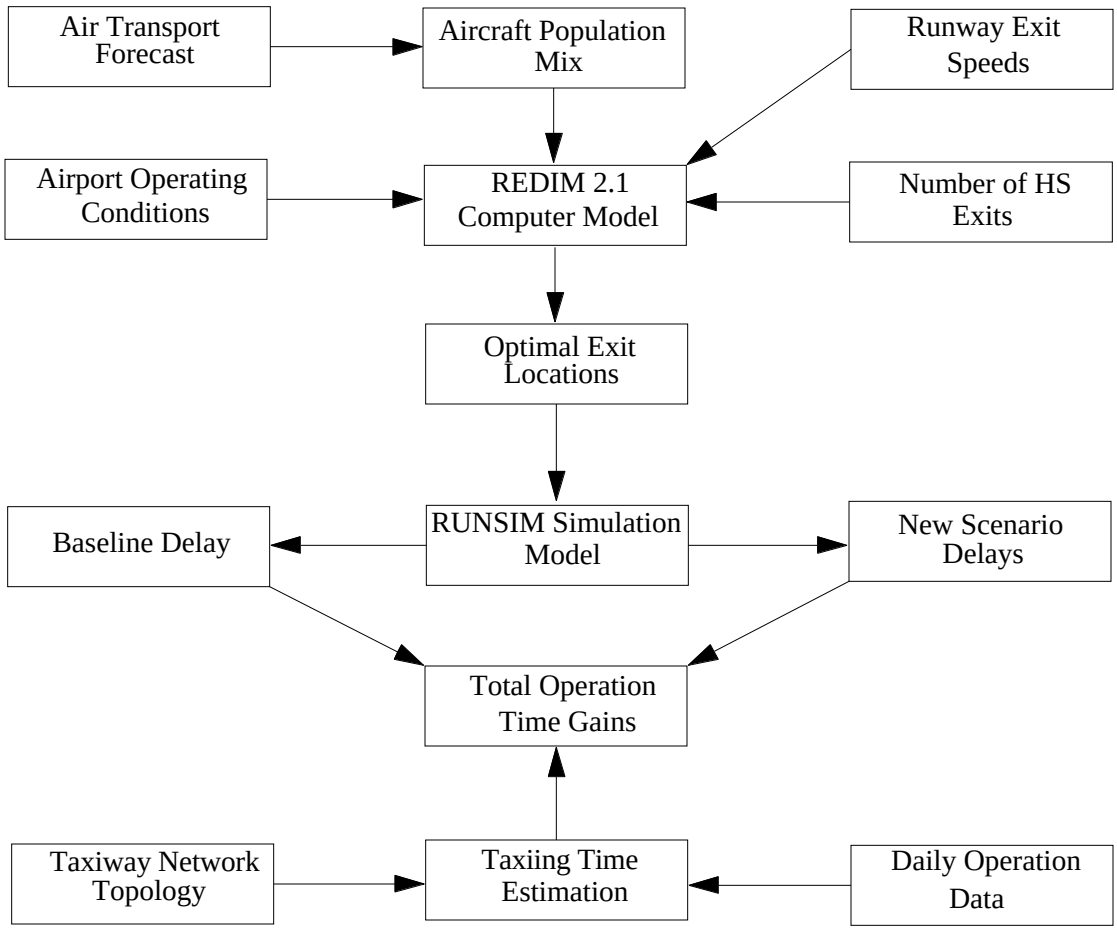

5.3 A Sample Application

In order to illustrate the use of the proposed method a baseline airport scenario was selected with a configuration similar to that shown in Figure 5.4. The baseline configuration has one runway and six 90 degree exits. Several input parameters were varied in the baseline scenario to test the sensitivity of cost/benefit results for selected exit speed turnoff configurations.

The following model parameters were investigated:

- Scenario 1- changes to aircraft mix index
- Scenario 2 - changes to landing fees
- Scenario 3 - taxing time and operating cost changes
- Scenario 4 - break even cost analysis

In the baseline scenario of Fig. 5.4 there is a single 3000 m. runway with four turnoffs. The major input parameters used for the analysis are discussed in the following paragraphs.

Arrival /Departure Ratio

In the analysis 50 percent of arrivals and 50 percent of departures were assumed for most of the scenarios. This implies that aircraft mixed operations apply.

Landing Weight Factors

This group of data is applied to landings only. The aircraft weight factor is a nondimentional parameter that indicates the percentage of the useful load carried by the aircraft at landing. A weight factor can vary from 0 to 1. The zero means the minimum landing weight and one means maximum landing weight.

In-trail Separations:

The current in-trail separations set by the federal Aviation Administration under both VFR and IFR conditions are used to simulate landing arrivals.

Airport Data

Data containing airport environment and runway exit characteristics for this baseline analysis are shown below.

5.3.1 Scenario 1

In a previous research effort [Trani et al., 1992], it was shown how the runway exit locations and configurations would affect the weighted runway occupancy time (WAROT) and hence the capacity of the runway to a specified aircraft mix index. However, it would be more helpful to have results for different aircraft mix indices so that the behavior of capacity changing with the aircraft mix could be readily ascertained. It is obvious that the hourly capacities for sixty general aviation aircraft and for sixty transport type aircraft are viewed differently by the airport managers.

Five aircraft mix indices were chosen to evaluate the capability of high-speed turnoff to increase the runway capacity. These data represent the aircraft mix comprising different aircraft categories as defined by current ATC standards (i.e., approach speed aircraft categories) and are shown in Table 5. 1. The simulation results indicated that when the aircraft mix index increases, as shown in Figure 5.5, the capacity decreases. This is reasonable because it is realized that when the runway has to operate with higher percentages of large aircraft, the runway occupancy times increase and the capacity decreases. However, if the

increased capacities were converted into percent increments of the baseline capacities as shown in Figure 5.6, we can see that the capacity gain does not increase monotonically.

When the aircraft mix index is low, as low as 57, the percentage of the increased capacity is relatively high, 11 percent; when the aircraft mix is near 72, the increased capacity decreased and then this percent increases again for higher mix indices. These results suggest that high-speed exits are capable of increasing the runway capacity under different aircraft mix indices; the percentage of the increase caused by the high-speed exits is sensitive to the aircraft mix specified. Also, we should notice that the lowest gain among the capacity values is not always associated with a fixed aircraft mix index. Results would be different from case to case depending upon the mix used in the analysis.

FIGURE 5.4 Airport Topology for Capacity and Delay Analysis.

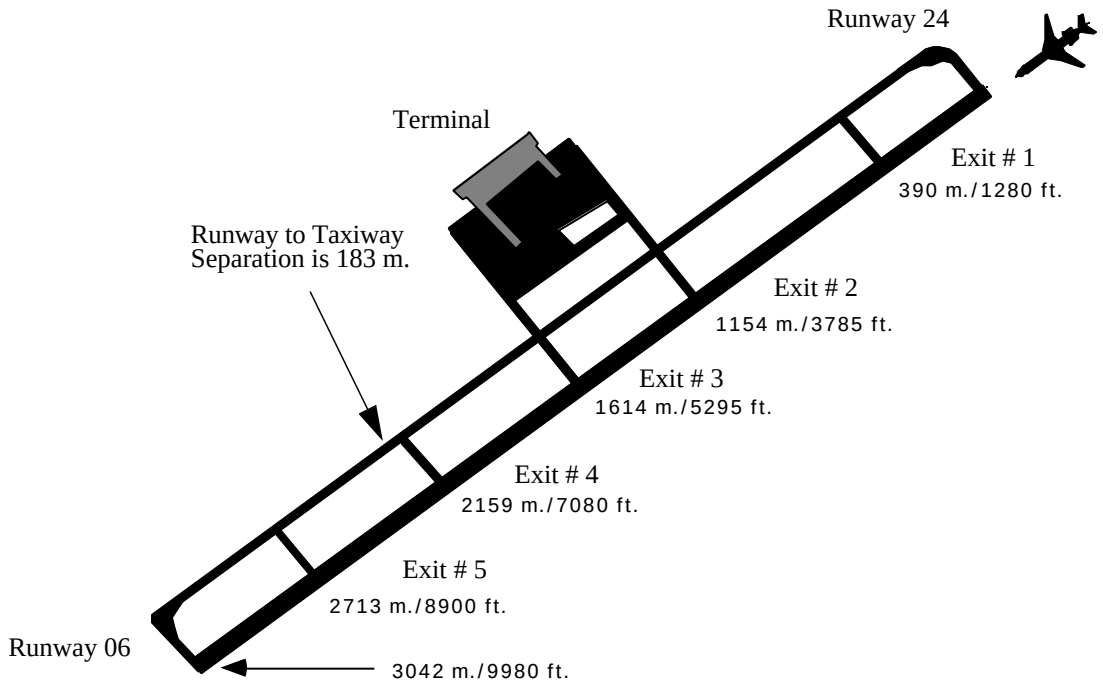

5.3.2 Scenario 2

Although high-speed exit can increase the capacity of a runway under certain conditions (i.e., VMC, mixed aircraft operations), it is difficult to evaluate the benefit of this improvement. Conceptually, the increase in capacity can allow more aircraft to land during the peak hours. The airport would therefore have more revenue from landing fees. Because landing fee depend on the take-off weight of aircraft, and the mean takeoff weights vary with the aircraft mix index, the landing fees are sensitive to both of the aircraft mix and the runway capacity which could be increased. Landing fees are also a function of the landing fee rate. To analyze the sensitivity of landing fee rate, values were varied from $1/1000 lb to $3/1000 lb, which are representative of landing fee rates for various airports. Besides

landing fee rates, the total operations per day in the baseline scenario were also considered as shown in Figure 5.1.

FIGURE 5.5 Runway Capacity vs. Aircraft Mix Index.

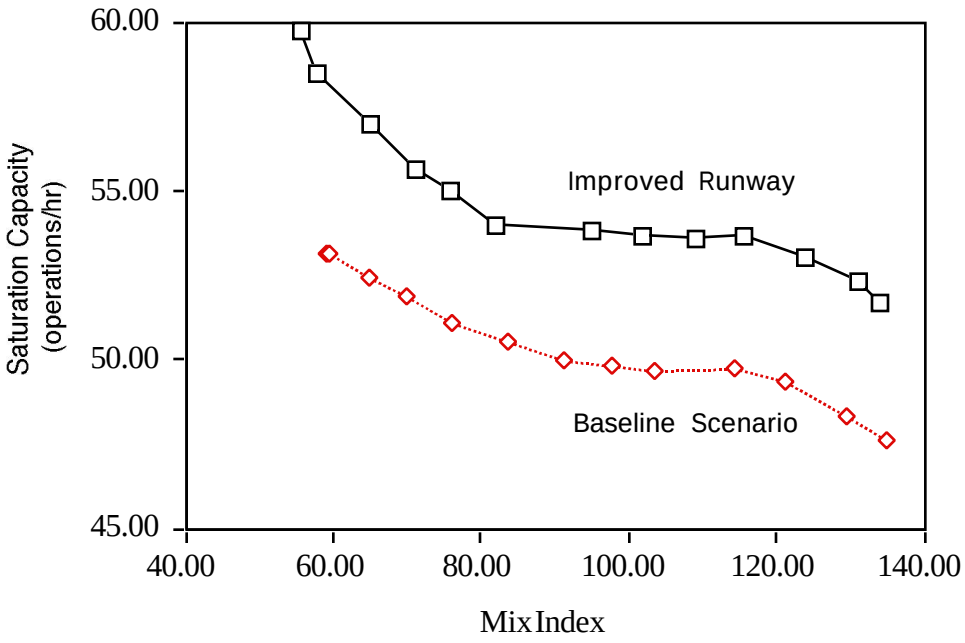

TABLE 5.1 Aircraft Fleet Mix Used in the Case Study.

Fleet Mix (%)	Group A	Group B	Group C	Group D
57	3	40	57	0
72	3	35	57	5
103	0	23	64	13
117	0	23	57	20
135	0	17	57	26

FIGURE 5.6 Capacity Gains for Different Aircraft Mixes.

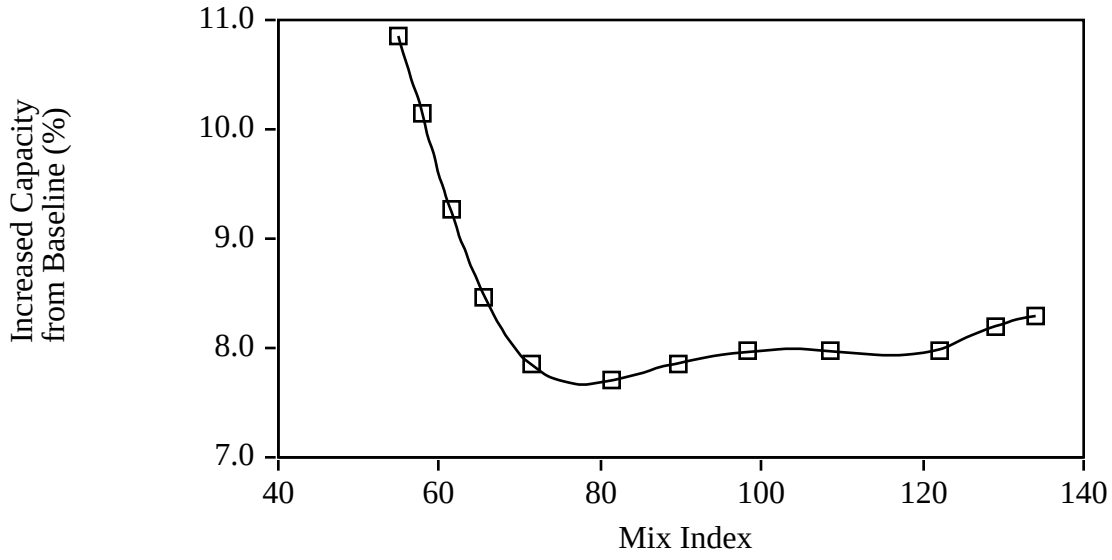

From the results shown in Figure 5.6 depicting the increased capacity for the baseline scenario, a certain percentage of capacity gain could be obtained by providing several high-speed exits with optimal locations along the runway. This means that the more operations per day (duration of peak hours) the baseline scenario has, the more new operations will be accommodated by high-speed taxiing. Thus, the number of operations during peak hours is also a sensitive parameter. Figure 5.7 illustrates the behavior of landing fee with aircraft mix along the life cycle. Figure 5.7 shows the behavior for a baseline scenario with 250 operations per day, landing fee rates of $1/1000 lb, $2/1000 lb, and $3/1000 lb were used. Contrary to the behavior of runway capacity, which indicates that capacity decreases when aircraft mix index increases, the total landing fee income increases if more transport or heavy aircraft are operated. Assuming a value of demand, high-speed exit infrastructure seem to offer clear benefits to the airlines, to the airport managers, and to passengers alike.

FIGURE 5.7 **Landing Fee Variations vs. Operations (20 Year Life Cycle).**

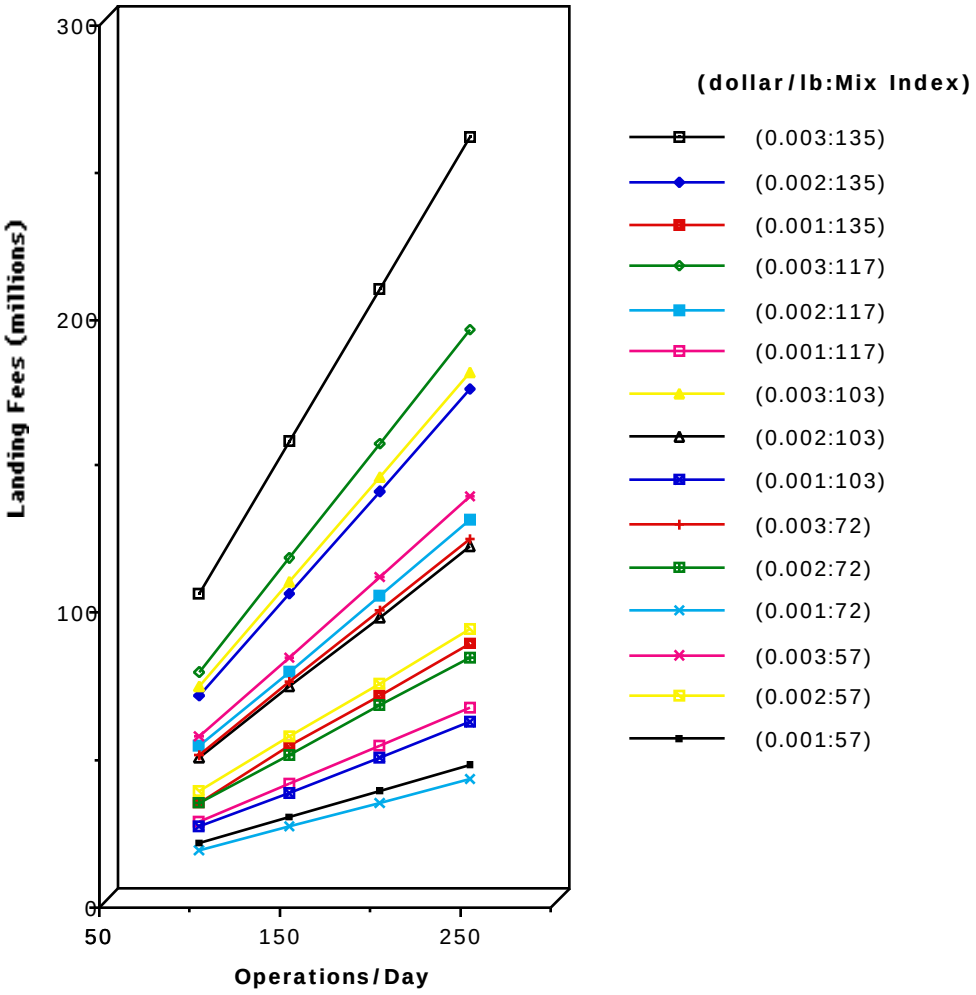

FIGURE 5.8 Landing Fees vs. Aircraft Mix.

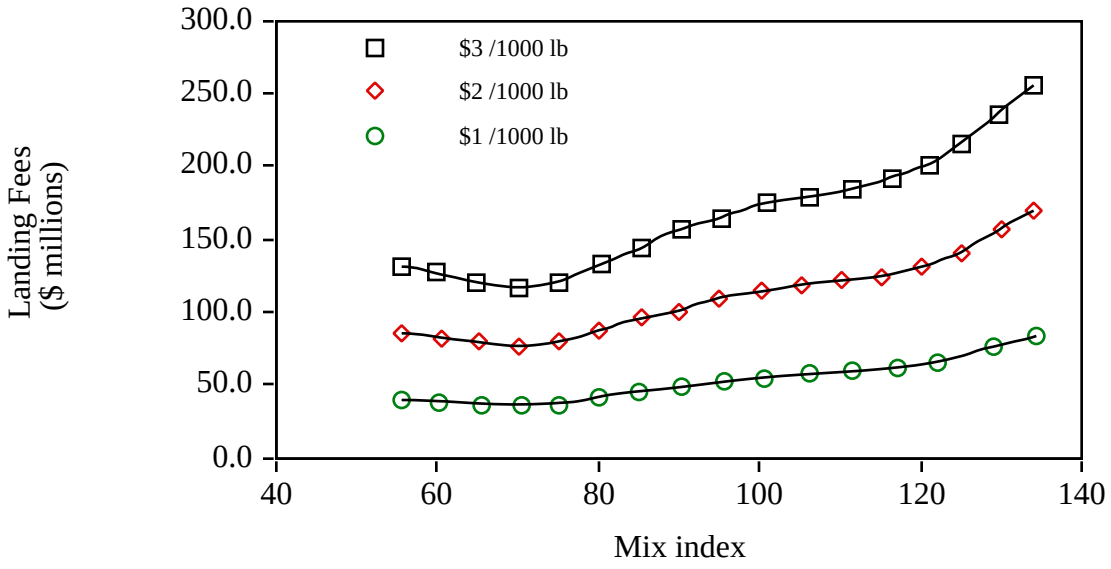

5.3.3 Scenario 3

The fact that high-speed exits are able to accommodate more landings and departures; taxiing time of the landing aircraft can also be reduced. Obviously, the saved taxiing time would reduce the airline operating cost. To get a quantitative perception of this idea, a typical aircraft mix was run by using RUNSIM to simulate the taxiing maneuver time saving due to the use of high-speed turnoff. This analysis used a configuration similar to SEATAC International Airport for the sake of illustration. and the aircraft mix is shown in Table 5.2. The taxiing optimal locations were generated from REDIM and put as parts of the input parameter in RUNSIM. Both of the saturation arrival and departure rates are 28 operations per hour which are the most expected operation rate under VFR condition (28 arrivals and 28 departures).

Figure 5.9 gives the taxiing times of baseline and improvement scenarios. From the figure we can see that, if four high-speed exits with optimal Locations are constructed eight types of aircraft will have significant reductions in taxing times. The highest reduction of taxiing time was 30 seconds for medium size transport aircraft. Also we can perceive from the data that the amount of taxiing time savings is associated with the proportion of a specified aircraft to some extent. For example, in the improved scenario, B 727 with the largest proportion in the mix, 19 percent, obtained 29.98 seconds of taxiing time saving, B 737, with the second largest proportion, 16 percent, obtained 19.41 seconds of taxiing time savings, and MD-83, with the third percentage, 12 percent, obtained 29.89 seconds of

taxiing time savings per operation. Another important result from the simulation was that

TABLE 5.2 SEATAC Airport Mix Index and Aircraft Landing Weight Factors.

Aircraft Name	Aircraft Mix	Weight Factor	Aircraft Name	Aircraft Mix	Weight Factor
A-300-600	2	0.8	DC-8-73	3	0.6
B-727-200	19	0.6	DHC-7	4	0.8
B-737-300	16	0.6	DHC-8-100	3	0.8
B-747-400	3	0.5	EMB-120	3	0.8
B-767-300	10	0.6	L-1011	3	0.6
BAe-31	10	0.8	MD-83	12	0.6
CE-208	1	0.8	PA-38-112	1	0.8
CE-421	4	0.8	SA-227-AT	12	0.8
CE-550	3	0.8			

no aircraft had the taxiing time increases caused the relocation of the exits. This speaks well of the capabilities of REDIM 2.1 as an optimization/allocation design tool. Figure 5.10 gives the total airline operation cost saving due to delay and taxiing time reduction. Figure 5.11 and 5.12 represent the cost savings from arrival and departure operations.

All the results described above support the following explanation: The high-speed exit location optimization procedure is able to reduce the runway occupancy time and hence increase the runway capacity; because the high-speed exit geometry can allow the aircraft to exit at a relatively very high-speed, taxiing times of the aircraft are also be reduced even when the exits are relocated and make a few aircraft taxi longer distances.

FIGURE 5.9 **Taxing Reductions for SEATAC International Airport.**

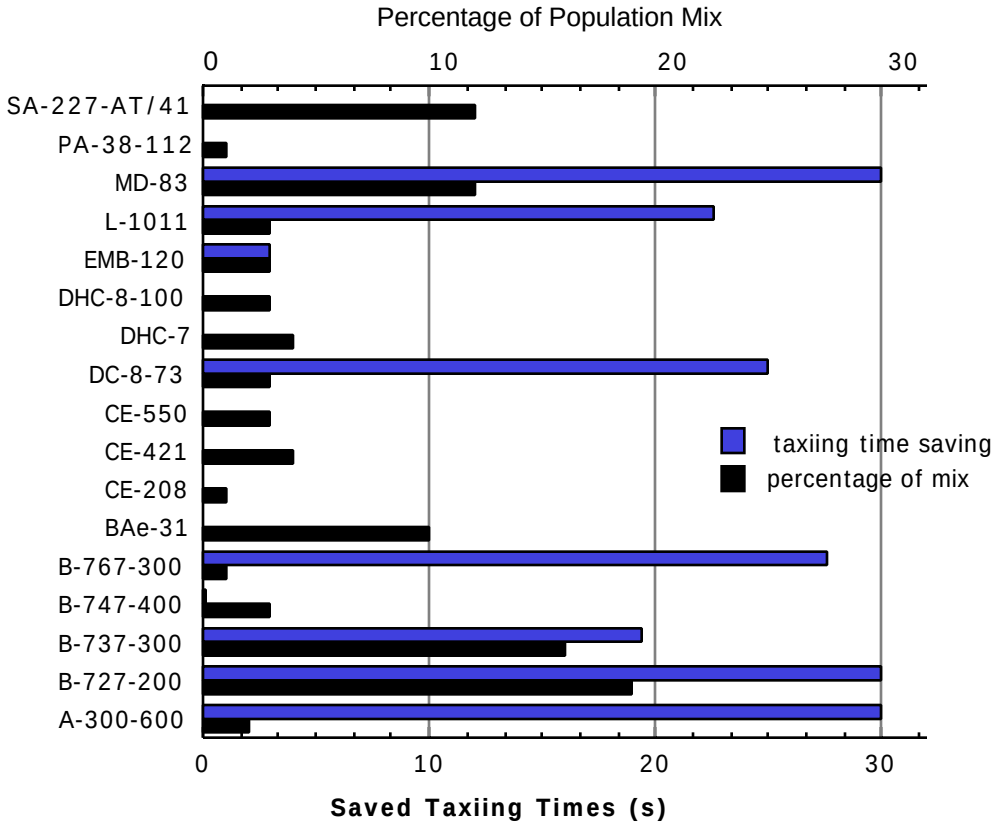

FIGURE 5.10 **Total Airline Operating Cost Reductions Along Life Cycle.**

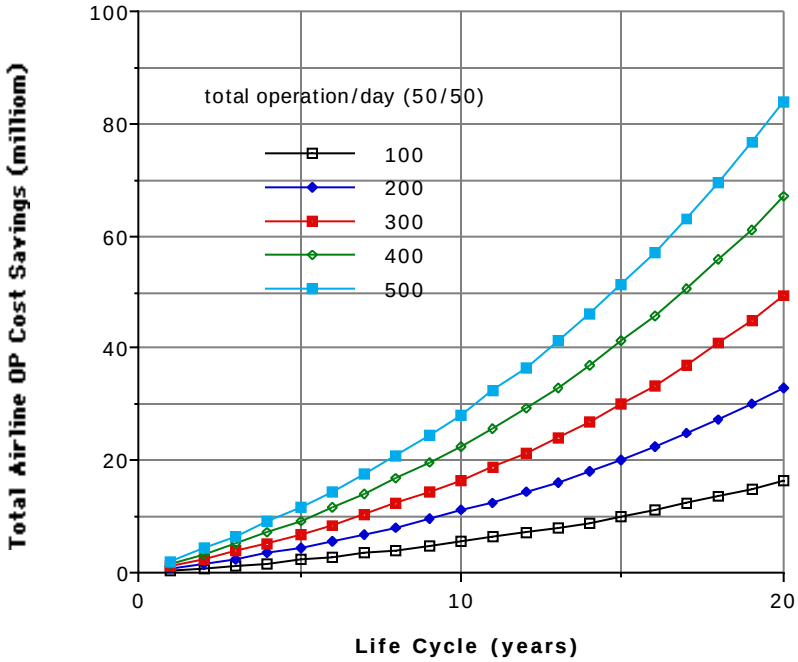

FIGURE 5.11 **Airline Operating Cost Savings Along Life Cycle Caused By Departure Delay Reductions.**

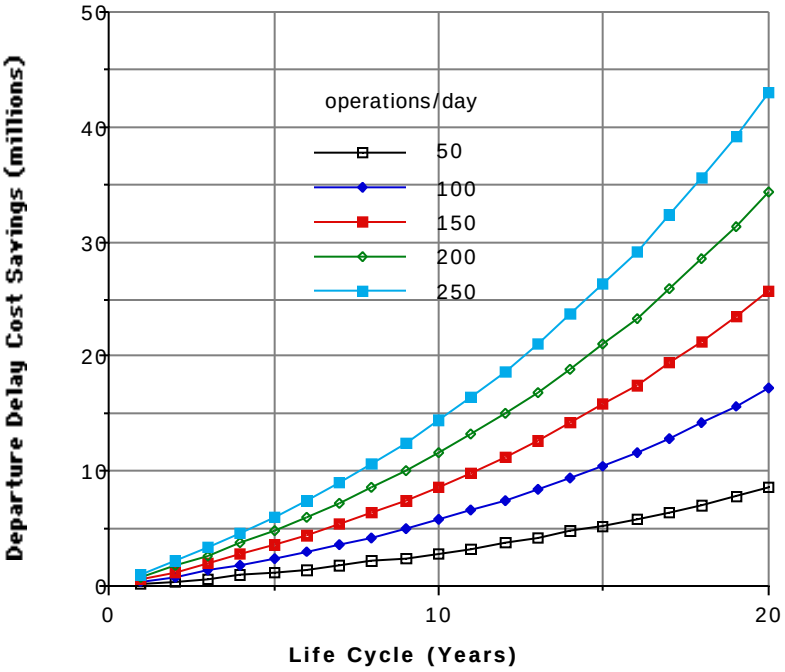

FIGURE 5.12 **Airline Operating Cost Savings Along Life Cycle Caused By Taxiing Time and Delay Reductions.**

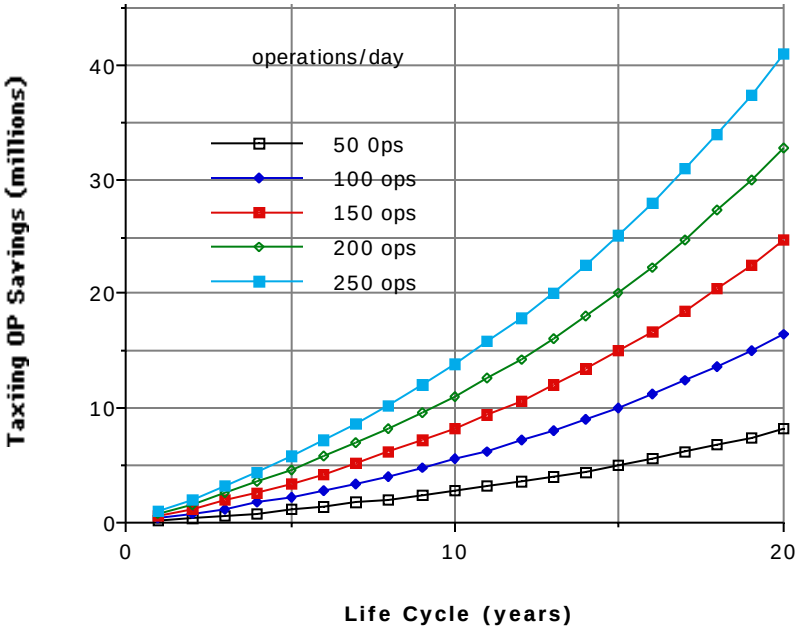

5.3.4 Scenario 4

It has been proved in scenario three that the installation of high-speed exits could increase the runway capacity and reduce the taxiing operation cost of the airlines. However, we should notice that the construction of high-speed exit needs some investment for the installation of the infrastructure at first. A preliminary cost-benefit analysis is necessary before any implementation of this type at an airport. Because construction costs are varied among construction firms and regions, this research will compute the break even cost given the potential revenue increases. The break even cost in this project is a pseudo construction and maintenance cost value of the facilities in the life cycle that, if the actual cost could be lower than this value, the high-speed exit construction project will be beneficial to the airport, passenger and airline operators. Because this analysis is from the point of view of the complete system, and it does not deal with any money flow between the airport and the airlines, the airline operating costs and passengers' savings were considered separately. It is believed that the break even cost contains more information than any computed net benefit or cost-benefit ratio derived from a specified construction cost.

Figure 5.13 gives results of the case study for SEATAC Airport Runway 16L including the limits of the construction and facility maintenance cost of the facilities in the life cycle per

single high-speed exit. Total requirements are two high-speed exits. From the diagram, we know the relationship between investment upper limits and the total daily peak hour operations (50/50). This case study assumes no air traffic growth exists which would be a very pessimistic case. The benefits are mainly from the delay reduction and taxiing time reduction. Simulation results show that the upper limit of investments vary from 2 million dollars to 13 million dollars per exit depending on the daily peak hour operations.

Figure 5.14 gives results for another case study (Greensboro Airport runway 23). From the diagram and given a specified aircraft mix index, we can find the break even limit of the construction and maintenance costs for a single exit (solid line). This case study applies for a scenario where the airport manager is planning to expand the airport service which can bring more landing fee revenue due to increased runway capacity. The net present value of break even costs vary from 6 to 13 million dollars per exit depending on the aircraft mix. Note that the region below the solid line represents a benefit region implying that any LCC cost in this region will result in a net benefit to the airport authority.

FIGURE 5.13 **Net Present Value of Break Even Cost for Each Exit. (Landing Fees Only over a 20 Year Life Cycle).**

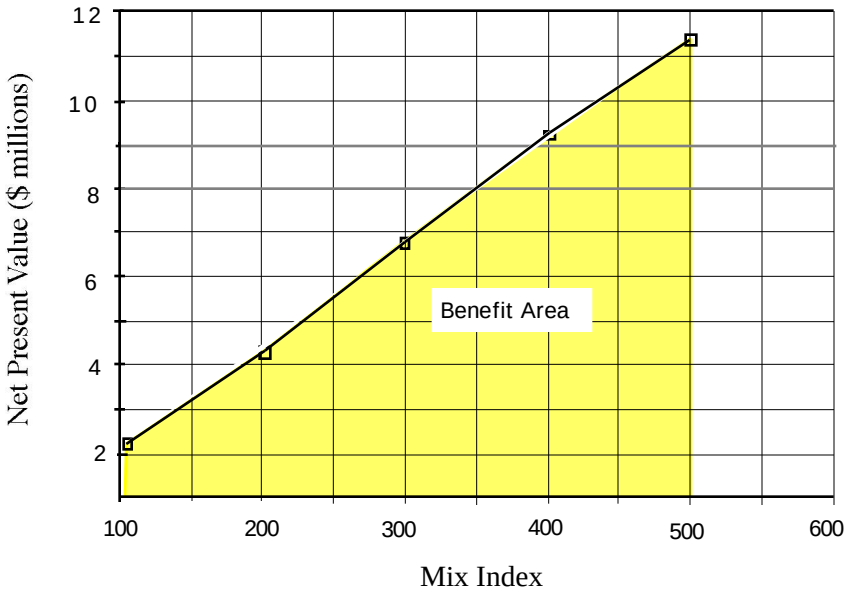

FIGURE 5.14 **Present Value of Break Even Cost for Each Exit (Airline Operation Cost Only over a 20 Year Life Cycle).**

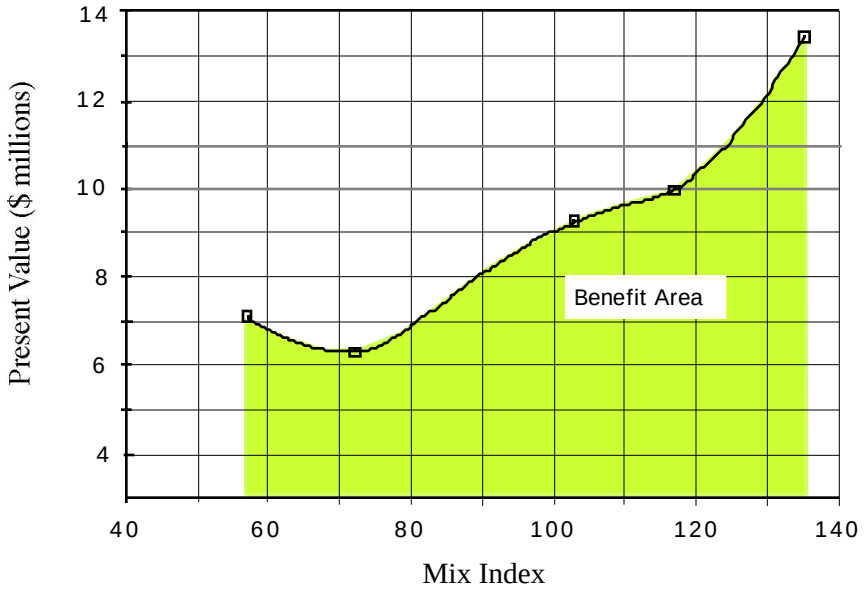

The runway occupancy time ROT is an important factor to estimate runway capacity under VMC conditions. The ROT and the aircraft mix conditionally influence the runway capacity and delay. The landing fee increases and operating cost reductions are derived from the increased capacity and departure delay reduction, and also depended on the aircraft mix.

Construction cost is also another constrain in the high-speed exit implementation. For a given set of airport and aircraft mix conditions, the optimal number exist. If more exits are build, the economic gain is less significant. Therefore the planning high-speed requires a system dynamic approach to balance the construction costs with delay and capacity benefits. This is illustrated in Figure 4.9

5.3.5 Simulation Results Using Existing and Futur e Air Traffic Control Rules

Under existing air traffic control conditions the interarrival separations under IFR conditions follow a 6/5/2.5 nautical mile rule. The simulations were carried out from the final approach fix for arrivals and from the gate for departures to simplify the analysis. An aircraft mix representative of a large hub airport facility was also used in these simulations. Several input parameters were varied from the "baseline scenario" to test the sensitivity of the model when the number of exits and their types are varied.

Data for arrival and departure rates was assumed to follow a poisson distribution. The interarrival and interdeparture times were varied from 125 seconds to 150 seconds to test the sensitivity of the runway delay to varying demand rates. In this range the total arrival delay is very sensitive to the demand rate because the demand is reaching the arrival capacity of the runway. The model however, is flexible enough to allow any combination of interarrival and interdeparture times. Due to the stochasticity of the model 500 arrivals and 500 departures were used per iteration to represent operations over a long period of time. Air traffic control time buffer data used were derived from observed values in ATC simulators [Credeur, 1989].

With this data, and for each interarrival time RUNSIM was run for five iterations to generate data for total delay for arrivals and departures, weighted average runway occupancy time (WAROT) and its standard deviation. The average values of these runs was used for plotting a demand versus average delay graph as shown in Fig. 5.15.

FIGURE 5.15 Arrival Delay Curves for Various Runway Scenarios.

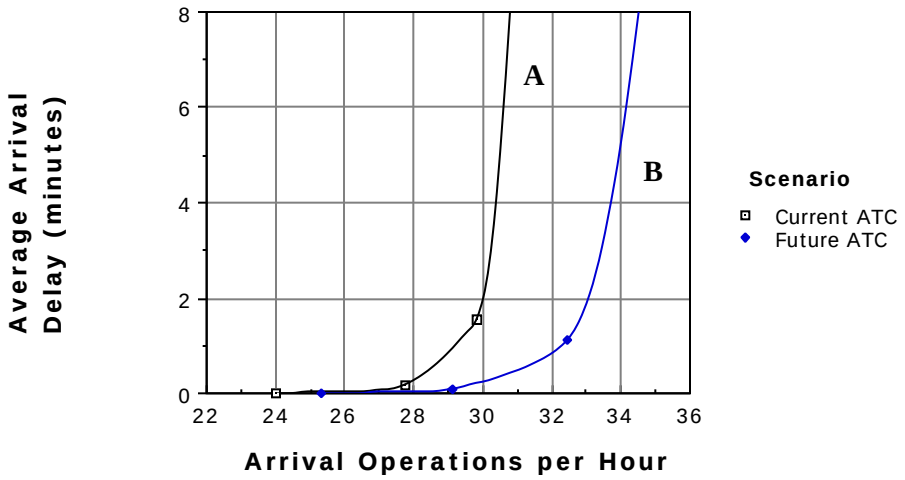

These figures illustrate that as the demand nears the ultimate capacity (i.e., capacity associated with an infinite delay) the total delay increases very rapidly. For the baseline scenario and an acceptable average delay of 4 minutes, the practical capacity for arrivals is 30.2 arrivals per hour under current ATC conditions. The resulting WAROT of the aircraft population is 54.5 seconds. In this study the effects of runway exit replacement are investigated to ascertain runway occupancy time gains possible with the implementation of standard high speed exits as well as REDIM generated geometries. The scenarios shown in Table 5.3

were investigated:

TABLE 5.3 Runway Scenarios Investigated for ROT Gain Analyses.

Scenario Number	Scenario	Runway Exits Description	Exit Speed (m/s)
1	Baseline	5 usable 90 degree runway exits	8.00
2	Wide Throat	Replace exits 1 through 4 with four optimally located “wide throat” turnoffs	15.00
3	30 Degree Standard FAA	Replace baseline exits 1-4 with four optimally located 30 degree acute angle exits	23.00
4	30 Degree Modified Exit	Replace baseline exits 1-4 with four optimally located 30 degree, modified entrance acute angle exits (i.e., 427 m. entrance spiral)	26.00
5	REDIM 3030	Replace baseline exits 1-4 with four optimally located REDIM generated turnoffs with 30 m/s exit design speed	30.00
6	REDIM 3530	Replace baseline exits 1-4 with four optimally located REDIM generated turnoffs with 35 m/s exit design speed	35.00

Table 5.5 illustrates the possible gains in weighted average runway occupancy time ranging from 54.5 seconds for the baseline scenario down to 36.8 seconds for the implementation of REDIM high speed geometries designed for 35 m./s. and an exit angle of 20 degrees. The reader should notice that these improvements apply for a runway whose exit locations have been replaced by optimally located turnoff on each category. Note from Table 5.5 that as the exit design speed (i.e., entry turnoff speed) is increased the optimal locations shift closer to the threshold as one might expect.

A plot of the average interarrival delay per aircraft are shown in Fig. 5.15 (curve labeled A) corresponding to existing final approach ATC separation rules. This result is not surprising since, under current ATC conditions, the interarrival separation and not the ROT of the aircraft is the critical factor governing the capacity and delay. An important result from this capacity and delay analysis is that the average delay for departures decreased significantly for a fixed level of departure operations. Figure 5.16 illustrates this for four of the six configurations studied where a significant shift in the departure delay curve is observed as the design exit speed is increased. The reason behind this shift is the availability of more acceptable gaps for departures, an effect of decreased WAROT for a single runway under mixed aircraft operations

The current ATC separation rules set by FAA is the critical parameter governing the delay at most airport facilities. By improving the technology in dealing with wake turbulence, improved radar technology for better air traffic control, the FAA proposes to decrease the interarrival separation to the values shown in Table 5.6. This scenario studies the effect of new ATC separation rules on capacity and delay. The model is run by changing the arrival separation to the new values and keeping the other values same as in "baseline scenario". Figure 5.16 shows the arrival delay relationship of this scenario, where the capacity (practical) has increased to 34.0 operations per hour, which is an increase of near 4 operations (arrivals) per hour as compared to the present rules.

TABLE 5.4 Current and Future ATC Aircraft Inter-Arrival Separation Criteria.

Leading Aircraft	Current ATC Separation				Future ATC Separation		
	Trailing Aircraft				Trailing Aircraft		
	Small	**Large**	**Heavy**		**Small**	**Large**	**Heavy**
Small	2.5 (84)	2.5 (64)	2.5 (60)		2.0 (65)	2.0 (51)	2.0 (48)
Large	4.0 (131)	2.5 (64)	2.5 (60)		3.0 (98)	2.0 (51)	2.0 (48)
Heavy	6.0 (196)	5.0 (129)	4.0 (96)		5.0 (163)	4.0 (103)	3.0 (72)

Cell values represent separations and headways in **nautical miles** and **seconds**, respectively.
Assumed approach speeds: 1) 110 knots for small, 2) 140 knots for large and 3) 150 knots for heavy aircraft.

Hence for REDIM exits to be more effective and to achieve a balance between the airspace arrival and runway practical capacities, the ATC separations have to be further decreased through the use of new technology. The ultimate goal is to allow smaller separations between adjacent arrivals and a corresponding reduction in the position errors of approaching aircraft.

TABLE 5.5 Aircraft Population Used for Capacity and Delay Analyses.

Aircraft	Percent Mix	TERP Classification	Aircraft	Percent Mix	TERP Classification
Cessna 208	3	A	Boeing 767	2	D
Saab 340	10	B	BAe-146	5	C
EMB 120	8	B	Boeing 727	15	C
SA 227	12	B	Boeing 737	15	C

TABLE 5.5 Aircraft Population Used for Capacity and Delay Analyses.

Aircraft	Percent Mix	TERP Classification	Aircraft	Percent Mix	TERP Classification
Boeing 757	5	C	Grumman IV	3	C
Boeing 747	3	D	MD 11	2	D
CE 550	5	B	MD 83	12	C

TABLE 5.6 Summary of Turnoff Locations for Capacity and Delay Airport Scenarios.

Scenario Number	Scenario	Runway Exits Description Exit Location (m.) Exit Type						Weighted Average ROT (s.)
		Exit # 1	Exit # 2	Exit # 3	Exit # 4	Exit # 5	Exit # 6	
1	Baseline	390 90 deg.	1154 90 deg.	1614 90deg.	2159 90 deg.	2713 90 deg.	3042 90 deg.	54.50
2	Wide Throat	390 90 deg.	950 WT	1225 WT	1425 WT	1900 WT	3042 90 deg.	51.20
3	30 Degree Standard FAA	390 30 deg.	950 30 deg.	1200 30 deg.	1400 30 deg.	1925 30 deg.	3042 90 deg.	44.63
4	30 Degree FAA Modified Exit[a]	390 90 deg.	900 30 deg. modified	1150 30 deg. modified	1350 30 deg. modified	1875 30 deg. modified	3042 90 deg.	43.00
5	REDIM 3020[b]	390 90 deg.	875 RE 3020	1125 RE 3020	1325 RE 3020	1825 RE 3020	3042 90 deg.	40.80
6	REDIM 3520[c]	390 30 deg.	825 RE 3520	1050 RE 3520	1250 RE 3520	1650 RE 3520	3024 90 deg.	36.80

a. The FAA modified 30 degree, acute angle geometry includes a 457 m. (1400 ft.) transition spiral.
b. The designation RE 3020 implies a high-speed exit designed for 30 m/s entry speed and a 20 degree exit angle.
c. The designation RE 3520 implies a high-speed exit designed for 35 m/s entry speed and a 20 degree exit angle.

CHAPTER 6

High Speed Turnoff Operational Requirements and Turnoff Geometric Design

In order to verify some of the mechanics associated with an aircraft turning at high speed a series of models were developed to estimate turnoff trajectories and possible side forces developed in aircraft tires. Two types of models were used in this regard: 1) first order turning models, and 2) multi-degree of freedom models. This chapter discusses some of these models in more detail.

6.1 Turnoff Models

Digital computer models can simulate aircraft ground trajectories describing the motion of an aircraft as it negotiates a high speed turnoff. The importance of the high order model is the possible incorporation of external forces and moments that could affect the stability characteristics of the vehicle as it travels at moderate speeds on the ground. The examples described here explore three basic sensitivity parameters judged important in the safe completion of a turnoff maneuver: 1) wind disturbances, 2) runway pavement friction characteristics, 3) aircraft speed variations and 4) human control tracking behavior.

6.1.1 First Order, Time Varying Turnoff Model

Although the simulation model used in the previous section serves well to predict the detail trajectory of an aircraft vehicle negotiating a runway exit its complexity to implement in an optimization procedure to find optimal locations of turnoff locations renders it impractical. A simple approximation to the nonlinear high order model can be stated if one considers the aircraft as a point mass free to move in the yawing aircraft axis. I this case the aircraft moment of inertia I_{zz} term acts as a damping mechanism introducing a time lag effect to the single degree of freedom equation of motion.

Neglecting the contribution of the rolling moments to the turning capabilities of an aircraft, the behavior can be described as a first order, time-varying system where the state variable is represented by the radius of the curvature, R. The differential equation of motion representing the time variations of R has been adapted from Schoen et. al. (Schoen et al., 1984) to include nonlinear skidding friction and lifting force terms as shown in Eq. 6.1. In this expression it is seen that the total nose gear lateral skidding friction coefficient, μ_{skid} is modeled as a linear combination of the yaw inertia, centripetal force and scrubbing force coefficient contributions as depicted in the first bracket term in Eq. 6.1.

$$\dot{R} = \text{Min} \left\{ \begin{array}{l} \dfrac{\left[f_{skid}\ (PSI, V) - \dfrac{V^2}{g\,R} - f_s\ (R) \right] R^2 \left\{ m - .5\ \rho V^2 S\, C_L \right\} g\ \ wb\ \ lm\ \left\{ 1 - \dfrac{lm}{100} \right\}}{100\ I_{zz}\ V} \\ \\ \dfrac{J_n\ R}{a_n} \end{array} \right. \qquad \textbf{(6.1)}$$

Where, V is the aircraft speed, m is the aircraft mass, ρ is the air density, S is the aircraft gross wing area, CL is the average lift coefficient in the landing ground roll configuration (i.e., low angle of attack and large flap deflections), lm the landing mass supported by the main landing gear, wb is the aircraft wheelbase, I_{zz} is the aircraft moment of inertia around the vertical axis, f_{skid} denotes the nonlinear functional relationship between the skid friction coefficient, tire pressure (PSI) and aircraft speed (V). Similarly, f_s is a nonlinear functional relationship between the scrubbing side friction coefficient contribution with turning radius approximated by suitable polynomial functions (Trani et al., 1990). The term f_{skid} is usually corrected by a safety factor in order to characterize the turn well below the impending skid condition.Note that in Eq. 6.1 it is necessary to introduce a human comfort factor constraint in terms of the normal acceleration and jerk, a_n and J_n, respectively.

This turnoff characterization algorithm was compared with actual aircraft landing gear path observations made by Horonjeff (Horonjeff et. al., 1958, 1960) for a Boeing KC-135 transport-type aircraft with an entry exit speed of 26.8 m./sec. (60 m.p.h.). The results were in excellent agreement for the KC-135 and the Boeing 707-131 aircraft. It is evident from this formulation that large increases in the aircraft yaw inertia term would result in larger turning radii as demonstrated in Fig. 6.1.

FIGURE 6.1 Comparison of Various Turnoff Trajectories for Transport-Type Aircraft.

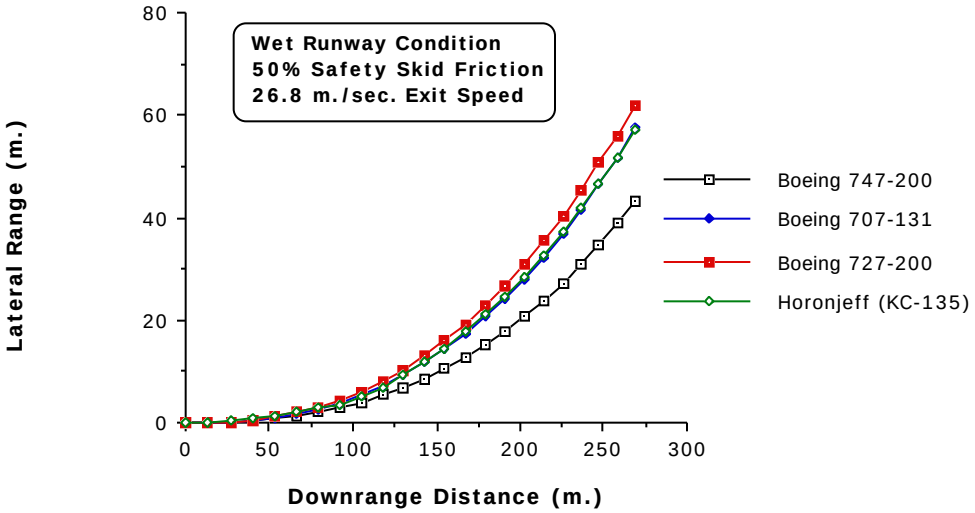

The integration of Eq. 6.1 can be executed numerically producing the instantaneous radius of curvature throughout the turnoff maneuver.

$$R_t = R_{t-1} + \int_{t-1}^{t} \dot{R}\, dt \qquad \textbf{(6.2)}$$

In a similar fashion the instantaneous Cartesian coordinates of the aircraft nose gear as it tracks the turnoff geometry are found by integrating the aircraft speed components in the lateral and downrange directions (a two degree of freedom model). This integrating procedure is also used to estimate the turnoff time (TOT) defined as the interval of time elapsed between the aircraft nose gear reaching the point of curvature (P.C.) of the turnoff and the time when all parts of the aircraft (i.e., wing tip or tailplane tip) clear the imaginary runway edge plane as depicted graphically in Fig. 6.2. In general, it has been found that, for a high-speed turnoff, the time consumed in the turn varies from 9 to 16 seconds depending upon the exit angle configuration, aircraft wingspan and runway width. This emphasizes the importance of the turnoff maneuver not only in terms of its geometric characterization but also in terms of the relative contribution of the Turnoff Time (TOT) to Runway Occupancy Time (ROT).

FIGURE 6.2 Basic Definitions of a High-Speed Runway Turnoff Model.

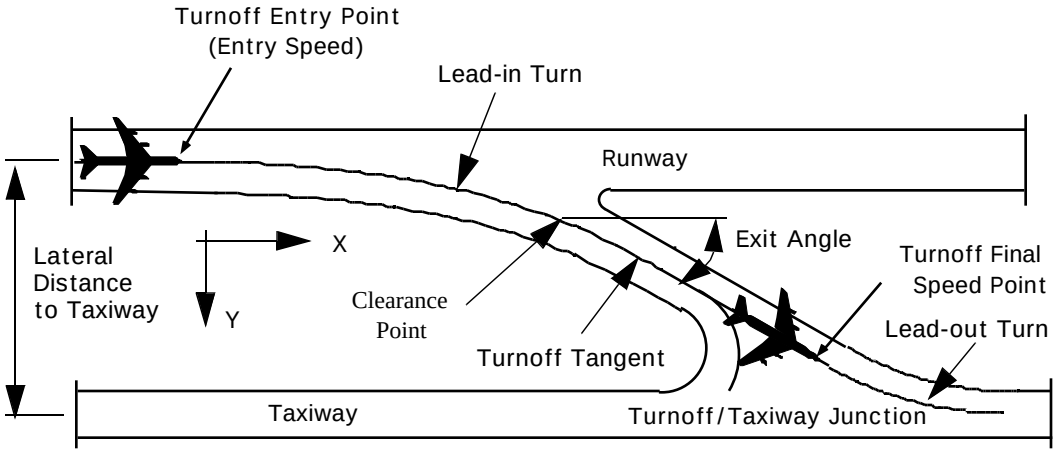

Geometries derived using Eq. 6.1 and having linear turnoff width tapers between metric stations 250 and 500 are were evaluated by pilots in a Boeing 727-200 simulator at the FAA Aeronautical Center in Oklahoma City. The results of these simulations seem to suggest that higher speed turnoffs are feasible at the same perceived level of safety if geometric changes are made to the throat section of the turnoff and if shallow turnoff angles are implemented (say 20 degrees instead of 30 degrees used in the standard acute angle exits today).

6.2 Runway Exit Design Implications

About 190 airports in United States have implemented FAA standard high-speed geometries (FAA, 1981). As many of these facilities were originally planned in the late forties and fifties they adopted lateral taxiway design standards that were not necessarily compatible with the lateral requirements of today's high-speed turnoffs. Many of these facilities have separation distances between runway and parallel taxiway centerlines of only 122 m. (400 ft.). These distances are, in general, inadequate to expedite aircraft from an arrival runway at high-speed unless a different turnoff design philosophy is adopted and smaller turnoff angles are used replacing existing 30 degree geometric design standards. A 122 m. separation distance between the runway and a parallel taxiway leaves pilots with very little room for decelerating an aircraft on the turnoff tangent and this might well be one of the leading contributing factors in the poor use of existing high-speed runway turnoffs at various airports reported in several field studies (HNTB, 1975; Koenig, 1978; Ruhl, 1990).

Using continuous simulation it is possible to derive lateral distance requirements to decelerate an aircraft for various turnoff entry and final speeds. Fig. 6.3 illustrates aircraft speed profiles for various aircraft deceleration values on the tangent segment of the turnoff. All curves were derived using a turnoff entry speed (V_{exit}) of 26.7 m/s at the point of intersection of the turnoff geometry and the runway centerline.

FIGURE 6.3 Aircraft Speed vs. Lateral Distance Traveled on a Modified FAA.

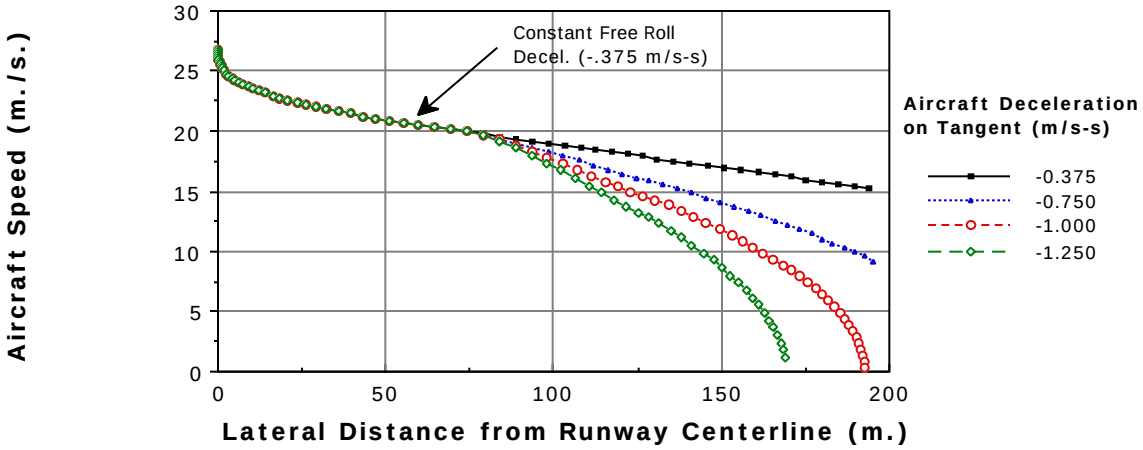

In Fig. 6.3 the abscissa represents the lateral distance of the aircraft nose gear (reference point) measured from the runway centerline. The construction of minimum recommended lateral distances measured from runway to taxiway centerlines for geometries using a 427 m. (1400 ft.) transition spiral is illustrated in Fig. 6.4. The results presented here were derived using a constant -.75 m/s^2 deceleration on the tangent with a third order deceleration time delay representing a realistic braking schedule. Other deceleration schedules and variations in the final exit angle can be derived using the same principle. The net effect of reducing the exit angle, θ, is a corresponding reduction in the minimum lateral space requirements needed to implement high-speed turnoff geometries at the expense of downrange distance. Using as illustration a turnoff with design entry speed of 26 m/s and a desired final speed at the starting point of the lead-out curve (see Fig. 6.2) of 15 m/s. it can be seen that a reduction of 33% in the lateral distance requirement is possible if the exit angle is reduced from 30 to 20 degrees (e.g., from 165 m. for $\theta = 30$ degrees to 110 m. for $\theta = 20$ degrees).

Deceleration values on tangents of up to 0.75 m/s^2 would seem acceptable for well designed turnoffs although further simulator testing is needed to confirm this point. This deceleration is about half of that used on runways by most transport-type aircraft [Horonjeff et al., 1959; HNTB, 1975; Hosang, 1978].

6.2.1 Runway Exit Entry Speed Limitations

Here we examine the limitations on turnoff entry speed as they apply to existing and newly proposed turnoff geometries (see Appendix H). Fig. 6.5 illustrates entry speed turnoff limitation curves for the most critical heavy transport-type aircraft currently in service (i.e., aircraft approach group D/Design Group V) derived from a study for NASA and FAA (Trani, Hobeika, et al., 1991).

FIGURE 6.4 Recommended Runway to Taxiway Separation Criteria for Modified.

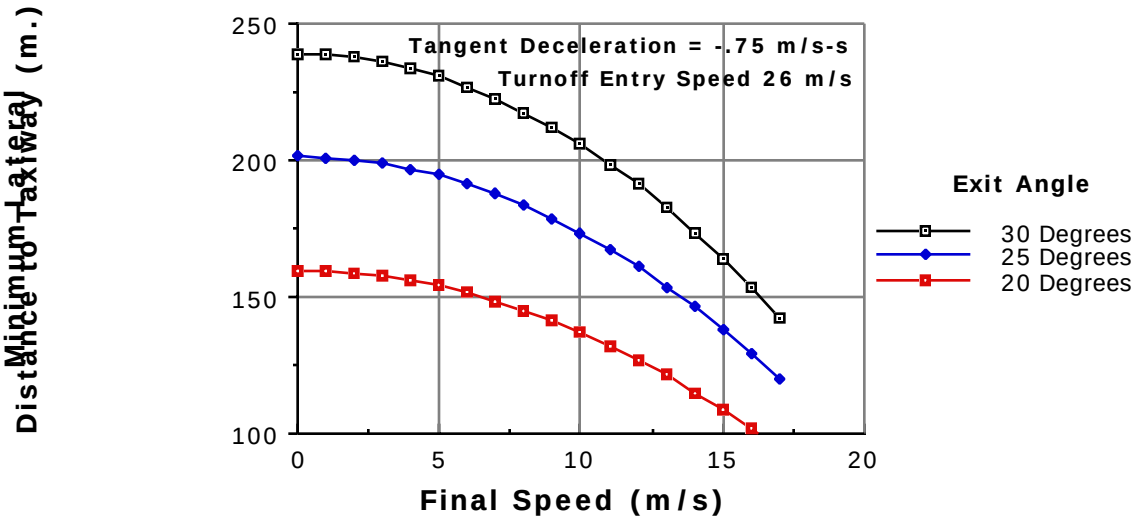

The interpretation of these curves is as follows: Select a desired turnoff exit speed (V_{exit}) on the horizontal axis and a final speed at the turnoff-taxiway junction (see Fig. 6.2 for nomenclature) then estimate the minimum lateral distance to a parallel taxiway in the ordinate axis. Taking as a numerical example an exit design turnoff speed of 30 m/s (67 m.p.h.) and using a final speed of 17.5 m/s (39 m.p.h.) it can be seen from Figure 6.5 that a minimum lateral separation of 182 m. (600 ft.) is required to execute the turn comfortably for an exit angle of 30 degrees. If the designer selects an exit angle to 20 degrees instead a minimum recommended lateral distance of 117 m. (383 ft.) could satisfy the same turnoff entry and final speed conditions. These curves are useful for design and planning purposes in the presence of lateral constraints. Similar curves have been derived for commuter aircraft (approach group B) and medium size transport aircraft (Trani, Hobeika et al., 1991).

In general there are two well defined types of constraints to be investigated before a high-speed turnoff is a feasible exit candidate on any runway: 1) geometric and 2) operational constraints. Fig. 6.5 addresses the operational constraints by limiting entry and final turnoff speeds. Geometric constraints refer to the minimum lateral separation distances between runways and the taxiway subsystem dictated by the physical shape of the turnoff. For example, the minimum desirable geometry of a standard 30 degree angle turnoff would consist of a lead-in turn segment followed by a lead-out segment with no tangent. This minimal configuration requires 106 m. (350 ft.) if a lead-out turn segment is provided with no double back. A double back solution would necessitate at least 167 m. (550 ft.) for design group V standards. Simple rules for the lateral characterization of turnoff geometries are contained in document DOT/FAA RD-92/6,II (Trani, Hobeika et al., 1992).

FIGURE 6.5 **Recommended Runway to Taxiway Separation Criteria for High Speed Turnoff Geometries Modeled Using a Boeing 747-400.**

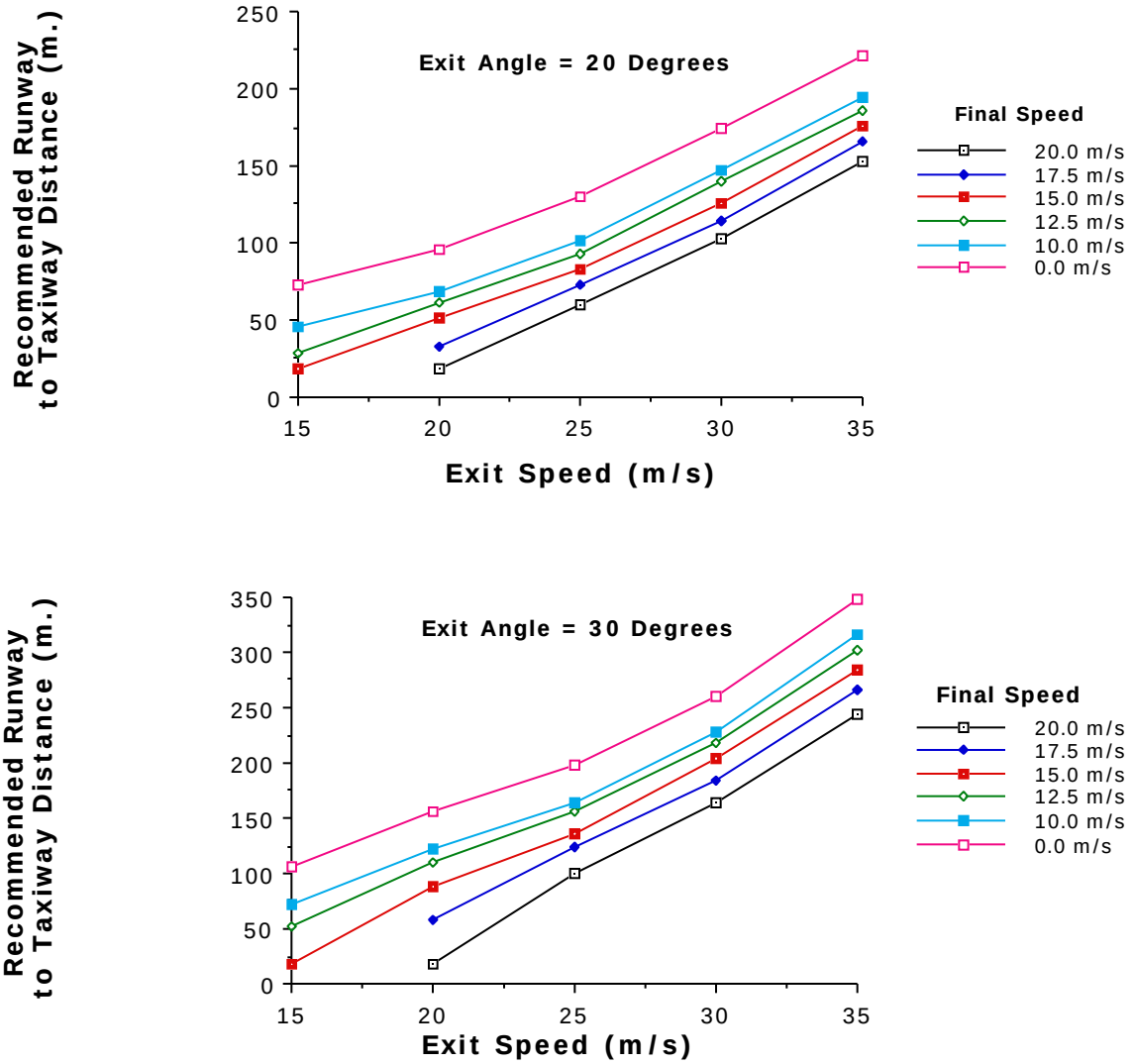

6.3 Runway Exit Longitudinal Constraints

Runway turnoff geometries designed for high exit speeds require large downrange distances between the runway/turnoff to turnoff/taxiway intersection points (see Fig. 6.3) for their implementation. A modified 30 degree angle turnoff geometry with a 427 m. (1400 ft.) transition spiral requires 670 m. (2198 ft.) between the P.C. of lead-in turn and the P.T. of lead-out turn if a 183 m. (600 ft.) lateral spacing between runway and taxiway centerlines is

used. Large downrange turnoff requirements have the potential drawback of limiting the number of turnoff geometries that could be implemented at a runway facility. A clear trade-off exists between the number of exits and the turnoff design exit speeds. Nevertheless the use of three or more optimally located high-speed turnoffs yields substantial reductions in weighted average runway occupancy time (WAROT).

6.3.1 Six Degree of Freedom Simulation Model

A six-degree-of-freedom (6 DOF) aircraft simulation model was developed in this research effort. The main objective of this model was to compare the maximum aircraft ground maneuvering envelope with the required turning commands necessary to steer the vehicle through some of the high speed turnoffs proposed in this research effort.

To simulate the aircraft turnoff maneuver, a flight vehicle can be represented as a ground vehicle moving in three dimensions. Mathematically, three aircraft force equations of motion with respect to a set of body axes with their origin located at the center of gravity are known to be of the form [Etkin, 1972],

$$\sum F_x = m(\dot{u} + wq - vr) \quad \textbf{(6.1)}$$

$$\sum F_y = m(\dot{v} + ur - wp) \quad \textbf{(6.2)}$$

$$\sum F_z = m(\dot{w} + vp - uq) \quad \textbf{(6.3)}$$

where, *m* is the aircraft mass, u, v and w are the aircraft velocity components in body axes, p, q and r are the angular rates about the x, y and z axes, respectively and F_x, F_y and F_z are the resultant external forces acting on the vehicle. Usually the left hand side terms represent the aggregate contribution of tire, gravity, aerodynamic and thrust forces. Three moment equations define the rotation of the vehicle along three orthogonal body axes.

$$\sum L = I_{xx}\dot{p} - I_{xz}(\dot{r} + pq) - (I_{yy} - I_{zz})qr \quad \textbf{(6.4)}$$

$$\sum M = I_{yy}\dot{q} - I_{xz}(r^2 - p^2) - (I_{zz} - I_{xx})rp \quad \textbf{(6.5)}$$

$$\sum N = I_{zz}\dot{r} - I_{xz}(\dot{p} - qr) - (I_{xx} - I_{yy})pq \quad \textbf{(6.6)}$$

In these equations u, v, w are linear velocities in the x, y, and z axes, respectively; p, q and r are roll, pitch and yaw rates (in radians per second) along the three body axes, I_{xx}, I_{yy} and I_{zz} are aircraft moments of inertia about the x, y, and z axes, respectively; L, M, N are the rolling, pitching, and yawing moments about x, y, and z axes, respectively. Equations (6.4-6.6) have assumed that each aircraft has a a plane of symmetry (xz) and thus the cross products of inertia I_{xy} and I_{yz} are zero.

The left handside forces and moments include wheel and landing gear forces, aerodynamic forces and moments, gravity forces and thrust induced forces.These forces and moments are shown in Figure 6.6 with their corresponding sign convention.

For this analysis the aircraft-tire assembly system can be modeled as a high-order differential system with six degrees of freedom: three rolling equations and three moment equations govern the motion of an aircraft as it travels at high speed through a runway exit. The mathematical formulation of this high order system follows the same general principles used in aircraft stability and control analysis found in various references (Etkin, 1972; Blalelock, 1979; Roskam, 1982, etc.) with the addition of corresponding ground force terms associated with the landing gear assembly.

Using some simplifying approximations regarding these equations we can decompose the problem into lateral and longitudinal aircraft dynamics. Moreover some simplifying assumptions regarding the rolling moments of the vehicle are possible.

FIGURE 6.6 Definition of Aircraft Forces and Moments in Body Axes.

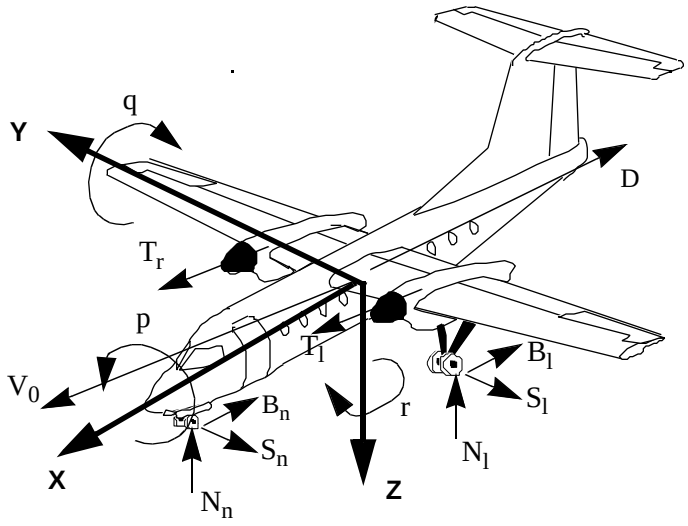

Aerodynamic forces
L = lift force
D = drag force

Tire forces
N = normal force
S = side force
B = braking force

Subscripts
n = nose gear
l = left gear
r = right gear

6.4 Testing the Simulation Procedure

A procedure to ascertain feasible aircraft ground trajectories is represented schematically in Figure 6.7. Here we feed a desired turnoff geometry into the six degree of freedom model and estimate desirable steering commands to execute the turnoff maneuver maintaining the aircraft nose gear as closely centered as possible to the turnoff centerline geometry. In the process a simple control system representing the dynamics of the human operator is used to introduce possible lags in the system that might be observed using real pilot operators. This ‘Pseudo-pilot model” uses a simple tracking algorithm similar to a PI controller (i.e., proportional and integral control).

FIGURE 6.7 Schematic Procedure for Aircraft Ground Trajectory Prediction (Closed Loop Analysis).

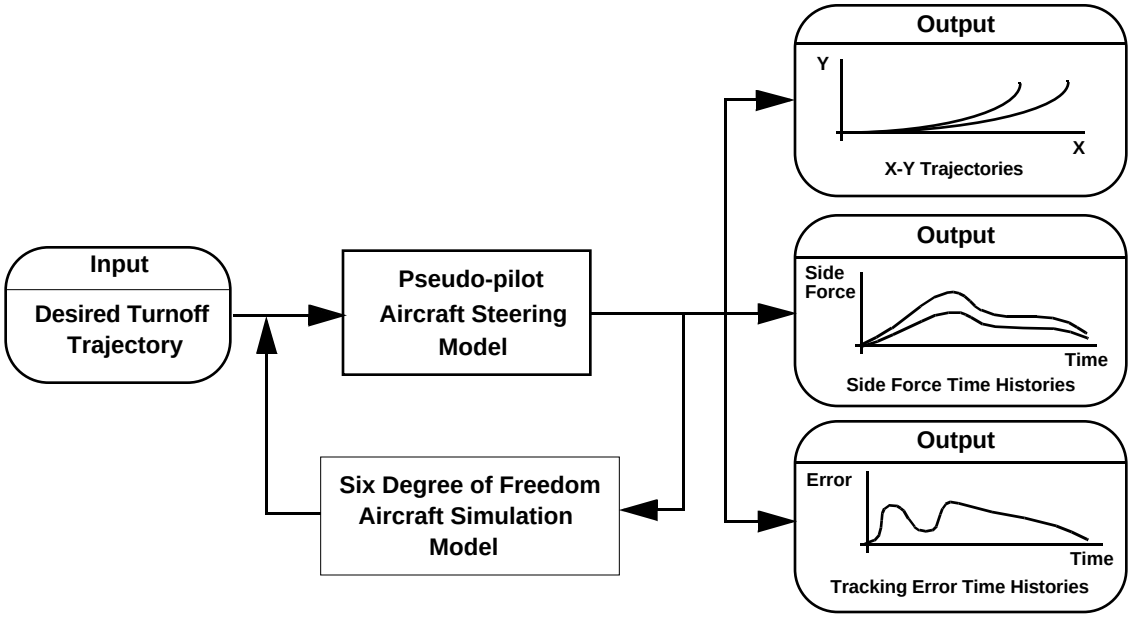

A second useful procedure to estimate the feasibility of the turnoff geometries proposed is to run the six-degree-of-freedom model previously described in an open loop configuration. That is to enter a desired steering time history and observe the dynamic motion of the aircraft on the ground resulting from an initial steering input disturbance. This procedure is illustrated in Figure 6.8.

Results of these procedures are illustrated in Figures 6.9 through 6.12 for a small business jet (Lockheed Jetstar) and for a four engine, wide body aircraft (with mass and inertia characteristics similar to those of the Boeing 747-200). The plots in Figures 6.10 and 6.11 show the side friction force and friction coefficient developed as the turnoff maneuvers are executed. Note that in both cases the expected side forces should be within the design capabilities of the landing gears. Figure 6.12 shows compares the x-y trajectories for a four engine wide body aircraft as it negotiates a high speed turnoff at 30 m/s. This figure was generated with the simulation code contained in Appendix E of this report.

FIGURE 6.8 **Schematic Procedure for Aircraft Ground Trajectory Prediction (Open Loop Analysis).**

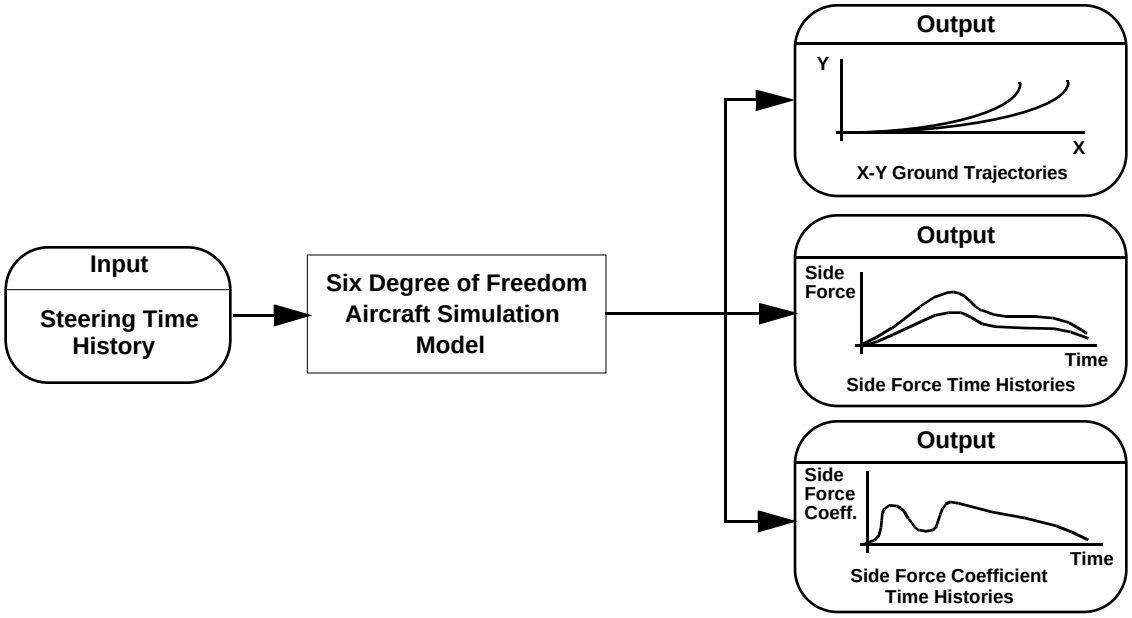

FIGURE 6.9 **Simulation Results for a Business Jet Negotiating a High Speed Turnoff (Maximum Turning Effort).**

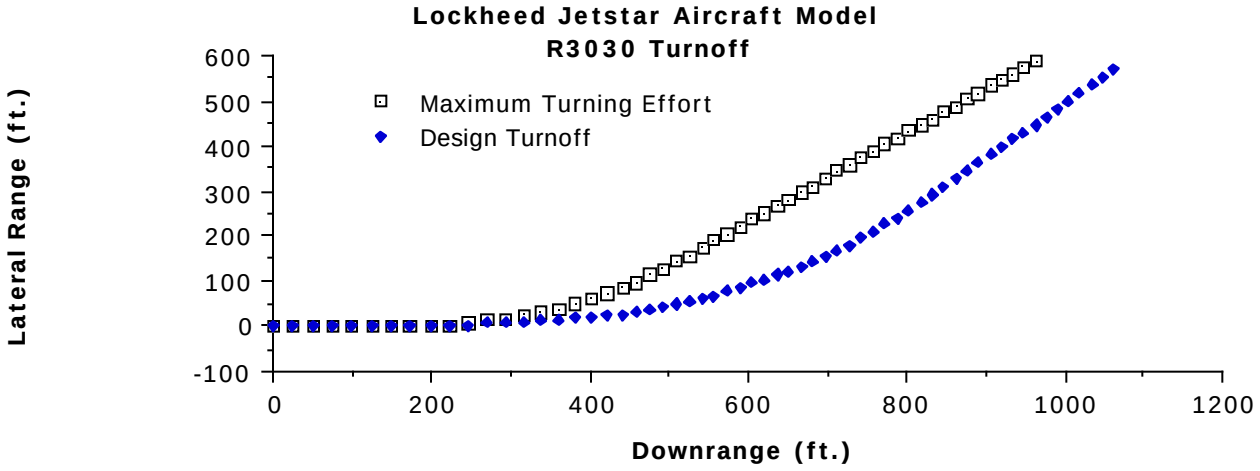

FIGURE 6.10 **Simulation Results for a Business Jet Negotiating a High Speed Turnoff (Tracking a High Speed Turnoff Centerline).**

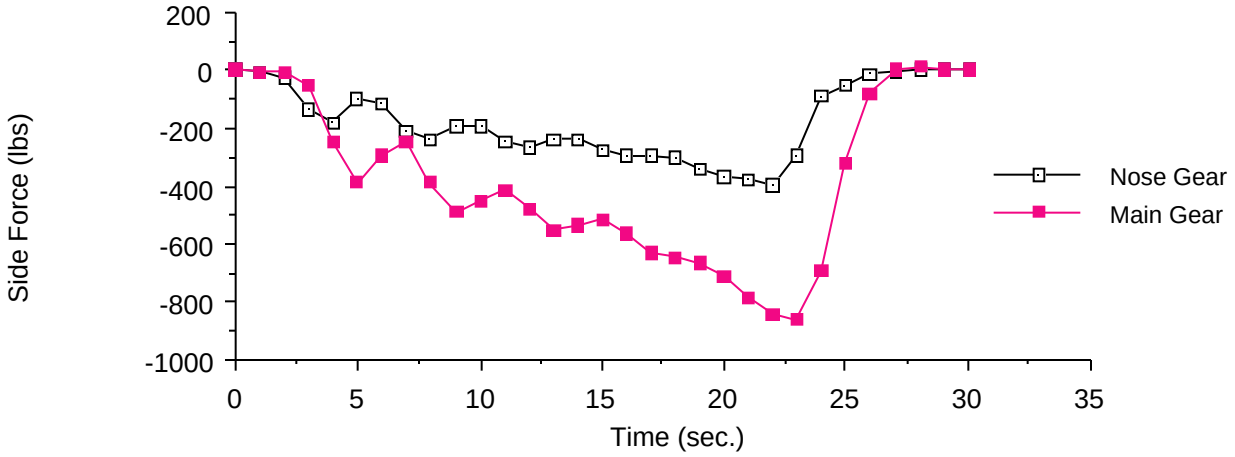

FIGURE 6.11 **Simulation Results for a Four Engine Wide Body Transport Negotiating a High Speed Turnoff (Tracking the Turnoff Centerline).**

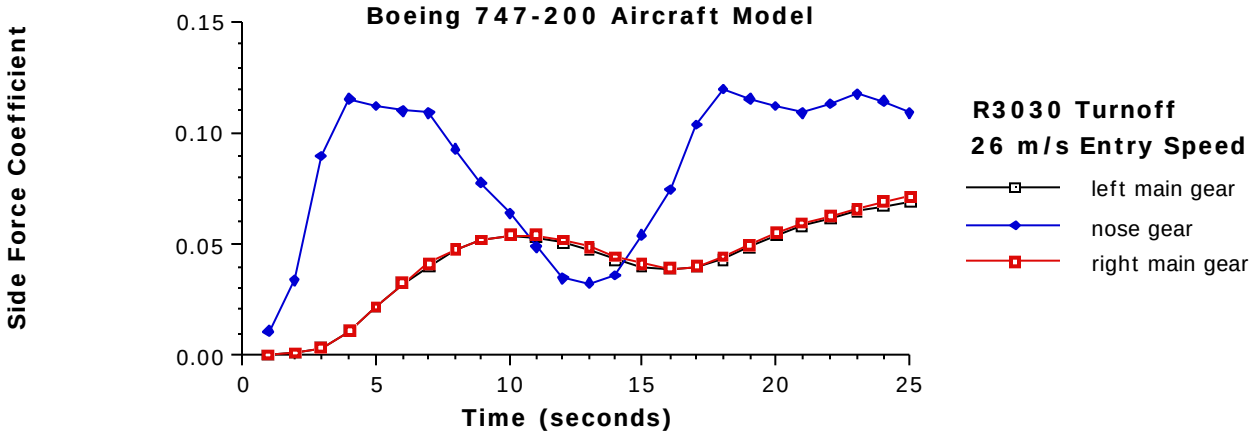

FIGURE 6.12 **Simulation Results for a Four Engine Wide Body Transport Negotiating a High Speed Turnoff (Tracking Offset Distance Diagram).**

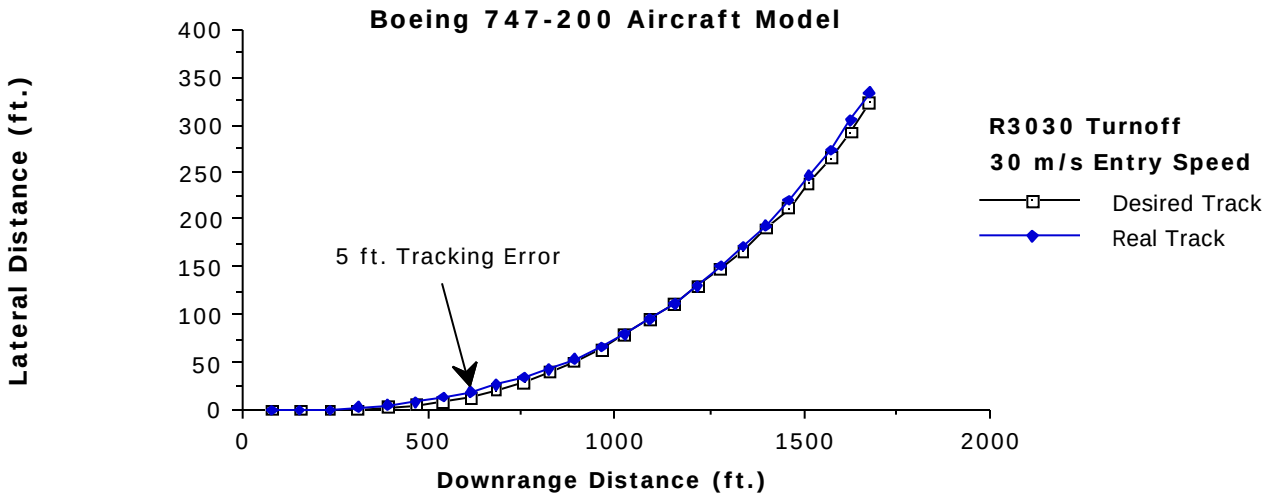

CHAPTER 7

Flight Simulation Experiments of High Speed Exits

This chapter summarizes the experiments conducted at Oklahoma City by the Federal Aviation Administration in conjunction with Virginia Tech to assess the operational suitability of rapid runway turnoff geometries under closed loop pilot simulations. The experiments analyzed pilot responses to “optimally-placed” rapid runway turnoff locations as well as aircraft state variable data to look at any possible implications of implementing the newly proposed high speed exits in real airports. A sample of the flight simulator questionnaire is shown in Appendix N of this report.

The piloted aircraft simulations were divided into two distinct experiments to maintain better control of the experimental output.

A first set of experiments was devoted to test the suitability of rapid runway turnoff geometries in "all ground" simulation runs.

The second part of the experiments assessed the suitability of optimal locations as predicted by the REDIM computer model using complete approaches to Oklahoma City runway 35.

The simulator used in the experiments was a CAE Electronics Phase C, full motion simulator (six degrees of freedom) owned and operated by the Federal Aviation Administration at the Mike Monroney Aeronautical Center in Oklahoma City. The simulator has an SPS-1 visual system capable of displaying dusk and night conditions over a 120^0 field of view. All simulation experiments were carried out with this simulator at near maximum landing weight (68,800kg) and with an aft center of gravity condition (i.e., 36% Mean Aerodynamic Chord - MAC - position) to simulate the most demanding conditions for ground control. Runway Visual Range (RVR) conditions for the experiment were set at 732 m. (2,400 ft.) providing little visual cues to pilots ahead of time and thus simulating poor visibility conditions. All simulation runs were conducted under night conditions.

Figure 7.1 shows the centerline tracks of the five turnoff geometries tested. Four new generation high speed geometries designated as RXXYY were developed according to the turnoff algorithms described by Trani et al. (1992). These geometries differ from the existing acute angle type by considering the turning limits of aircraft dictated by the yaw inertia of the vehicle instead of using a spiral geometry representation. In the five letter designator of these new geometries XX represents the design speed in m/s and YY stands for the turnoff exit angle. The four turnoff geometries evaluated have different degrees of curvature associated with two design entry speeds (i.e., 30 and 35 m/s) and two different exit angles (i.e., 200 and 300) used as design parameters. Figure 7.2 illustrates the differences between the acute angle exit with a 427 m spiral transition and geometry R3530 designed for 35 m/s and with a 30 degree exit angle. Both geometries were designed with the Boeing 727-200 as the critical aircraft.

FIGURE 7.1 Centerline REDIM Generated High Speed Runway Exit Geometries.

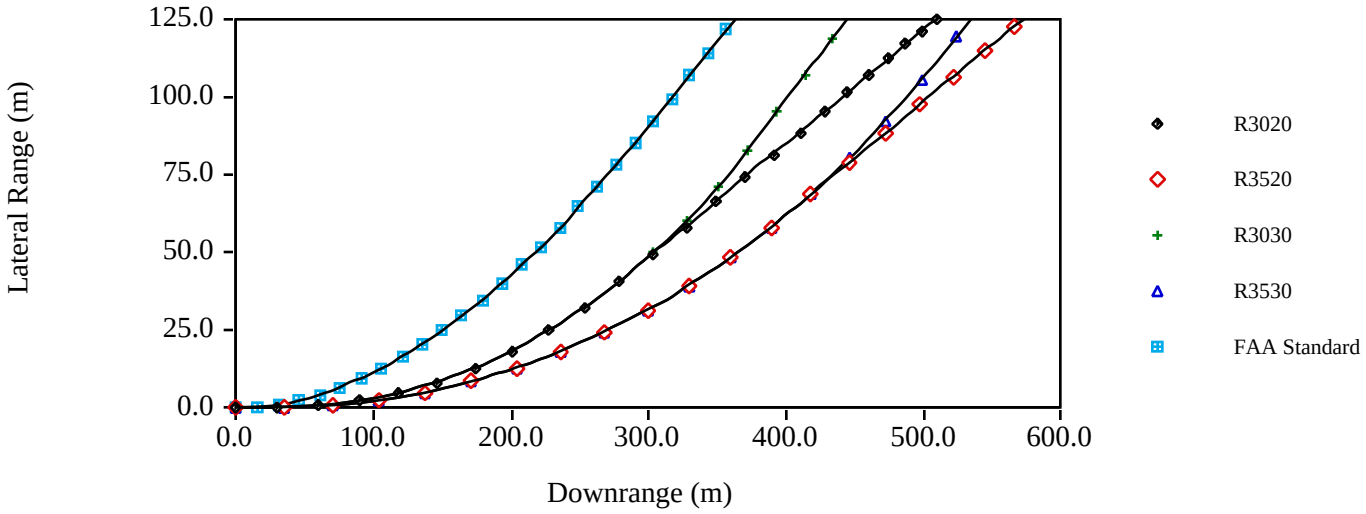

Figure 7.2 clearly shows differences in radii of curvature (variable in both exit geometries with increasing stationing) with a significant advantage to the R3530 geometry. Another significant difference is the throat taper of both geometries. The FAA acute angle exit uses a fairly aggressive taper starting at station 0.0 that quickly brings the high speed taxiway edges to coincide with the 22.9 m wide taxiway (for design group III) at metric station 519.0. The R3530 geometry on the other hand uses a less pronounced taper starting at metric station 250.00 and ending with a 30.5 m wide taxiway at metric station 750.0. The rationale for this design was to provide pilots more situational awareness and better visual cues while negotiating the turnoff at higher speeds. Finally, another clear difference in the geometric design standards used in these experiments was the distance between runway and taxiway. The FAA currently recommends 152 m (500 ft.) as the recommended distance between taxiway and runway centerlines for design group III (assuming high elevation conditions). However in our experience this value would have been unrealistic as

pilots would have to break hard during the turnoff maneuver to decelerate the aircraft to comfortable speeds at the end of the tangent section of the turnoff. All new geometries used a 228 m (750 ft.) distance between taxiway and runway centerlines thus providing pilots with ample deceleration distance on the turnoff tangent section.

FIGURE 7.2 Comparison of REDIM R3530 and FAA Acute Angle High Speed Exit.

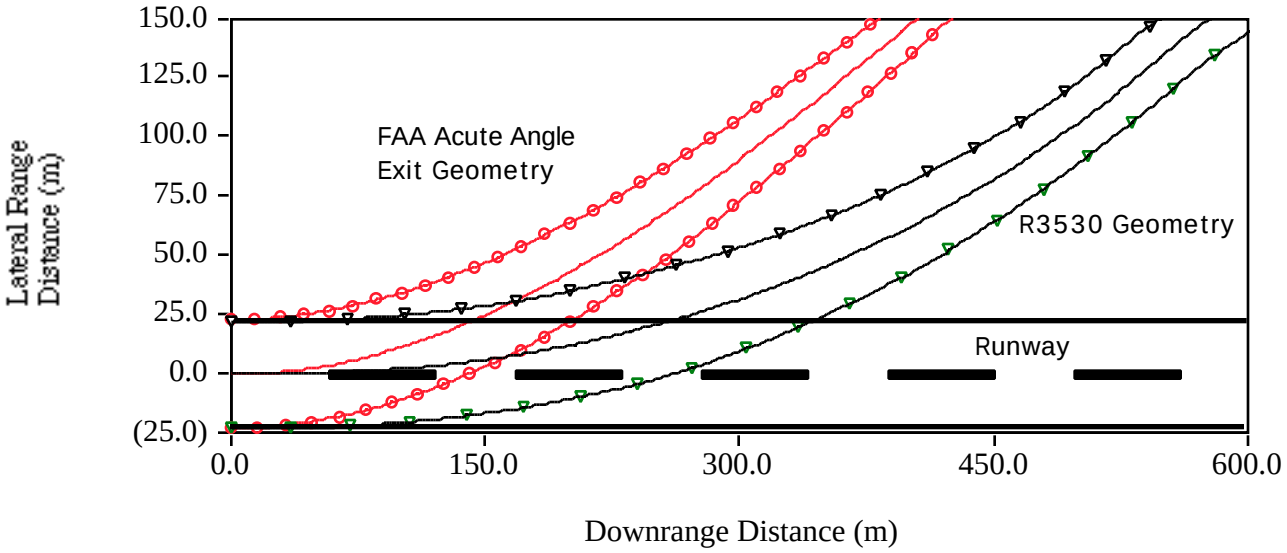

7.1 Runway Turnoff Assessment (Experiment Set # 1).

This part of the experiment ascertained pilot responses of various high-speed runway turnoff geometries. The experiments were conducted by exposing a selected group of FAA pilots to four different experimental geometry configurations. The standard FAA acute angle geometry (30 degree exit angle) was used as baseline scenario as shown in Table 7.1

Each run was evaluated by every pilot using a simple questionnaire (see Appendix M) to quantify each pilot opinion. The questionnaire responses were compared with aircraft state variable traces derived from each simulation run to cross check turnoff deficiencies and strengths. The turnoff geometries shown in Table 7.1 have different degrees of curvature associated with two design entry speeds (i.e., 30 and 35 m/.s) and two different exit angles used as design parameters.

TABLE 7.1 Turnoff Geometries for Experiment Set # 1.

Scenario	Geometry Label	Turnoff Angle	Design Speed (m/s)	REDIM Geometry
1	VII	30	30	R-3030
2	VIII	20	30	R-3020
3	V	30	35	R-3530
4	VI	20	35	R-3520
Baseline	FAA	30	27	N/A

7.1.1 Aircraft and Simulator Confi guration

The simulator used in the experiments was a CAE Electronics Phase C, full motion simulator (six degrees of freedom) owned and operated by the Federal Aviation Administration at the Mike Monroney Aeronautical Center in Oklahoma City. The simulator has an SPS-1 visual system capable of displaying dusk and night conditions over 120^0 field of view.

Table 7.2 shows the aircraft and airport parameters used in the simulation. Note that an aft center of gravity position was used to realistically simulate poor nose gear guidance effectiveness while negotiating high-speed exits. The turbulence level was kept to a minimum to avoid introduction of an external parameter in the simulation. The aircraft was loaded near its maximum allowable landing weight of 68,800 kg. and the c.g. position aft. Runway visual range was set to 731.7 m. (2,400 ft.) thus allowing us to learn landing roll strategies under low visibility conditions. All centerline turnoff lights were illuminated and a 100 foot spacing between edge lights was used to provide adequate peripheral vision to enhance situational awareness during the guidance task.

The experiments were randomized to minimize pilot learning during the experiment. Each run was evaluated by every pilot using a simple questionnaire to quantify pilot opinions. The questionnaire addressed issues related to: a) perceived geometry safety, b) aircraft steering effort, and c) overall rating of each turnoff geometry. The questionnaire responses were compared with aircraft state variable traces derived from each simulation run to cross check turnoff deficiencies and strengths.

All output parameters were collected at approximately one sample every 2 seconds. A high-speed modem connection from the CAE flight simulator was used to extract aircraft parameters in real-time. Up to twenty eight parameters were monitored during these experiments to understand aircraft dynamics and pilot behaviors. These parameters included: indicated airspeed, ground speed, pressure altitude, yaw angle, nose gear compression, left gear compression, longitudinal velocity, lateral velocity, longitudinal accel-

eration, lateral acceleration, centerline deviations, rudder pedal forces, wind speed, and wind direction among others.

TABLE 7.2 Aircraft and Airport Configuration for Experiment Set # 1.

Aircraft/Airport Parameter	Remarks
Mass	Maximum Allowable Landing Weight (MALW) 68,800 Kg. for Boeing 727-200 (typical)
C.G. Position	Aft c.g. condition (32% MAC)
Flaps	30 degrees down (consistent with MALW)
Runway Visual Range (RVR)	731 m. (2400 ft.)
Simulator Visual	Night conditions
Simulator Sampling Rate	Variable sampling rate (1-1/2 per second)
Simulator Starting Position	At runway threshold
Airport Temperature	15^0 C
ILS and HIRL	Operational
Turbulence Level	7% (light)
Wind Conditions	6.19 m/s (12 knots) crosswind

FIGURE 7.3 Scenario for Simulation Experiment Set # 1.

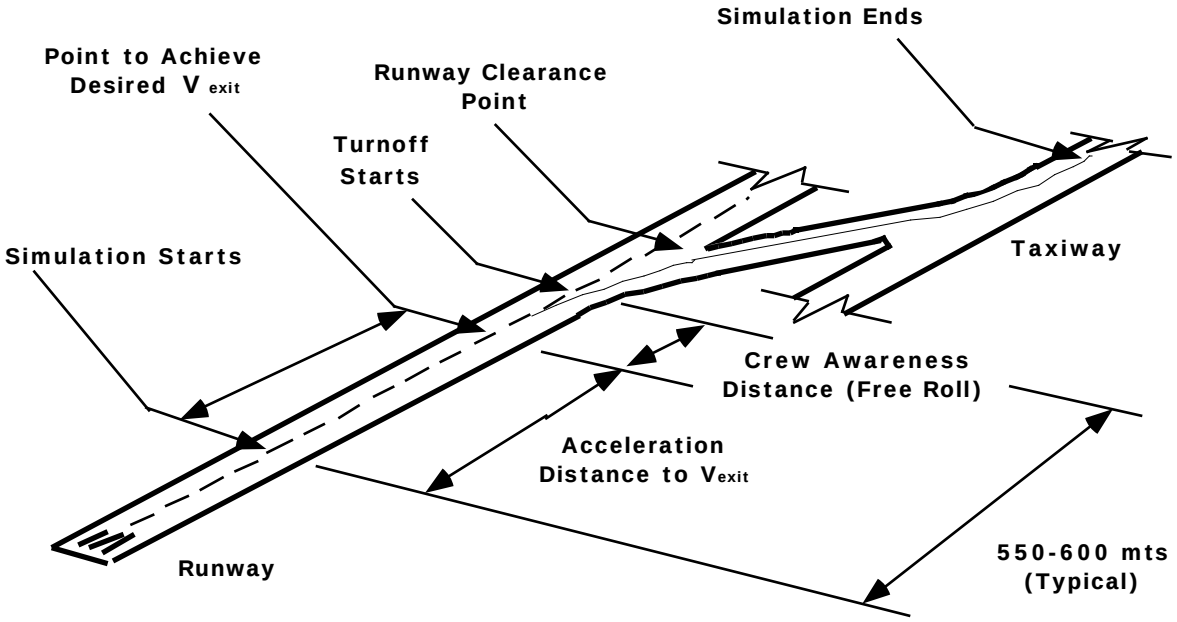

7.1.2 Test Pilots Tasks

Before attempting each simulation trial each pilot performed two familiarization runs to each turnoff geometry. Refer to Figure 7.3 to see a graphical representation of the testing scenario of experiment set # 1. The exit geometries were rotated from subject to subject to avoid preconditioning during monitored trial runs. The following pre-briefing information was given to each pilot prior to each simulation run.

1) Accelerate the aircraft on the ground until reaching a maximum perceived operational speed to negotiate the turnoff presented in each run. The distance from the initial aircraft position and the turnoff point of curvature is about 550 m. (see Figure 1) and thus should allow you to accelerate a Boeing 727 and then turnoff at any speed below 80 knots.
2) Since airspeed indicators are usually unreliable below 60 knots use the on-board INS system to monitor desired entry speeds in successive runs. The maximum perceived exit speed should consider passenger comfort, aircraft skidding characteristics, c.g. condition, etc. We are interested in learning from your experience the maximum operational speed considered safe for each turnoff.
3) Negotiate the turnoff at or near the maximum operational turnoff speed using standard aircraft steering procedures (i.e., tiller and rudder inputs). Maintain the turnoff centerline over the cockpit as close as possible.
4) Once reaching the turnoff tangent section (i.e., straight segment) proceed normally until reaching a position 100 m. (330 ft.) from the point of tangency. The trial run is now completed.
5) Repeat another four monitored trial runs (five trials per turnoff geometry) following steps 2) through 4).
6) Record your experience in the questionnaire handed in to you by the test monitor. It is very important to record the turnoff geometry number given to you by the experiment monitor. Also, record the time of the simulation as this will allow me to cross reference each simulation trial.
7) Proceed with a new turnoff geometry. Repeat steps 1) through 6) for each set of 5 monitored trial runs.

7.1.3 Simulator Coordinator Tasks

The following information was used by the simulator coordinator to verify each simulation run.

1) Verify the turnoff geometry to be tested prior to each trial run. Cross check with experiment monitor. If necessary coordinate with simulator ground personnel as they need to load the proper disk with each visual)
2) Allow two dry runs (i.e., not monitored) to get each pilot familiarized with the turnoff geometry to be tested.
3) Record time and turnoff geometry in the experiment worksheet provided.
4) Start simulator at reference position (i.e., at the active runway threshold).

5) Once the aircraft reaches a position of 100 m. (330 ft.) or about 10 seconds after crossing the point of tangency the trial run is completed.

5) Reset the simulator for another monitored trial run. There will be five trial runs per geometry for each pilot to gather better statistics.

6) After the fifth monitored trial run is completed (for one turnoff geometry) reset the simulator to the new turnoff geometry.

The following variables will be collected from the simulator at approximately one sample per second.

TABLE 7.3 Simulator Output Parameters for Experiment Set # 1.

Parameters	Parameters
1) Indicated Airspeed 2) Ground Speed 3) Pressure Altitude 4) Yaw Angle 5) Total Thrust 6) Ground Distance 7) Nose Gear Compression 8) Left Gear Compression 8) Longitudinal Velocity 9) Lateral Velocity 10) Longitudinal Acceleration	11) Lateral Acceleration 12) Ground Distance Travelled 13) Pilot Eye Height 14) Rudder Pedal Force 15) Column Force 16) Wheel Force 17) Flap Angle 18) Centerline Deviation 19) Longitudinal Wind Velocity 20) Lateral Wind Velocity

7.1.4 Test Monitor Tasks

The following information was used by the test monitor to verify each simulation run.

1) Verify the turnoff geometry to be tested prior to each trial run. Cross check with simulation coordinator monitor.

2) Allow two familiarization runs (not monitored) to get each pilot familiarized with the turnoff geometry to be tested.

3) Record time and turnoff geometry in the experiment worksheet provided.

4) Record approximate entry speed from the on-board INS system for each monitored trial run.

5) Record any behaviors observed during monitored trial runs.

6) After the fifth monitored trial run is completed (for one turnoff geometry) the simulator will be switched to show a new turnoff geometry.

7) Record the simulation ending times.

8) Coordinate with simulator coordinator the new turnoff geometry to be selected.

7.2 Runway Turnoff Location (Experiment Set # 2).

This part of the experiment estimated the pilots acceptance of various high speed runway turnoff locations. The experiments were conducted by exposing the same group of pilots

to five different turnoff location/geometry configurations (see Table 7.4). Each run will be evaluated by pilots to verify their assessment using response questionnaires and later compared with time histories derived from the simulation runs.

TABLE 7.4 Runway-Turnoff Scenarios for Experiment Set # 2.

Scenario	Optimal Exit Location	Location Description	REDIM Geometry
I	1215	Short	VI (R-3520)
II	1355	Medium	VI (R-3020)
III	1315	Short	VIII (R-3020)
IV	1450	Medium	VIII (R-3020)
Baseline	1500	Standard	N/A

The turnoff locations were modified according to the design exit speed and geometry configuration. Speeds of 30 and 35 m/s were used as data points to asses the validity of the REDIM model landing roll kinematics under three different exit location scenarios labeled short and medium.

The simulations were conducted in a relatively long runway (i.e., 3,050 m.) to assess crew landing roll behavioral patterns under relatively unconstrained runway length conditions.

7.2.1 Aircraft and Simulator Confi guration

The aircraft and airport configurations are shown for these trials is in Table 7.5. It should be mentioned that the simulator was usually in fuel freeze mode while executing these trials to maintain the same center of gravity characteristics throughout all the simulations. This maintained an aft center of gravity value to lighten the nose gear response.

TABLE 7.5 Aircraft and Airport Configuration for Experiment Set # 2.

Aircraft/Airport Parameter	Remarks
Mass	Maximum Allowable Landing Weight (MALW) 68,800 Kg. for Boeing 727-200 (typical)
C.G. Position	Aft c.g. condition (36% MAC)
Flaps	30 degrees down (consistent with MALW)
Runway Visual Range (RVR)	2400 ft.
Simulator Visual	Night Conditions
Simulator Sampling Rate	1 to 1/2 samples per second
Simulator Starting Position	at Final Approach Fix (or 5.3 miles out)

7.2.2 Pilot's Tasks

Before attempting each simulation trial each pilot performed one familiarization run to each turnoff geometry. The exit geometries were rotated from subject to subject to avoid preconditioning during monitored trial runs. The following pre-briefing information was given to each pilot prior to each simulation run.

1) Execute a familiarization trial run to familiarize yourself with given runway-turnoff scenario.
2) The exit geometries will be rotated from subject to subject to avoid preconditioning during monitored trial runs.
3) Fly a standard approach with the aircraft at near maximum landing weight (30 degrees flap angle setting). The landing c.g. position will be aft to unload the nose gear (critical issue in turnoff design).
4) The flare and touchdown locations should be nominal according to airline practices.
5) Apply normal thrust reversers and braking effort as needed to negotiate the best runway exit available.
6) Negotiate the turnoff at or near the maximum operational turnoff speed using standard aircraft steering procedures (i.e., tiller and rudder inputs). Maintain the turnoff centerline over the cockpit as close as possible.
7) Once reaching the turnoff tangent section (i.e., straight segment) proceed normally until reaching a position 100-200 m. (300-650 ft.) from the point of tangency. The trial run is now completed.
8) Repeat another two monitored trial runs (three trials per runway-turnoff combination) following steps 2 through 6.
9) Record your experience in the questionnaire handed in to you by the test monitor. It is very important to record the runway-turnoff geometry number given to you by the test monitor. Also please record the time of the simulation as this will allow me to cross reference each simulation trial.

This should be done while the new visual is loaded.

10) Proceed with a new runway-turnoff scenario (five total). Repeat steps 1) through 6) for each set of monitored trial runs.

7.2.3 Simulator Coordinator Tasks

The following information was used by the simulator coordinator to verify each simulation run.

1) Verify the runway-turnoff geometry to be tested prior to each trial run. Cross check with experiment monitor. If necessary coordinate with simulator ground personnel as they need to load the proper disk with each visual)
2) Allow one dry run (not monitored) to get each pilot familiarized with the runway-turnoff geometry to be tested (start at FAF).
3) Record time and turnoff geometry in the experiment worksheet provided.
4) Turn on the video camera inside the simulator.
5) Start simulator at reference position (i.e., at the FAF).

6) Once the aircraft reaches a position of 100-200 m. (300-650 ft.) or about 5-6 seconds after crossing the point of tangency the trial run is completed.

7) Reset the simulator for another monitored trial run. There will be three trial runs per runway-turnoff scenario per pilot.

8) After the third monitored trial run is completed (for one turnoff geometry) reset the simulator to the new runway-turnoff scenario.

Parameters collected from the simulator for these experiments were as follows:

TABLE 7.6 Simulator Output Parameters for Experiment Set # 2.

Parameters	Parameters
1) Indicated Airspeed 2) Ground Speed 3) Radio Altitude 4) Pitch Angle 5) Roll Angle 6) Yaw Angle 7) Total Thrust 8) Ground Distance 9) Nose Gear Compression 10) Left Gear Compression 11) Longitudinal Velocity	12) Lateral Velocity 13) Vertical Velocity 14) Longitudinal Acceleration 15) Lateral Acceleration 16) Vertical Acceleration 17) Rudder Pedal Force 18) Ground Distance Travelled 19) Spoiler Deployed Flag 20) On Ground Flag

7.2.4 Test Monitor

The following information was used by the test monitor to verify each simulation run.

1) Verify the turnoff geometry to be tested prior to each trial run. Cross check with simulation coordinator monitor.

2) Allow one familiarization run (not monitored) to get each pilot exposed to the runway-turnoff geometry to be tested (start at FAF).

3) Record time and turnoff geometry in the experiment worksheet.

4) Record speeds at threshold crossing point and the turnoff entry point from the on-board INS system for each monitored trial run.

5) Record any behaviors observed during monitored trial runs.

6) After the third monitored trial run is completed (for one runway-turnoff scenario) the simulator will be reset.

7) Record the simulation ending times.

8) Coordinate with simulator coordinator the new turnoff geometry to be selected.

7.3 Simulation Results

Appendix K contains results of the simulation experiments carried out in March 13-16, 1995 using a Boeing 727-200 simulator. The data gathered was analyzed using a simple

post-processor program written in C and Matlab. Sample results are shown in Figures 7.2-7.7.

Figure 7.4 details a composite plot showing time history for true airspeed and a velocity-distance profile for a single simulation run. These data was analyzed and milestone points were extracted to estimate runway exit speeds for all five scenarios tested. Appendix K contains histograms of the exit speeds for each geometry tested. Also, statistical summaries are found in the same appendix. Figure 7.5 illustrates a typical x-y trace for the same aircraft trial and also shows the gear compression parameter extracted from the simulator. Figure 7.6 shows further details of the x-y trace and velocity-distance profile for the turnoff section of the run. Velocity profiles on the turnoff were also analyzed to learn the type of pilot behaviors once on a turnoff. Figure 7.7 illustrates a three dimensional plot of airspeed and distance.

FIGURE 7.4 Typical Speed Time History and Speed-Distance Profile for Experiment Set # 1.

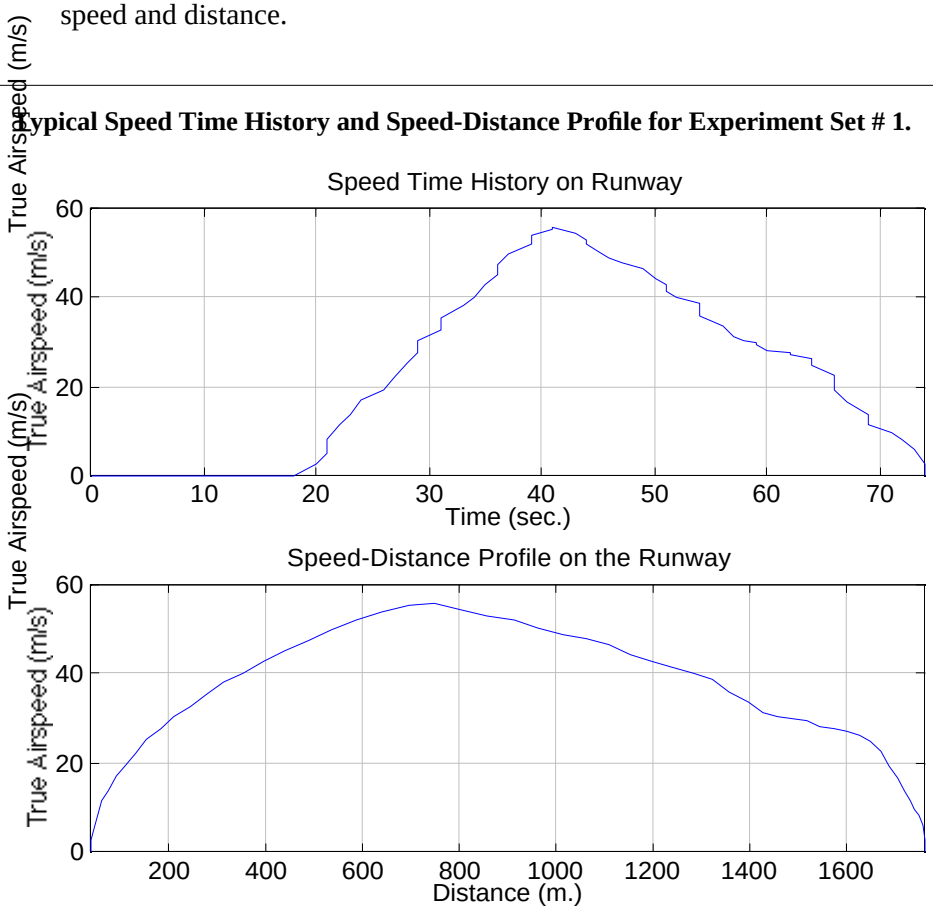

FIGURE 7.5 **X-Y Trajectory and Main Gear Compression Parameter Plots.**

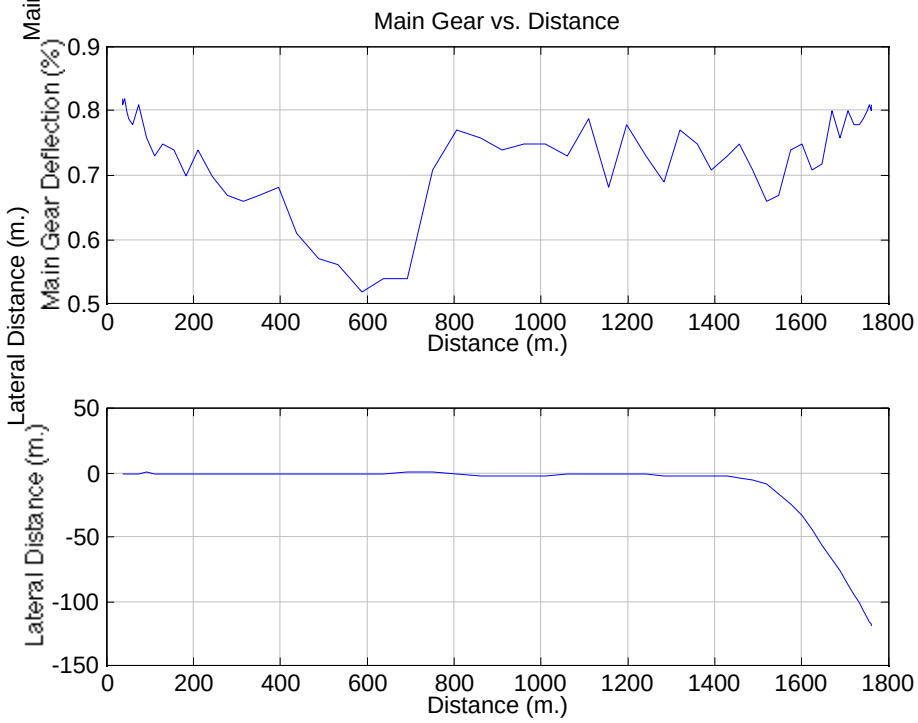

FIGURE 7.6 **X-Y Trajectory and Speed-Distance Profile on High Speed Turnoff.**

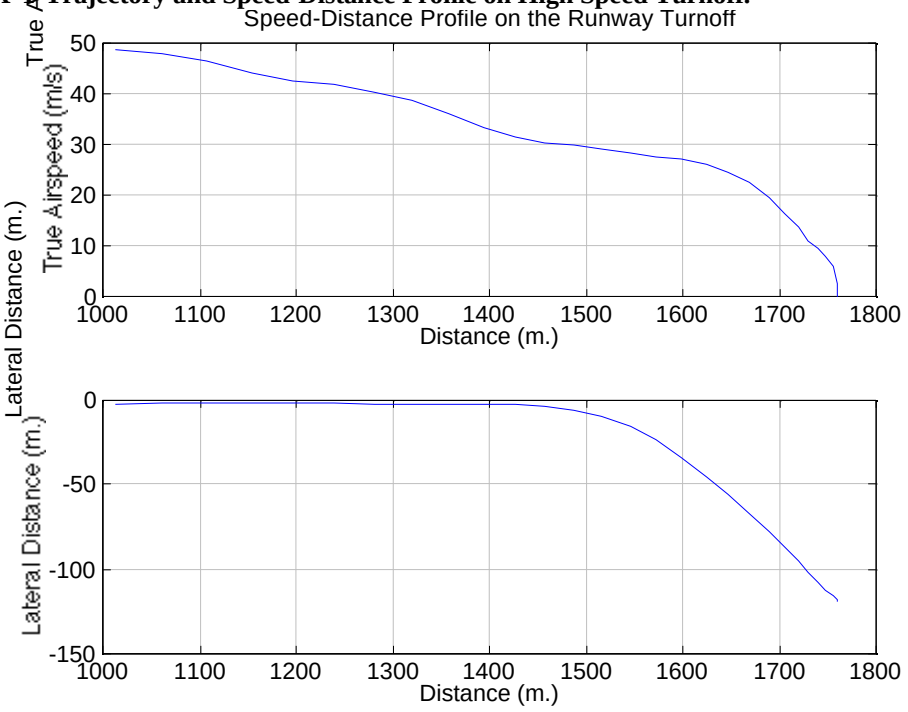

FIGURE 7.7 **Three Dimensional Plot of Aircraft Position and Airspeed.**

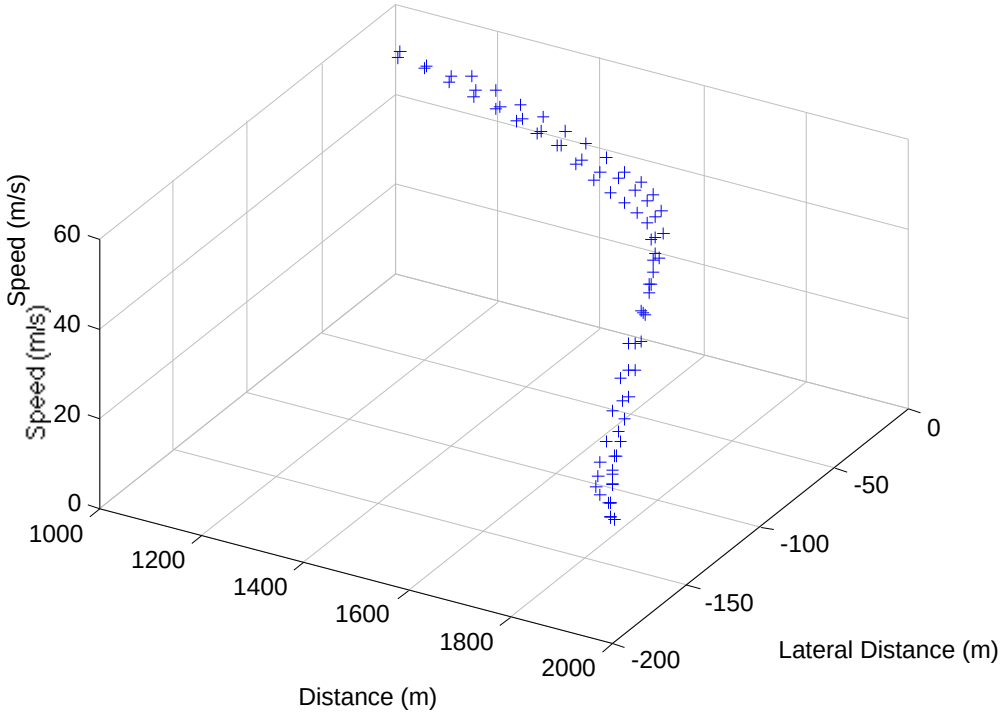

7.4 Discussion of Simulation Results

The flight simulator data was reduced using a post-processor written in C and Matlab. Two independent statistical analyses were carried out to assess the feasibility and acceptance of the proposed high speed exit designs: 1) unpaired t-test analysis of exit speed and questionnaire responses, and 2) two-way factor analysis of aircraft exit parameters and non-parametric tests for questionnaire responses. Sections 7.4.1 through 7.4.4 discuss these results.

7.4.1 Unpaired Tests for Exit Speed Obser vations

Exit speed data was reduced and analyzed to see if indeed there were significant differences between the new proposed geometries and the current FAA acute angle exit. Table 7.7 shows the t-test results of the experiment for all five exit geometries tested

TABLE 7.7 Summary Information for Various High Speed Exits Tested.

Exit Geometry	FAA Acute Angle	REDIM 3530	REDIM 3520	REDIM 3030	REDIM 3020
Mean Exit Speed - m/s (knots)	38.96 (75.60)	45.62 (88.51)	45.54 (88.35)	49.19 (95.43)	45.66 (88.58)
Standard Deviation of Exit Speed - m/s (knots)	5.32 (10.32)	6.08 (11.80)	4.20 (8.15)	6.40 (12.42)	5.24 (10.16)
Standard Error - m/s (knots)	1.00 (1.95)	1.11 (2.15)	0.79 (1.54)	1.15 (2.23)	0.94 (1.83)
Range - m/s (knots)	23.7 (46.0)	23.7 (46.0)	19.1 (37.0)	21.6 (42.0)	25.3 (49.0)
Count	28	30	29	31	31

The results indicate that there are significant differences in behavior while using the newly proposed geometries and the current FAA standard. These differences were attributed to a better design of the throat section of the turnoff which gave pilots more situational awareness in how to execute the guidance during the high speed maneuver. Note from Table 7.8 that differences between the new high speed exits is not statistically significant (high values of P in the last column of the table). Further consideration of the questionnaires validated this results. Note that in some cases the new turnoffs were being executed comfortably 5-10 m/s higher than the current FAA standard. The exit angle of 20 degrees while preferred by most pilots in the questionnaires did not seem to have any impact on the exit speed observed. It was mentioned in most questionnaires that 20 degrees seems to ease the transition between a high speed roll-out and the tangent portion of the turnoff.

TABLE 7.8 Unpaired t-test Results for Various High Speed Exits.

Unpaired t-test	Mean Difference (knots)	Degrees of Freedom	t-value	P-Value
FAA - REDIM 3530	-12.860	56	-4.409	< 0.0001
FAA - REDIM 3520	-12.669	55	-5.153	< 0.0001
FAA - REDIM 3030	-19.796	57	-6.620	< 0.0001
FAA - REDIM 3020	-12.877	57	-4.825	< 0.0001
REDIM V - REDIM 3520	0.191	57	0.072	0.9428
REDIM V - REDIM 3030	-6.937	59	-2.237	0.0291
REDIM V - REDIM 3020	-0.017	59	-0.006	0.9951
REDIM VI - REDIM 3030	-7.127	58	-2.609	0.0115
REDIM VI - REDIM 3020	-0.208	58	-0.087	0.9309
REDIM VII - REDIM 3020	6.919	60	2.401	0.0195

7.4.2 Unpaired Tests of Questionnair e Responses

Each question asked in the questionnaire was judged among all pilots that participated in this study. The results of Experiment set #1 are shown in Table 7.9. the rating scale used varied from 1 to 7 for all questions to ensure continuity in the results. In the rating scale used 1 was associated with a poor design and great steering effort to keep the aircraft in the turnoff centerline. Seven was the highest score and it usually meant easy steering requirements and good geometric designs.

Table 7.10 shows the results of an unpaired t-test for the questionnaire responses. Judging from the P values of this table one can conclude that the levels of safety and skill required to negotiate all turns was about the same. In general most pilots said the workload was reasonable and no steering reversals were observed in the data except for two occasions when the pilot admitted entering the runway exit at an unreasonable speed.

TABLE 7.9 Summary Information for Various High Speed Exits Evaluated.

Exit Geometry	FAA Acute Angle	REDIM 3530	REDIM 3520	REDIM 3030	REDIM 3020
Mean response (1-7 scale)	5.00	5.00	5.43	4.51	4.75
Std. deviation	1.55	1.53	1.51	1.72	1.72
Count	7	7	7	7	7

TABLE 7.10 Unpaired t-test Results (Questionnaire Responses for Exit Evaluation).

Unpaired t-test	Mean Difference	Degrees of Freedom	t-value	P-Value
FAA - REDIM 3530	0.000	11	0.00	1.0000
FAA - REDIM 3520	-.429	11	-.504	0.6243
FAA - REDIM 3030	.429	11	.469	0.6484
FAA - REDIM 3020	.429	11	.469	0.6484
REDIM V - REDIM 3520	-.429	12	-.528	0.6074
REDIM V - REDIM 3030	.429	12	.493	0.6308
REDIM V - REDIM 3020	.429	12	.493	0.6308
REDIM VI - REDIM 3030	.857	12	.991	0.3413
REDIM VI - REDIM 3020	.857	12	.991	0.3413
REDIM VII - REDIM 3020	0.00	12	0.00	1.0000

Based on the information collected from the flight simulator and questionnaires, two statistical experiments were formulated to assess the feasibility and acceptance of the proposed high speed exit designs: (1) a two-factor ANOVA analysis of exit speed and (2) nonparametric tests of pilot questionnaire responses.

7.4.3 Two-factor ANOVA Analysis of Exit Speeds

The REDIM turnoff geometries were designed to allow higher exit speed than usual FAA standard exit geometry. The relevant data collected from the flight simulation was analyzed to see if there were any significant difference between the new geometries and current FAA acute angle exit in terms of exit speed. Table 7.7 gives a summary information of exit speed taken by pilots on the five geometries in experiment set 1.

In this experimental design, runway exit geometry was considered as the main factor. However, to reduce experimental error, a second factor - each pilot, was also considered. All the pilots in the flight simulation experiment had different levels of flight experience and total flight times in the Boeing 727-200. By considering this second factor, the variation between pilots, which is most likely significant compared to the uniformity of one pilot, could be removed from the experimental error in the analysis of variance. Although the pilot effect on exit speed was not of our interest, because of the possible interactions between pilot and exit geometry, two-factor ANOVA analysis was conducted for the evaluation.

The two-factor experiment was carried out for every combination of two turnoff geometries. The mathematical expression of this test can be written as:

$$y_{ijk} = \mu + \alpha_i + \beta_j + (\alpha\beta)_{ij} + \varepsilon_{ijk} \quad \textbf{(7.1)}$$

Where: y_{ijk} is the observed kth trial exit speed by pilot j on ith turnoff geometry i, μ is the mean of exit speed, α_i is the effect of ith geometry, β_j is the effect of jth pilot, $(\alpha\beta)_{ij}$ is the interaction effect, and ε_{ijk} is the term for random errors. A significance level of 0.05 was selected to test the following hypotheses: (1) H1: there is no significant interaction between the turnoff geometries and the pilots, (i.e., $(\alpha\beta)_{ij} = 0$); (2) H2: there is no major difference in the exit speed when different exit geometries are tested, (i.e., $\alpha_i = 0$).

The results of the experiment are shown in Table 7.11. The results show that there are significant differences in behavior when comparing the new REDIM geometries and the current FAA standard geometry. The interaction between the exit geometries and the pilots is not significant (high p-value). This exit speed difference could be attributed to the better design of the throat section of the turnoff which gives pilots more situational awareness during the high speed maneuver (see Figure 1). However, the difference between the four high speed turnoffs is not statistically significant. The exit angle of 20 degree while preferred by most pilots in the questionnaires did not seem to have much impact on the observed exit speed.

TABLE 7.11 Two-factor Exit Speed Analysis for Various High Speed Runway Exits.

Two factor Experiment	Mean Difference (knots)	f-value for Geometry	f-value for Interaction	P-value for Geometry	P-value for Interaction
FAA-R3530	-13.72	34.26	0.23	0.000	0.945
FAA-R3520	-14.06	40.90	0.74	0.000	0.601
FAA-R3020	-14.83	43.47	0.87	0.000	0.515
FAA-R3030	-20.67	86.27	0.58	0.000	0.714
R3530-R3520	-0.33	0.03	1.39	0.856	0.264
R3530-R3020	-1.11	0.35	1.60	0.560	0.197
R3530-R3030	-6.94	14.09	1.59	0.001	0.200
R3520-R3020	-0.78	0.21	0.04	0.650	0.999
R3520-R3030	-6.61	15.86	0.91	0.001	0.493
R3020-R3030	-5.83	11.39	1.10	0.003	0.389

7.4.4 Nonparametric Tests of Questionnair e Responses

The objective of the second test was to find out the difference between the new geometries and the FAA standard geometry regarding to safety, steering effort, and overall acceptance. After each simulation run in the experiment, pilots were asked to answer the questions in the questionnaire. This procedure gave pilots ample time to respond in detail as new visual files containing various runway exit geometries were loaded in the simulator CGI computer. Three parameters were chosen for the evaluation of high speed turnoff geometries: safety, steering requirements, and overall assessment. The rating scale used varied from 1 to 7 for all questions to ensure continuity in the results. In our scale, 7 was associated with a poor design and great steering effort to keep the aircraft on the turnoff centerline, while 1 was associated with good geometric design and easy steering requirements. A summary of all questionnaire responses collected from experiment set 1 is shown in Table 7.12.

TABLE 7.12 Summary Information of Questionnaire Responses.

	Exit Geometry	FAA Standard	REDIM R3530	REDIM R3520	REDIM R3030	REDIM R3020
Safety (1-7 Scale)	Mean	4.00	3.00	2.57	3.29	3.14
	Std. Dev.	0.00	1.53	1.51	1.60	1.22
	Count	7	7	7	7	7
Steering Effort (1-7 Scale)	Mean	4.00	3.29	2.57	3.43	2.86
	Std. Dev.	0.00	1.50	1.51	1.51	1.35
	Count	7	7	7	7	7
Overall (1-7 Scale)	Mean	4.00	3.00	2.71	3.29	2.86
	Std. Dev.	0.00	1.29	1.38	1.50	1.35
	Count	7	7	7	7	7

Several factors were considered in choosing a nonparametric statistics method to test questionnaire responses: (1) for each geometry, the observations may not come from normal distributions; (2) only a small sample size was available (7 data points for each geometry); (3) all the observations were defined on ordinal a scales instead of on ratio scales; (4) in order to separate pilot effect, the observations should be paired to remove external errors.

A Wilcoxon signed rank test was used to compare the means of five treatments (5 geometries) for each of these three parameters: safety, steering effort, and overall acceptance. Taking FAA standard acute angle exit as the baseline scenario, three hypotheses to be tested were:

(1) The proposed geometries have better safety features than standard FAA acute angle design;

(2) The new geometries require less steering effort in the turnoff maneuver;

(3) Overall, the new geometries are better than the FAA acute angle high-speed exit.

The significance level of 0.05 was used in this analysis. Table 7.13 shows the results of Wilcoxon signed rank tests of the pilot questionnaire responses. Judging from the P-values in this table, we can **conclude that the level of safety was improved over the FAA acute angle turnoff geometry**. The steering effort required to negotiate all turns was less demanding, and the overall performance of new geometries was judged to be better. However, the difference between all new four exit geometries is not significant thus implying that differences between REDIM geometries are not perceived by most pilots.

TABLE 7.13 Wilcoxon Signed Rank Test of Questionnaire Responses

Signed Rank Test	P-value for Safety Evaluation	P-value for Steering Effort Evaluation	P-value for Overall Evaluation
FAA-R3530	0.947	0.896	0.963
FAA-R3520	0.977	0.977	0.977
FAA-R3030	0.909	0.860	0.896
FAA-R3020	0.969	0.970	0.970
R3530-R3520	0.181	0.273	0.465
R3530-R3030	0.371	0.789	0.371
R3530-R3020	0.789	0.593	1.000
R3520-R3030	0.181	0.201	0.273
R3520-R3020	0.225	1.000	1.000
R3030-R3020	0.789	0.273	0.584

To summarize the results from these two experiments, we find that new high speed runway exits could be used to increase exit speed without compromising safety or inducing extra workload. By increasing exit speed, runway occupancy time is reduced thus capacity could be increased.

CHAPTER 8

Research Conclusions and Recommendations

The simulation/optimization approach adopted in this new version of REDIM provides airport planners and researchers alike with a better understanding of the complex issue of locating optimal runway exits and their associated geometries. Looking at existing data on runway occupancy times [Koenig, 1978; Weiss and Barrer, 1984, Weiss, 1985; and Ruhl, 1990] it is believed that the new REDIM model behaves in a realistic fashion for a multitude of scenarios tested. Comparison of previous empirical results obtained by previous researchers support the validity of this argument. Further empirical studies are being pursued in Phase III of this research project at six large and medium size airport hubs.

Following the approach adopted in the previous version of the REDIM model the description of fully variable turnoff geometries is approximated with two large radii of curvature. This simplifies the presentation of results within the model yet approximates very closely a turnoff geometry resembling a large transition spiral. The reader can compare results of high speed geometries defined with variable radii of curvature and the standardized spiral transitions used in association with the 30 degree FAA standard geometry.

In order to provide guidance for implementation of high speed geometries a series of nomographs have been suggested in this report providing preliminary design guidelines for future use by airport planners. The graphs contained in Section 6.1 of the report document suggested lateral separations between runways and turnoffs for combinations of exit type, exit angle, and aircraft operational turnoff speeds (i.e., entry and final speeds). The lateral constraints dictated by operational aircraft criteria and runway exit geometric constraints were also programmed into the software package to allow further compliance with these proposed standards. Design nomographs have been derived for FAA standard high-speed exits (i.e., 30 deg. standard and 30 deg. modified geometry with 427 m. transition spiral) as well as for REDIM generated geometries. The results are presented in Chapter 6of this report.

Another aspect deserving attention are the calibration of some of the safety margins and assumptions made in the present modeling effort. In the overall conceptualization of REDIM safety margins were implemented in some of the dynamic module subroutines to account for the usual uncertainties associated with manual control tasks, such as the landing of an aircraft, the activation of braking devices, etc. However, the reduction of these uncertainties could significantly reduce the runway occupancy time (ROT) by reducing the margins of safety needed to cope with the original assumptions. This phenomena is similar to the anticipated reductions in the aircraft interarrival time (IAT) to the runway threshold through an improvement of the aircraft delivery accuracy (e.g., by reducing the final approach IAT separation buffers). The underlying assumptions made in this model have tried to establish a good balance between operational safety and the efficiency of the runway subsystem. This compromise was necessary because the model is expected to be applied in a variety of scenarios where the manual control uncertainties will be, in general, quite high. That is, the model could be either applied to small community airports where the proficiency and accuracy of the pilots might dictate slightly larger safety margins or to large transport-type airports where an increased number of automated landing rollout operations could take place in the future.

The resulting simulation/optimization model called REDIM 2.1 (runway exit design interactive model) is a stand alone application requiring minimal computer hardware (i.e., an IBM or compatible personal computer and EGA capabilities) that can be used in the planning and design of new runway turnoff upgrades or in the location of turnoffs for future runway facilities. REDIM 2.1 is capable of handling all existing turnoff geometries (including “wide throat” geometries) for added flexibility as well as newly proposed high-speed geometries with user-defined turnoff angles.

8.1 Conclusions

The main conclusions found during the development of the REDIM 2.1 computer model can be summarized as follows:

- The computer program developed uses a combination of a Monte Carlo simulation and a Polynomial Dynamic Programming algorithm to estimate turnoff candidates and optimize locations that minimize the aircraft weighted average runway occupancy time (WAROT).
- The model results computed for various runway/turnoff configurations seem to be in good agreement with empirical observations made by previous researchers [Koenig, 1978; Weiss and Barrer, 1984, Weiss, 1985 and Ruhl, 1990]. It must be pointed out that most of the previous data reported aircraft per approach group [except for Ruhl, 1990] while the model described in this report considers the differences in landing aircraft dynamics between individual vehicles even if they belong to the same approach speed group classification.
- Significant reductions in runway occupancy time are possible with the optimal location and geometric tailoring of turnoff geometries for a known aircraft population. For a single runway reductions in WAROT of up to 15% are possible with the use of

proposed super-acute angle exits (i.e., 20 degree turnoff angle) compared with standard 30 degree angle geometries. Further reductions are possible while converting right angle turnoffs to super-acute angle exits. This reduction in WAROT could translate in moderate gains in runway capacity under mixed operations due to the stretching effect on the departure slots.

- Reductions in WAROT down to 36-40 seconds seem feasible with the use of optimally located super-acute turnoffs. This WAROT could support a 2.0 nautical mile interarrival separation (assuming some advances in terminal ATC automation take place and solutions to the wake vortex problem are found).
- Six degree of freedom aircraft simulations seem to indicate that super-acute turnoff geometries could allow consistent exit speeds of up to 35 m./s. (78 m.p.h.) for transport type aircraft operations. While the land use requirements of these turnoffs are high it might well payoff in runways operated almost exclusively by transport-type aircraft over a 20 year life cycle.
- Proposed lateral separation distance nomographs between a runway and parallel taxiways were derived for all types of high-speed geometries using fairly conservative aircraft deceleration assumptions on the tangent portion of a turnoff. These nomographs could be used in preliminary airport planning to estimate land use requirements.
- The airfield observations confirm that REDIM 2.1 can indeed predict the weighted ROT parameter for many aircraft individually. In several occasions the WAROT values predicted by the model are within 2-3 seconds of those observed. Chapter 4 of this report addresses this issue in more detail.
- The airfield observations reported fill an important gap in aviation operations today. The data was derived from video sources thus making it more reliable than standard counts taken at airports in previous studies.
- The flight simulation experiments conducted at the FAA Mike Monroney Aeronautical Center confirm that high speed exits are being misused in practice by conservative practices. These results also show that widening the throat of high speed exits has a substantial effect in the perception of high speed geometries by pilots.
- The flight simulation results indicate that pilots could take four new high speed exit geometries at higher speeds than the FAA acute angle standard. The data showed however, that in doing so pilots did not feel any safety compromises in the process. The exits tested have spiral transitions based upon the aircraft inertia and not based on geometric principles.

8.2 Some Recommendations

Several recommendations derived from this report are:

- Investigate in detail the aircraft landing gear dynamics associated with the proposed high-speed turnoffs as this might eventually be a deterrent for their operational implementations from the airline point of view. This will require actual aircraft runs and not just flight simulations in order to assess landing gear loads realistically.

- An extension to the existing model is possible where further consideration is given to the complex interactions between existing taxiway/runway subsystems and the placement of new runway turnoff locations. Also some consideration could be given in this analysis to airline/ATC motivational practices in locating runway turnoffs.
- Implement the algorithms of REDIM in a real-time ground control advisory system to help ATC personnel to make decisions regarding exit assignment in real time. This automated advisory system could in principle reduce ground delays prevalent at major airports by assigning aircraft to unused taxiways and runway exits. This project could easily tie the algorithmic development done here with ASTA-2 automation initiatives.
- Implement new lateral distance guidelines between runway and taxiway centerlines in FAA AC/150-5300-13 to provide minimum requirements for the implementation of high-speed runway turnoffs. Most pilots felt that 225 m (750 ft) was a minimum to execute high speed roll-outs from real runways. These standards are proposed in Chapter 6 of this report.

APPENDIX A

REDIM 2.1 Aircraft Data File

This appendix contains pertinent aircraft data spanning four aircraft classification groups. The data has been gathered from reliable sources such as aircraft manufacturer data, Jane's All the World's Aircraft, Aviation Week and Space Technology, Business and Commercial Aviation Planning Handbook and several other respected magazines covering the world of aviation.

The appendix lists pertinent aircraft data characteristics used in REDIM 2.1to execute both the optimization and dynamic aircraft simulation procedures. Table A.1 illustrates the characteristics of transport-type aircraft corresponding to aircraft categories C and D.

TABLE A.1 Aircraft Data for Approach Groups C and D.

Aircraft Name	REDIM Code	Max. Landing Mass (Kg)	Oper. Empty Mass (Kg.)	Aircraft Wingspan (m.)	Aircraft Wheel-Base (m.)	% Load on Main Gears
Airbus A-300-600	A-300	140,000	92,160	44.80	18.60	92.50
Airbus A-310-300	A-310	124,000	80,050	43.90	15.21	91.60
Airbus A-320-200	A-320	64,500	39,750	33.91	12.63	90.50
Fokker 100	F100	39,915	24,375	28.08	14.00	89.50

TABLE A.1 Aircraft Data for Approach Groups C and D.

Aircraft Name	REDIM Code	Max. Landing Mass (Kg)	Oper. Empty Mass (Kg.)	Aircraft Wingspan (m.)	Aircraft Wheel-Base (m.)	% Load on Main Gears
BAe 146-200	BAe-146	36,741	23,882	26.34	11.20	92.30
Boeing 727-200	B-727-200	73,028	46,164	36.75	16.75	92.50
Boeing 737-300	B-737-300	51,710	31,561	28.88	12.35	93.50
Boeing 747-200	B-747-200	255,825	170,180	28.88	12.50	92.50
Boeing 747-400	B-747-400	285,765	177,374	59.64	25.60	94.60
Boeing 757-200	B-757-200	89,813	57,267	63.30	25.60	94.00
Boeing 767-200	B-767-200	116,573	79,923	38.05	18.29	93.50
McDonnell MD-83	MD-83	63,276	36,546	47.57	19.69	92.20
McDonnell MD-87	MD-87	58,967	33,183	32.87	22.07	90.30
Mc. Donnell DC-10-30	DC-10-30	182,766	121,198	32.87	19.18	91.20
Douglas DC-8-73	DC-8-73	117,000	75,500	50.40	22.05	94.00
McDonnell MD-11	MD-11	195,047	125,646	53.00	28.27	93.80
Lockheed L-1011	L-1011	166,920	111,312			

Table A.2 illustrates the aircraft data representative of aircraft in approach group A aircraft. Note that the sequence of this table is the same as that used in the REDIM 2.1 master file definition. The number of aircraft in every aircraft database can be increased to 20 aircraft.

TABLE A.2 Data for Single Engine Aircraft (Approach Group A).

Aircraft Name	REDIM Code	Max. Landing Mass (Kg)	Oper. Empty Mass (Kg.)	Aircraft Wingspan (m.)	Aircraft Wheel-Base (m.)	% Load on Main Gears
Piper PA-38-112	PA-38-112	757	502	10.36	1.45	77.45
Piper PA-28-161	PA-28-161	1,109	596	10.67	2.03	82.18

TABLE A.2 Data for Single Engine Aircraft (Approach Group A).

Aircraft Name	REDIM Code	Max. Landing Mass (Kg)	Oper. Empty Mass (Kg.)	Aircraft Wingspan (m.)	Aircraft Wheel-Base (m.)	% Load on Main Gears
Piper PA-28-235	PA-28-235	1,363	705	10.92	1.98	81.73
Piper PA-32-301	PA-32-301	1,636	878	11.02	2.36	85.92
Piper PA-46-310P	PA-46-310P	1,772	1,118	13.66	2.44	83.31
Beechcraft F33A	BE F33F	1,545	964	10.21	2.13	81.51
Cessna 172	CE 172	1,090	676	10.92	1.70	77.93
Cessna 208	CE 208	3,615	2,230	15.88	2.11	81.20
Cessna 182	CE 182	1,338	790	10.92	1.69	78.85
Cessna 210	CE 210	1,772	1,007	11.20	1.81	77.60

TABLE A.3 Data for Twin-Engine Business Aircraft (Approach Group B).

Aircraft Name	REDIM Code	Max. Landing Mass (Kg)	Oper. Empty Mass (Kg.)	Aircraft Wingspan (m.)	Aircraft Wheel-Base (m.)	% Load on Main Gears
Beechcraft BE-58	BE-58	2,500	1,579	11.53	2.72	84.73
Beechcraft 300	BE 300	6,363	3,851	16.81	4.56	89.13
Cessna 402C	CE 402C	3,107	1,863	13.45	3.18	88.12
Cessna 421	CE 421	3,266	2,298	12.53	3.20	87.19
Beechcraft 2000	BE 2000	6,366	4,323	16.46	6.86	92.27
Cessna 406	CE 406	4,250	2,287	15.04	3.81	85.37
Piper PA-34-220T	PA-34-220T	2,160	1,296	11.85	2.13	82.13
Piper PA-42-1000	PA-42-1000	5,477	3,493	14.53	3.23	87.22
Piaggio P180	PD 180	4,777	3,27245	13.84	5.80	91.41

TABLE A.4 Data for Business, Turbofan-Powered Aircraft (Approach Groups B and C).

Aircraft Name	REDIM Code	Max. Landing Mass (Kg)	Oper. Empty Mass (Kg.)	Aircraft Wingspan (m.)	Aircraft Wheel-Base (m.)	% Load on Main Gears
Cessna CE-550	CE-550	5,773	3,351	15.90	5.55	92.61
Cessna CE-650	CE-650	9,090	5,306	16.31	6.50	92.95
Learjet 31	LEAR-31	6,940	4,514	13.34	6.15	93.42
Learjet 55	LEAR-55	8,165	5,737	13.34	7.01	93.27
Grumman G-IV	G1159	26,535	18,098	23.72	11.62	93.70
British Aeros. 125-800	BAE125	10,590	7,858	15.66	6.41	93.10
IAI 1124 (Westwind II)	IAI-1124	8,636	6,022	13.65	7.79	94.77
Beechcraft 400	BE-400	6,454	4,500	13.25	5.86	92.68
IAI 1125 (Astra)	IAI-1125	9,409	5,759	16.05	7.34	94.38
Dassault Falcon 100	DA-100	8,020	4,909	13.08	5.30	92.77
Dassault Falcon 200	DA-200	13,090	8,545	16.30	5.74	90.94
Dassault Falcon 50	DA-50	17,857	9,590	18.86	7.24	92.19
Canadair CL-601-3A	CL-601	16,363	11,220	19.61	7.99	92.86

TABLE A.5 Aircraft Data for Commuter Aircaft (Approach Group B).

Aircraft Name	REDIM Code	Max. Landing Mass (Kg)	Oper. Empty Mass (Kg.)	Aircraft Wingspan (m.)	Aircraft Wheel-Base (m.)	% Load on Main Gears
Saab 340-2	SAAB-340	12,020	7194	21.44	7.14	90.88

TABLE A.5 Aircraft Data for Commuter Aircaft (Approach Group B).

Aircraft Name	REDIM Code	Max. Landing Mass (Kg)	Oper. Empty Mass (Kg.)	Aircraft Wingspan (m.)	Aircraft Wheel-Base (m.)	% Load on Main Gears
British Aeros. 31	BAE-31	6,600	4,131	15.05	4.60	87.18
Embraer 120	EMB-120	11,250	6,878	19.78	6.97	90.77
Boeing DeHavilland 6	DCH-6	5,579	3,363	19.81	4.53	87.16
Boeing DeHavilland 7	DHC-7	19,958	12,560	28.35	8.38	90.89
Boeing DeHavilland 8	DHC-8-200	15,375	9,793	25.91	9.60	91.63
Beechcraft 1900C	BE-1900	7,302	3,946	16.61	7.25	93.72
Fairchild Metro III	SA-227	6,590	3,963	16.60	5.38	88.74
Embraer 110-P1	EMB-110	5,712	3,855	15.33	5.10	90.70
CASA 212-200	CASA-212	7,465	3,780	19.00	5.55	88.07
NRT 235-200	NRT-235	14,229	9,892	25.81	6.92	89.70
Aeros./Alenia ATR-72	ATR-72	21,385	13,460	27.05	10.70	93.26
Aeros./Alenia ATR-42	ATR-42	15,500	9,973	25.57	8.78	92.71
Fokker 50	F-50	18,890	12,520	29.00	9.70	92.13
British Aeros. ATP	BAE-ATP	21,773	13,594	30.63	9.70	92.62
Dornier 228-100	DO-228	6,213	3,547	16.97	6.29	91.05
Shorts 360	S-360	10,251	7,689	22.76	6.15	87.93

APPENDIX B

Airfield Data Used for Model Calibration

Tables B.1 through B.3 contain selected data used in the calibration of REDIM 2.1 for Washington National (DCA), Charlotte-Douglas and Atlanta Hartsfield International Airports, respectively. This data subset was selected for calibration of the landing roll profiles typical of small and large transport aircraft.

TABLE B.1 Data Subset Collected at Washington National Airport and Used in the Calibration of REDIM 2.1.

No.	A/C	Vfl (m/s)	Vtd (m/s)	TDL (m)	Lbr (m)	Vini (m/s)	LD (m)	DEC (m/s/s)	ROT (s)	EXIT
1	B-727	60.84	56.09	438.65	605.03	55.35	1132	2.05	50.83	RWY
2	B-727	68.2	66.69	258.92	268.22	66.69	1124.35	2.07	40.37	I
3	B-727	64.56	61.34	578.95	728.47	60.89	1280.89	2.54	42.2	RWY
4	B-727	67.59	64.04	387.92	474.57	58.35	1076.27	2.08	47.5	I
5	B-727	68.31	69.81	332.52	347.47	70.03	1276.63	2.15	43.53	RWY
6	B-727	73.04	73.71	258.92	347.47	73.71	1119.49	2.94	43.97	I
7	B-727	62.57	59.37	552.71	605.03	58.35	1139.23	2.35	43.7	RWY
8	B-727	67.82	58.49	344.67	347.47	58.35	1059.85	1.76	50.77	RWY

TABLE B.1 **Data Subset Collected at Washington National Airport and Used in the Calibration of REDIM 2.1.**

No.	A/C	Vfl (m/s)	Vtd (m/s)	TDL (m)	Lbr (m)	Vini (m/s)	LD (m)	DEC (m/s/s)	ROT (s)	EXIT
9	B-727	72.23	61.89	460.61	474.57	60.89	1121.36	2.17	42.43	RWY
10	B-727	62.62	63.47	355.94	474.57	60.89	1164.72	2.03	53.87	RWY
11	B-727	65.57	58.71	465.9	728.47	58.35	1131.22	3.11	38.9	RWY
12	B-727	72.07	73.63	342.55	347.47	73.71	1284.05	2.42	38.1	RWY
13	B-727	65.82	61.08	664.97	850.39	58.35	1526.53	1.85	58.43	J
14	B-727	68.21	59.55	822.86	972.31	58.37	1463.29	2.55	57.8	J
15	B-727	63.2	58.37	831.6	850.39	58.37	1450.52	2.09	67	J
16	B-727	71.59	67.43	446.31	474.57	66.69	1137.42	2.68	43.43	I
17	B-727	67.82	60.54	422.1	605.03	58.35	1164.42	2.24	47.83	RWY
18	B-727	68.56	63.29	364.39	474.57	60.89	1010.15	2.62	46.87	I
19	B-727	69.37	65.22	409.1	474.57	63.66	1243.28	2.05	41.83	RWY
20	B-727	69.95	66.42	358.56	474.57	63.66	1124.23	2.43	40.33	I
21	B-727	69.39	61.44	287.06	347.47	58.35	981.43	1.98	46.17	I
22	B-727	69.1	61.04	471.33	474.57	60.89	1137.95	2.12	42.6	I
23	B-727	65.41	62.99	506.24	605.03	60.89	1281.85	2.07	40.37	RWY
24	B-727	60.37	58.29	477.8	605.03	56.02	1069.8	2.41	43.23	I
25	B-727	69.68	65.49	567.44	728.47	63.66	1569.32	1.87	61.37	J
26	B-727	66.43	63.66	430.23	474.57	63.66	1026.75	2.86	42.07	H
27	B-727	67.89	66.41	480.86	728.47	60.89	1207.64	2.93	42.77	RWY
28	B-727	65.28	61.66	540.84	728.47	56.02	1263.58	2.09	42.2	I
29	B-727	66.51	61.48	399.67	474.57	58.35	1086.93	2.05	44.27	I
30	B-727	65.21	60.02	275.67	474.57	58.35	1107.18	1.98	42.87	I
31	B-727	62.74	60.89	386.03	474.57	60.89	1177.73	2	47.1	RWY
32	B-727	66.47	65.81	567.33	605.03	66.69	1265.73	2.69	40.43	RWY
33	B-727	70.31	64.5	439.15	474.57	63.66	1183.82	2.22	46.83	RWY

TABLE B.1 Data Subset Collected at Washington National Airport and Used in the Calibration of REDIM 2.1.

No.	A/C	Vfl (m/s)	Vtd (m/s)	TDL (m)	Lbr (m)	Vini (m/s)	LD (m)	DEC (m/s/s)	ROT (s)	EXIT
34	B-727	64.66	61.29	314.9	347.47	60.89	1081.97	1.91	40.07	I
35	B-727	69.18	66.69	474.19	474.57	66.69	1552.89	1.65	71	J
36	B-727	64.38	60.89	586.21	728.47	60.89	1352.22	2.25	69.97	J
37	B-727	65.65	62.26	234.35	474.57	60.89	1050.49	2.44	42.43	I
38	B-727	72.05	66.69	669.49	850.39	66.69	1374.13	3.39	42.67	RWY
39	B-727	66.14	61.39	451.68	605.03	60.89	1418.27	1.73	64.27	J
40	B-727	64.88	62.72	892.51	972.31	60.9	1580.83	2.31	62.37	J
41	B-727	67.7	66.66	481.24	605.03	66.66	1245.81	2.77	41.23	RWY
42	B-727	64.69	60.89	412.42	474.57	60.89	1313.96	1.67	40.43	RWY
43	B-727	68.35	61.88	558.46	728.47	60.89	1533.88	1.74	57.57	J
44	B-727	60.92	57.96	368.8	605.03	56.02	1090.3	2.31	43.93	I
45	B-727	60.87	56.02	474.57	728.47	53.86	1185.52	2.19	44.17	RWY
46	B-727	64.01	57.39	399.6	474.57	56.02	914.43	2.54	36.27	H
47	B-727	65.12	60.77	353.55	474.57	58.35	1112.3	1.96	41.37	I
48	B-727	68.94	64.81	426.45	605.03	63.66	1101.07	3.18	42.27	I
49	B-727	70.7	70.03	305.61	347.47	70.03	1307.94	2.08	38.47	RWY
50	B-727	70.89	66.69	658.38	728.47	66.69	1607.09	2.02	59.07	J
51	B-727	66.54	63.66	392.03	474.57	63.66	1101.98	2.51	43.27	I
52	B-727	66.68	63.86	332.48	474.57	63.66	1301.89	1.91	41.83	RWY
53	B-727	65.87	63.11	372.83	474.57	60.89	1207.44	1.92	48.27	RWY
54	B-727	69.05	63.66	347.47	474.57	60.89	1094.14	2.27	39.3	I
55	B-727	65.19	63.39	487.28	728.47	60.89	1279.4	2.55	85.23	J
56	B-727	71.88	65.77	367.6	474.57	60.89	1130.75	2.14	40.6	I
57	B-727	68.03	64.59	564.57	605.03	63.65	1546.54	1.67	61.67	J
58	B-727	67.52	63.11	259.89	347.47	60.89	976.32	2.23	47.57	I

TABLE B.1 Data Subset Collected at Washington National Airport and Used in the Calibration of REDIM 2.1.

No.	A/C	Vfl (m/s)	Vtd (m/s)	TDL (m)	Lbr (m)	Vini (m/s)	LD (m)	DEC (m/s/s)	ROT (s)	EXIT
59	B-727	65.64	60.89	347.47	474.57	58.35	1116.8	1.95	39.7	I
60	B-727	66.86	63.66	472.67	474.57	63.66	1175.28	2.25	37.9	I
61	B-727	64.17	60.84	477.38	605.03	58.35	1099.11	2.54	46.1	I
62	B-727	64.96	63.52	353.83	474.57	60.89	1111.95	2.2	42.57	I
63	B-727	63.72	59.06	568.49	850.39	58.35	1276.79	2.94	44.37	RWY
64	B-727	61.56	60.12	367.64	605.03	53.86	1044.45	2.28	49.37	I
65	B-727	63.26	58.35	567.93	728.47	58.35	1170.14	2.84	41.53	I
66	B-727	66.15	63.66	440.83	474.57	63.66	1132.09	2.4	38.07	I
67	B-727	67.56	61.93	427.07	474.57	60.89	1044.45	2.46	43	I
68	B-727	68.4	66.69	471.97	474.57	66.69	1336.59	2.06	40.4	RWY
69	B-727	65.91	63.66	576.43	605.03	63.66	1252.13	2.44	44.03	I
70	B-727	62.19	58.35	490.13	728.47	58.35	1445.71	1.75	68.7	J
71	B-727	62.91	58.35	661.86	850.39	58.35	1531.02	1.84	61.8	J
72	B-727	68.8	66.69	423.05	605.03	66.69	1485.86	2.01	64.17	J
73	B-737	56.04	53.72	631.89	728.47	53.72	1075.67	2.86	48.8	I
74	B-737	72.33	70.8	366.47	474.57	66.11	1148.11	2.58	41.3	RWY
75	B-737	66.4	62.63	428.75	474.57	61.06	1120.64	2.19	39.53	RWY
76	B-737	73.26	65.42	404.17	605.03	65.42	1238.94	2.67	37.97	RWY
77	B-737	64.19	57.19	349.38	474.57	53.87	902.1	2.34	34.8	H
78	B-737	61.08	54.4	465.26	605.03	53.87	1146.04	1.85	42.57	I
79	B-737	66.71	61.43	463.67	605.03	61.06	1446.71	1.68	61.17	J
80	B-737	62.53	61.06	247.11	347.47	61.06	1026.92	2.08	39.97	I
81	B-737	69.36	63.43	405.56	605.03	61.06	1102.2	2.84	42.23	I
82	B-737	63.82	57.73	458.43	605.03	57.24	1093.67	2.43	44.1	I
83	B-737	68.08	65.42	476.75	605.03	65.42	1129.13	3.23	39.57	I

TABLE B.1 Data Subset Collected at Washington National Airport and Used in the Calibration of REDIM 2.1.

No.	A/C	Vfl (m/s)	Vtd (m/s)	TDL (m)	Lbr (m)	Vini (m/s)	LD (m)	DEC (m/s/s)	ROT (s)	EXIT
84	B-737	67.39	65.82	377.16	605.03	62.62	1135	2.85	44.8	RWY
85	B-737	69.19	59.15	343.54	474.57	58.94	1037.07	2.29	44.3	RWY
86	B-737	71.68	70.36	364.6	474.57	62.62	1102.46	2.41	39.93	RWY
87	B-737	57.4	55.66	474.57	605.03	55.66	1061.77	2.41	43.57	RWY
88	B-737	68.52	66.79	337.08	347.47	66.79	1223.94	2.03	42.8	RWY
89	B-737	61.5	55.66	364.17	474.57	55.66	1075.91	1.83	41.8	I
90	B-737	67.55	60.77	411.29	474.57	58.94	1132.18	1.96	39.93	I
91	B-737	62.45	58.81	352.28	474.57	55.66	1010.66	2.05	47.1	I
92	B-737	70.17	67.21	327.73	347.47	66.79	1048.49	2.54	43.57	I
93	B-737	62.48	62.52	341.18	347.47	62.62	1124.93	1.94	44.2	RWY
94	B-737	65.98	59.42	333.48	347.47	58.94	1134.38	1.64	47.4	I
95	B-737	65.57	62.62	460.19	474.57	62.62	1237.54	1.98	43.13	RWY
96	B-737	63.28	61.36	390.91	474.57	58.94	1010.2	2.4	48.03	I
97	B-737	64.29	58.94	414.26	474.57	58.94	1114.09	2.01	41.57	I
98	B-737	62.77	58.25	501.91	728.47	55.66	1229.39	2.19	47.07	RWY
99	B-737	68.75	61.49	368.18	474.57	55.66	1098.67	1.76	39.6	I
100	B-737	63.1	58.94	361.22	474.57	58.94	1116.12	2.01	42.43	I
101	B-737	64.93	62.62	549.72	605.03	62.62	1132.47	2.86	43.53	I
102	B-737	61.83	57.14	417.15	474.57	55.66	1063	1.87	43.6	I
103	B-737	66.94	63.57	295.18	347.47	62.62	1039.89	2.18	42.47	I
104	B-737	63.11	59.17	230.9	347.47	57.54	1027.37	1.77	47.83	I
105	B-737	70.8	64.31	483.14	605.03	64.31	1244.59	2.53	42.07	RWY
106	B-737	68.62	67.05	388.15	474.57	64.31	1134.88	2.45	39.4	I
107	B-737	70.55	65.03	452.02	728.47	64.31	1262.17	3.03	42.2	RWY
108	B-737	65.1	64.31	333.27	474.57	64.31	1016	2.99	40.1	H

TABLE B.1 **Data Subset Collected at Washington National Airport and Used in the Calibration of REDIM 2.1.**

No.	A/C	Vfl (m/s)	Vtd (m/s)	TDL (m)	Lbr (m)	Vini (m/s)	LD (m)	DEC (m/s/s)	ROT (s)	EXIT
109	B-757	65.82	59.68	510.28	605.03	56.78	1225.4	1.87	47.6	RWY
110	B-757	66.12	59.22	266.09	347.47	54.59	885.45	1.93	38.9	H
111	B-757	73.38	64.52	418.45	474.57	64.52	1317.06	1.94	38.67	RWY
112	B-757	64.69	54.59	763.05	972.31	52.57	1475.25	1.85	61.33	J
113	B-757	62.19	59.14	416.48	474.57	59.14	1138.42	1.96	43.13	I
114	B-757	78.32	78.86	344.84	347.47	78.86	1138.04	3.36	46.3	I
115	B-757	78.59	77.31	394.9	474.57	74.71	1107.2	3.7	49.73	I
116	B-757	77.75	73.9	489.45	850.39	67.6	1263.82	4.44	44.27	RWY
117	B-757	67.92	59.3	466.67	474.57	59.14	1039.9	2.3	42.73	I
118	B-757	65.4	57.06	261.56	474.57	50.7	1081.06	1.38	47.1	I
119	B-757	62.85	59.63	450.7	474.57	59.14	1150.42	1.92	50.1	RWY
120	B-757	64.56	61.73	346.8	347.47	61.72	1094.45	1.95	49.6	RWY
121	B-757	62.43	56.78	493.5	728.47	56.78	1301.13	2.03	41.63	RWY
122	B-757	64.93	59.55	454.76	474.57	59.14	1179.83	1.84	41.2	I
123	B-757	58.94	55.05	448.14	605.03	54.59	1059.66	2.29	44.27	I
124	B-757	59.96	54.59	396.61	474.57	54.59	1101.58	1.66	44.97	I
125	B-757	63.16	57.91	381.84	474.57	54.59	1034.43	1.86	44.4	I
126	B-757	63.76	60.61	376.05	474.57	56.78	1155.49	1.71	34.93	J
127	B-757	68.31	61.76	412.85	474.57	59.14	1148.37	1.93	41	I
128	B-757	62.69	57.48	436.97	474.57	56.78	1099.89	1.86	40.43	I
129	B-757	62.88	57.43	380.56	605.03	50.7	1075.13	1.78	46.17	I
130	B-757	64.21	57.02	468.46	474.57	56.78	1137.7	1.75	41.77	I
131	B-757	57.44	54.1	378.27	474.57	52.57	874	2.33	46.43	H
132	B-757	60.11	54.84	467.67	474.57	54.59	1072.56	1.74	45.13	I
133	B-757	62.31	61.72	299.92	347.47	61.72	1027.29	2.14	39.57	I

TABLE B.1 Data Subset Collected at Washington National Airport and Used in the Calibration of REDIM 2.1.

No.	A/C	Vfl (m/s)	Vtd (m/s)	TDL (m)	Lbr (m)	Vini (m/s)	LD (m)	DEC (m/s/s)	ROT (s)	EXIT
134	B-757	59.09	59.14	523.85	605.03	59.14	1234.58	2.06	45.43	RWY
135	DC-9	63.35	54.68	311.87	474.57	53.03	1130.9	1.46	41.63	I
136	DC-9	62.33	57.19	484.13	605.03	54.54	1110.82	2.05	42.83	RWY
137	DC-9	67.86	64.16	375.27	474.57	64.16	1084.55	2.64	44	I
138	DC-9	66.03	61.91	427.35	605.03	60.61	1281.19	2.05	45.2	I
139	DC-9	58.28	57.41	475.68	605.03	57.4	1239.28	1.89	43.43	RWY
140	DC-9	58.82	57.4	344.68	347.47	57.4	1003.17	1.83	48.8	I
141	DC-9	66.72	62.54	533.75	728.47	60.6	1283.04	2.50	38.77	RWY
142	DC-9	64.86	59.74	381.57	474.57	57.4	1092.02	1.94	41.57	I
143	DC-9	62.03	60.6	326.92	347.47	60.6	1083.69	1.88	40.2	I
144	DC-9	66.92	67.97	336.03	347.47	68.17	1159.29	2.31	40.77	I
145	DC-9	68.6	62.3	510.47	605.03	57.4	1295.97	1.73	46.77	RWY
146	DC-9	67.19	62.25	383.34	474.57	57.4	1113.48	1.87	39.83	I
147	DC-9	66.23	64.16	452.27	605.03	64.16	1500.02	1.80	67.5	J
148	DC-9	66.45	61.33	703.12	728.47	60.6	1436.78	1.96	63.57	J
149	DC-9	65.08	62.03	552.4	728.47	60.6	1487.94	1.83	61.23	J
150	DC-9	67.62	62.81	372.88	605.03	57.4	1049.8	2.69	45	I
151	DC-9	66.55	61.04	406.08	474.57	57.4	1112.1	1.88	39.73	I
152	DC-9	63.41	60.17	744.57	850.39	57.4	1418.23	2.11	68.9	J
153	DC-9	66.75	62.25	383.35	605.03	57.4	934.49	3.64	37.87	H
154	DC-9	61.21	57.4	593.22	728.47	57.4	1566.47	1.43	67.03	J
155	DC-9	62.62	60.6	466.65	474.57	60.6	1012.6	2.58	47.37	I
156	DC-9	75.46	68.27	345.08	347.47	68.17	1252.92	2.07	42.3	I
157	DC-9	66.85	62.97	389.89	474.57	60.6	1072.55	2.32	43.23	I
158	DC-9	68.92	60.6	569.51	605.03	60.6	1362.93	1.83	36.03	RWY

TABLE B.1 **Data Subset Collected at Washington National Airport and Used in the Calibration of REDIM 2.1.**

No.	A/C	Vfl (m/s)	Vtd (m/s)	TDL (m)	Lbr (m)	Vini (m/s)	LD (m)	DEC (m/s/s)	ROT (s)	EXIT
159	DC-9	60.95	57.4	456.55	474.57	57.4	1036.76	2.13	46.83	I
160	DC-9	64.56	62.79	396.18	474.57	60.6	1125.66	2.13	53	RWY
161	DC-9	64.47	60.3	486.67	605.03	57.4	1245.48	1.87	42.17	RWY
162	DC-9	60.95	56.62	510.13	605.03	54.54	1130.23	1.98	41.53	I
163	DC-9	61.9	56.21	400.52	474.57	54.54	1030.53	1.87	51.43	I
164	DC-9	62.46	60.6	252.18	347.47	60.6	1052.21	1.97	40.27	I
165	DC-9	69.35	64.67	318.23	474.57	64.16	1362.44	1.81	47.1	RWY
166	DC-9	63.76	59.49	391.5	605.03	57.4	1189.88	2.05	47.53	RWY
167	DC-9	71.59	67.74	361.16	474.57	64.16	1109.41	2.53	42.13	I
168	DC-9	66.78	60.79	341.68	347.47	60.6	1051.61	1.97	42.33	I
169	DC-9	62.84	58.4	434.78	605.03	57.4	1112.4	2.36	44.03	RWY
170	DC-9	61.1	57.4	437.41	474.57	57.4	1058.38	2.05	46.07	I
171	MD-80	77.29	68.26	427.64	443.48	67.58	1414.32	1.89	67.27	J
172	MD-80	69.89	66.22	503.58	728.47	61.44	1294.38	2.54	42	RWY
173	MD-80	84.5	79.51	405.57	474.57	79.51	1507.88	2.62	71.3	J
174	MD-80	76.22	72.93	404.94	474.57	75.09	1125.24	3.64	43.73	RWY
175	MD-80	73.44	68.14	454.47	474.57	67.58	1326.11	2.15	42.27	RWY
176	MD-80	79.01	76.07	446.44	728.47	75.09	1566.9	2.83	68.47	J
177	MD-80	64.34	61.44	447.82	474.57	61.44	1105.73	2.28	39.67	RWY
178	MD-80	71.55	68.59	438.5	474.57	67.58	1305.8	2.21	38.77	RWY
179	MD-80	71.26	68.28	449.87	474.57	67.58	1668.41	1.54	60.97	J
180	MD-80	72.3	64.12	358.17	474.57	61.44	1089.14	2.34	43.33	I
181	MD-80	63.92	61.44	447.82	605.03	61.44	1108.99	2.85	43.8	I
182	MD-80	72.55	71.12	475.53	605.03	67.58	1591.97	1.86	56.83	J
183	MD-80	67.83	64.84	313.57	347.47	64.37	1105.73	2.14	44.1	I

TABLE B.1 Data Subset Collected at Washington National Airport and Used in the Calibration of REDIM 2.1.

No.	A/C	Vfl (m/s)	Vtd (m/s)	TDL (m)	Lbr (m)	Vini (m/s)	LD (m)	DEC (m/s/s)	ROT (s)	EXIT
184	MD-80	67.31	63.92	366.72	474.57	61.44	1137.09	2.17	40.37	I
185	MD-80	70.09	67.95	323.88	347.47	67.58	998.71	2.82	37.2	H
186	MD-80	64.33	60.84	376.01	474.57	58.77	1250.41	1.65	42.67	RWY
187	MD-80	64.24	57.81	305.09	474.57	56.32	1051.38	1.97	46.37	I
188	MD-80	67.44	63.68	377.37	474.57	61.44	1089.21	2.34	40.7	I
189	MD-80	68.5	65.41	433.24	474.57	64.37	1472.28	1.63	61.8	J
190	MD-80	65.1	59.54	567.29	605.03	58.77	1210.88	2.11	39.73	I
191	MD-80	65.53	64.38	450.47	474.57	64.38	1155.3	2.38	37.67	I
192	MD-80	64.4	61.08	457.32	474.57	61.44	1333.37	1.67	69.83	J
193	MD-80	65.3	58.77	636.37	850.39	58.77	1417.67	2.25	62	RWY
194	MD-80	70.1	64.37	377.51	474.57	64.37	1262.59	2.06	42.6	RWY
195	MD-80	64.52	58.15	558.28	728.47	56.32	1380.47	1.74	37.1	RWY
196	MD-80	76.12	64.25	350.05	474.57	58.77	1096.1	2.05	98.17	I
197	MD-80	65.69	62.39	273.24	347.47	61.44	1150.82	1.79	40.97	I
198	MD-80	64.63	60.76	364.3	605.03	56.32	1069.48	2.45	41.83	I
199	MD-80	64.58	60.81	505.14	605.03	58.77	1567.21	1.33	67.57	J
200	MD-80	67.23	60.17	507	728.47	56.32	1137.33	2.78	40	I
201	MD-80	67.63	60.9	292.19	605.03	61.45	1224.93	2.32	40.4	I
202	MD-80	63.57	58.77	818.58	850.39	58.77	1466.06	2.07	64.9	J
203	MD-80	72.55	66.73	381.07	474.57	64.37	1294	1.98	41.1	RWY
204	MD-80	66.92	63.58	381.61	474.57	61.44	1114.45	2.25	38.97	I
205	MD-80	67.09	60.72	492.89	728.47	56.32	1245.35	2.20	46.4	RWY
206	MD-80	65.2	62.87	381.44	605.03	58.77	1162.8	2.29	39.6	I
207	MD-80	67.63	64.97	304.83	347.47	64.37	1108.03	2.13	39.8	I
208	MD-80	66.37	59.54	457.09	605.03	58.77	1366.9	1.68	72.4	J

TABLE B.1 Data Subset Collected at Washington National Airport and Used in the Calibration of REDIM 2.1.

No.	A/C	Vfl (m/s)	Vtd (m/s)	TDL (m)	Lbr (m)	Vini (m/s)	LD (m)	DEC (m/s/s)	ROT (s)	EXIT
209	MD-80	64.86	62.32	436.29	474.57	61.44	1138.71	2.16	44.03	I
210	MD-80	62.24	58.77	474.57	728.47	56.32	1257.55	2.15	67.93	J
211	MD-80	68.13	66.76	364.44	474.57	61.44	1230.33	1.90	45.3	RWY
212	MD-80	65.07	64.18	351.75	474.57	58.77	1090.02	2.07	41.73	I
213	MD-80	66.38	61.89	454.91	474.57	61.44	1181.21	2.03	39.77	I
214	MD-80	65.6	59.25	401.89	474.57	56.32	1184.55	1.60	49	RWY
215	MD-80	73.74	70.02	387.5	474.57	67.58	1455.89	1.87	63.53	J
216	MD-80	65.32	58.78	533.35	728.47	58.75	1218.56	2.60	48.8	RWY
217	MD-80	68.19	64.94	306.82	347.47	64.37	1510.35	1.39	62.6	J
218	MD-80	69.35	64.46	470.99	474.57	64.37	1479.78	1.61	67.37	J
219	MD-80	66.29	61.44	400.71	474.57	61.44	1046.75	2.51	44	I
220	MD-80	66.25	66.25	391.64	474.57	66.25	1152.53	2.57	43.1	I
221	MD-80	65.25	59.55	350.67	474.57	56.78	1087.12	1.90	43.47	I

TABLE B.2 Data Subset Collected at Charlotte/Douglas International Airport and Used in the Calibration of REDIM 2.1

No.	A/C	Vfl (m/s)	Vtd (m/s)	TDL (m)	Lbr (m)	Vini (m/s)	LD (m)	DEC (m/s/s)	ROT (s)	EXIT
222	B-727	68.19	67.11	708.13	845.82	65.65	1849.8	1.75	56.07	E
223	B-727	63.63	62.62	593.99	690.68	63.61	1786.7	1.49	60.3	E
224	B-727	68.57	67.29	640.18	845.82	67.57	1785.3	2	61.63	E
225	B-727	64.99	62.87	461.52	690.68	61.93	1794.3	1.38	61.83	E
226	B-727	69.46	66.86	603.2	845.82	66.59	1709.9	2.1	63.13	E

TABLE B.2 Data Subset Collected at Charlotte/Douglas International Airport and Used in the Calibration of REDIM 2.1

No.	A/C	Vfl (m/s)	Vtd (m/s)	TDL (m)	Lbr (m)	Vini (m/s)	LD (m)	DEC (m/s/s)	ROT (s)	EXIT
227	B-727	75.01	75.67	724.29	845.82	74	1922.9	2.17	51.63	E
228	B-727	67.02	65.39	423.51	690.68	61.93	1664.2	1.56	61.2	E
229	B-727	67.85	64.99	485.25	690.68	65.41	1226.1	3.2	40.07	B
230	B-727	68.48	67.03	574.22	845.82	66.59	1812.7	1.88	56.9	E
231	B-727	68.77	66.7	883.77	1133.9	60.96	1942.8	1.79	50.97	E
232	B-727	72.95	71.61	333.85	369.42	71.44	1746.3	1.58	59.83	E
233	B-727	64.45	63.27	367.82	845.82	60.56	1466.8	2.28	66.97	E
234	B-727	66.82	65.37	309.46	369.42	65.37	1819.1	1.21	59.07	E
235	B-737	62.16	57.97	496.34	690.68	57.33	1232.7	2.25	37.9	B
236	B-737	62.9	61.49	391.69	690.68	55.96	1225.3	2.14	47.63	B
237	B-737	63.96	62.56	343.07	369.42	62.24	1145	1.97	45.9	B
238	B-737	73.96	71.41	479.68	690.68	70.37	1275.1	3.52	40.33	B
239	B-737	60.9	58.67	354.82	690.68	54.01	1141.5	2.29	48.1	B
240	B-737	65.71	62.75	406.26	690.68	61.11	1414.9	2.01	64.97	E
241	B-737	63.2	61.44	315.37	369.42	61.23	1204.4	1.76	43.2	B
242	B-737	62.55	60.79	417.63	690.68	58.06	1792.8	1.17	60.13	E
243	B-737	60.48	58.53	429.77	690.68	56.63	1122.6	2.72	48	B
244	B-737	60.18	59.05	390.75	690.68	55.96	1176	2.35	47.03	B
245	B-737	62.98	61.33	405.89	690.68	58.06	1226	2.36	43.03	B
246	B-737	63.57	62.78	381.19	523.49	57.27	1097.3	2.12	54	B
247	B-737	67.08	66.22	449.5	690.68	66.35	1742.5	1.72	58.4	E
248	B-737	67.92	65.98	390.15	690.68	61.11	1134.2	3.25	42.47	B
249	B-737	64.95	65.06	298.29	369.42	64.31	1173	2.06	41.53	B
250	B-737	69.83	70.07	353.9	369.42	70.16	1186.9	2.51	40.57	B

TABLE B.2 Data Subset Collected at Charlotte/Douglas International Airport and Used in the Calibration of REDIM 2.1

No.	A/C	Vfl (m/s)	Vtd (m/s)	TDL (m)	Lbr (m)	Vini (m/s)	LD (m)	DEC (m/s/s)	ROT (s)	EXIT
251	B-737	66.29	64.15	462	690.68	63.61	1212.5	3.06	40.47	B
252	B-737	59.8	58.15	278.81	369.42	56.72	1042.8	1.77	52.17	B
253	B-737	65.42	64.42	313.81	369.42	63.24	1183	1.96	43.3	B
254	B-737	69.85	69.57	270.41	369.42	68.88	1193.3	2.38	41.03	B
255	B-737	65.94	61.88	498.41	690.68	61.11	1249.4	2.59	42.3	B
256	B-737	67.65	64.77	453.63	690.68	64.49	1676.6	1.7	63.6	E
257	B-737	65.63	64.28	391.81	690.68	63.61	1209.3	3.08	44.8	B
258	B-737	67.91	64.59	462.45	690.68	63.61	1215.2	3.05	44.03	B
259	B-737	68.01	66.4	374.53	690.68	61.11	1193.7	2.87	46.5	B
260	B-737	62.43	60.26	372.54	690.68	57.33	1346.3	1.87	70.8	E
261	B-737	68.79	67.09	648.76	690.68	67.29	1234.7	3.39	38.9	B
262	B-737	68.43	67.06	449.5	690.68	66.35	1798.4	1.63	59.77	E
263	B-737	68.79	66.49	423.37	690.68	68.3	1766.6	1.8	58.67	E
264	B-737	69.8	69.18	282.03	369.42	66.5	1214.2	2.14	40.67	B
265	B-737	68.29	67.53	309.6	369.42	67.69	1171.2	2.35	43.6	B
266	B-737	69.07	66.99	458.52	690.68	66.35	1772.9	1.67	58.13	E
267	B-737	69.88	68.38	443.07	845.82	65.65	1879.6	1.7	54.4	E
268	B-737	72.38	71.75	403.87	690.68	68.3	1787.9	1.77	62.4	E
269	B-757	59.26	58.04	305.1	369.42	57.57	1073.8	1.76	53.67	B
270	B-757	60.79	60.39	644.62	845.82	59	1524.9	1.95	74.87	E
271	B-757	61.88	60.19	499.66	690.68	60.31	1621.3	1.52	71.77	E
272	B-757	64.29	60.76	508.97	690.68	61.93	1741.8	1.45	66.07	E
273	DC-9	70.76	69.46	397.8	690.68	67.29	1766.6	1.74	62.3	E
274	DC-9	63.18	61.68	456.86	690.68	60.31	1191.8	2.78	45.5	B

TABLE B.2 Data Subset Collected at Charlotte/Douglas International Airport and Used in the Calibration of REDIM 2.1

No.	A/C	Vfl (m/s)	Vtd (m/s)	TDL (m)	Lbr (m)	Vini (m/s)	LD (m)	DEC (m/s/s)	ROT (s)	EXIT
275	DC-9	66.75	63.87	497.52	690.68	63.61	1235.5	2.94	43.8	B
276	DC-9	62.73	63.41	260.38	269.14	63.45	1220.6	1.69	43.13	B
277	DC-9	71.82	70.99	398.39	690.68	67.29	1738.6	1.78	62.13	E
278	DC-9	70.57	66.9	505.5	690.68	68.3	1710.9	1.9	62.1	E
279	DC-9	65.67	64.51	407.56	690.68	60.31	1220.3	2.64	42.53	B
280	DC-9	67.21	64.81	477.89	690.68	64.49	1782	1.54	63.07	E
281	MD-80	67.58	67.04	867.94	1133.9	60.65	1893.5	1.88	52.67	E
282	MD-80	67.82	65.83	412.4	690.68	64.49	1612.4	1.82	59.37	E
283	MD-80	64.91	62.24	472.12	845.82	59.77	1748.7	1.53	68.4	E
284	MD-80	62.89	61.6	399.97	690.68	59.52	1192.9	2.68	49.53	B
285	MD-80	64.81	63.88	754.22	845.82	63	1814.7	1.63	63.03	E
286	MD-80	70.54	69.22	400.52	690.68	67.29	1792.8	1.7	61.13	E
287	MD-80	67.64	65.07	547.35	845.82	65.65	1833.8	1.78	62.53	E

TABLE B.3 Data Subset Collected at Atlanta Hartsfield International Airport and Used in the Calibration of REDIM 2.1

No.	A/C	Vfl (m/s)	Vtd (m/s)	TDL (m)	Lbr (m)	Vini (m/s)	LD (m)	DEC (m/s/s)	ROT (s)	EXIT
288	B-727	64.5	61.41	408.5	665.99	58.95	1305.72	2.04	49.4	D
289	B-727	66.06	61.96	664.74	918.97	58.11	1356.55	2.86	47.1	D
290	B-727	67.22	66.37	521.73	579.58	66.22	1623.8	1.70	55.5	B11
291	B-727	70.5	69.16	552.48	579.58	69.06	1656.85	1.83	56.27	B11

TABLE B.3 Data Subset Collected at Atlanta Hartsfield International Airport and Used in the Calibration of REDIM 2.1

No.	A/C	Vfl (m/s)	Vtd (m/s)	TDL (m)	Lbr (m)	Vini (m/s)	LD (m)	DEC (m/s/s)	ROT (s)	EXIT
292	B-727	67.26	60.37	1069.1	1559.35	52.99	1869.01	3.11	45.7	B11
293	B-727	71.45	68.31	450.3	752.55	65.71	1683	1.87	52.53	B11
294	B-727	69.87	60.74	759.34	1005.38	58.39	1751.25	1.71	49.8	B11
295	B-727	71	68.12	687.01	1178.05	57.7	1770.86	2.08	48.13	B11
296	B-727	72.47	71.06	583.34	918.97	65.37	1786.52	1.97	49.27	B11
297	B-727	73.94	72.73	552.72	745.24	70.68	1708.39	2.16	50.53	B11
298	B-727	73.87	74.51	583.34	657.91	72.89	1691.03	2.17	53.5	B11
299	B-727	75.81	77.48	646.25	745.24	76.92	1815.23	2.37	44.7	B11
300	B-727	77.39	73.27	603.47	657.91	70.92	1747.66	1.93	48.83	B11
301	B-737	61.06	58.09	568.32	745.24	52.3	1229.39	1.93	49.57	B7
302	B-737	64.35	63.57	686.97	918.21	59.87	1838.96	1.49	48.7	B11
303	B-737	65.49	63.08	586.87	623.16	62.84	1312.4	2.24	41.93	B7
304	B-737	65.65	60.98	513.26	665.99	58.95	1440.04	1.69	65.23	B11
305	B-737	66.47	64.24	513.5	918.97	53.37	1347.98	2.30	39.67	B7
306	B-737	68.06	62.4	660.99	918.97	58.11	1360.16	2.84	51.03	D
307	B-737	70.7	69.78	635.77	1091.48	63.33	1814.83	2.18	46.97	B7
308	B-737	69.8	71.06	455.5	492.71	71.22	1726.56	1.72	51.07	B11
309	B-737	71.25	68.11	643.17	1005.38	55.85	1374.19	3.04	38.97	B7
310	B-737	72.81	69.79	677.3	709.27	69.56	1812.58	1.82	46.23	B11
311	B-737	72.71	68.29	624.55	1005.38	58.39	1809.49	1.59	48.53	B11
312	B-737	76.48	71.65	673.58	918.97	68.82	1691.77	2.51	50.07	B11
313	B-757	51.97	49.28	635.47	918.97	44.32	1157.71	2.26	47.47	C
314	B-757	65.45	63.76	589.89	788.52	59.22	1696.76	1.47	53.83	B11
315	B-757	64.45	61.52	890.74	1264.61	55.25	1764.58	2.18	52.67	B11

TABLE B.3 Data Subset Collected at Atlanta Hartsfield International Airport and Used in the Calibration of REDIM 2.1

No.	A/C	Vfl (m/s)	Vtd (m/s)	TDL (m)	Lbr (m)	Vini (m/s)	LD (m)	DEC (m/s/s)	ROT (s)	EXIT
316	B-757	65.8	64.66	580	1005.38	58.39	1722.78	1.78	51.37	B11
317	B-757	64.86	58.27	762.48	1005.38	54.66	1739.63	1.45	53.67	B11
318	B-757	64.46	65.05	598.93	745.24	60.81	1735.61	1.44	52.27	B11
319	B-757	67.24	66.6	652.46	788.52	64.34	1751.25	1.71	50	B11
320	B-757	68.03	63.79	803.96	1005.38	59.75	1762.39	1.79	47.35	B11
321	B-757	67.92	64.4	638.27	1005.38	53.53	1569.02	1.77	59.47	B11
322	B-757	72.65	71.3	847.24	918.97	70.68	1801.46	2.35	46.83	B11
323	DC-9	58.98	60.11	389.66	492.71	60.56	1336.35	1.67	43.63	B7
324	DC-9	64.84	60.89	506.66	874.93	54.15	1622.51	1.39	59.43	B11
325	DC-9	67.58	62.96	489.13	752.55	59.71	1736.19	1.39	52.23	B11
326	DC-9	69.43	69.28	582.46	623.16	69.26	1616.94	1.99	57.67	B11
327	DC-9	66.32	68.99	376.05	448.97	69.8	1246.63	2.52	49.53	D
328	DC-9	69.23	68.11	619.31	623.16	68.1	1770.86	1.66	51	B11
329	DC-9	70.99	70.07	633	832.1	68.34	1754.53	2.07	51.2	B7
330	DC-9	70.98	67.94	579.28	657.91	65.6	1695.6	1.67	52.43	B11
331	DC-9	70.65	67.89	628.55	832.1	64.68	1862.73	1.62	47.33	B11
332	DC-9	70.96	67.17	626.8	752.55	66.02	1770.86	1.73	47.37	B11
333	DC-9	72.34	71.01	854.18	918.97	70.68	1884.14	2.15	52.6	B11
334	DC-9	68.37	70.13	626.72	918.97	68.82	1779.89	2.26	49.57	B7
335	DC-9	74.44	70.16	810.19	918.97	68.82	1889.12	2.01	43.57	B11
336	MD-80	56.46	55.28	469.06	657.91	48.59	1096.89	1.69	42.67	C
337	MD-80	57.73	56.77	409.16	492.71	56.47	1097.43	1.92	51.47	C
338	MD-80	59.47	59.25	504.13	788.52	48.25	1202.15	1.76	43.5	C
339	MD-80	63.4	63.61	461.23	492.71	63.63	1295.72	1.99	44.3	B7

TABLE B.3 Data Subset Collected at Atlanta Hartsfield International Airport and Used in the Calibration of REDIM 2.1

No.	A/C	Vfl (m/s)	Vtd (m/s)	TDL (m)	Lbr (m)	Vini (m/s)	LD (m)	DEC (m/s/s)	ROT (s)	EXIT
340	MD-80	64.42	59.95	660.91	832.1	60.39	1348.52	2.69	42.27	B7
341	MD-80	65.31	66.09	572.42	1005.38	58.39	1687.23	1.87	56.73	B11
342	MD-80	66.27	63.38	603.21	788.52	56.04	1285.26	2.29	46.23	B7
343	MD-80	67.76	66.17	554.05	657.91	64.00	1319.61	2.45	45.37	D
344	MD-80	66.92	67.95	486.93	657.91	64.00	1862.49	1.36	49.00	B11
345	MD-80	68.66	68.16	703.73	918.97	67.06	1797.06	2.08	48.07	B11
346	MD-80	68.09	66.04	646.86	1005.38	58.39	1688.41	1.87	60.5	B11
347	MD-80	68.76	67.16	800.31	1264.61	56.45	1828.19	2.06	45.23	B11
348	MD-80	67.93	69.15	532.89	918.97	62.26	1811.75	1.7	48	B11
349	MD-80	67.54	68.83	573.8	745.24	63.78	1400.1	2.45	77.43	B11
350	MD-80	70.86	67.35	660.15	745.24	65.37	1704.62	1.79	58.5	B11
351	MD-80	71.19	70.33	402.61	492.71	70.03	1699.06	1.69	55.83	B11
352	MD-80	71.28	68.71	385.83	665.99	66.47	1799.84	1.58	49.07	B11
353	MD-80	68.24	69.07	541.24	657.91	65.6	1678.06	1.7	54.7	B11
354	MD-80	71.5	69.4	622.05	918.97	62.26	1732.83	1.86	51.23	B11
355	MD-80	72.12	66.02	569.84	1091.48	57.7	1728.03	1.94	53.4	B11
356	MD-80	73.04	72.53	520.17	579.58	72.44	1750.9	1.89	52.43	B11
357	MD-80	69.16	72.67	395.93	448.97	73.42	1735.36	1.78	52.33	B7
358	MD-80	71.29	72.29	474.07	745.24	63.79	1810.78	1.52	47	B11
359	MD-80	74.41	72.49	537.88	745.24	70.68	1778.2	2.01	48.97	B11
360	MD-80	73.51	71.35	639.18	745.24	70.68	1810.78	1.95	47.93	B11
361	MD-80	73.34	66	942.78	1178.05	63.33	1850.5	2.34	45.2	B11
362	MD-80	74.38	70.08	608.82	709.27	69	1867.88	1.7	46.03	B11
363	MD-80	76.95	74.52	673.03	788.52	72.38	1843.71	2.09	47.77	B11

APPENDIX C

Runway Occupancy Time and Exit Assignment Tables (Right Angle Turnoffs)

This appendix contains the simulation results presented in Chapters 3 and 4 and applied to a runway with selected aircraft mixes. The main motivation of these results is to provide quick guidance on the optimal location of standard and high speed exits for various aircraft mixes and exit locations to airport designers.

The aircraft populations selected are representative of the United States fleet operating at the largest 100 airports. The aircraft mix data was obtained from the Federal Aviation Administration Statistics for Carrier Airports [FAA, 1992] and the Aviation and Aerospace Almanac. The procedure employed here uses the existing population aircraft mix in the US fleet and assigns them to a hypothetical scenario testing the percentage of aircraft exiting at discrete runway exit locations. The data was derived with REDIM 2.1 for a runway 3000 m. long and sea level standard atmosphere conditions.

Table C.1. through C.4 contain the percentage information for standard runway exits (i.e., 90 degree turnoffs). Figures C.1 through C.4 illustrate graphically the results contained in Tables C.1 through C.4, respectively. Information on high speed exit assignments can be found in Chapter 3 of this document.

The use of this information should beviewed as a guideline for airport designers to locate optimal exits subjected to aircraft population mixes comparable to those found in the average US fleet mix. All tables and figures in this appendix assign aircraft into approach speed categories using the standard Air Traffic Control classification. The data shows dry and wet exit assignments as well as the corresponding runway occupancy times associated with each assignment.

FIGURE C.1 Typical Aircraft Exit Assignment and ROT Data for Approach Speed Group A (Right Angle Turnoffs).

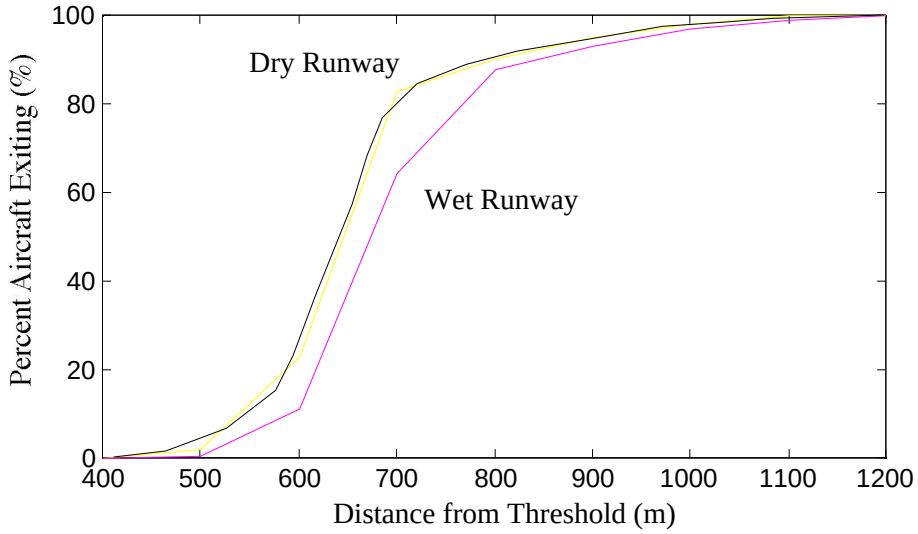

TABLE C.1 Aircraft Exit Assignment for Approach Group A (Right Angle Turnoffs).

Exit Location (m.)	Percent Exiting (Dry Runway)	Average ROT (s) Dry Runway	Percent Exiting (Wet)	Average ROT (s) Dry Runway
400	0	31	0	32
500	2	33	0	35
600	23	36	11	37
700	83	38	65	38
800	90	42	88	41
900	95	45	93	46
1000	98	47	97	48
1100	100	51	99	51
1200	100	55	100	54

FIGURE C.2 Typical Aircraft Exit Assignment and ROT Data for Approach Speed Group B (Right Angle Turnoffs).

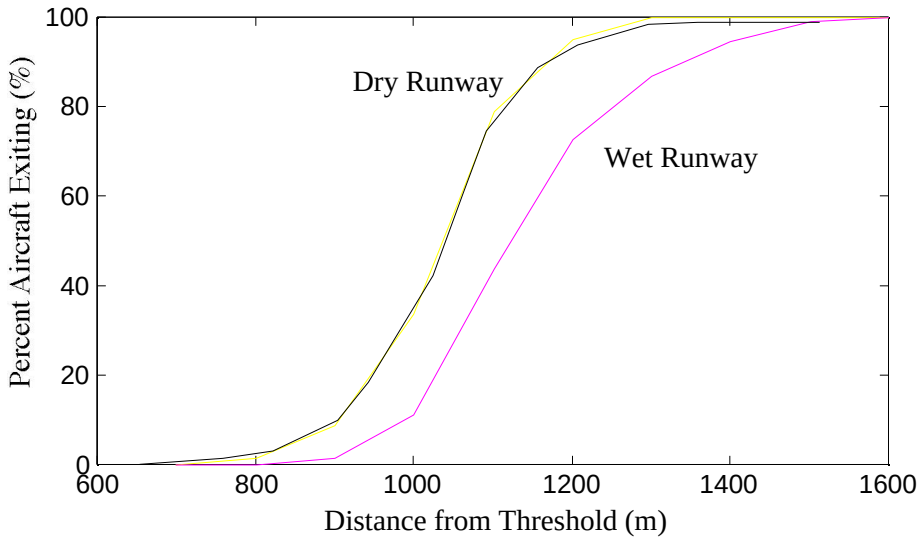

TABLE C.2 Aircraft Exit Assignment for Approach Group B (Right Angle Turnoffs).

Exit Location (m.)	Percent Exiting (Dry Runway)	Average ROT (s) Dry Runway	Percent Exiting (Wet)	Average ROT (s) Dry Runway
700	0	43	0	42
800	2	45	0	46
900	9	49	1	50
1000	34	53	11	53
1100	79	54	44	54
1200	95	56	73	57
1300	99	58	87	58
1400	100	59	95	59
1500	100	61	99	60
1600	100	62	100	61

FIGURE C.3 Typical Aircraft Exit Assignment and ROT Data for Approach Group C (Right Angle Turnoffs).

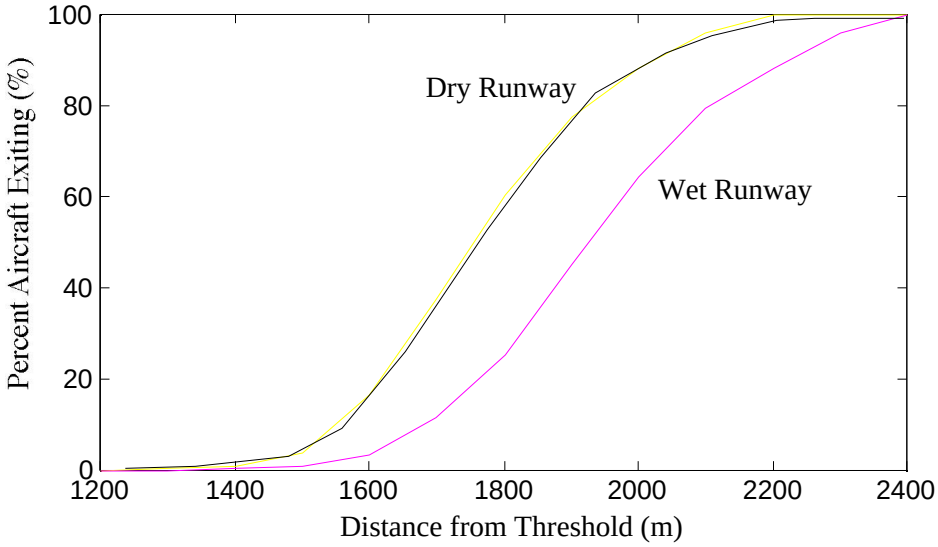

TABLE C.3 Aircraft Exit Assignment and ROT Data for Approach Speed Group C (Right Angle Turnoffs).

Exit Location (m.)	Percent Exiting (Dry Runway)	Average ROT (s) Dry Runway	Percent Exiting (Wet)	Average ROT (s) Dry Runway
1200	0	61	0	61
1300	1	62	0	62
1400	2	64	1	64
1500	4	66	1	66
1600	17	68	4	68
1700	37	69	12	69
1800	60	70	25	70
1900	78	72	46	72
2000	89	72	64	71
2100	96	74	80	75

TABLE C.3 Aircraft Exit Assignment and ROT Data for Approach Speed Group C (Right Angle Turnoffs).

Exit Location (m.)	Percent Exiting (Dry Runway)	Average ROT (s) Dry Runway	Percent Exiting (Wet)	Average ROT (s) Dry Runway
2200	100	74	88	74
2300	100	75	96	75
2400	100	78	100	79

FIGURE C.4 Typical Aircraft Exit Assignment and ROT Data for Approach Speed Group D (Right Angle Turnoffs).

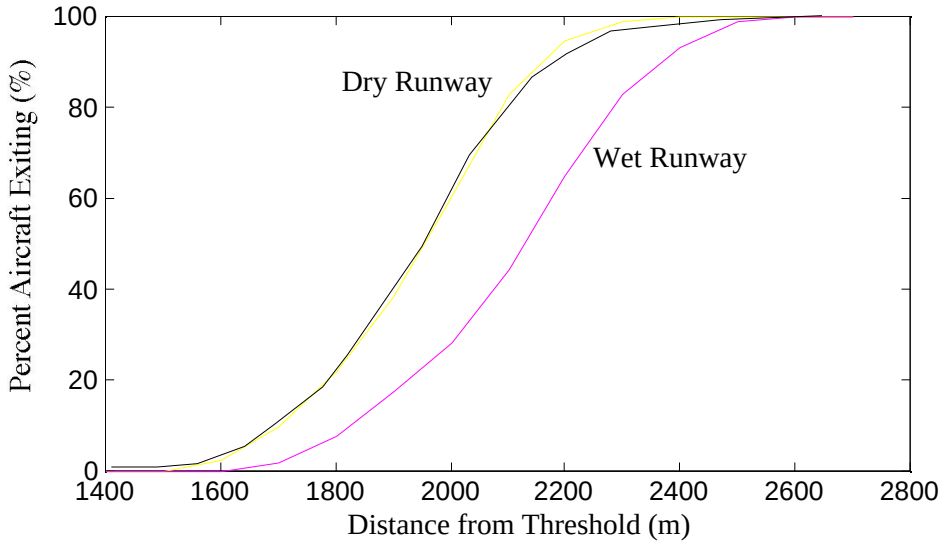

TABLE C.4 Aircraft Exit Assignment for Approach Speed Group D (Right Angle Turnoffs).

Exit Location (m.)	Percent Exiting (Dry Runway)	Average ROT (s) Dry Runway	Percent Exiting (Wet)	Average ROT (s) Dry Runway
1400	0	66	0	66
1500	1	69	0	69

TABLE C.4 Aircraft Exit Assignment for Approach Speed Group D (Right Angle Turnoffs).

Exit Location (m.)	Percent Exiting (Dry Runway)	Average ROT (s) Dry Runway	Percent Exiting (Wet)	Average ROT (s) Dry Runway
1600	2	69	1	70
1700	10	72	2	73
1800	22	73	8	73
1900	38	74	18	74
2000	61	76	29	76
2100	83	77	45	77
2200	94	76	65	76
2300	99	80	83	79
2400	100	79	93	79
2500	100	81	99	82
2600	100	82	100	81
2700	100	82	100	82

APPENDIX D

Recommended High Speed Turnoff Geometries

This appendix contains information on the proposed high speed turnoff geometries discussed in Chapter 4 of this report. The geometries are generically named REDIM XXYY denoting the parent application from which they were derived. The letters XX correspond to the turnoff design speed (in meters per second) whereas YY represents the final exit angle with respect to the runway centerline. To illustrate this principle a geometry denoted REDIM 3520 will represent a turnoff designed for a speed of thirty five meters per second entry speed and having a final exit angle at the tangent point of twenty degrees. In this research many turnoff geometries having so-called high-speed design characteristics were investigated. However, for standardization purposes the following two categories of geometries are proposed: 1) High-speed turnoffs with 30 degree turning angles and 2) High speed turnoff with 20 degree turning angles. A further classification can be made if various types of aircraft are considered (i.e., heavy, large and small transport aircraft). For this treatment only two types of transport aircraft are considered since they are representative critical vehicles in airport planning and design.

Figure D.1 illustrates some of the relevant data for turnoff geometry REDIM 3520 using as an aircraft generator a trijet, medium size aircraft. Note that this geometry has a linear taper from metric stations 250 and 750 as this will provide pilots with better situational awareness of the turnoff. Table D.1 contains pertinent information regarding the x-y coordinates of a turnoff geometry sized for a Boeing 747-200 and that could be used for airport designs for design group V. The coordinate points have been generated using a lateral separation between runway and nearest taxiway of 229 m. (750 ft.). Note that if a different lateral distance is used a corresponding adjustment should be made to the lead-out turn.

Table D.1: Cartesian Coordinates for Turnoff Geometry REDIM 3520 (all coordinates in feet) Generated by a Large Transport Aircraft.

Station (ft.)	X Centerline Coordinate	Y Centerline Coordinate	X Left Edge (Coordinate)	Y Left Edge (Coordinate)	X Right Edge (Coordinate)	Y Rigth Edge (Coordinate)
0.00	0.00	0.00	0.00	75.00	0.00	-75.00
50.00	50.00	0.03	49.88	75.08	50.11	-75.03
100.00	100.00	0.20	99.55	75.28	100.45	-74.88
150.00	149.99	0.68	148.97	75.77	151.02	-74.42
200.00	199.98	1.59	198.25	76.68	201.73	-73.50
250.00	249.97	3.01	247.44	78.08	252.51	-72.06
300.00	299.93	4.98	296.55	80.02	303.30	-70.06
350.00	349.86	7.51	345.60	82.50	354.12	-67.47
400.00	399.77	10.66	394.59	85.59	404.94	-64.28
450.00	449.62	14.42	443.50	89.28	455.75	-60.44
500.00	499.43	18.82	492.34	93.59	506.51	-55.97
550.00	549.17	23.85	541.10	98.53	557.24	-50.83
600.00	598.85	29.56	589.77	104.12	607.92	-45.01
650.00	648.44	35.93	638.35	110.37	658.53	-38.50
700.00	697.94	43.00	686.82	117.27	709.06	-31.29
750.00	747.33	50.75	735.16	124.86	759.50	-23.37
800.00	796.61	59.19	783.38	133.14	809.84	-14.74
850.00	845.77	68.37	831.62	141.31	859.91	-4.58
900.00	894.78	78.25	879.84	149.65	909.73	6.84
950.00	943.63	88.85	927.92	158.71	959.35	19.00
1000.00	992.33	100.20	975.89	168.41	1008.78	31.98
1050.00	1040.85	112.28	1023.75	178.69	1057.94	45.88
1100.00	1089.18	125.12	1071.47	189.72	1106.88	60.54

Table D.1: Cartesian Coordinates for Turnoff Geometry REDIM 3520 (all coordinates in feet) Generated by a Large Transport Aircraft.

Station (ft.)	X Centerline Coordinate	Y Centerline Coordinate	X Left Edge (Coordinate)	Y Left Edge (Coordinate)	X Right Edge (Coordinate)	Y Rigth Edge (Coordinate)
1150.00	1137.29	138.73	1119.00	201.49	1155.57	75.97
1200.00	1185.18	153.10	1166.36	214.03	1204.00	92.17
1300.00	1280.22	184.17	1260.44	241.43	1300.00	126.93
1350.00	1327.34	200.89	1307.18	256.32	1347.50	145.48
1400.00	1374.31	218.04	1354.64	271.93	1393.97	164.15
1450.00	1421.28	235.18	1402.16	287.57	1440.40	182.79
1500.00	1468.25	252.33	1449.70	303.15	1486.80	201.50
1550.00	1515.21	269.46	1497.26	318.64	1533.16	220.29
1600.00	1562.18	286.61	1544.84	334.14	1579.53	239.08
1650.00	1609.15	303.75	1592.28	349.97	1626.02	257.54
1700.00	1656.13	320.90	1639.26	367.11	1672.99	274.68
1750.00	1703.10	338.04	1686.23	384.26	1719.97	291.82
1800.00	1750.06	355.18	1733.20	401.40	1766.93	308.96
1850.00	1797.04	372.32	1780.17	418.54	1813.91	326.11
1900.00	1844.00	389.46	1827.13	435.68	1860.87	343.24
1950.00	1890.98	406.60	1874.11	452.82	1907.84	360.39
2000.00	1937.94	423.75	1921.07	469.97	1954.81	377.53
2050.00	1984.91	440.89	1968.04	487.11	2001.78	394.68
2100.00	2031.89	458.03	2015.02	504.25	2048.76	411.81
2150.00	2078.86	475.17	2061.99	521.39	2095.72	428.95
2200.00	2125.82	492.32	2108.96	538.54	2142.69	446.10
2250.00	2172.79	509.46	2155.92	555.68	2189.66	463.24
2300.00	2219.77	526.60	2202.90	572.82	2236.63	480.38
2350.00	2266.76	543.66	2250.51	590.10	2283.02	497.22

Table D.1: Cartesian Coordinates for Turnoff Geometry REDIM 3520 (all coordinates in feet) Generated by a Large Transport Aircraft.

Station (ft.)	X Centerline Coordinate	Y Centerline Coordinate	X Left Edge (Coordinate)	Y Left Edge (Coordinate)	X Right Edge (Coordinate)	Y Rigth Edge (Coordinate)
2400.00	2314.34	559.00	2300.44	606.19	2328.26	511.80
2450.00	2362.64	571.93	2351.10	619.76	2374.18	524.10
2500.00	2411.52	582.43	2402.39	630.78	2420.65	534.09
2550.00	2460.86	590.48	2454.16	639.22	2467.57	541.74
2600.00	2510.54	596.05	2506.28	645.07	2514.81	547.04
2650.00	2560.44	599.14	2558.64	648.30	2562.25	549.97
2700.00	2610.43	599.80	2610.50	649.00	2610.37	550.60

Table D.2: Cartesian Coordinates for Turnoff Geometry REDIM 3530 (all coordinates in feet)Generated by a Large Transport Aircraft.

Station (ft.)	X Centerline Coordinate	Y Centerline Coordinate	X Left Edge (Coordinate)	Y Left Edge (Coordinate)	X Right Edge (Coordinate)	Y Rigth Edge (Coordinate)
0.00	0.00	0.00	0.00	75.00	0.00	-75.00
50.00	50.00	0.03	57.21	75.09	57.51	-75.02
100.00	100.00	0.20	113.94	75.38	115.13	-74.79
150.00	149.99	0.68	170.12	76.11	172.76	-74.09
200.00	199.98	1.59	225.87	77.40	230.23	-72.76
250.00	250.60	3.03	281.22	79.35	287.44	-70.75
300.00	299.93	4.98	336.19	81.98	344.37	-68.02
350.00	349.86	7.51	390.78	85.33	400.99	-64.55
400.00	399.77	10.66	444.98	89.40	457.28	-60.32
450.00	449.62	14.42	498.79	94.20	513.22	-55.33
500.00	499.43	18.82	552.20	99.74	568.80	-49.56

Table D.2: Cartesian Coordinates for Turnoff Geometry REDIM 3530 (all coordinates in feet)Generated by a Large Transport Aircraft.

Station (ft.)	X Centerline Coordinate	Y Centerline Coordinate	X Left Edge (Coordinate)	Y Left Edge (Coordinate)	X Right Edge (Coordinate)	Y Rigth Edge (Coordinate)
550.00	549.63	23.90	605.20	106.03	623.99	-43.02
600.00	598.85	29.56	657.79	113.05	678.79	-35.69
650.00	648.44	35.93	709.95	120.82	733.19	-27.60
700.00	697.94	43.00	761.66	129.32	787.16	-18.72
750.00	747.33	50.75	812.99	138.27	840.65	-8.79
800.00	796.61	59.19	864.08	146.84	893.46	3.02
850.00	845.77	68.37	914.75	156.15	945.76	15.58
900.00	894.78	78.25	964.97	166.17	997.55	28.91
950.00	943.63	88.85	1014.80	176.71	1048.75	43.21
1000.00	992.33	100.20	1064.17	187.97	1099.40	58.24
1050.00	1040.85	112.28	1113.07	199.97	1149.50	73.99
1100.00	1089.18	125.12	1161.48	212.70	1199.02	90.46
1150.00	1137.29	138.73	1209.40	226.14	1247.95	107.63
1200.00	1185.18	153.10	1256.80	240.30	1296.29	125.51
1250.00	1232.82	168.25	1303.69	255.17	1344.02	144.08
1300.00	1280.22	184.17	1350.04	270.74	1391.12	163.34
1350.00	1327.34	200.89	1395.84	287.01	1437.58	183.28
1400.00	1374.17	218.42	1441.10	303.92	1483.38	203.93
1450.00	1420.68	236.75	1485.83	321.43	1528.47	225.34
1500.00	1466.87	255.90	1529.98	339.62	1572.88	247.38
1550.00	1512.71	275.86	1573.52	358.50	1616.61	270.04
1600.00	1558.19	296.66	1615.70	379.53	1660.39	291.86
1650.00	1603.26	318.29	1657.21	401.17	1703.49	314.33

Table D.2: Cartesian Coordinates for Turnoff Geometry REDIM 3530 (all coordinates in feet)Generated by a Large Transport Aircraft.

Station (ft.)	X Centerline Coordinate	Y Centerline Coordinate	X Left Edge (Coordinate)	Y Left Edge (Coordinate)	X Right Edge (Coordinate)	Y Rigth Edge (Coordinate)
1700.00	1647.93	340.76	1698.04	423.41	1745.92	337.45
1750.00	1692.15	364.09	1738.25	446.31	1787.57	361.16
1800.00	1735.91	388.26	1778.64	469.70	1827.95	384.55
1850.00	1779.26	413.20	1818.36	492.70	1867.68	407.55
1900.00	1822.52	438.26	1857.28	515.24	1906.59	430.09
1950.00	1865.79	463.31	1895.34	537.28	1944.65	452.13
2000.00	1909.05	488.37	1932.52	558.82	1981.84	473.67
2050.00	1952.32	513.43	1968.82	579.84	2018.14	494.69
2100.00	1995.59	538.49	2004.24	600.36	2053.55	515.21
2150.00	2038.86	563.55	2038.77	620.35	2088.08	535.20
2200.00	2082.13	588.61	2072.41	639.84	2121.73	554.69
2250.00	2125.40	613.67	2105.33	658.90	2154.32	573.57
2300.00	2169.23	637.70	2139.29	677.58	2185.11	590.49
2350.00	2214.22	659.50	2173.39	694.73	2216.01	606.04
2400.00	2260.24	679.04	2207.71	710.47	2247.10	620.30
2450.00	2307.18	696.24	2242.23	724.82	2278.39	633.31
2500.00	2354.93	711.08	2276.93	737.83	2309.83	645.09
2550.00	2403.35	723.51	2311.75	749.50	2341.39	655.67
2600.00	2452.34	733.51	2346.65	759.86	2373.02	665.06
2650.00	2501.75	741.05	2381.57	768.93	2404.66	673.28
2700.00	2551.50	746.11	2416.47	776.73	2436.28	680.34
2750.00	2601.42	748.67	2451.29	783.28	2467.84	686.28
2800.00	2651.42	748.99	2486.00	788.60	2499.29	691.10

Table D.2: Cartesian Coordinates for Turnoff Geometry REDIM 3530 (all coordinates in feet)Generated by a Large Transport Aircraft.

Station (ft.)	X Centerline Coordinate	Y Centerline Coordinate	X Left Edge (Coordinate)	Y Left Edge (Coordinate)	X Right Edge (Coordinate)	Y Rigth Edge (Coordinate)
2850.00	2701.42	748.91	2520.54	792.73	2530.59	694.85
2900.00	2751.42	748.82	2554.88	795.69	2561.71	697.53
2950.00	2801.41	748.73	2588.97	797.51	2592.61	699.17
3000.00	2851.42	748.65	2622.79	798.21	2623.25	699.81
3050.00	2901.42	748.57	2655.03	798.18	2654.87	699.78

Figure D.2 compares the same standard FAA 30 deg. angle geometries (top figure is the modified geometry with a 427 m. spiral) with a 35 m./s. exit speed REDIM geometry sized for a Boeing 727-200. Notice that the entrance fillet in REDIM generates geometries is significantly changed providing pilots with better visibility of the turnoff.

FIGURE D.1 Comparison of REDIM High-Speed Exits Generated by a Boeing 727-200 Aircraft.

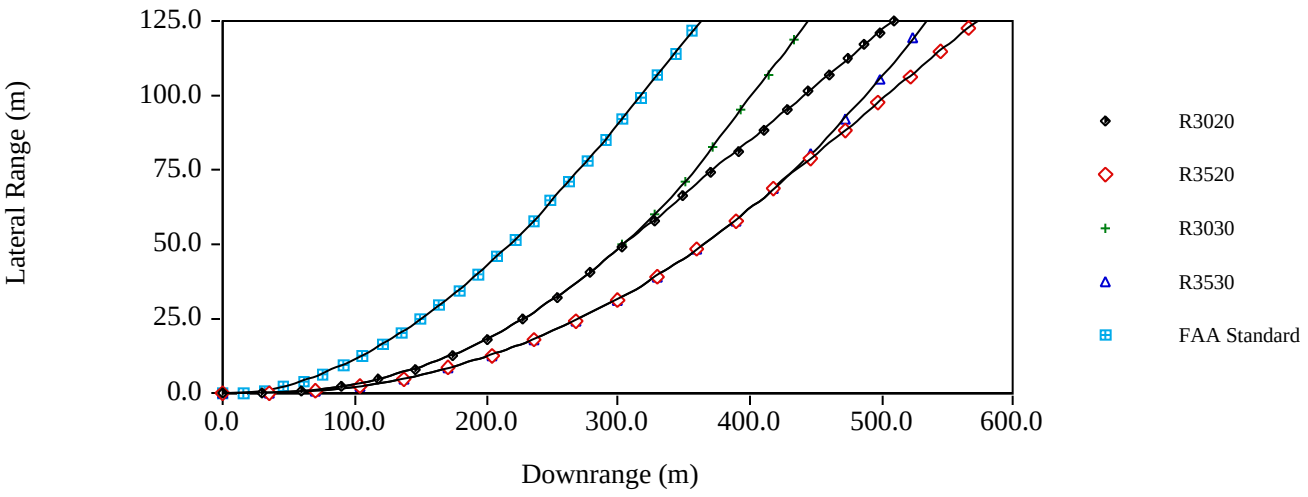

FIGURE D.2 Comparison of Runway Turnoff Goemetry Generated by a Medium Size Trijet Aircraft (Boeing 727-200) and FAA Acute Angle Exit.

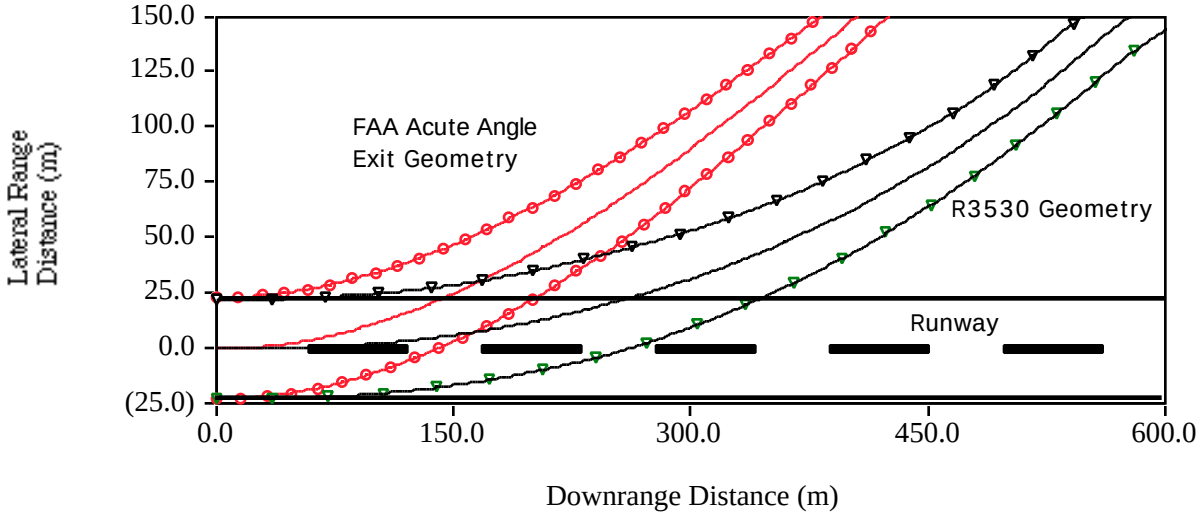

APPENDIX E

Six Degrees of Freedom Aircraft/Turnoff Simulation Equations

This appendix contains the equations used to test the mechanical characteristics of the aircraft model as it negotiates a high-speed turnoff. The equations shown here were developed in STELLA II[1], a continuous simulation graphical language, available in Apple Macintosh[2] computers. Model parameters shown below are those of the four-engine Lockheed Jetstar.

```
TXDXI(t) = TXDXI(t - dt) + (TXDDXI) * dt
INIT TXDXI = 0.0
TXDDXI = TXDD
TXXI(t) = TXXI(t - dt) + (TXDXII) * dt
INIT TXXI = TXO
DOCUMENT:  Variable to estimate the initial position

TXDXII = TXD
TYDXI(t) = TYDXI(t - dt) + (TYDDXI) * dt
INIT TYDXI = 0.0

TYDDXI = TYDD
TYXI(t) = TYXI(t - dt) + (TYDXII) * dt
INIT TYXI = TYO
```

1. STELLA II is a registered trademark of High Performance Systems, New Hampshire.
2. Macitintosh is a registered trademark of Apple Computers Inc., Cupertino, California.

```
TYDXII = TYD
TZDXI(t) = TZDXI(t - dt) + (TZDDXI) * dt
INIT TZDXI = TZDO

TZDDXI = TZDD
TZXI(t) = TZXI(t - dt) + (TZDXII) * dt
INIT TZXI = TZO

TZDXII = TZD
XDXI(t) = XDXI(t - dt) + (XDDXI) * dt
INIT XDXI = XDO

XDDXI = XDD
XIXI(t) = XIXI(t - dt) + (XDIXI) * dt
INIT XIXI = 0.0

XDIXI = XDI
YDXI(t) = YDXI(t - dt) + (YDDXI) * dt
INIT YDXI = YDO

YDDXI = YDD
YIXI(t) = YIXI(t - dt) + (YDIXI) * dt
INIT YIXI = 0.0

YDIXI = YDI
ZDXI(t) = ZDXI(t - dt) + (ZDDXI) * dt
INIT ZDXI = ZDO

ZDDXI = ZDD
ZIXI(t) = ZIXI(t - dt) + (ZDIXI) * dt
INIT ZIXI = ZIO

ZDIXI = ZDI
AI = 0.0
B = ARCTAN(YD/XD)
CBLM = 0.01
CBN = 0.01
CBRM = 0.01
CFAD = CFAD1+CFADTY*TY+CFADE*ELV
CFAD1 = 0.0397
DOCUMENT:  j 0.031

CFADE = 0.06
```

CFADTY = 0.13
CFAL = CFAL1+CFALTY*TY+CFALE*ELV+CFLTYD*TYD
CFAL1 = 0.17
DOCUMENT: j 0.31

CFALE = 0.4
DOCUMENT: j 0.43

CFALTY = 5.0
DOCUMENT: j 4.6

CFAS = CFASB*B+CFASAI*AI+CFASR*RUD+CFSTZD*TZD+CFSTXD*TXD
CFASAI = 0.0
CFASB = -0.72
DOCUMENT: j -0.31

CFASR = 0.187
CFLTYD = 3.9
CFSTXD = -0.037
CFSTZD = 0.175
DOCUMENT: j 0.21

CH = 10.39
CLM = 1242.279
CLM1 = 0.90*FTZWLM
CLM2 = 15340.5*(FTZWLM+1.0)^(-1.0916)
CLM3 = IF (-CLM2)*ABS(SLPALM)<=-180.0 THEN -180.0 ELSE (-CLM2)*ABS(SLPALM)
CLM4 = IF SLPALM<0.0 THEN -1.0 ELSE 1.0
CMAX = 0
CMAXAI = 0.054
DOCUMENT: j 0.178

CMAXB = 0.103
DOCUMENT: j -0.089

CMAXR = 0.025
DOCUMENT: j 0.01447

CMAY = 0
CMAYE = -0.81
DOCUMENT: j -1.28

```
CMAYTY = -0.8
DOCUMENT:  j -0.89

CMAZ = 0
CMAZAI = -0.075
DOCUMENT:  j -0.053

CMAZB = 0.137
DOCUMENT:  j 0.065

CMAZR = -0.063
DOCUMENT:  j -0.0657

CMO = 0.0908
CMXTXD = -0.37
DOCUMENT:  j -0.47
CMXTZD = -0.11
DOCUMENT:  j 0.096

CMYTYD = -8.00
DOCUMENT:  j -12.4

CMZTXD = -0.14
DOCUMENT:  j -0.03

CMZTZD = -0.16
DOCUMENT:  -0.099

CN = 437.922
CN1 = 0.9*FTZWN
CN2 = 15340.5*(FTZWN+1.0)*(-1.0916)
CN3 = IF (-CN2)*ABS(SLPAN)<=-180.0 THEN -180.0 ELSE (-CN2)*ABS(SLPAN)
CN4 = IF SLPAN<0.0 THEN -1.0 ELSE 1.0
CRM = 1242.279
CRM1 = 0.90*FTZWRM
CRM2 = 15340.5*(FTZWRM+1.0)^(-1.0916)
CRM3 = IF (-CRM2*ABS(SLPARM))<=-180.0 THEN -180.0 ELSE (-CRM2*ABS(SLPARM))
CRM4 = IF SLPARM<0.0 THEN -1.0 ELSE 1.0
DZLM = ZLMF-ZLM
DOCUMENT:  AILERON

DZN = ZNF-ZN
DZRM = ZRMF-ZRM
```

```
ELV = 0.0
FAD = (CFAD*ROW*S*V^2)/2
FAL = (CFAL*ROW*S*V^2)/2
FAS = (CFAS*ROW*S*V^2)/2
FAX = -FAD*COS(TY)+FAL*SIN(TY)
FAY = FAS
FAZ = -FAD*SIN(TY)-FAL*COS(TY)
DOCUMENT:  AILERON

FGX = -M*G*SIN(TY)
FGY = M*G*COS(TY)*SIN(TX)
FGZ = M*G*COS(TY)*COS(TX)
FTXLM = -FTXWLM*COS(TY)+FTZWLM*SIN(TY)
FTXN = -FTXWN*COS(TY)+FTZWN*SIN(TY)
FTXRM = -FTXWRM*COS(TY)+FTZWRM*SIN(TY)
FTXWLM = IF XD<0.0 OR XD = 0.0 THEN 0.0 ELSE CBLM*FTZWLM
FTXWN = IF XD < 0.0 OR XD = 0.0 THEN 0.0 ELSE CBN*FTZWN
DOCUMENT:  AILERON

FTXWRM = IF XD<0.0 OR XD = 0.0 THEN 0.0 ELSE CBRM*FTZWRM
FTYLM = -FTXWLM*SIN(TX)*SIN(TY)-FTYWLM*COS(TX)-FTZWLM*SIN(TX)*COS(TY)
FTYN = -FTXWN*SIN(TX)*SIN(TY)-FTYWN*COS(TX)-FTZWN*SIN(TX)*COS(TY)
FTYRM = -FTXWRM*SIN(TX)*SIN(TY)-FTYWRM*COS(TX)-FTZWRM*SIN(TX)*COS(TY)
FTYWLM = CLM1*CLM4*ABS(SLPALM)
FTYWN = CN1*CN4*ABS(SLPAN)
FTYWRM = CRM1*CRM4*ABS(SLPARM)
DOCUMENT:  AILERON

FTZLM = -FTXWLM*COS(TX)*SIN(TY)+FTYWLM*SIN(TX)-FTZWLM*COS(TY)*COS(TX)
FTZN = -FTXWN*COS(TX)*SIN(TY)+FTYWN*SIN(TX)-FTZWN*COS(TX)*COS(TY)
FTZRM = -FTXWRM*COS(TX)*SIN(TY)+FTYWRM*SIN(TX)-FTZWRM*COS(TY)*COS(TX)
FTZWLM = IF (KLM*DZLM-CLM*VZLM)<=0.0 THEN 0.0 ELSE (KLM*DZLM-CLM*VZLM)
DOCUMENT:  AILERON

FTZWN = if (KN*DZN-CN*VZN)<=0.0 then 0.0 else (KN*DZN-CN*VZN)
FTZWRM = if (KRM*DZRM-CRM*VZRM)<=0.0 THEN 0.0 ELSE (KRM*DZRM-CRM*VZRM)
FX = FAX+FGX+FTXN+FTXRM+FTXLM
FY = FAY+FGY+FTYN+FTYRM+FTYLM
FZ = FAZ+FGZ+FTZN+FTZRM+FTZLM
G = 32.17
IX = 42273
IY = 126099
IZ = 160104
```

KLM = 3393.77
KN = 1180.45
KRM = 3393.77
M = 734
MAXAI = (CMAXAI*AI*ROW*S*WS*V^2)/2
DOCUMENT: AILERON

MAXB = (CMAXB*B*ROW*S*WS*V^2)/2
MAXR = (CMAXR*RUD*ROW*S*WS*V^2)/2
MAXTXD = (CMXTXD*TXD*ROW*S*WS*V^2)/2
MAXTZD = (CMXTZD*TZD*ROW*S*WS*V^2)/2
MAY = MAYTY+MAYE+MAYTYD
MAYE = (CMAYE*ELV*ROW*S*CH*V^2)/2
MAYTY = ((CMO+CMAYTY*TY)*ROW*S*CH*V^2)/2
MAYTYD = (CMYTYD*TYD*ROW*S*CH*V^2)/2
DOCUMENT: AILERON

MAZ = MAZB+MAZR+MAZAI+MAZTZD+MAZTXD
MAZAI = (CMAZAI*AI*ROW*S*WS*V^2)/2
MAZB = (CMAZB*B*ROW*S*WS*V^2)/2
MAZR = (CMAZR*RUD*ROW*S*WS*V^2)/2
MAZTXD = (CMZTXD*TXD*ROW*S*WS*V^2)/2
MAZTZD = (CMZTZD*TZD*ROW*S*WS*V^2)/2
MGX = -FTYN*ZN-FTYRM*ZRM-FTYLM*ZLM+FTZRM*YRM+FTZLM*YLM
DOCUMENT: AILERON

MGY = -FTZN*XN+FTXN*ZN+FTXRM*ZRM+FTXLM*ZLM-(FTZRM+FTZLM)*XM
MGZ = (FTYRM+FTYLM)*XM+FTYN*XN-FTXRM*YRM-FTXLM*YLM
MGZM = MGZ-MGZN
MGZN = FTYN*XN
MX = M_AX+MGX
MY = MAY+MGY
MZ = MAZ+MGZ
DOCUMENT: AILERON

M_AX = MAXB+MAXAI+MAXR+MAXTZD+MAXTXD
ROW = 0.002378
RUD = 0.0
S = 542.5
SLPALM = ARCTAN(YDWLM/XDWLM)
SLPAN = ARCTAN(YDWN/XDWN)-STEERING
SLPARM = ARCTAN(YDWRM/XDWRM)
TX = TXXI

```
DOCUMENT:

TXD = TXDXI
TXDD = (MX+(IY-IZ)*TYD*TZD)/IX
TXO = 0.0
TY = TYXI
TYD = TYDXI
TYDD = (MY+(IZ-IX)*TZD*TXD)/IY
DOCUMENT:  AILERON

TYO = 0.0
TZ = TZXI
TZD = TZDXI
TZDD = (MZ+(IX-IY)*TXD*TYD)/IZ
TZDO = 0.0
TZO = 0
V = (XDI^2+YDI^2)^0.5
VZLM = ((XD-TZD*YLM+TYD*ZLM)*SIN(TY)-(YD+TZD*XM-TXD*ZLM)*SIN(TX)*COS(TY)-
(ZD-TYD*XM+TXD*YLM)*COS(TX)*COS(TY))/(COS(TX)*COS(TY))
VZN = ((XD+TYD*ZN)*SIN(TY)-(YD+TZD*XN-TXD*ZN)*SIN(TX)*COS(TY)-(ZD-
TYD*XN)*COS(TX)*COS(TY))/(COS(TX)*COS(TY))
DOCUMENT:
VZRM = ((XD-TZD*YRM+TYD*ZRM)*SIN(TY)-(YD+TZD*XM-TXD*ZRM)*SIN(TX)*COS(TY)-
(ZD-TYD*XM+TXD*YRM)*COS(TX)*COS(TY))/(COS(TX)*COS(TY))
WS = 53.75
XD = XDXI
XDD = FX/M-ZD*TYD+YD*TZD
XDI = COS(TY)*COS(TZ)*XD+(SIN(TX)*SIN(TY)*COS(TZ)-
COS(TX)*SIN(TZ))*YD+(COS(TX)*SIN(TY)*COS(TZ)+SIN(TX)*SIN(TZ))*ZD
XDO = 100
XDWLM = COS(TY)*(XD-TZD*YLM+TYD*ZLM)+SIN(TX)*SIN(TY)*(YD+TZD*XM-
TXD*ZLM)+COS(TX)*SIN(TY)*(ZD+VZLM-TYD*XM+TXD*YLM)
XDWN = COS(TY)*(XD+TYD*ZN)+SIN(TX)*SIN(TY)*(YD+TZD*XN-
TXD*ZN)+COS(TX)*SIN(TY)*(ZD+VZN-TYD*XN)
XDWRM = COS(TY)*(XD-TZD*YRM+TYD*ZRM)+SIN(TX)*SIN(TY)*(YD+TZD*XM-
TXD*ZRM)+COS(TX)*SIN(TY)*(ZD+VZRM-TYD*XM+TXD*YRM)
XI = XIXI
XM = -3.28
XN = 18.9
YD = YDXI
YDD = FY/M-XD*TZD+ZD*TXD
YDI =
COS(TY)*SIN(TZ)*XD+(SIN(TX)*SIN(TY)*SIN(TZ)+COS(TX)*COS(TZ))*YD+(COS(TX)*SIN(T
Y)*SIN(TZ)-SIN(TX)*COS(TZ))*ZD
DOCUMENT:
```

YDO = 0

YDWLM = COS(TX)*(YD+TZD*XM-TXD*ZLM)-SIN(TX)*(ZD+VZLM-TYD*XM+TXD*YLM)

YDWN = COS(TX)*(YD+TZD*XN-TXD*ZN)-SIN(TX)*(ZD+VZN-TYD*XN)

YDWRM = COS(TX)*(YD+TZD*XM-TXD*ZRM)-SIN(TX)*(ZD+VZRM-TYD*XM+TXD*YRM)

YI = YIXI

YLM = -6.55

YM = 0

YRM = 6.55

ZD = ZDXI

ZDD = FZ/M-YD*TXD+XD*TYD

ZDI = (-SIN(TY))*XD+(SIN(TX)*COS(TY))*YD+(COS(TX)*COS(TY))*ZD

ZDO = 0

ZI = ZIXI

ZIO = -5.9

ZLM = (-ZI+XM*SIN(TY)-YLM*SIN(TX)*COS(TY))/(COS(TX)*COS(TY))

ZLMF = 6.07

ZN = (-ZI+XN*SIN(TY))/(COS(TX)*COS(TY))

ZNF = 6.59

ZRM = (-ZI+XM*SIN(TY)-YRM*SIN(TX)*COS(TY))/(COS(TX)*COS(TY))

ZRMF = 6.07

STEERING = GRAPH(TIME)

(0.00, 0.00), (2.63, 0.0615), (5.26, 0.0795), (7.89, 0.0735), (10.5, 0.0606), (13.2, 0.0471), (15.8, 0.0336), (18.4, 0.0215), (21.1, 0.0093), (23.7, -0.00555), (26.3, -0.0177), (28.9, -0.0285), (31.6, -0.0298), (34.2, -0.0177), (36.8, 0.00255), (39.5, 0.0106), (42.1, 0.012), (44.7, 0.0133), (47.4, 0.012), (50.0, 0.012)

APPENDIX F

Aircraft Velocity Profile Data from ATL, DCA and CLT Airports

This appendix contains graphical information on the aircraft velocity profiles used in the calibration of the model. As it was discussed in Chapter 3, three major airports and five medium and short range transports were used in the calibration procedure thus resulting in a subset of all data collected at five airport locations. Figures F-1 through F-5 illustrate the velocity profiles for five transport aircraft landing on runway 08L at Atlanta Hartsfield International Airport (VMC conditions). The observations have been plotted as bivariate graphs of distance vs. aircraft velocity. The reader should recall that aircraft used in the calibration process are: Boeing 727-200, 737-200/300, 757-200, Douglas DC9-30 and the McDonnell Douglas MD-80 (series 83 and 87).

Also shown in these plots are the upper and lower bound aircraft landing roll trajectories predicted by REDIM 2.1. Note that in most cases the observed trajectories lie well within the upper and lower bound profiles thus providing a qualitative assessment of the computer model predictions.

Figures F-6 through F-10 depict the profiles for the same aircraft population landing at Washington National Airport runway 36 (VMC conditions). It can be seen that once again the prediction capabilities of the model seem very adequate as most of the observations fall well within the REDIM predicted bounds.

Finally, Figures F-11 through F-15 present graphical information on landing observations at Charlotte International runway 23. Note that in this case the main deviations from the landing roll observations are motivated by the long separation between two available runway turnoffs (i.e., see runway turnoff Echo and Bravo in Figure 3.3).

FIGURE F.1 **Observed and Predicted Velocity Profiles for Boeing 727-200 Aircraft Landing at Atlanta International Airport (Runway 08L).**

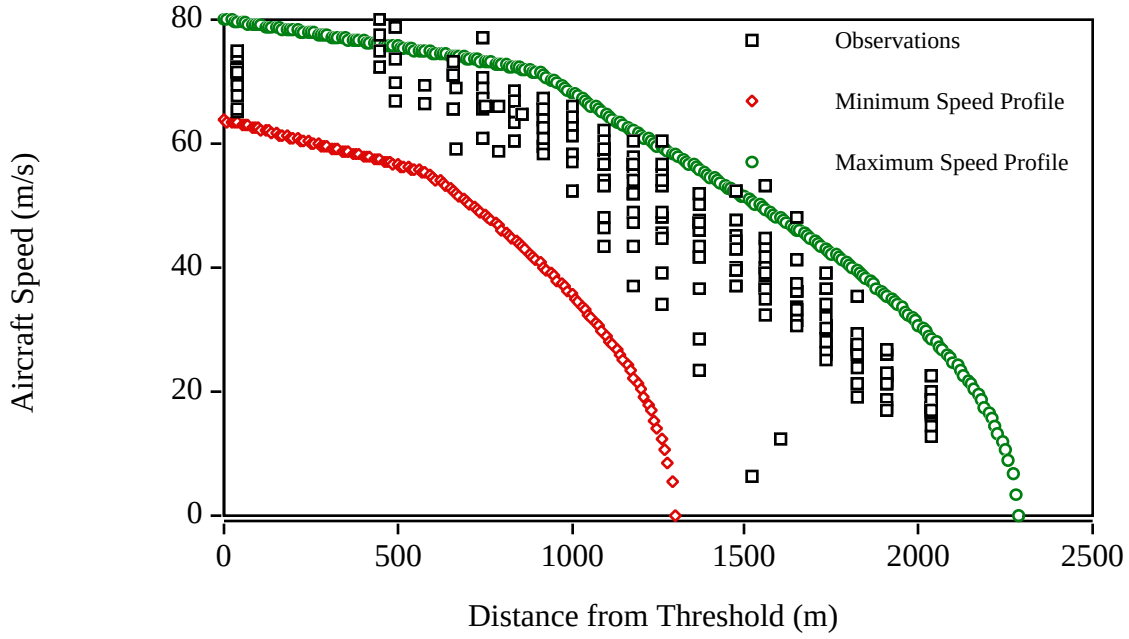

FIGURE F.2 **Observed and Predicted Velocity Profiles for Boeing 737-200/300 Aircraft Landing at Atlanta International Airport (Runway 08L).**

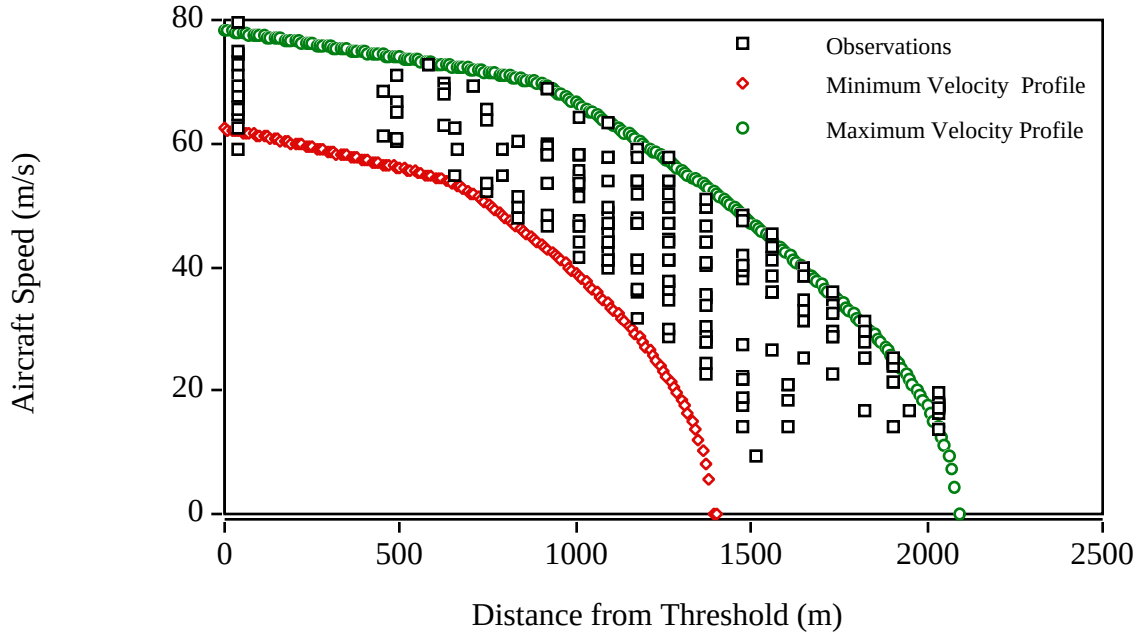

FIGURE F.3 **Observed and Predicted Velocity Profiles for Boeing 757-200 Aircraft Landing at Atlanta International Airport (Runway 08L).**

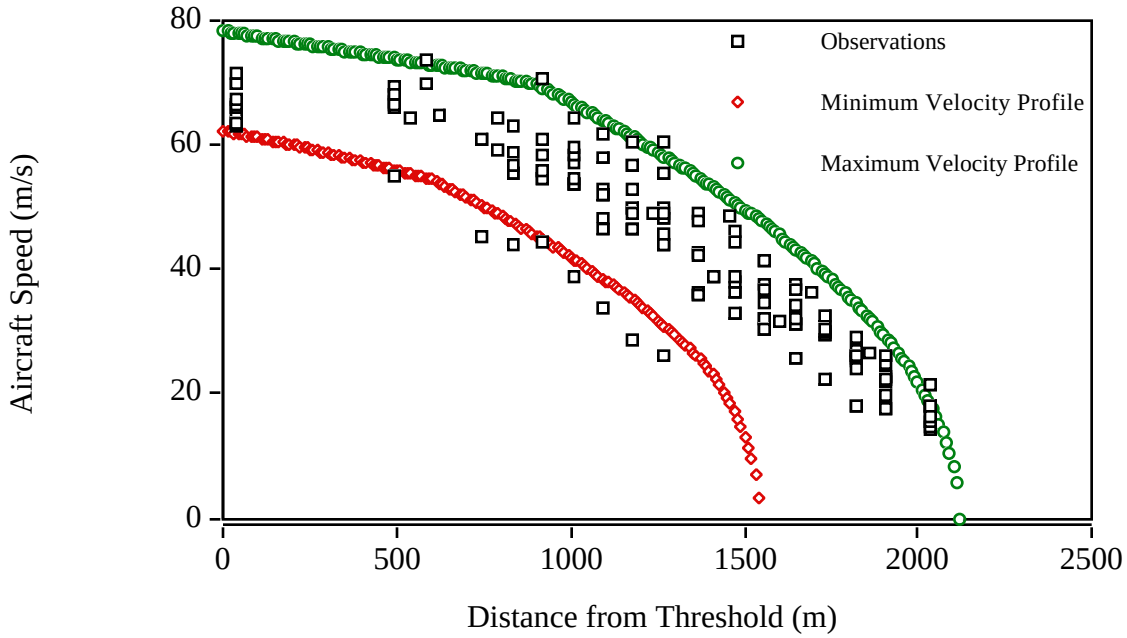

FIGURE F.4 **Observed and Predicted Velocity Profiles for Douglas DC9-30 Aircraft Landing at Atlanta International Airport (Runway 08L).**

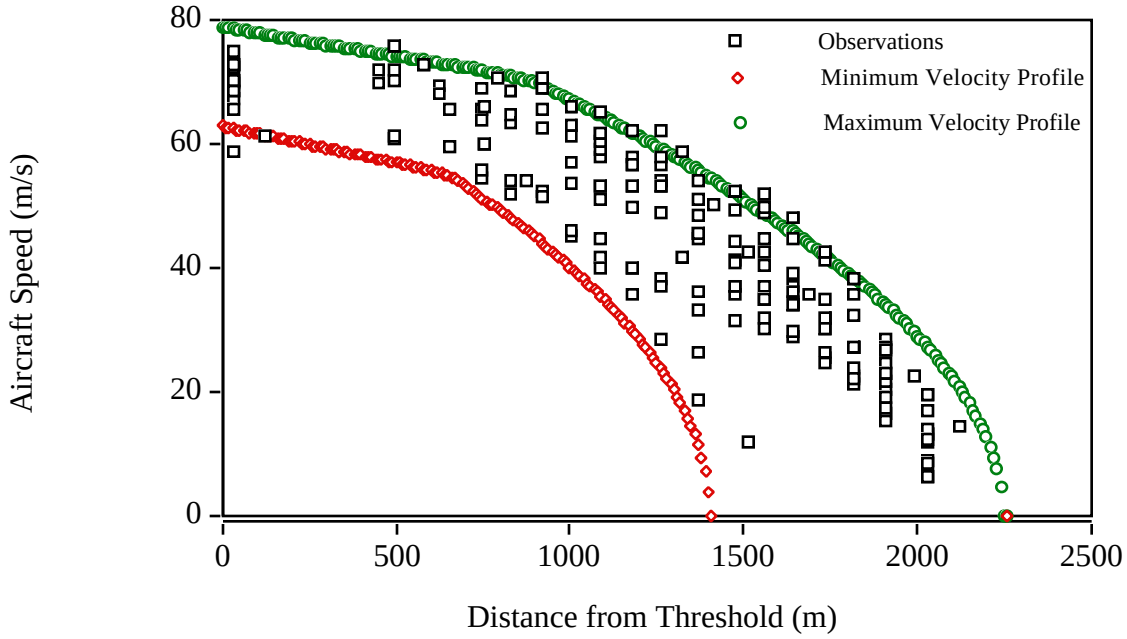

FIGURE F.5 **Observed and Predicted Velocity Profiles for McDonnell Douglas MD-80 Aircraft Landing at Atlanta International Airport (Runway 08L).**

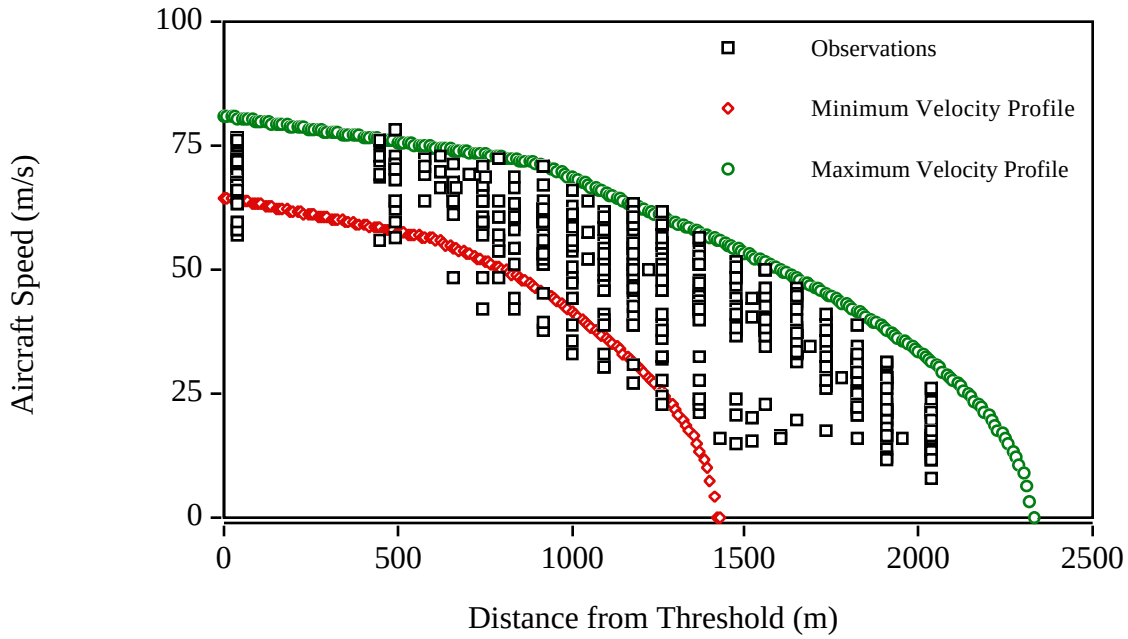

FIGURE F.6 **Observed and Predicted Velocity Profiles for Boeing 727-200 Aircraft Landing at Washington National Airport (Runway 36).**

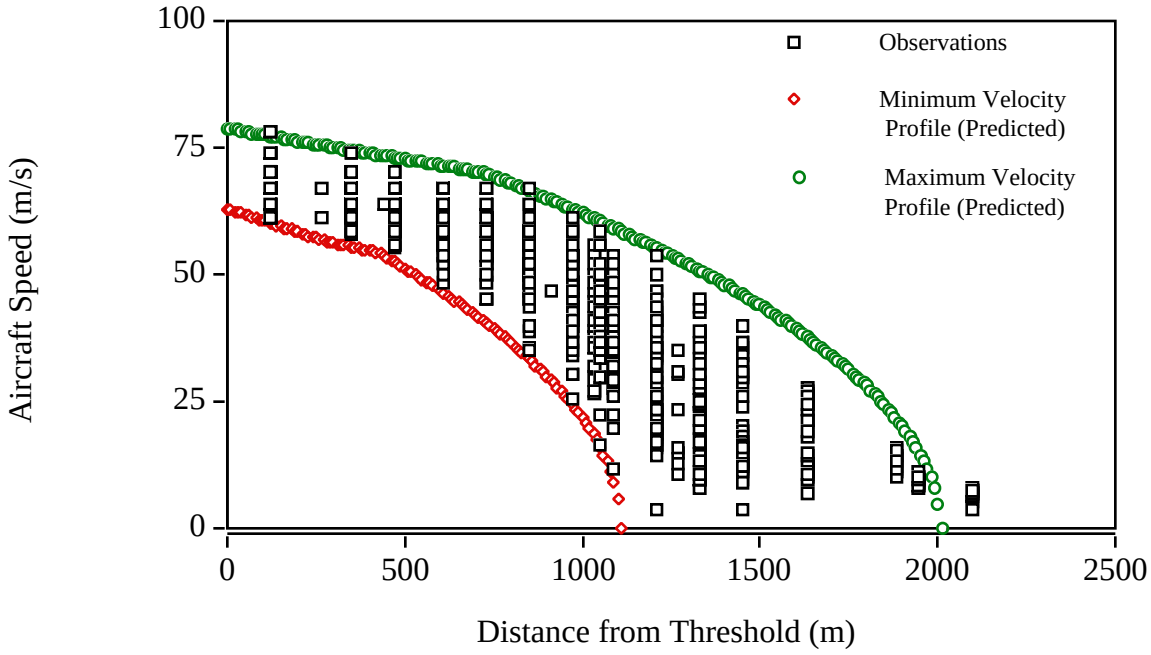

FIGURE F.7 **Observed and Predicted Velocity Profiles for Boeing 737-200/300 Aircraft Landing at Washington National Airport (Runway 36).**

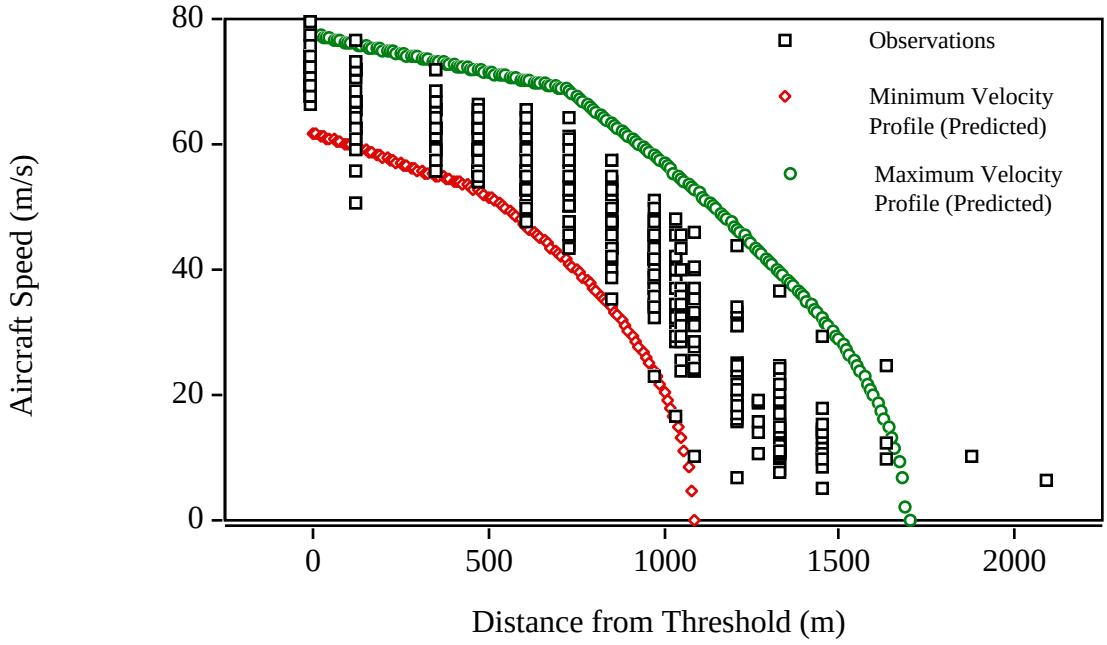

FIGURE F.8 **Observed and Predicted Velocity Profiles for Boeing 757-200 Aircraft Landing at Washington National Airport (Runway 36).**

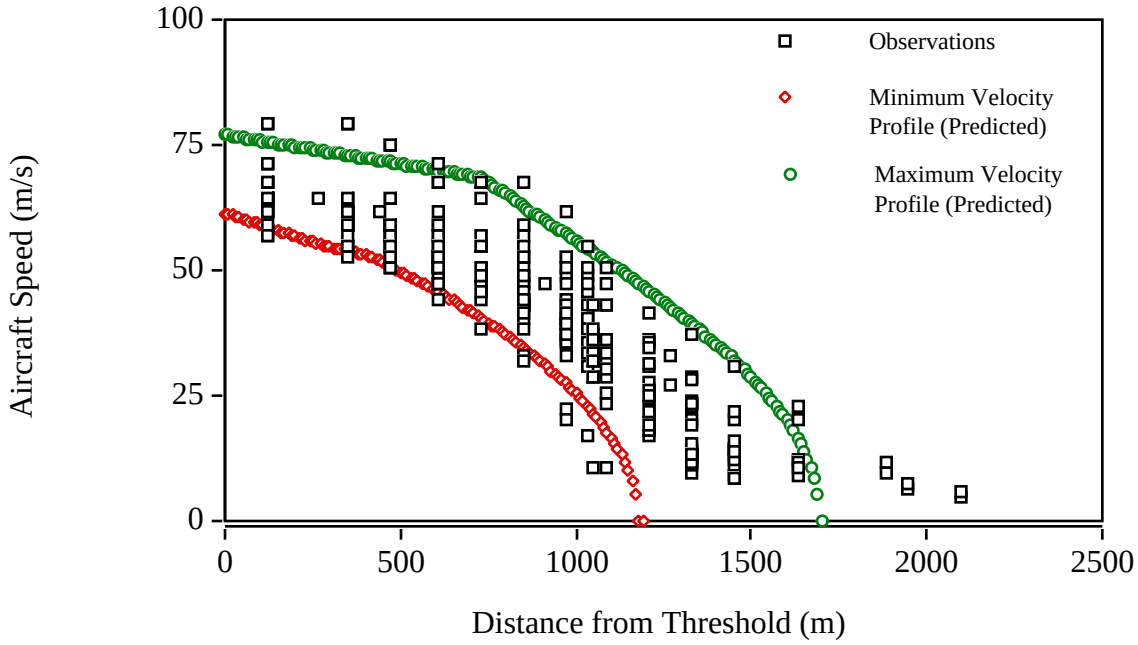

FIGURE F.9 **Observed and Predicted Velocity Profiles for Douglas DC9-30 Aircraft Landing at Washington National Airport (Runway 36).**

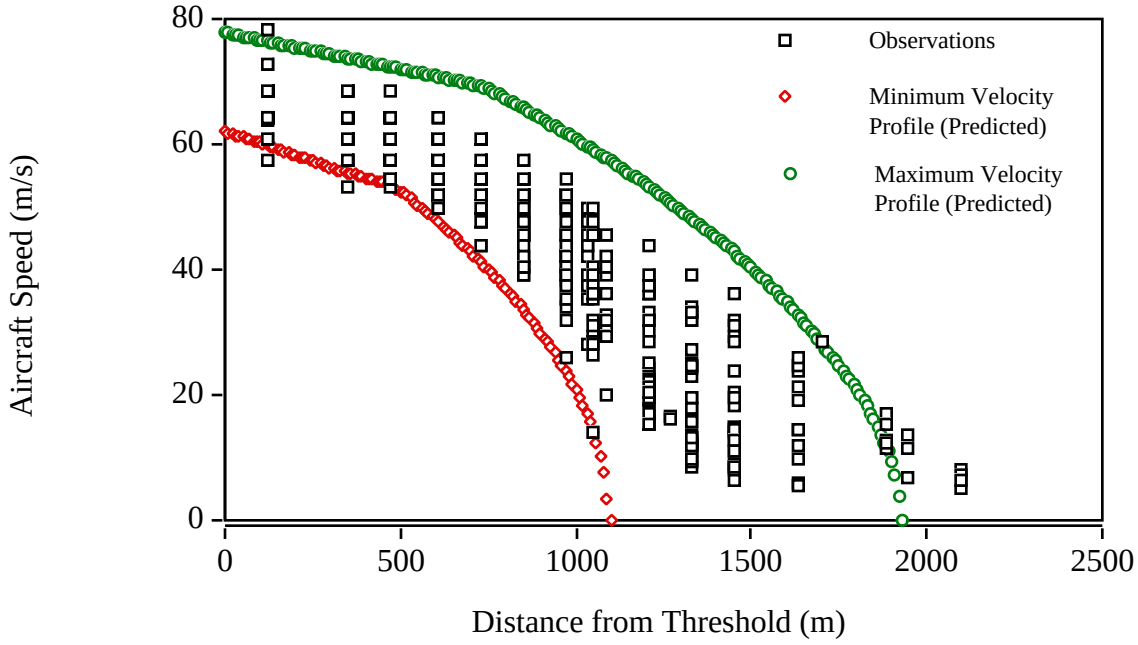

FIGURE F.10 **Observed and Predicted Velocity Profiles for McDonnell Douglas MD-80 Aircraft Operating at Washington National Airport (Runway 36).**

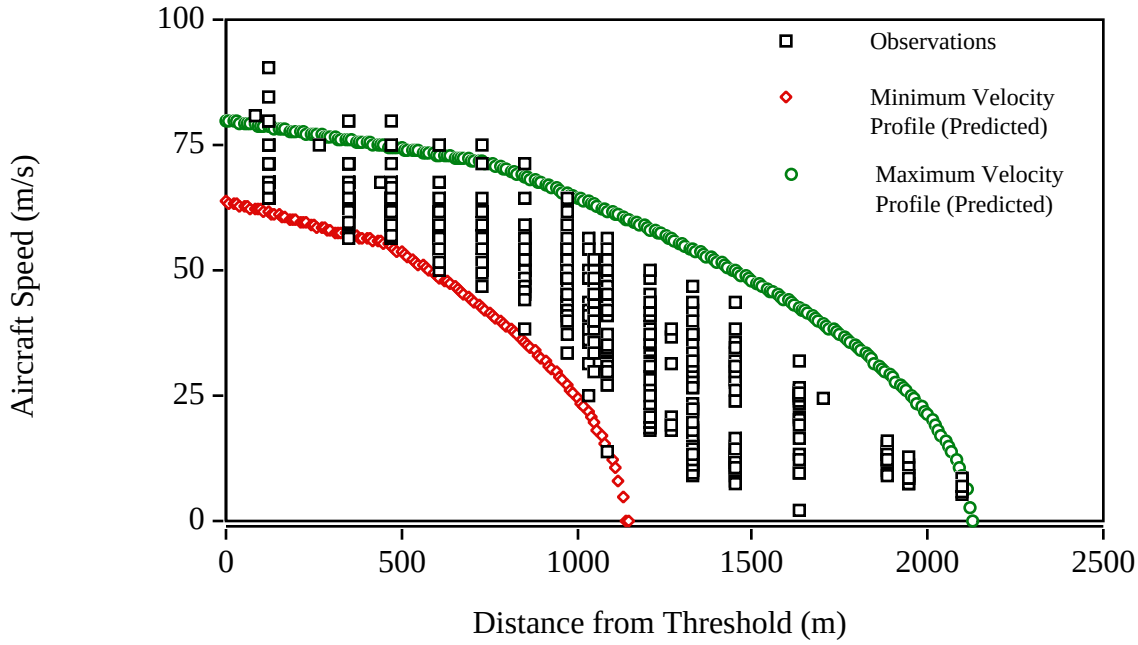

FIGURE F.11 **Observed and Predicted Velocity Profiles for Boeing 727-200 Aircraft Landing at Charlotte International Airport (Runway 23).**

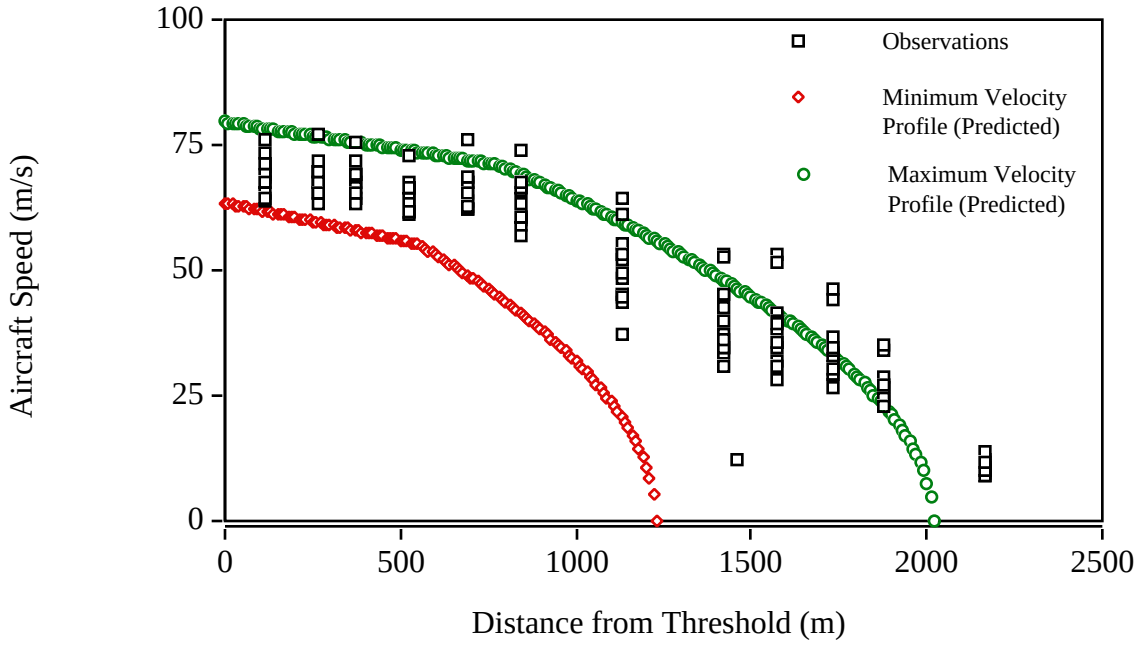

FIGURE F.12 **Observed and Predicted Velocity Profiles for Boeing 737-200/300 Aircraft Landing at Charlotte International Airport (Runway 23).**

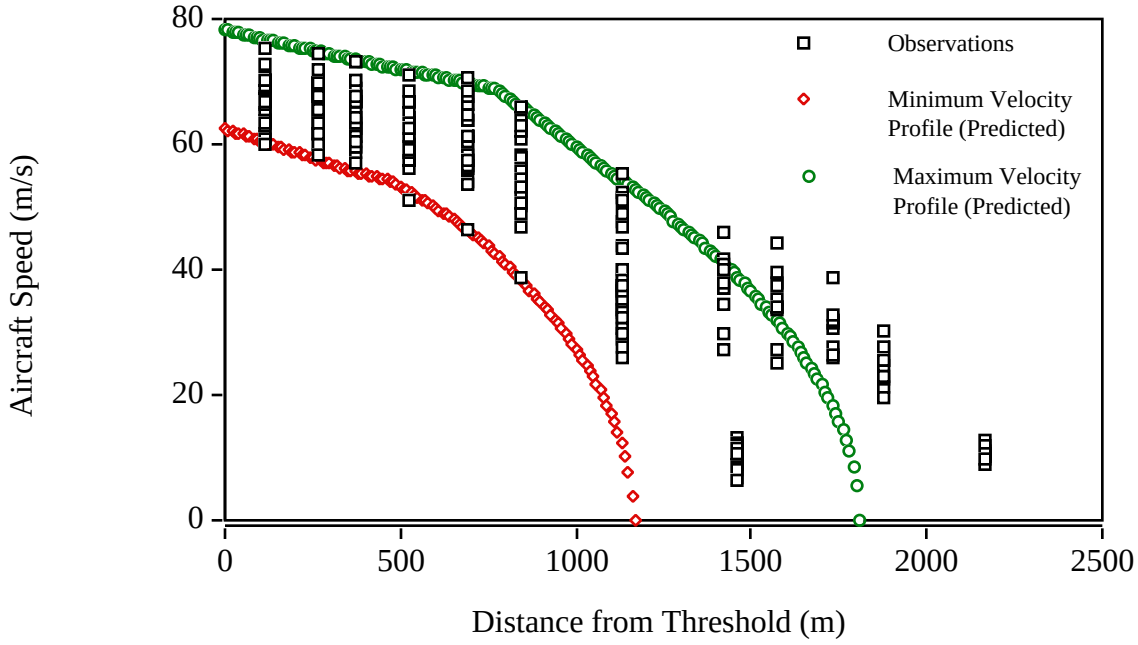

FIGURE F.13 **Observed and Predicted Velocity Profiles for Boeing 757-200 Aircraft Landing at Charlotte International Airport (Runway 23).**

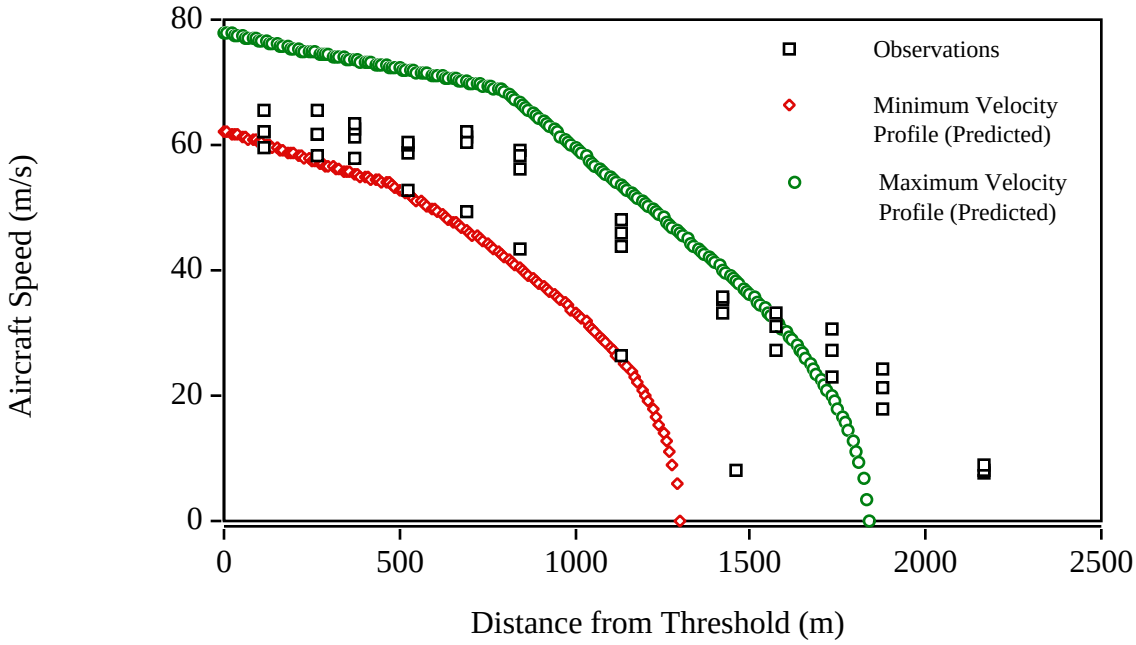

FIGURE F.14 **Observed and Predicted Velocity Profiles for Douglas DC9-30 Aircraft Landing at Charlotte International Airport (Runway 23).**

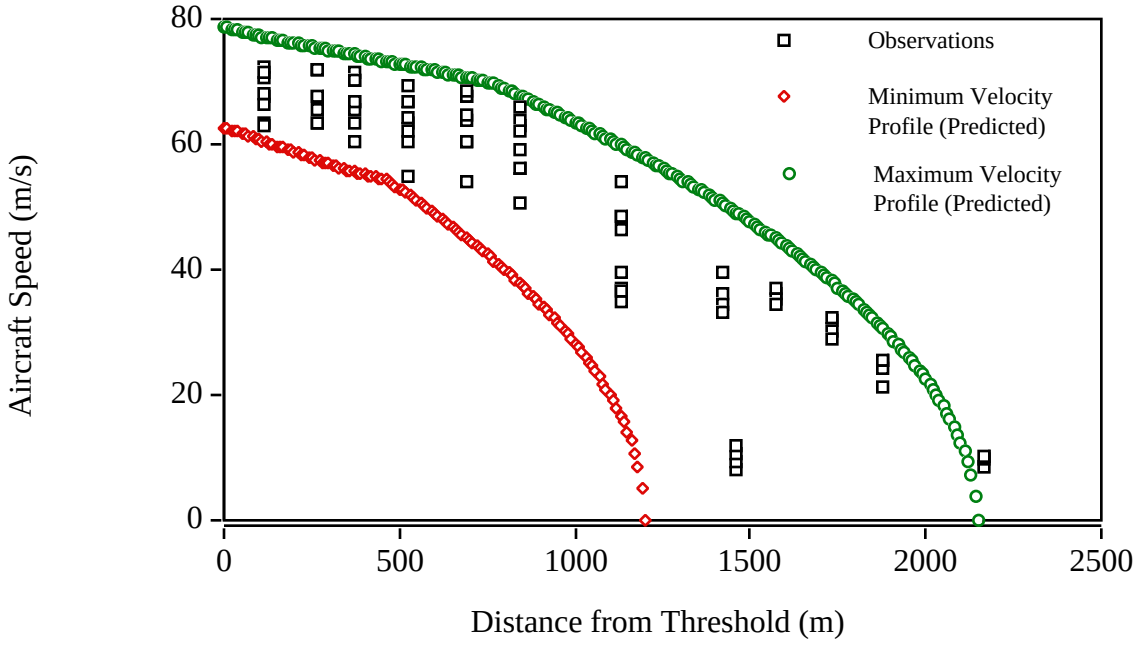

FIGURE F.15 **Observed and Predicted Velocity Profiles for McDonnell Douglas MD-80 Aircraft Operating at Charlotte International Airport (Runway 23).**

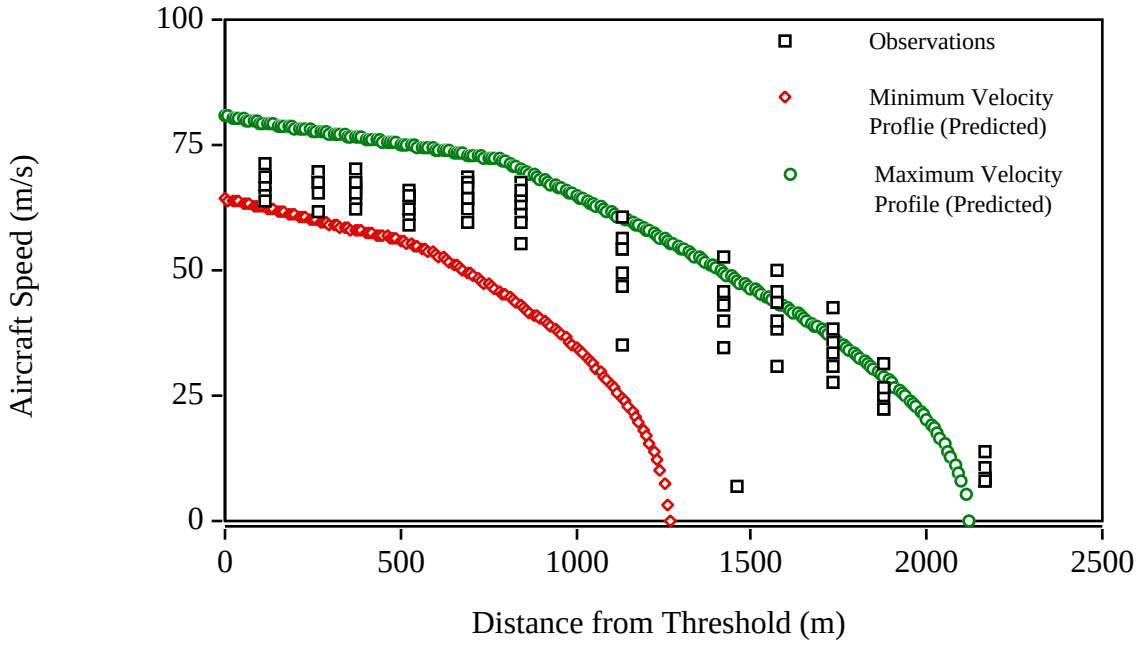

APPENDIX G

Aircraft Exit Speed Data Obtained at Various Airports

This appendix contains graphical information on the aircraft exit histograms used in the calibration of the model. Four major airports are included in this analysis and no distinction at the moment is made of individual aircraft as it was found that both, transport aircraft and commuters, display somewhat similar characteristics while taking various exit turnoffs.

Figure G.1 illustrate the exit speed histograms observed at Charlotte Douglas International Airport Runway 23 under VMC conditions. The observations have been plotted as histograms to better inform the reader the exit speed trends observed. Table G.1 summarizes the results for CLT and also includes a brief description of the types of exits at this facility. It should be noted that CLT Runway 23 has only two runway exits capable of accommodating transport aircraft (i.e., Bravo and Echo) and a third one located 900 m. from the threshold being used primarily by commuter traffic.

Figures G.2 through G.5 show exit speed histograms for data collected at Washington National, Atlanta International and Dulles international Airports, respectively. Note that in the case of National Airport the total exit speed distribution is actually normally distributed (i.e., using Chi-Square analysis) even though not all exits are of the same type as CLT.

Finally, Figures G-11 through G-15 present graphical information on landing observations at Charlotte International runway 23. Note that in this case the main deviations from the landing roll observations are motivated by the long separation between two available runway turnoffs (i.e., see runway turnoffs Echo and Bravo in Figure 3.3).

FIGURE G.1 **Observed Exit Speed Histogram for All Aircraft Landing on Runway 23 at Charlotte International Airport.**

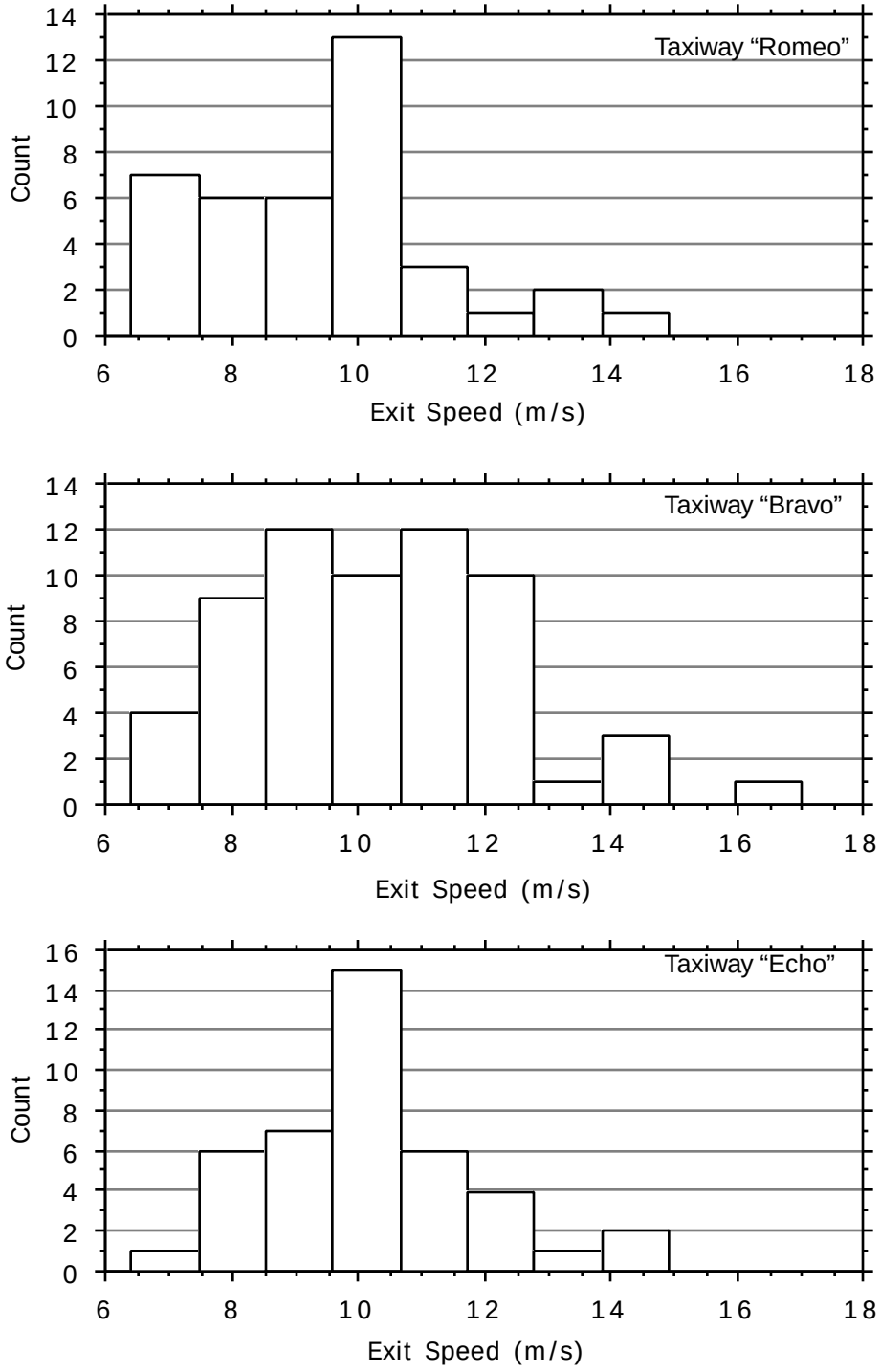

FIGURE G.2 **Exit Speed Histogram Observed at Charlotte Douglas International Airport (Runway 23).**

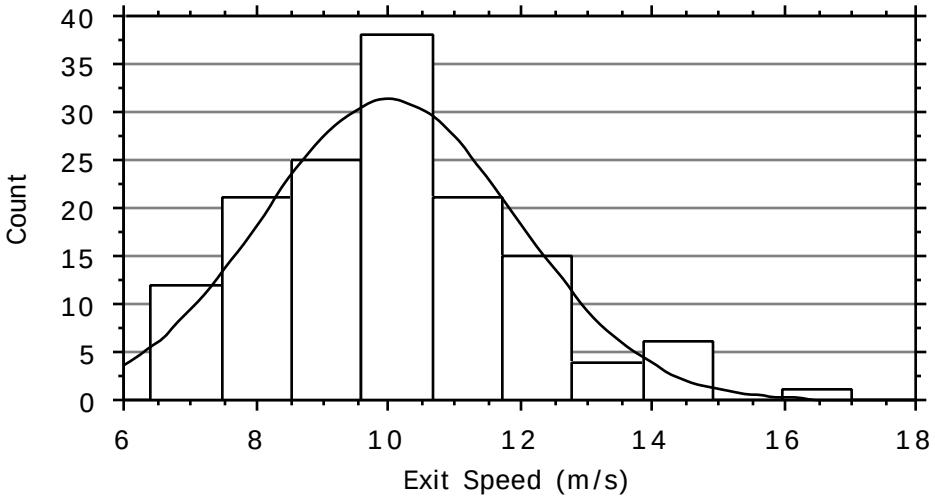

TABLE G.1 **Summary of Statistics for Exit Speed Analysis at CLT Runway 23.**

Parameter	Taxiway Name and Description			
	Romeo (Std. 90 degree)	Bravo (Std. 90 degree)	Echo (Std. 90 degree)	Total
Mean (m/s)	9.4	10.3	10.2	10.0
Std. Dev. (m/s)	1.9	2.0	1.6	1.9
Std. Error (m/s)	0.31	0.26	0.25	0.16
Count	39	62	42	143
Minimum (m/s)	6.4	6.3	6.8	6.4
Maximum (m/s)	13.9	17.0	14.2	17.0

FIGURE G.3 **Observed Exit Speed Histograms for All Aircraft Landing on Runway 36 at National Airport.**

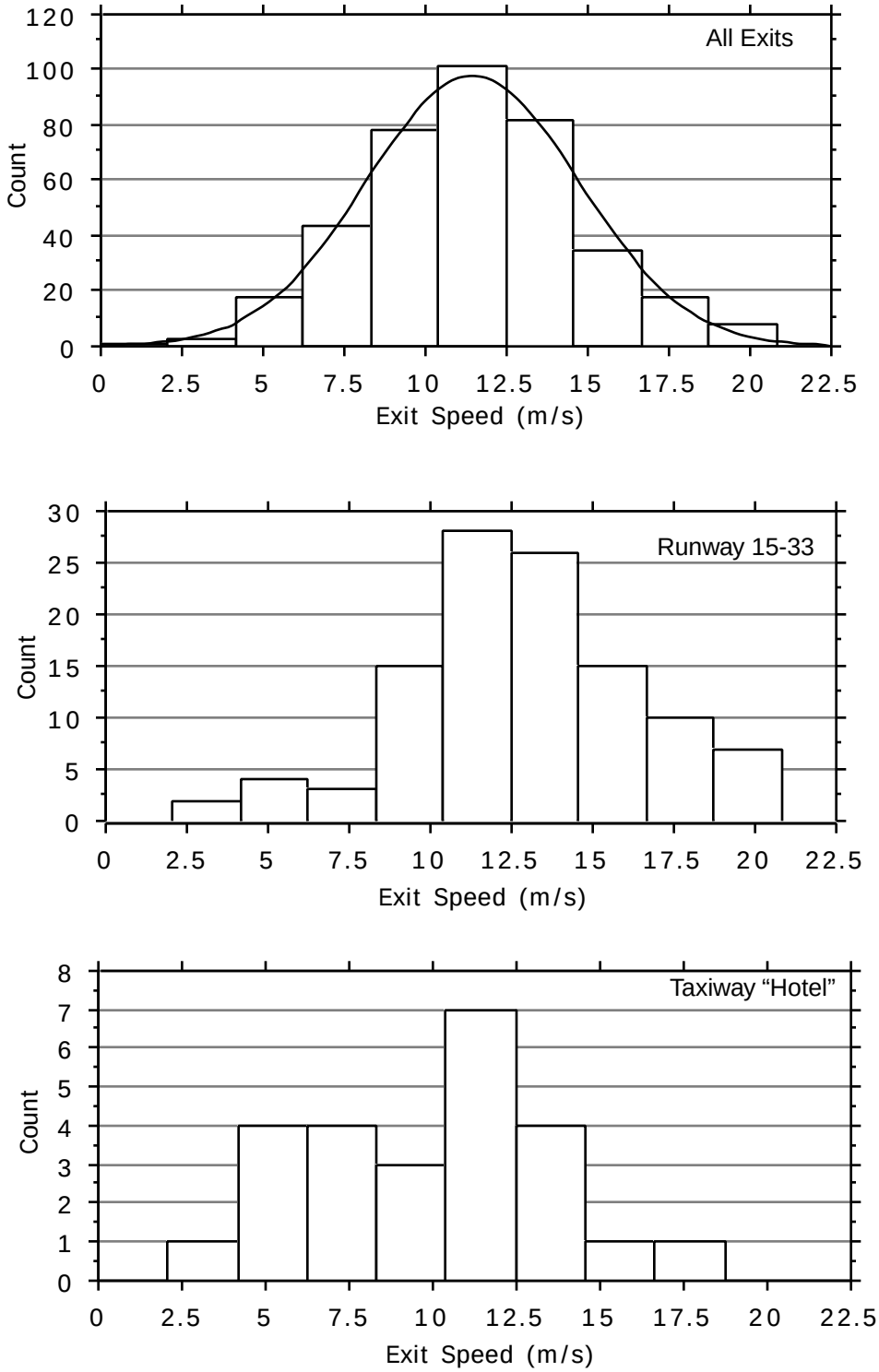

FIGURE G.4 **Observed Exit Speed Histograms for All Aircraft Landing on Runway 36 at DCA (Cont.).**

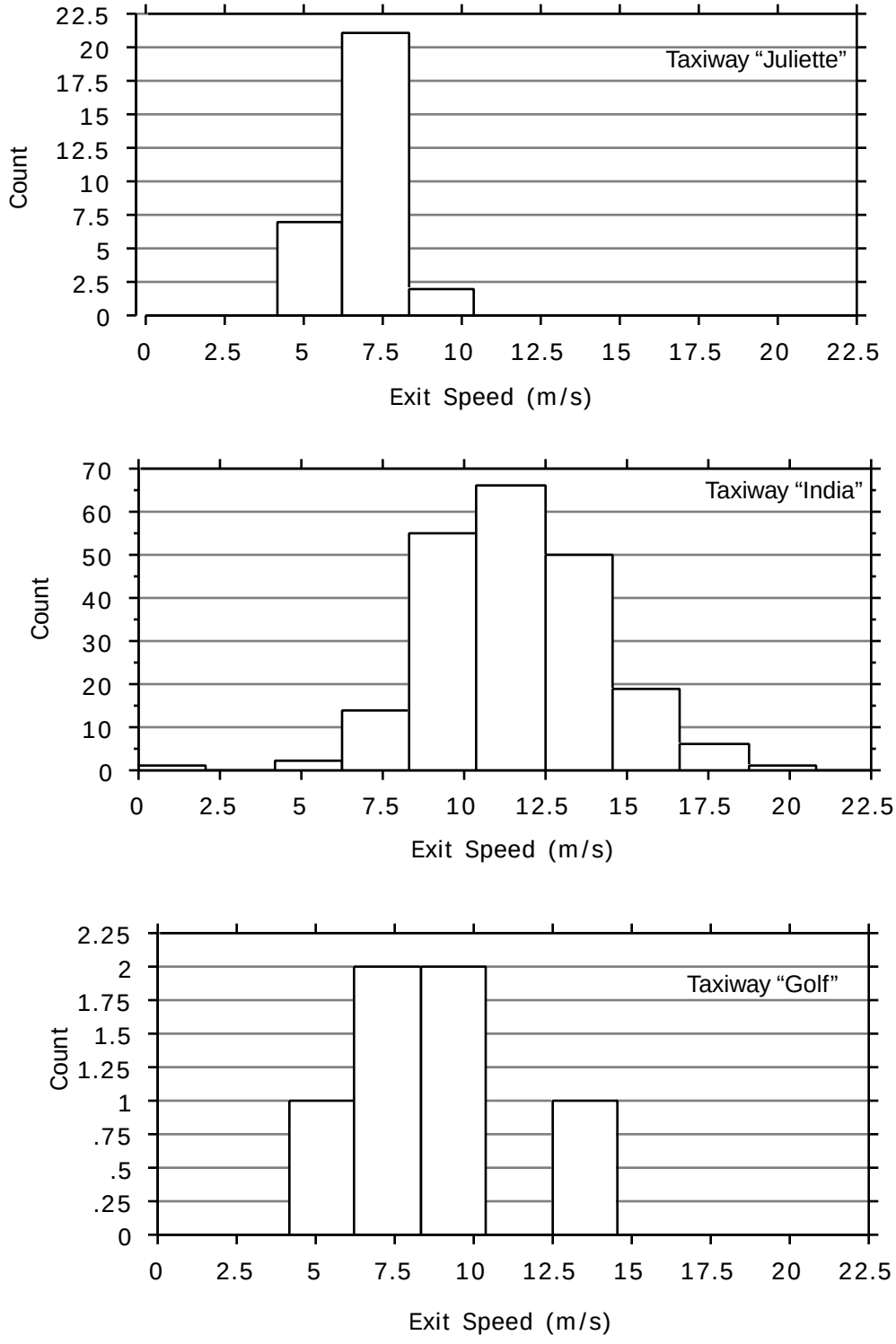

FIGURE G.5 Observed Exit Speed Histograms for All Aircraft Landing on Runway 36 at DCA (Cont.).

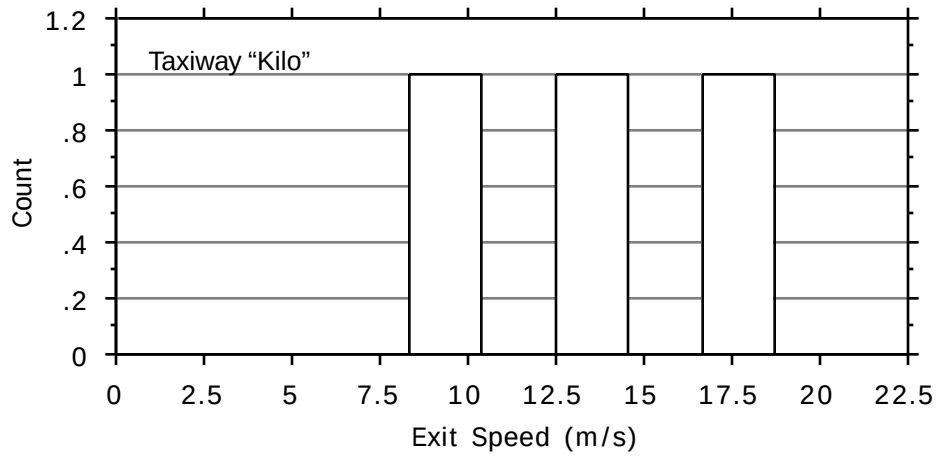

TABLE G.2 Summary of Statistics for Exit Speed Analysis at DCA Runway 36.

Parameter	Taxiway Name and Description					
	Golf	Hotel	India	Juliette	Runway	Foxtrot
Mean (m/s)	8.7	10.2	11.6	6.9	12.7	13.0
Std. Dev. (m/s)	3.1	3.7	2.6	1.1	3.6	3.6
Std. Error (m/s)	1.3	0.7	0.2	0.2	0.3	2.1
Count	6	25	214	30	110	3
Minimum (m/s)	5.6	3.8	5.2	5.1	8.4	9.5
Maximum (m/s)	14.3	17.8	20.6	8.9	20.8	16.7

FIGURE G.6 **Observed Exit Speed Histograms for All Aircraft Landing on Runway 08-L at ATL.**

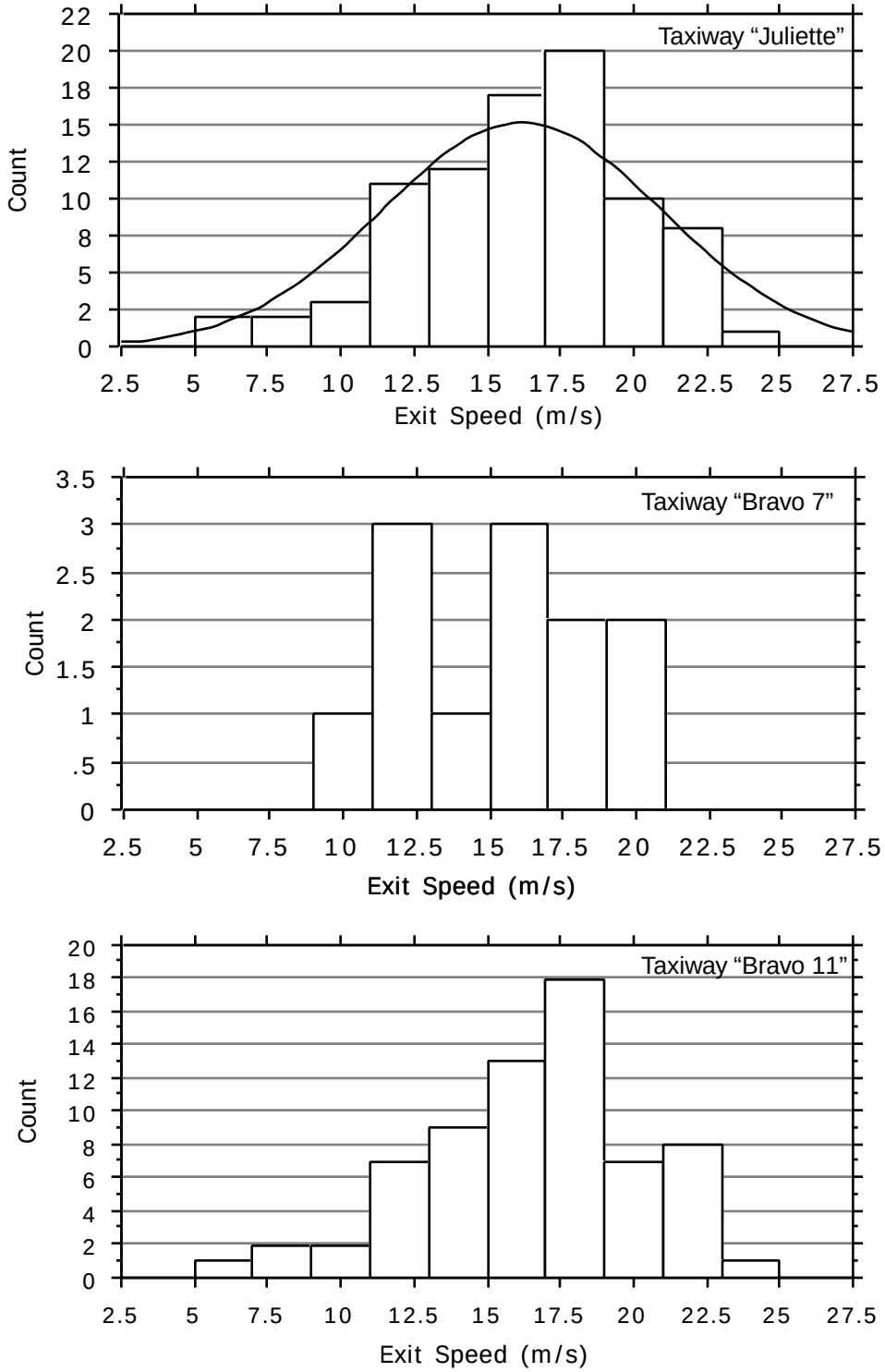

TABLE G.3 Summary of Statistics for Exit Speed Analysis at ATL Runway 08-L.

Parameter	Taxiway Name and Description			
	Charlie (Wide 90 degrees)	Delta (Wide 90 degrees)	Bravo-7 (Std. 30 degrees)	Bravo-11 (Std. 30 degrees)
Mean (m/s)	13.3	13.3	15.4	16.9
Std. Dev. (m/s)	N/A	8.54	3.64	4.03
Std. Error (m/s)	N/A	3.23	1.05	0.48
Count	1	7	12	70
Minimum (m/s)	13.3	8.3	9.6	7.2
Maximum (m/s)	13.3	15.3	20.9	26.3

FIGURE G.7 Observed Exit Speed Histograms for All Aircraft Landing on Runway 01-R at IAD.

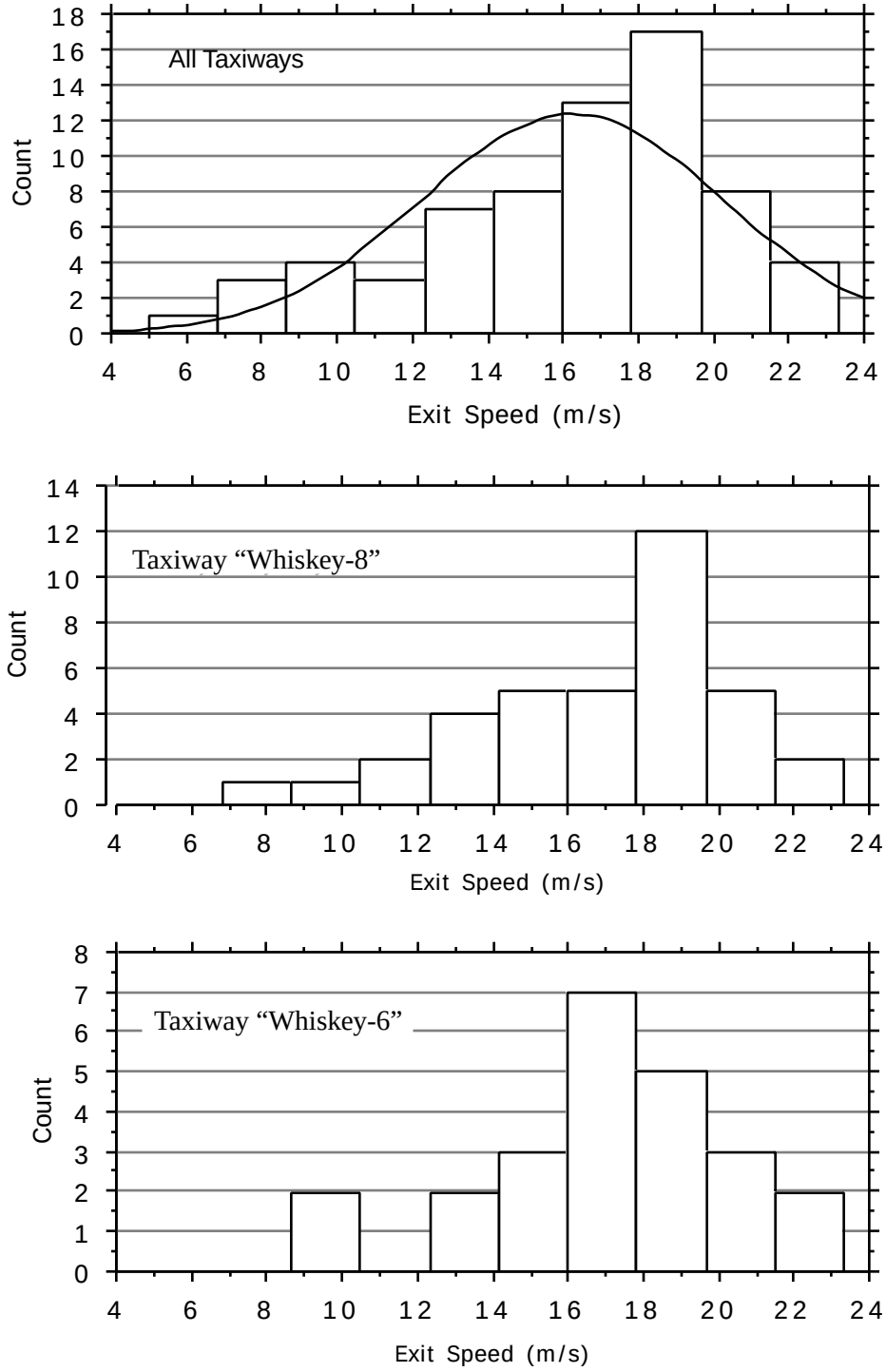

TABLE G.4 Summary of Statistics for Exit Speed Analysis at IAD Runway 01-R.

Parameter	Taxiway Name and Description				
	Whiskey-4 (Std. 30 degrees)	Whiskey-7 (Std. 30 degrees)	Whiskey-6 (Std. 30 degrees)	Whiskey-8 (Std. 30 degrees)	Totals[a]
Mean (m/s)	12.5	7.7	16.9	16.9	16.2
Std. Dev. (m/s)	2.92	0.22	3.45	3.44	4.02
Std. Error (m/s)	1.458	0.159	0.705	0.566	0.488
Count	4	2	24	37	68
Minimum (m/s)	9.6	7.6	9.4	8.5	7.6
Maximum (m/s)	16.0	7.9	23.3	23.3	23.3

a. Includes one observation on Whyskey-5 clocked at 5.6 m/s.

APPENDIX H

Aircraft Runway Occupancy Time Data Obtained at Various Airports

This appendix contains graphical and tabular information on the aircraft runway occupancy times used in the calibration of the REDIM 2.1 model. Four major airports are included in this analysis and no distinction at the moment is made of individual aircraft as it was found that both, transport aircraft and commuters, display somewhat similar characteristics while taking various exit turnoffs.

Figure H.1 illustrate the exit speed histograms observed at Charlotte Douglas International Airport Runway 23 under VMC conditions. The observations have been plotted as histograms to better inform the reader the exit speed trends observed. Table H.1 summarizes the results for CLT and also includes a brief description of the types of exits at this facility. It should be noted that CLT Runway 23 has only two runway exits capable of accommodating transport aircraft (i.e., Bravo and Echo) and a third one located 900 m. from the threshold being used primarily by commuter traffic.

Figures H.2 through H.5 show exit speed histograms for data collected at Washington National, Atlanta International and Dulles international Airports, respectively. Note that in the case of National Airport the total exit speed distribution is actually normally distributed (i.e., using Chi-Square analysis) even though not all exits are of the same type as CLT.

Finally, Figures H.11 through H.15 present graphical information on runway occupancy time landing observations at Charlotte International runway 23. Note that in this case the main deviations from the landing roll observations are motivated by the long separation between two available runway turnoffs (i.e., see runway turnoff Echo and Bravo in Figure 3.3).

FIGURE H.1 **Runway Occupancy Time Histogram for All Aircraft Landing on Runway 23 at Charlotte International Airport.**

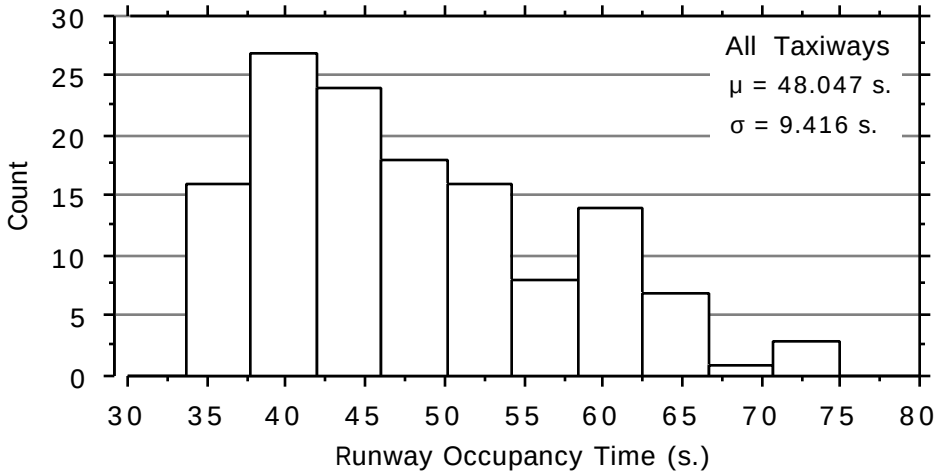

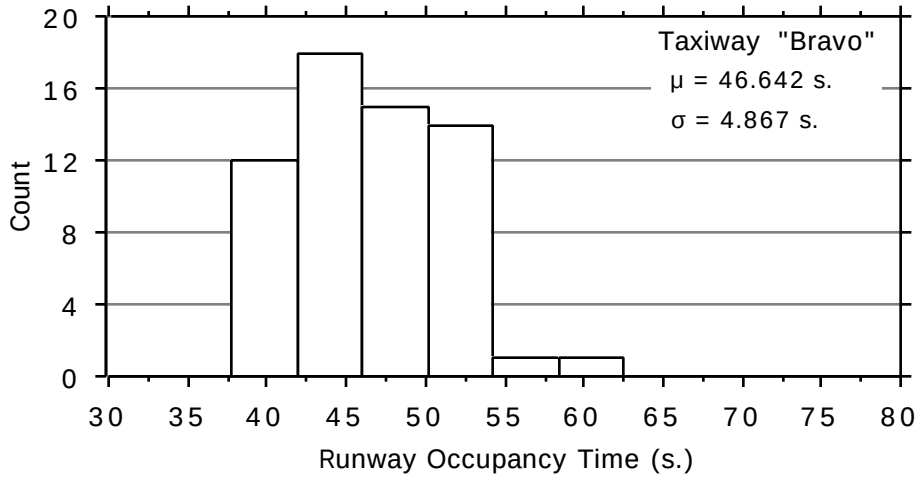

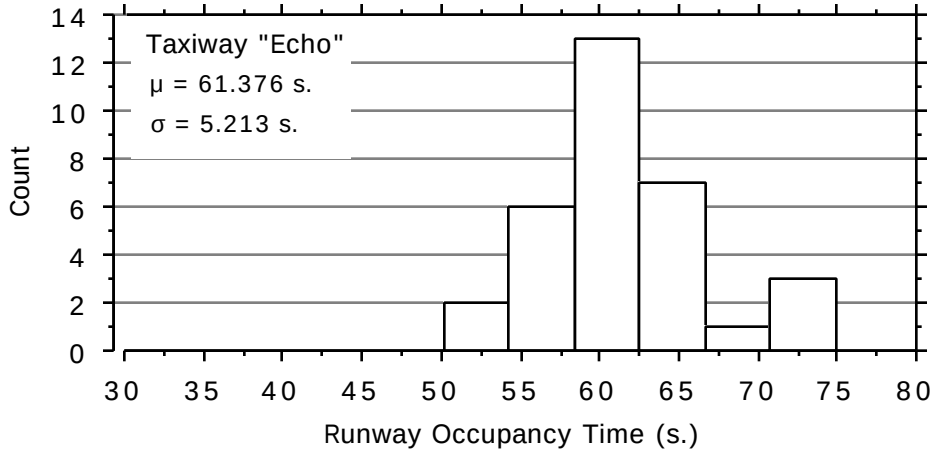

FIGURE H.2 **Runway Occupancy Time Histogram Observed at Charlotte Douglas International Airport (Runway 23).**

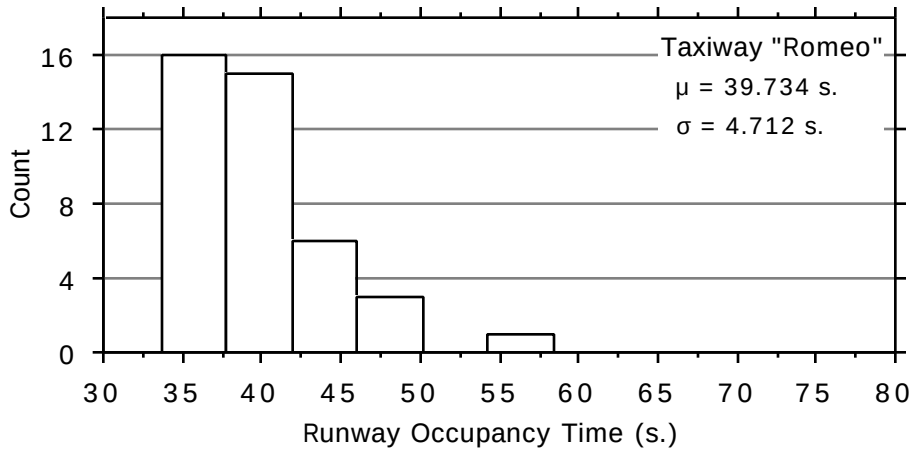

TABLE G.1 **Summary of Statistics for Runway Occupancy Time Analysis at CLT Runway 23.**

Parameter	Taxiway Name and Description			
	Romeo (Std. 90 degree)	Bravo (Std. 90 degree)	Echo (Std. 90 degree)	Total
Mean (s.)	39.7	46.6	61.4	48.0
Std. Dev. (s.)	4.71	4.87	5.12	9.42
Std. Error (s.)	0.74	0.62	0.92	0.81
Count	41	61	32	134
Minimum (s.)	33.6	37.9	50.9	33.6
Maximum (s.)	55.2	60.1	74.8	74.8

FIGURE H.3 **Observed Runway Occupancy Time Histograms for All Aircraft Landing on Runway 36 at National Airport.**

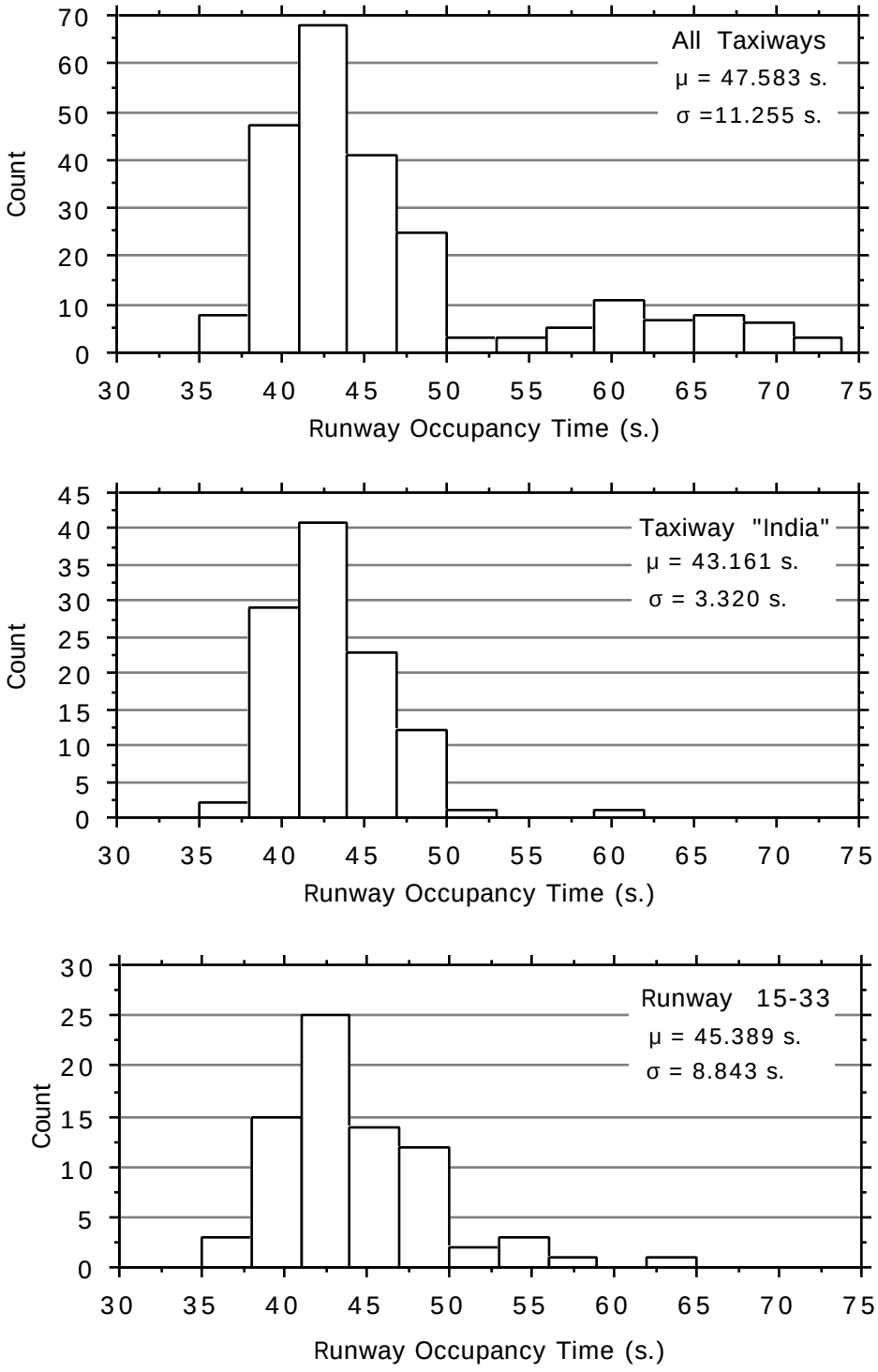

FIGURE H.4 **Observed Runway Occupancy Time Histograms for All Aircraft Landing on Runway 36 at DCA (Cont.).**

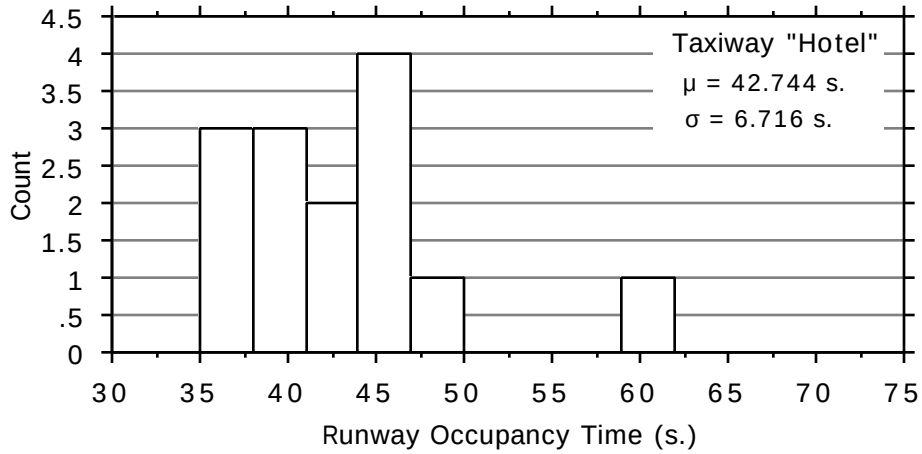

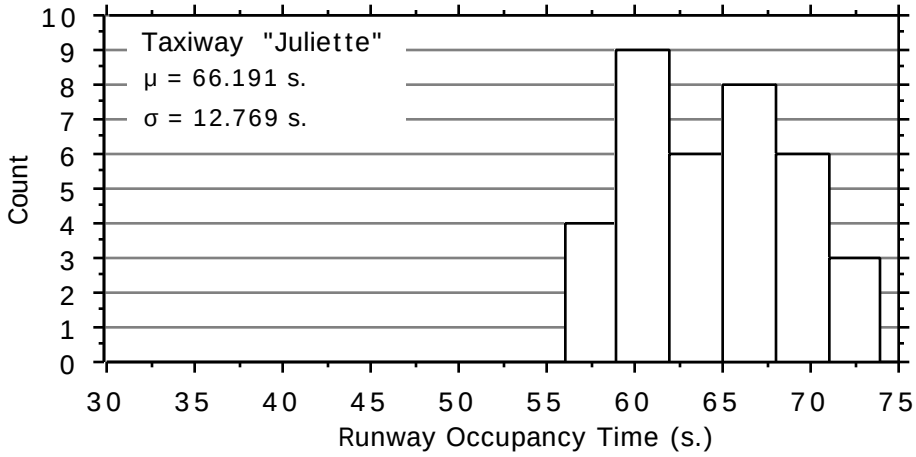

TABLE G.2 Summary of Statistics for Runway Occupancy Time Analysis at DCA Runway 36.

Parameter	Taxiway Name and Description				Total
	Hotel	India	Juliette	Runway	
Mean (s.)	42.7	43.1	66.2	45.4	47.6
Std. Dev. (s.)	6.71	3.32	12.77	8.84	11.3
Std. Error (s.)	1.73	0.318	2.05	1.00	0.73
Count	15	109	39	79	241
Minimum (s.)	34.8	37.7	34.9	36.0	34.8
Maximum (s.)	61.1	60.7	130.4	98.2	130.4

FIGURE H.5 Observed Runway Occupancy Time Histograms for Aircraft Landing on Runway 08-L at ATL.

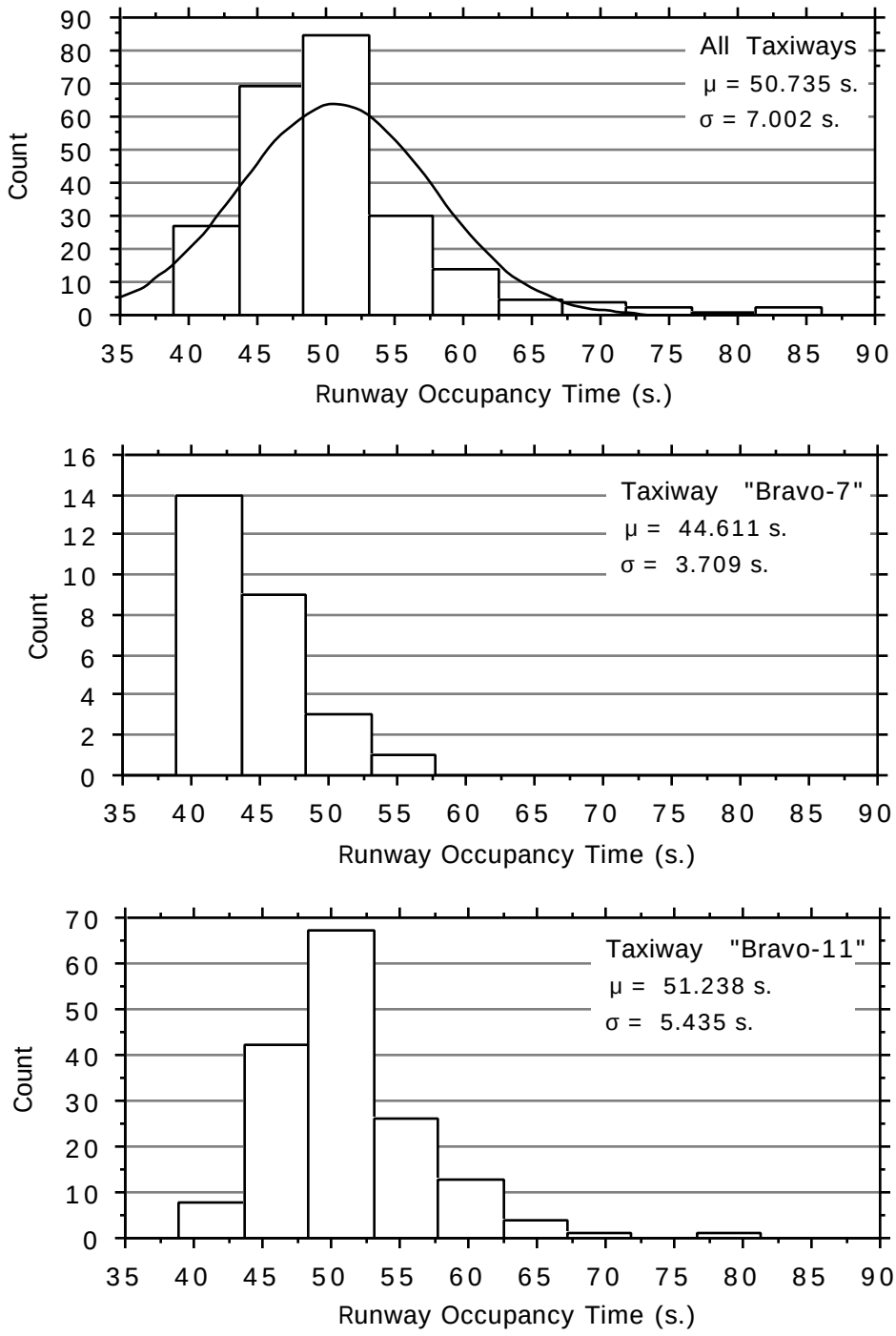

FIGURE H.6 **Observed Runway Occupancy Time Histograms for Aircraft Landing on Runway 08-L at ATL.**

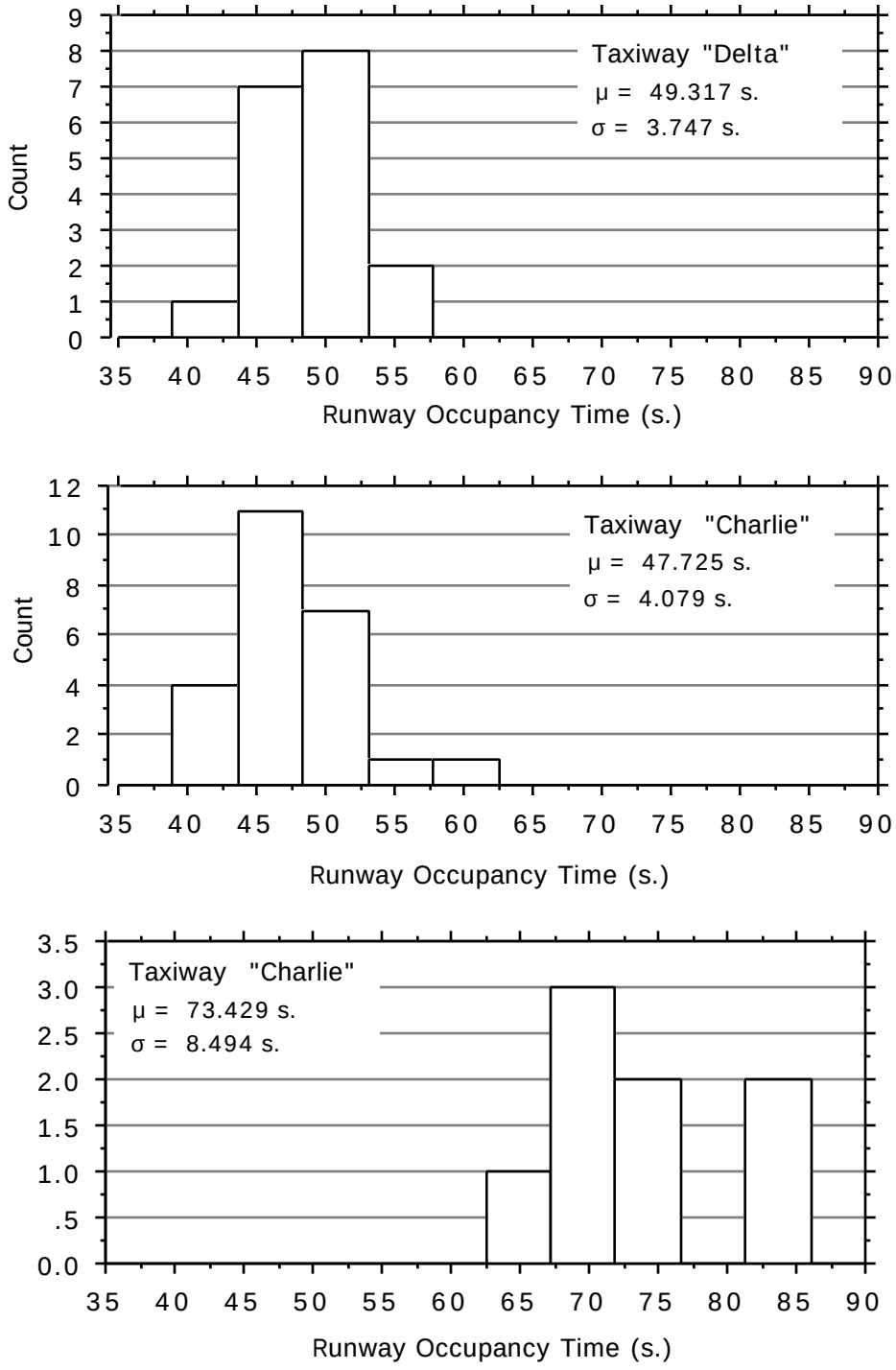

TABLE G.3 Summary of Statistics for Runway Occupancy Time Analysis at ATL Runway 08-L.

Parameter	Taxiway Name and Description					Total
	Charlie (Wide 90 degrees)	Delta (Wide 90 degrees)	Bravo-7 (Std. 30 degrees)	Bravo-11 (Std. 30 degrees)	Bravo-13 (Std. 30 degrees)	
Mean (s.)	47.7	49.3	44.6	52.2	73.4	50.7
Std. Dev. (s.)	4.08	3.75	3.71	5.44	8.49	7.00
Std. Error (s.)	0.83	0.88	0.71	0.43	3.00	0.45
Count	24	18	27	162	8	239
Minimum (s.)	41.1	41.0	39.0	41.0	62.6	39.0
Maximum (s.)	60.5	57.2	53.4	77.4	86.0	86.0

FIGURE H.7 Observed Runway Occupancy Time Histograms for Aircraft Landing on Runway 01-R at IAD.

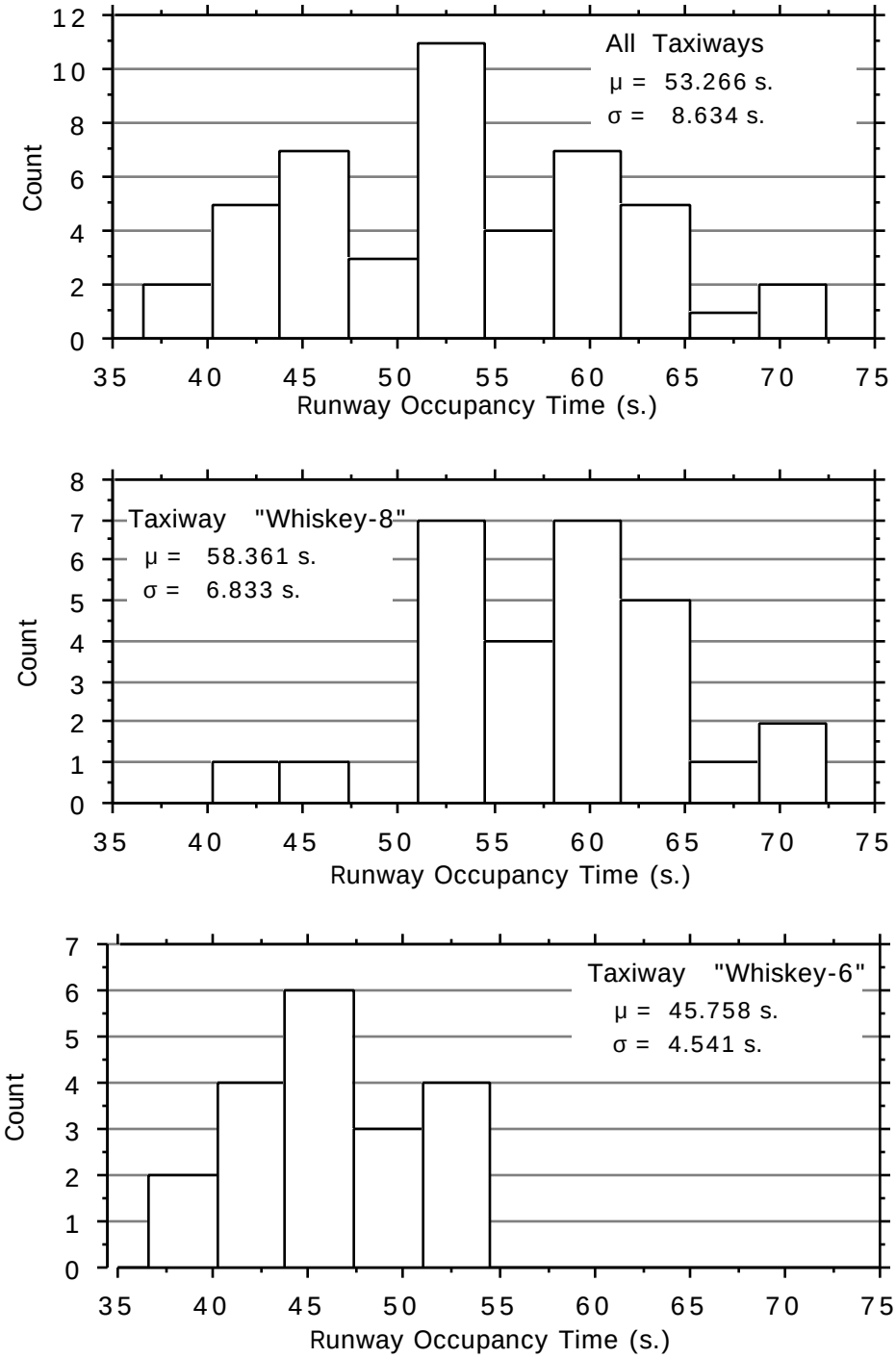

TABLE G.4 Summary of Statistics for Runway Occupancy Time Analysis at IAD Runway 01-R.

Parameter	Taxiway Name and Description				
	Whiskey-4 (Std. 30 degrees)	Whiskey-7 (Std. 30 degrees)	Whiskey-6 (Std. 30 degrees)	Whiskey-8 (Std. 30 degrees)	Totals
Mean (s.)	43.2	48.3	45.8	58.4	53.3
Std. Dev. (s.)	4.20	N/A	4.54	6.83	8.63
Std. Error (s.)	1.03	N/A	1.04	1.29	1.26
Count	4	1	19	28	47
Minimum (s.)	36.3	N/A	36.6	42.8	36.6
Maximum (s.)	50.4	N/A	52.7	72.5	72.5

APPENDIX J Airport Layouts

This appendix contains layouts of the airports used during the data collection procedure. The layouts have been adapted from the 1994 Aviation Capacity Enhancement Plan (FAA, 1994). Note that the diagrams include specific runway taxiways used in the calibration process.

Figure J.1 shows the airport layout for Washington National Airport. At this facility runway 36 was the primary runway in use during the two day visit. Runway taxiways labeled E, F, G, H, I and J were in use for both transport and General Aviation aircraft.

Figure J.2 depicts graphically Charlotte/Douglas International Airport. At this facility most of the observations were recorded on runway 23 with three feasible exit locations: R, B, and E. All the landing aircraft were assigned to the new terminal building.

Figure J.3 illustrates a simple airport layout for the William B. Hartsfield International Airport in Atlanta. Runway 8L was the primary focus of our observations with feasible exits labeled C, D, B7, B9, and B-11. A small percentage of landings were recorded on runway 9R .

Figure J.4 shows graphically a layout for Washington Dulles Airport. Runways 19R and 19L were in operation during our visit with 19R being the primary landing runway at the time. Exits labeled W4, W6, and W8 were the main focus of the observations at this airport.

FIGURE J.1 **Washington National Airport Layout (Adapted from the 1994 Aviation Capacity Enhancement Plan).**

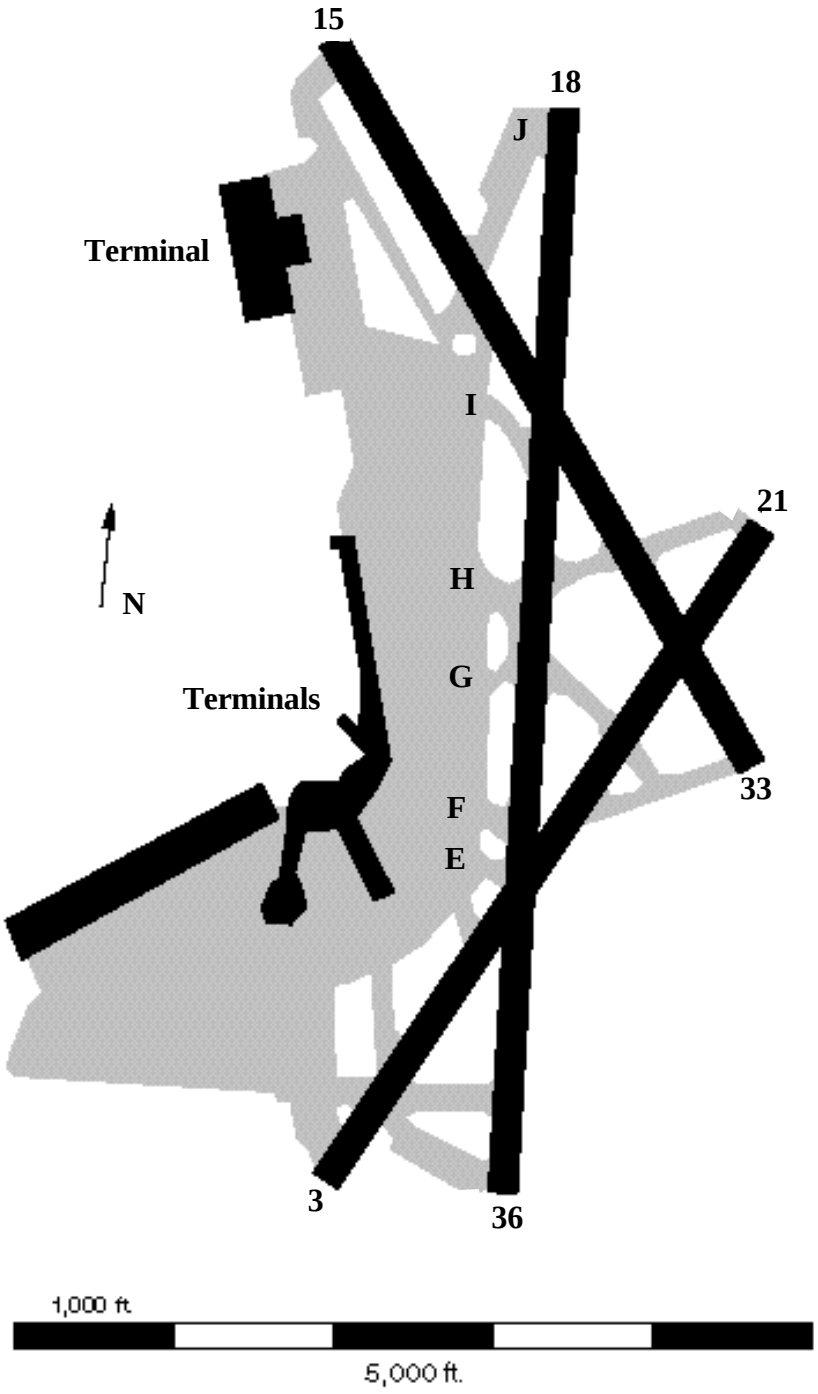

FIGURE J.2 **Charlotte/Douglas International Airport Layout (Adapted from the 1994 Aviation Capacity Enhancement Plan).**

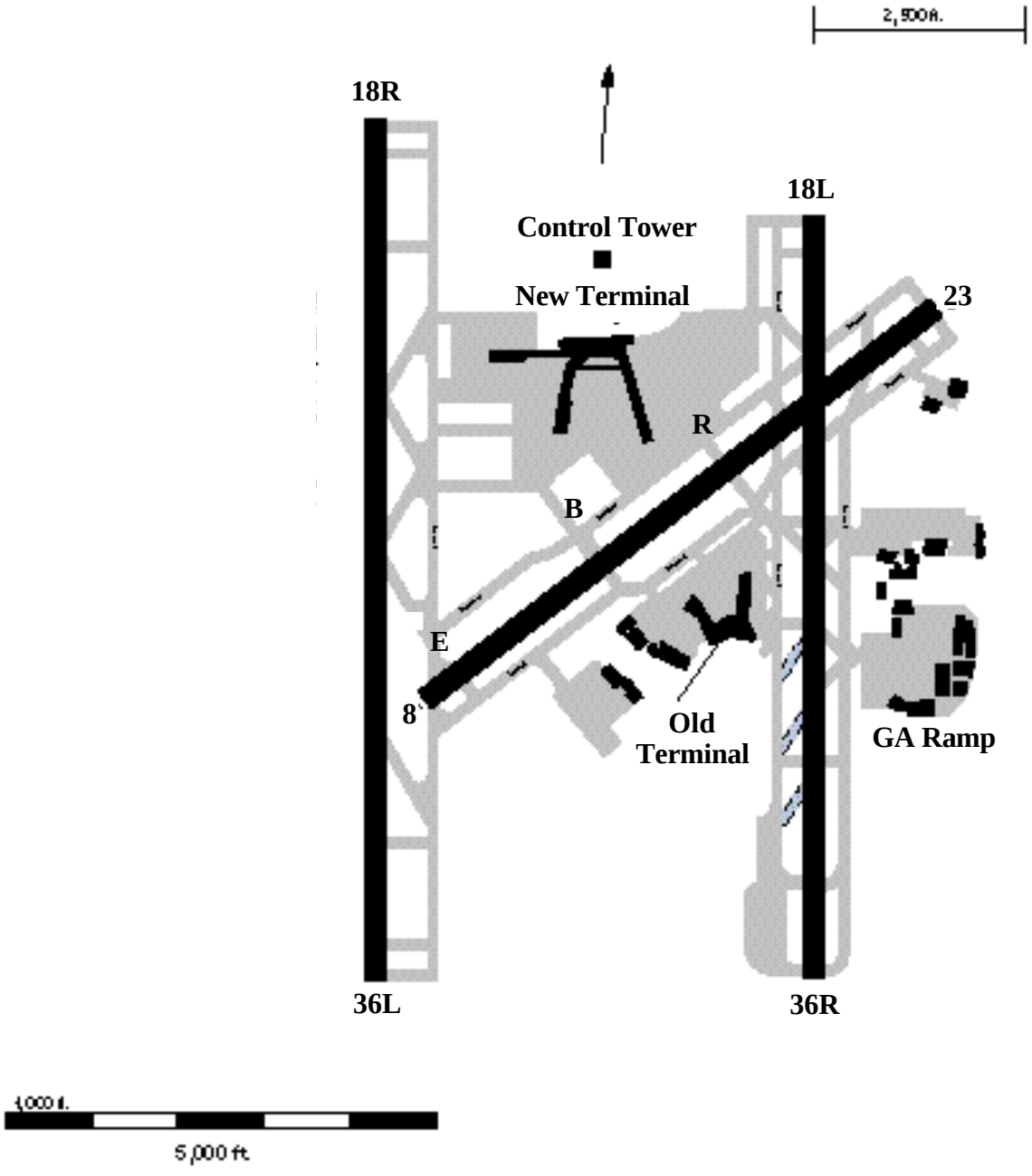

FIGURE J.3 **Atlanta Hartsfield International Airport Layout (Adapted from the FAA 1994 Enhancement Capacity Plan).**

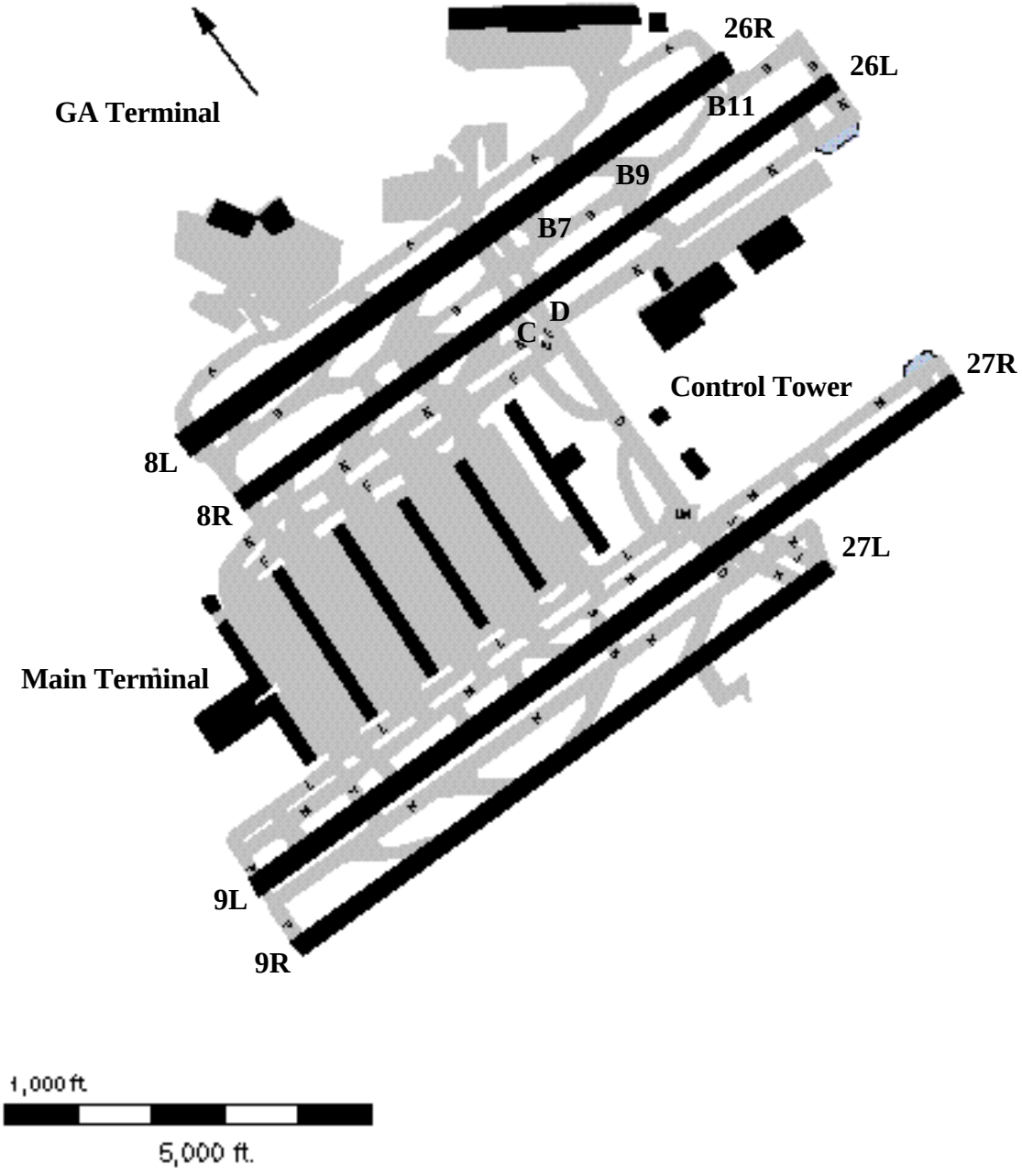

FIGURE J.4 **Washington Dulles International Airport Layout (Adapted from the FAA 1994Enhancement Capacity Plan).**

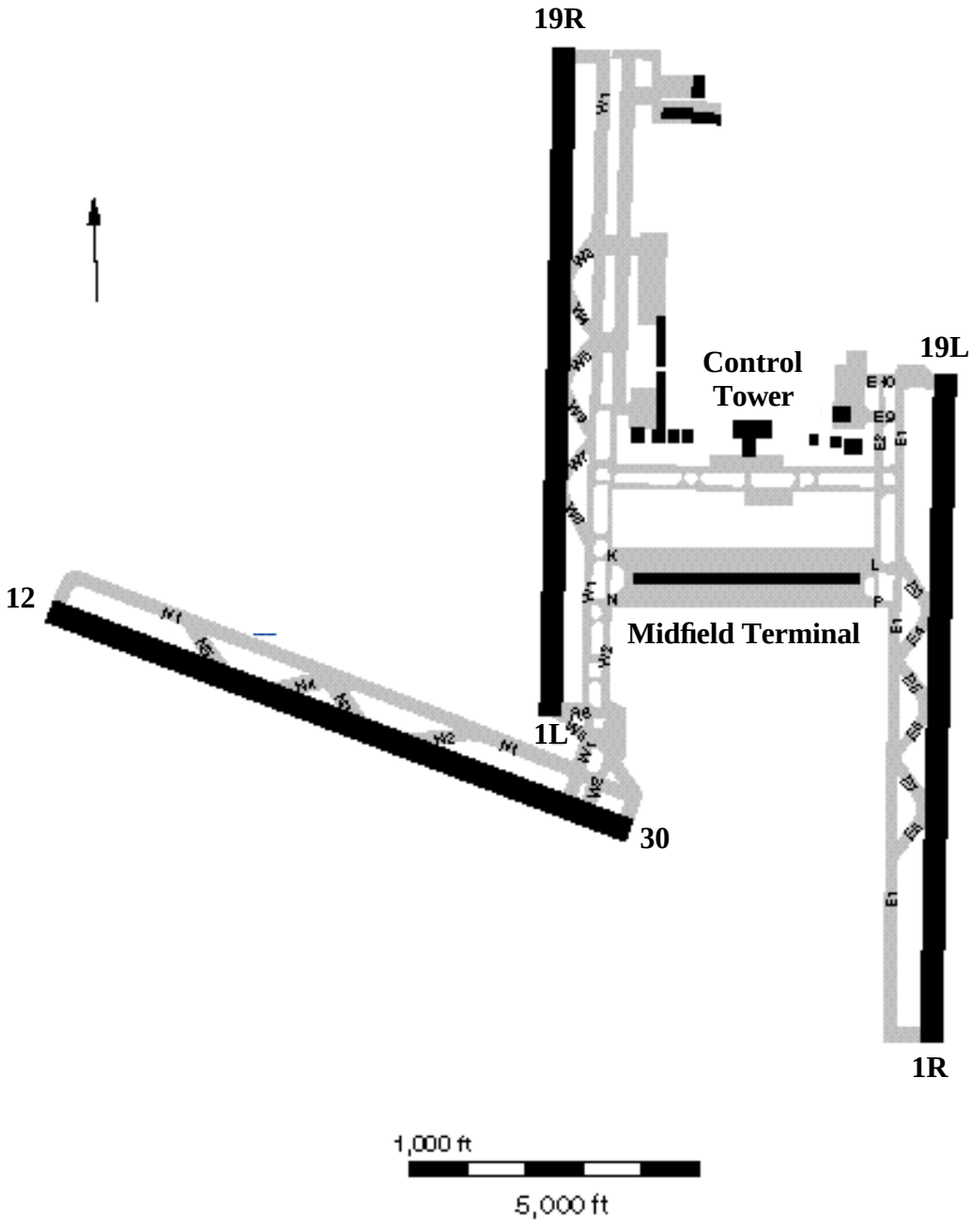

APPENDIX K

Fligh Simulation Experimental Data (Exit Speeds)

This appendix contains exit speed data derived from flight simulation experiments conducted at the Mike Monroney Aeronautical Center using the FAA Boeing 727-200 flight simulator in December, 1994 and March, 1995. The data presented here contains information on actual exit speeds observed during flight simulation runs.The exit speed parameter gives an idea of the willingness of pilots to execute and negotiate a high speed exit at the maximum permissible exit speed. Table K.1 contains summary information on exit speeds recorded 61.0 m (200 ft.) from the point of curvature (i.e., where centerline guidance lights start). Figures K.1 through K.5 contain histograms showing graphically the exits speeds for five high speed turnoff geometries tested.

Unpaired t-tests of the exit speed data shows that the hypothesized differences between the means are non zero. Table K.2 illustrates the t-test results for the five geometries tested comparing the FAA acute angle exit with others. Note that in all cases there are significant differences between the results of the pilot run and the new geometries thus indicating that pilots indeed behaved differently while negotiating the new exit geometries.

It is interesting to point out that in most cases the differences in perceived safety among the exits tested were not significant as shown in Table K.2. This is probably due to the overall perception by pilots that the new exits have a significant widening in the throat section compared with the current FAA standard geometries. writing

TABLE K.1 Summary Information for Various High Speed Exits Tested in the Boeing 727-200 Flight Simulator.

Exit Geometry	FAA Acute Angle	REDIM 3030	REDIM 3020	REDIM 3530	REDIM 3520
Mean Exit Speed - m/s (knots)	38.96 (75.60)	45.62 (88.51)	45.54 (88.35)	49.19 (95.43)	45.66 (88.58)
Standard Deviation of Exit Speed - m/s (knots)	5.32 (10.32)	6.08 (11.80)	4.20 (8.15)	6.40 (12.42)	5.24 (10.16)
Standard Error - m/s (knots)	1.00 (1.95)	1.11 (2.15)	0.79 (1.54)	1.15 (2.23)	0.94 (1.83)
Range - m/s (knots)	23.7 (46.0)	23.7 (46.0)	19.1 (37.0)	21.6 (42.0)	25.3 (49.0)
Count	28	30	29	31	31

TABLE K.2 Unpaired t-test Results for Various High Speed Exits.

Unpaired t-test	Mean Difference (knots)	Degrees of Freedom	t-value	P-Value
FAA - REDIM V	-12.860	56	-4.409	< 0.0001
FAA - REDIM VI	-12.669	55	-5.153	< 0.0001
FAA - REDIM VII	-19.796	57	-6.620	< 0.0001
FAA - REDIM VIII	-12.877	57	-4.825	< 0.0001
REDIM V - REDIM VI	0.191	57	0.072	0.9428
REDIM V - REDIM VII	-6.937	59	-2.237	0.0291
REDIM V - REDIM VIII	-0.017	59	-0.006	0.9951
REDIM VI - REDIM VII	-7.127	58	-2.609	0.0115
REDIM VI - REDIM VIII	-0.208	58	-0.087	0.9309
REDIM VII - REDIM VIII	6.919	60	2.401	0.0195

FIGURE K.1 Exit Speed Data for the Acute Angle High Speed Exit.

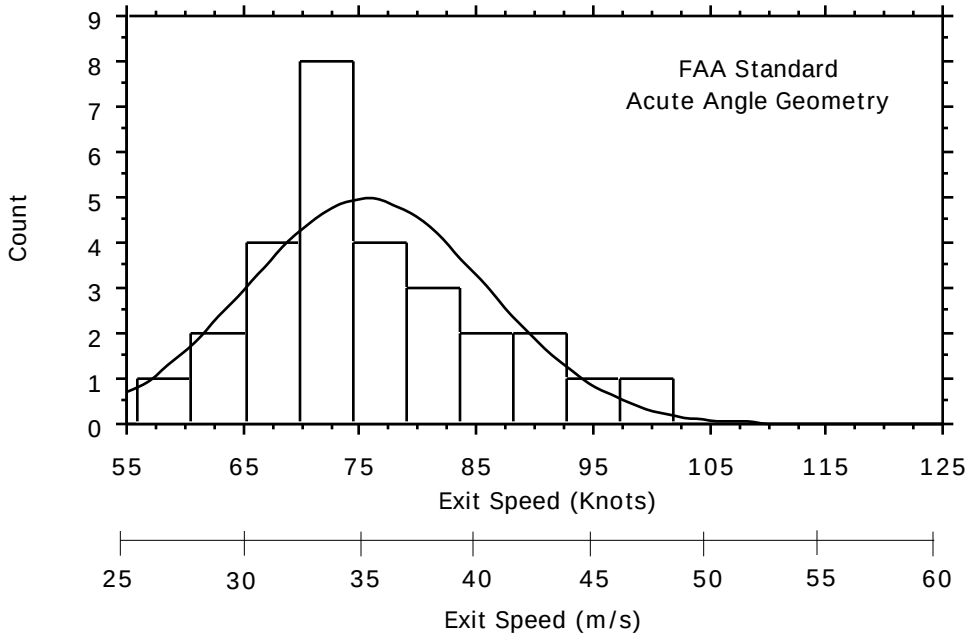

FIGURE K.2 **Exit Speed Data for Geometry V.**

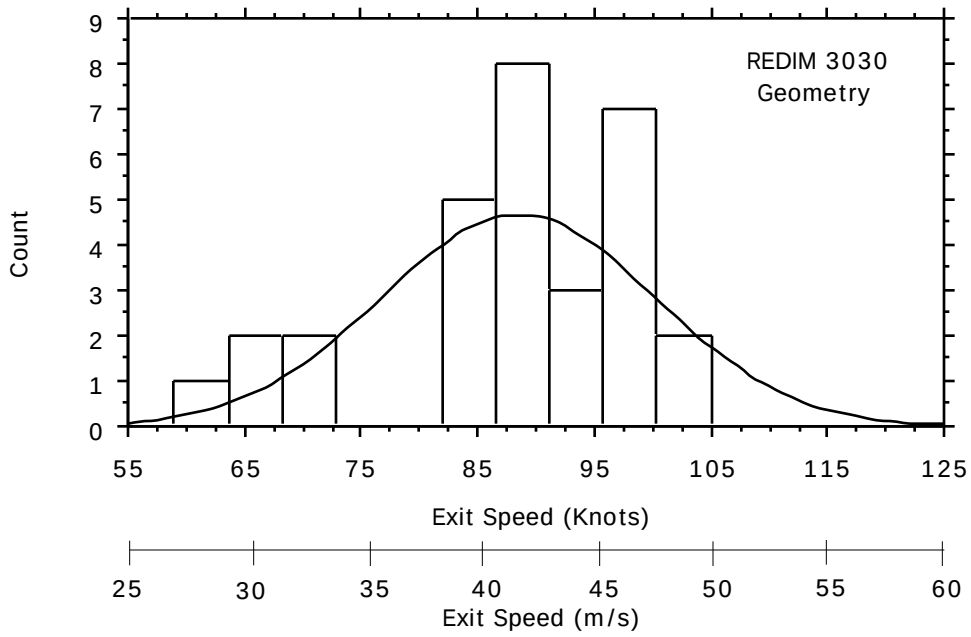

FIGURE K.3 **Exit Speed Data for Geometry VII.**

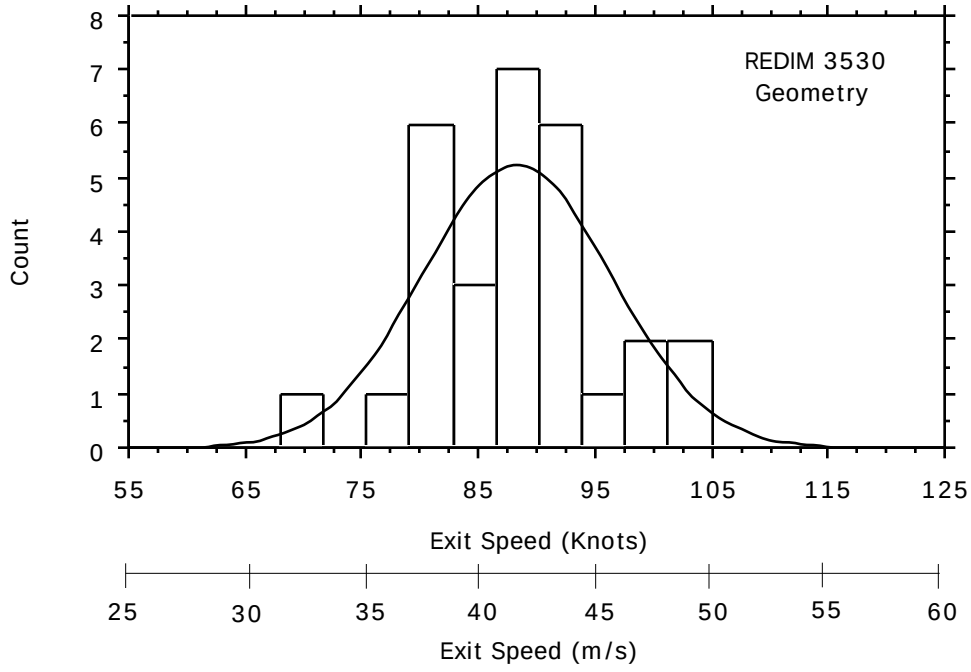

FIGURE K.4 **Exit Speed Data for Exit Geometry VI.**

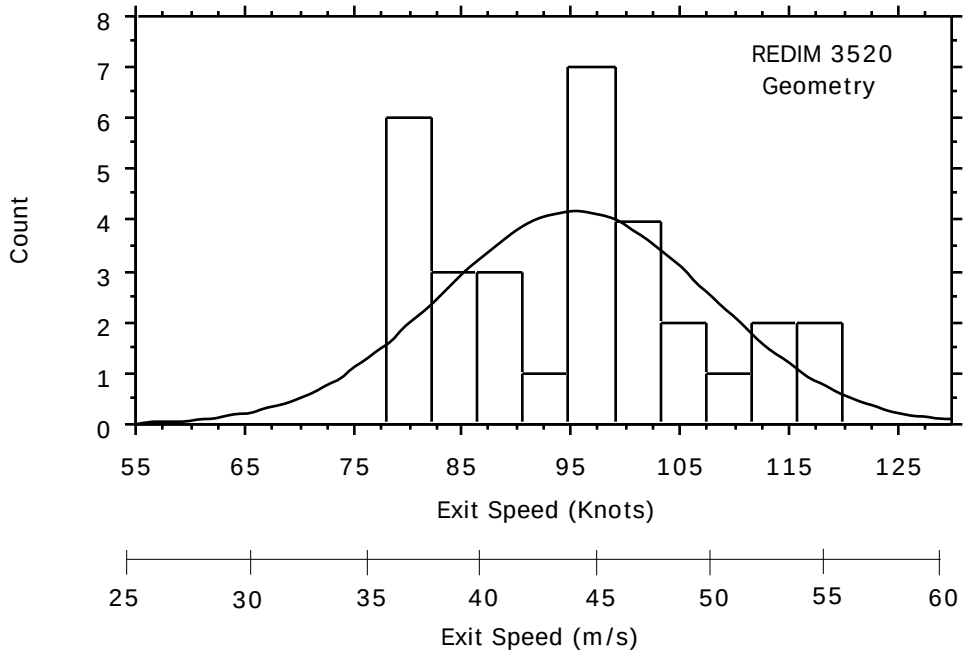

FIGURE K.5 **Exit Speed Data for Exit Geometry VIII.**